Investigation of an LNG fuel system for a Norwegian coast guard ship

Undersøkelse av LNG drivstoffsystem for skip
i den norske kystflåten

Joseph DiRenzo

NTNU

Norwegian University
of Science and Technology

Department of Energy
and Process Engineering

EPT-M-2014-25

MASTER THESIS

for

Student Joseph DiRenzo

Spring 2014

Investigation of an LNG fuel system for a Norwegian coast guard ship

Undersøkelse av LNG drivstoffsystem for skip i den norske kystflåten

Background and objective

LNG is being introduced as fuel for both land based and marine transport applications. For use in marine applications, some of the drivers for the introduction are:
- To comply with new emission regulations related to NOx and other gases
- Reduced fuel costs
- Environmental aspects related to reduced CO_2 emissions

The Norwegian Coast Guard has introduced three vessels that use LNG as their primary source of fuel and the US Coast Guard is currently evaluating an introduction in their vessels. These as well as other LNG fuelled ships has experienced situations where a drop in fuel tank pressure has led to motor power outage.

The aim of this Master's project is to perform theoretical, experimental and modelling and simulation efforts in order to understand this phenomenon in more detail.

The following tasks are to be considered:

1. Perform a literature survey related to storage and transport of cryogenic liquids
2. Plan and perform an experimental campaign onboard a coast guard vessel to understand the changing conditions of LNG in the fuel tank, with emphasis on a bunkering condition
3. Participate in model experiments investigating fluid movements and mixing in a typical LNG fuel tank, to the extent possible
4. Make a detailed model of the tank system in order to be able to simulate the consequence of different events
5. Propose different measures to avoid conditions where a drop in tank pressure can be avoided

-- " --

Within 14 days of receiving the written text on the master thesis, the candidate shall submit a research plan for his project to the department.

When the thesis is evaluated, emphasis is put on processing of the results, and that they are presented in tabular and/or graphic form in a clear manner, and that they are analyzed carefully.

The thesis should be formulated as a research report with summary both in English and Norwegian, conclusion, literature references, table of contents etc. During the preparation of the text, the candidate should make an effort to produce a well-structured and easily readable report. In order to ease the evaluation of the thesis, it is important that the cross-references are correct. In the making of the report, strong emphasis should be placed on both a thorough discussion of the results and an orderly presentation.

The candidate is requested to initiate and keep close contact with his/her academic supervisor(s) throughout the working period. The candidate must follow the rules and regulations of NTNU as well as passive directions given by the Department of Energy and Process Engineering.

Risk assessment of the candidate's work shall be carried out according to the department's procedures. The risk assessment must be documented and included as part of the final report. Events related to the candidate's work adversely affecting the health, safety or security, must be documented and included as part of the final report. If the documentation on risk assessment represents a large number of pages, the full version is to be submitted electronically to the supervisor and an excerpt is included in the report.

Pursuant to "Regulations concerning the supplementary provisions to the technology study program/Master of Science" at NTNU §20, the Department reserves the permission to utilize all the results and data for teaching and research purposes as well as in future publications.

The final report is to be submitted digitally in DAIM. An executive summary of the thesis including title, student's name, supervisor's name, year, department name, and NTNU's logo and name, shall be submitted to the department as a separate pdf file. Based on an agreement with the supervisor, the final report and other material and documents may be given to the supervisor in digital format.

☐ Work to be done in lab (Water power lab, Fluids engineering lab, Thermal engineering lab)
☒ Field work

Department of Energy and Process Engineering, 14. January 2014

Olav Bolland
Department Head
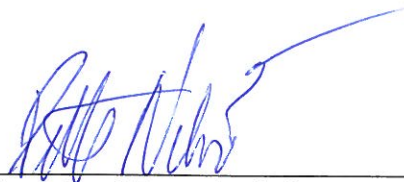
Adjunct Prof. Petter Nekså
Academic Supervisor

Research Advisors:
Kjell Kolsaker, NTNU EPT
Dag Stenersen, SINTEF MARINTEK

Preface

This master's thesis is an original intellectual product of the author, Joseph DiRenzo IV and is submitted as a partial requirement for the degree of Masters of Science in Natural Gas Technology from the Norwegian University of Science and Technology (NTNU).

Executive Summary

This report examines the reasons behind Natural Gas (NG) engine de-loading on LNG fuelled vessels. Two instances of NG engine de-loading due to low tank pressure have been document on KV Bergen in the Norwegian Coast Guard. Results from this study revealed that NG engine de-loading was caused by the disruption of the liquid surface layer in the LNG tank initiated by tank sloshing. Research found that when the surface layer between the bulk liquid and vapor in the tank was modified by sloshing the rate of vapor condensation increased faster than the mass flow rate produced by the Pressure Build Up (PBU) circuit inside the Vaporizer. Using the difference between the mass flow rate entering the vapor region and exiting through condensation, the time which a NG engine de-loading situation occurs was predicted.

These conclusions were drawn from different models and calculations which analyzed factors affecting tank pressure. One model calculated the PBU mass flow rate by balancing the change in pressure in each section of the PBU. Another model developed an idealized set of equations for the time required to pressurize the LNG tank. A mixing model was also produced which calculated the lowest fall in tank pressure possible if the liquid in the tank mixed completely with the vapor in the tank. These mixing calculations proved the criteria for NG engine de-loading can be met if there is enough interaction between the liquid and vapor in the tank.

A measurement campaign was carried out to understand how the different sub-components of the LNG system (LNG tank, PBU, Evaporator, and water glycol circuit) behaved during normal operations. The goal of the measurement campaign was to find real values which may be used to predict the conditions leading to NG engine de-loading. Using a heat balance from the different streams entering and leaving the Vaporizer, the average mass flow rate through the PBU circuit was determined to be 0.16 kg/s. This vapor mass flow rate is an indication of the PBU's ability to build up the tank pressure. The time required to build up the tank pressure from 295 kPa to 495 kPa was measured to be approximately 18 minutes on MF Korsfjord the morning after bunkering.

The calculated and measured results were combined to draw conclusions about the main factors leading to gas engine de-loading. By comparing the idealized and actual amount of time required to pressurize the tank, it was possible to estimate that 66.2% of the vapor mass flow from the PBU condensed while the tank was being pressurized. Using the rate of vapor condensation, it was possible to calculate that the thickness of an effective conduction layer, representative of the surface layer, is 1.71 mm in undisturbed conditions. The thickness of an undisturbed tank was used as a base case to examine how modifying the thickness of the surface layer and area of the vapor liquid interface changes the rate of vapor condensation. In situations where the vapor condensation exceeded the PBU mass flow rate, the difference was used to calculate how quickly the tank pressure fell.

This report also includes items for further research which would provide additional understanding of the factors leading to NG engine de-loading. Included is a detailed description of an experimental rig which may be used to find the relationship between disturbances occurring

outside the tank and sloshing happening inside. Different abatement technologies are also discussed to improve the reliability of LNG systems on LNG fueled vessels.

Table of Contents

List of Figures

List of Tables

List of Equations

Abbreviations

ECA	Emission Control Area
EVAP	Product Evaporator
HFO	Heavy Fuel Oil
IMO	International Maritime Organization
LA	Liquefied Argon
LCH4	Liquefied Methane
LIN	Liquefied Nitrogen
LNG	Liquefied Natural Gas
LOX	Liquefied Oxygen
MARPOL	International Convention for the Prevention of Pollution from Ships
NASA	National Aeronautics and Space Administration
NG	Natural Gas
NIST	National Institute of Standards and Technology
PBU	Pressure Build Up Unit

Nomenclature

Parameter	Description	Units
$\dot{Q}$	Volume Flow	[m^3/s]
$\dot{m}$	Mass Flow	[kg/s]
A	Area	[m^2]
B	Propagation Velocity	[m/s]
b	Thickness	[m]
C	Effective Length Hardware	[ft]
Cp	Heat Capacity (constant P)	[J/(kg*K)]
d	Diameter	[m]
D	Thermal Diffusivity	[m^2/s]
E	Energy	[kJ]
e	Surface Roughness	[m]
f	Friction Factor	[-]
G	Mass velocity per area	[kg/(m^2*s)]
h	Enthalpy	[J/kg]
J	Mechanical Equivalent of Heat	[ft*lb/Btu]
Ja	Jacob Number	[-]
k	Thermal Conductivity	[W/(m*K)]
l	Length (coil)	[m]
L	Length	[m]
m	Mass	[kg]
M	Molecular Weight	[g/mol]
N	Number of PBU coil rows	[-]
n	Number of PBU tubes	[-]
nr	Countable number	[-]
p	Pitch	[m]
P	Pressure	[kPa]
Pr	Prandtl Number	[-]
r	Radius	[m]
R	Universal Gas Constant	[J/K*mol]
Re	Reynolds Number	[-]
S	Free Surface Area	[m^2]
s	Ratio of Specific Heats (Cp/Cv)	[-]
SR	Slip Ration	[-]
t	time	[s]
T	Temperature	[K]
u	Velocity	[m/s]
U	Overall Heat Transfer Coefficient	[W/(m^2/s)]
V	Volume	[m^3]
W	Power (Electric / Thermal)	[kW]
x	Position	[m]
X	Thermo-physical constant	[-]
y	Mole fraction	[-]
z	Height	[m]
Z	Compressibility Factor	[-]

α	Molecular Evaporation Coefficient	[-]
θ	Concentration Percent	[%]
μ	Dynamic Viscosity	[Pa*s]
ρ	Density	[kg/m^3]
ε	Void Fraction	[-]

Sub-script	Description	Units
a	Annulus	[-]
A	Point A	[-]
AB	Length AB	[-]
acc	Acceleration	[-]
avg	Average	[-]
b	Inner cylinder	[-]
bulk	Bulk LNG Condition in tank	[-]
bunk	Bunkering Condition	[-]
B	Point B	[-]
BC	Length BC	[-]
c	Outer cylinder	[-]
C	Point C	[-]
CD	Length CD	[-]
coil	Coil	[-]
cond	Conduction	[-]
conv	Convection	[-]
crit	Critical	[-]
D	Point D	[-]
DA	Length DA	[-]
e	Equivalent /Effective	[-]
evap	Evaporation	[-]
exit	Exit Condition	[-]
eng	Natural Gas Engine	[-]
fric	Friction	[-]
f	Final	[-]
flat	Flat Surface	[-]
gas	Gas	[-]
gly	Water / Glycol mixture	[-]
hard	Hardware	[-]
heel	Heel, liquid	[-]
hom	Homogeneous	[-]
i	Inner / Inlet	[-]
int	Initial	[-]
inter	Interface transfer	[-]
l	Liquid	[-]
lat	Latent Heat of Evaporation / Condensation	[-]
lam	Laminar	[-]
leak	Leakage, Heat	[-]
lng	Liquid Natural Gas (liquid)	[-]

mol	Molecules (specific)	[-]
m	Log mean difference	[-]
min	Minimum	[-]
ng	Natural Gas (vapor)	[-]
o	Outer / Outlet	[-]
press	Pressurization	[-]
purge	Top Tank Purging	[-]
ramp	Ramp Up Pressurization	[-]
sl	Sloshing	[-]
sat	Saturated	[-]
sc	Sub-cooled	[-]
stat	Static	[-]
surf	Surface	[-]
tank	Tank	[-]
tot	Total	[-]
trans	Transitional	[-]
tube	Tubing	[-]
turb	Turbulent	[-]
v	Vapor	[-]
vap	Vaporizer	[-]
w	Wall	[-]
x	Various fluid properties	[-]
xfer	Transfer (heat/energy)	[-]
1	State One	[-]
2	State Two	[-]
3	State Three	[-]

Super-Script	Description	Units
t	Time	[s]
-	Average	[-]
'	Total Time Elapsed	[-]

1. Introduction

In the past decade, there has been growing interest in the use of LNG as a maritime fuel. This growing interest may be attributed to economic motivation and more stringent maritime emissions standards. Given the growing interest in LNG as a maritime fuel, efforts should be made to continually improve the reliability of LNG systems on maritime vessels.

1.1 Economic Motivations

One reason for the shift from classic marine fuels like Heavy Fuel Oils (HFO) to LNG is cost considerations. According to Lowell, Lutsey et al. (2013) between 2010 and 2012 the price of LNG was between 45 and 60 percent of the price of HFO used on marine vessels. Burel, Taccani et al. (2013) claims that this price difference may be caused, in part, by shrinking oil reserves and easier access to natural gas reserves with improved extraction techniques. The price advantage of LNG is clearly shown in Figure 1.
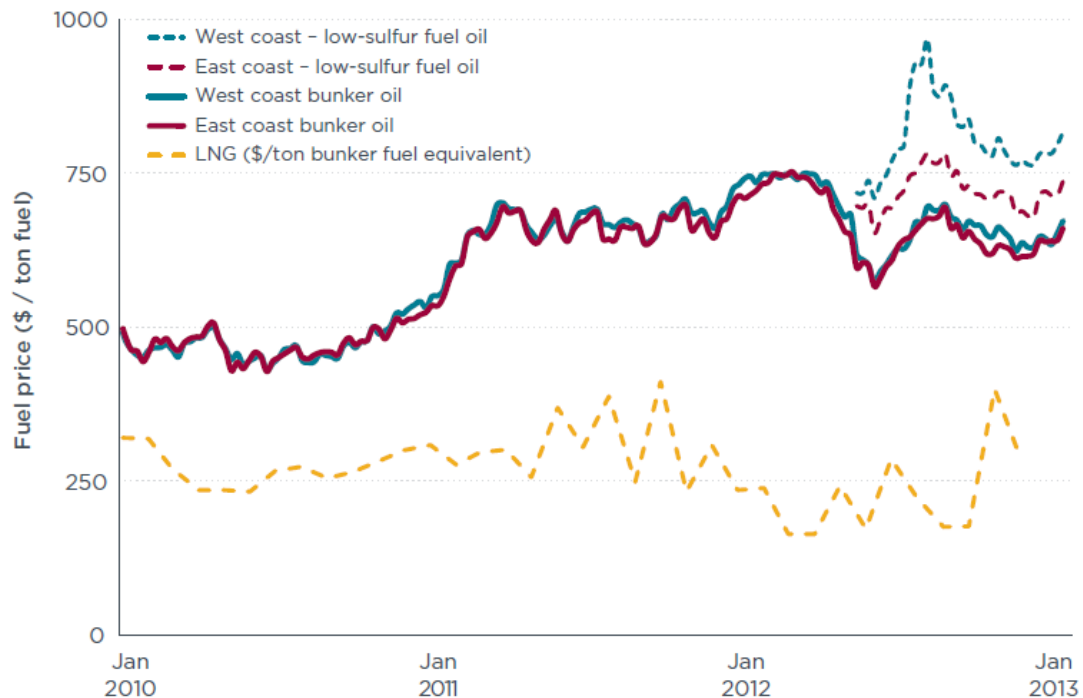
Figure 1: LNG price compared to other maritime fuels (Lowell, Lutsey et al. 2013)

Besides fuel costs there are also environmental reasons and more stringent pollution regulations causing the shift from classic marine fuels to LNG. The push by governments to better regulate the amount of pollution produced by maritime vessels is best encapsulated by the creation of Emissions Control Areas (ECAs) around Europe and North America. These ECAs place a limit on the amount of pollution that a certain vessel is allowed to produce. Pollution limits are set by the International Maritime Organization (IMO) through regulations enacted by the International

Convention for the Prevention of Pollution from Ships (MARPOL) (Burel, Taccani et al. 2013). Figure 2 and Figure 3 show the Sulfur and NO_x limits imposed by MARPOL in the ECAs.

Date	Global limit [% mass]	Date	ECA limit [% mass]
Prior to 1/1/2010	4.5%	Prior to 1/7/2010	1.5%
After 1/1/2012	3.5%	After 1/7/2010	1.0%
After 1/1/2020	0.5%	After 1/1/2015	0.1%

Figure 2: Global and ECA Sulfur Limits [% mass] by date (Burel, Taccani et al. 2013)

Tier	Date	NO_x limit [g/kWh]		
		$n < 130$	$130 \leq n \leq 2000$	$n \geq 2000$
Tier I	2000	17.0	$45 \times n^{-0.2}$	9.8
Tier II	2011	14.4	$44 \times n^{-0.23}$	7.7
Tier III	2016*	3.4	$9 \times n^{-0.2}$	1.96

*Only for NOx ECAs (TIER II applies outside ECAs).
n = engine speed [rpm].

Figure 3: NOx Emission Limits for ECA by date (Burel, Taccani et al. 2013)

There are a number of ways to achieve the emissions limits within the ECAs. These pollution reduction measures include using gas scrubbers, internal engine modifications, switching to different types of HFO, etc. (Burel, Taccani et al. 2013). A list of existing technology used to reduce pollution and by what amount is shown in Figure 4. Switching to LNG as a maritime fuel has a clear advantage over other methods used to reduce emissions from maritime vessels.

Abatement technology/measure	Emission reduction (%)			
	SO_x	NO_x	PM	CO_2
Basic internal engine modifications for 2 strokes, slow speed only	0	−20	0	0
Advanced internal engine modifications	0	−30	0	0
Direct water injection	0	−50	0	0
Humid air motors	0	−70	0	0
Exhaust gas recirculation + scrubbing	−93	−35	−63	0
Selective catalytic reduction (2.7% S residual oil fuel)	0	−90	0	0
Sea water scrubbing	−75	0	−25	0
Fuel switching (from 2.7% S to 1.5% S HFO)	−44	0	−18	0
Fuel switching (from 2.7% > 0.5% S HFO)	−81	0	−20	0
Low S marine diesel (from 0.5 to >0.1% S)	−80	0	0	0
Liquefied Natural Gas (LNG)	−90	−80	−100	−20

Figure 4: Maritime Emissions Abatement Technology (Burel, Taccani et al. 2013)

The shift from classic marine fuels to LNG is currently occurring in Norway and other Scandinavian countries. Lowell, Lutsey et al. (2013) notes that the Bit Viking "a 25,000 metric-ton product tanker" and the 12 LNG ferries operated by Fjord 1 mark a shift toward using LNG as a maritime fuel in Norway. Additionally, the Norwegian Coast Guard maintains three patrol vessels which are powered by Natural Gas (NG) engines. The growing number of small scale production and storage facilities being built along the Norwegian coast line is another indication that the shift from classic marine fuel to LNG is occurring (Lowell, Lutsey et al. 2013). The growing number of vessels using LNG in Norway and other Scandinavian countries indicates that there is interest in ensuring that maritime LNG systems are reliable.

This sub-section outlined the motivation behind switching to LNG as a source of maritime fuel. Besides the cost compared to other fuels, using LNG as a source of fuel allows vessels to meet standards imposed in ECAs by MARPOL. The next section discusses one particular challenge which should be addressed in future designs of LNG powered vessels.

1.2 System Reliability Motivation

Given the benefits of using LNG as a source of fuel, LNG systems onboard vessels should be as reliable as possible. This report focuses on the issue of NG engine de-loading caused by low tank pressure. Though not formally addressed in other publications, internal reports and discussions with operators on LNG fueled vessels suggest that this issue should be addressed to improve the reliability of LNG fueled vessels.

One instance where this problem has disrupted operations is on KV Bergen, a LNG fueled patrol vessel in the Norwegian Coast Guard vessel. According to a report produced by KV Bergen on 18 October 2012, NG engine de-loading occurred approximately two hours after bunkering during full engine trails (Espeland 2012). Before the NG engine de-loading occurred, three NG engines were producing 2200 kW at 88% of the full engine capacity. The majority of the engine load was used to power the electric motor for a full engine trial. After the first engine de-loading, the LNG system was reset and the NG engines were brought to 92% capacity. The Chief Engineer noticed, while the second full engine trail was conducted, the pressure in the LNG tank dropped from 4.6 bara to 3.6 bara. A second de-loading of the NG engines occurred shortly after this drop in tank pressure was noted. In response to the second de-loading, the engineers onboard decreased the load on the NG engines and allowed the pressure in the LNG tank to increase to an unspecified pressure. This was the first de-loading event documented on KV Bergen.

A second de-loading event occurred on KV Bergen during the first week of November 2013. Before the de-loading event, KV Bergen received 101 m^3 (approximately 44000 kg) of LNG during bunkering. Once the bunkering was finished, the Chief Engineer increased the LNG tank pressure to 4.6 bara using the Pressure Build Up (PBU) circuit. After 1 hour of producing 1400 kW from two gas engines, the LNG tank pressure began to fall while the PBU circuit was in operation. When the top tank pressure reached 3.9 bara, the Chief Engineer switched to the diesel engine to avoid an unintentional de-loading of the NG engines. Espeland (2014) noted the waves

were approximately 3 meters high during this event. When KV Bergen re-positioned for better coverage from the weather it was possible to increase the top tank pressure again. The factors leading to these de-loading events are explored later in this report.

This sub-section provided details on two unplanned instances of NG engine de-loading on KV Bergen due to low LNG tank pressure. The next chapter discusses what pressure will cause the NG engines to de-load and proposes a hypothesis for this fall in LNG tank pressure.

2. Thesis Objectives

2.1 Purpose

This report explores and quantifies the changing conditions in a LNG system on a maritime vessel during and after bunkering. The objective of this study is to gain a better understanding of the reasons for NG engine de-loading due to low LNG tank pressure. The theoretical basis of these changes are explored and supported by data collected during different measuring campaigns. Measurements were carried out on MF Korsfjord, a ferry owned by Fjord 1, and KV Bergen, a patrol vessel in the Norwegian Coast Guard. A methodology is proposed which predicts the behavior inside the LNG tank given different bunkering conditions. In the last section of the report, recommendations are made for further research which will provide additional insight into NG engine de-loading cause by low LNG tank pressure.

2.2 Scope and Limitation

This study focuses on the conditions inside the LNG tank during and after bunkering. Currently, there exists little information about how the LNG system on maritime vessels reacts directly after bunkering. This report will quantify the changing conditions in the following components: the LNG tank, Pressure Build Up (PBU) Unit, Product Evaporator (EVAP), and water glycol piping. Specifically, this report will attempt to find the fluid properties of the NG and LNG inside the LNG tank before and after bunkering. Simulations and measurements are made to project pressure conditions in the LNG tank as a result of bunkering. This report is limited in that it only considers the drop in tank pressure as a reason for NG engine de-loading. Other causes for NG engine de-loading are not considered in this report.

2.3 How de-loading occurs

Operating specifications for the gas engines used onboard MF Korsfjord and KV Bergen indicate what conditions must be in place to cause engine de-loading due to low LNG tank pressure. Both KV Bergen and MF Korsfjord use Mitsubishi gas engines (model GS16). Table 1 provides the main features of this gas engine model (Mitsubishi 2014).

Table 1: Mitsubishi Model GS16 Features

Feature	Description
Model	GS16
Type	4 cycle
Fuel System	Water cooled spark ignition pre-mixed fuel gas and air
Cylinder	16 cylinders
Minimum Inlet Gas Pressure	350 kPa
Maximum Inlet Gas Pressure	800 kPa
Governor Type	Electronic air-fuel mixture control
Output	1250 kVA/ 1000 kW

NG entering the gas engine fuel system is taken down from its entering pressure (>350 kPa) to approximately 20 kPa (200 mbar) with the Gas Ramp Unit (GRU). The purpose of the GRU is to "govern and regulate the gas supply and gas pressure to the engines" (CryoAB 2009). The starboard side GRU on MF Korsfjord is shown in Figure 5. Once the natural gas is taken down to 200 mbar it is mixed with air before being injected into the gas engines.

Figure 5: Gas Ramp Unit (GRU)

If the NG pressure before the GRU is below 350 kPa as specified in Table 1 then an unintended de-loading of the gas engines on KV Bergen and MF Korsfjord will occur. On both KV Bergen and MF Korsfjord, the pressure before the GRU is determined by the pressure in the LNG tank. The analysis in this report will focus on understanding why the pressure in the LNG tank would cause the pressure before the GRU to fall below this minimum pressure. The next sub-section provides two hypotheses for why the LNG tank pressure would fall below this lower pressure limit.

2.4 Hypothesis

One hypothesis for the unintended fall in tank pressure is the PBU circuit is not able to supply enough vaporized NG to the top of the LNG tank to keep the LNG tank pressure above 350 kPa. The PBU is a sub-unit of the vaporizer, which is a large helically-wound heat exchanger. Heat is exchanged between the water glycol mixture entering from the top of the vaporizer and the LNG contained in the coils of the PBU and EVAP. It is possible that not enough LNG is evaporated in PBU to stop the fall in LNG tank pressure which occurs when LNG is drawn from the LNG tank by the NG engines and evaporated through the EVAP.

A second hypothesis is that the LNG in tank mixes with the NG at the top of the LNG tank and causes the NG to condensate. Vapor condensation in the LNG tank causes the tank pressure to fall. There are several different mechanisms which may cause the LNG in the tank to interact with the NG in the top of the tank. Based on the two reports detailing the documented de-loading events, it possible that disturbances within the LNG system introduced during the full engine trial or bunkering caused the tank pressure to fall. Another possibility is that external disturbances, such as the rocking motions of waves, may have caused greater interaction between the LNG and NG in the tank.

Both of these hypotheses will be explored throughout the report. The literature review will delve into existing literature and provide insight into these two hypotheses. Specifically, the literature review will explore the heat transfer between liquid and vapor surface layers in cryogenic storage tanks, pressurization studies, and the relationship between the fall in tank pressure and sloshing.

3. Literature Review

The literature review is broken into three distinct sections which will provide an understanding of relevant studies related to pressure in cryogenic tanks. The first sub-section explores the fundamental relationships controlling heat transferred from the liquid through the vapor liquid interface. The second sub-section examines pressurization experiments conducted in cryogenic tanks used to validate a set of equations governing the total amount of time required to pressurize the tank. The third sub-section explores the fall in tank pressure recorded during sloshing experiments using tanks with cryogenic material.

3.1 Vapor Liquid Interface

The first section of the literature review provides an overview of the research conducted on vapor and liquid interaction inside LNG tanks at the liquid interface. Numerous experiments on evaporation mechanisms in cryogenic fluids have been conducted by Ralph G. Scurlock at Southampton University in the United Kingdom. The focus of Scurlock's experiments was to quantify heat transfer occurring between the bulk cryogenic liquid and vapor inside cryogenic storage tanks through the top surface layer of the cryogenic liquids. Driving the experiments was the goal of gaining a better understanding of heat transfer mechanisms leading to the creation of boil-off gas in cryogenic storage tanks (Scurlock 2006). A discussion of the experiments' relevancy to NG engine de-loading from low tank pressure is provided at the end of this sub-section.

To explain how surface evaporation takes place, Scurlock examined how heat enters cryogenic storage containers and travels to the surface. Scurlock found that heat is absorbed into the cryogenic fluid by natural convection through the insulation of the storage container. On vertical surfaces in the storage tank, cryogenic fluid is superheated and forms a "boundary layer" of fluid which is approximately 1-5 mm thick. This boundary layer carries the superheated fluid to the surface where it is released through surface evaporation. The "boundary layer" carrying superheated fluid to the surface is illustrated in Figure 6 as a line drawn parallel to the side of the container. Scurlock noted that if the ratio of tank depth to the diameter is less than 0.5 then vertical thermals will form "at interval approximating the liquid depth" (2006). A vertical thermal is illustrated in Figure 6 as the downward pointing arrow perpendicular to the liquid surface.

Heat flow OUT
via surface evaporation

Superheated
liquid
(boundary
layer flow)

Heat flow IN
(absorbed by
liquid boundary
layer flow)
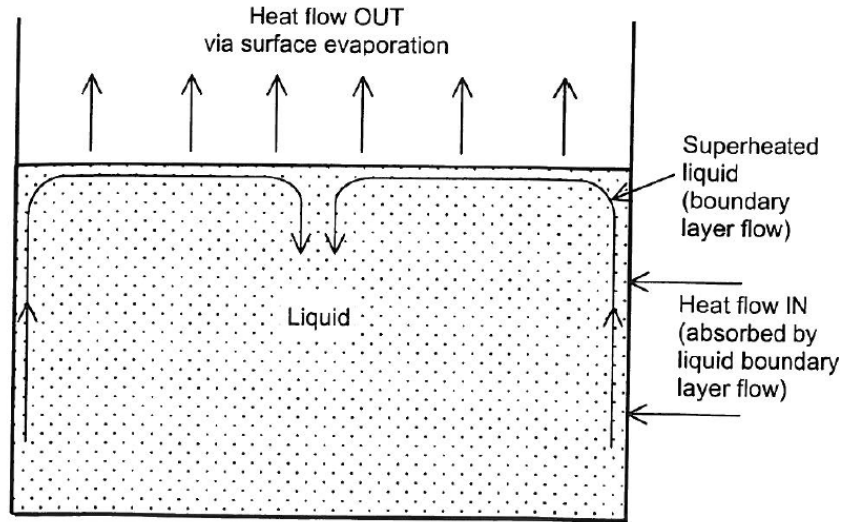
Liquid

Figure 6: Surface Evaporation Illustration (Scurlock 2006)

Scurlock devised an experiment to quantify the evaporation impedance presented by the liquid surface. The experimental rig used for these evaporation experiments is shown in Figure 7 with the following description:

> The boil-off vessel was an 80 mm inner diameter, double walled, vacuum insulated dewar surrounded by a second liquid bath of 120 mm inner diameter. The boil-off from the inner vessel could be varied via a uniform heat-flux electrical heater mounted in the vacuum space around the inner wall. The micro-thermometers consisted of 25 micron diameter copper/constantan thermocouple junctions mounted horizontally in differential or absolute configurations.

The thermocouples used in the boil-off container were spaced with 100 mm increments in order to measure the temperature across the entire span of the surface region. Scurlock examined the surface evaporation of the following fluids: Liquid Nitrogen (LIN), Liquid Oxygen (LOX), Liquid Argon (LA), Liquid Methane (LCH4) and LNG. Using the experimental rig shown in Figure 7, Scurlock found the evaporation mass flux versus bulk superheating shown in Figure 8.
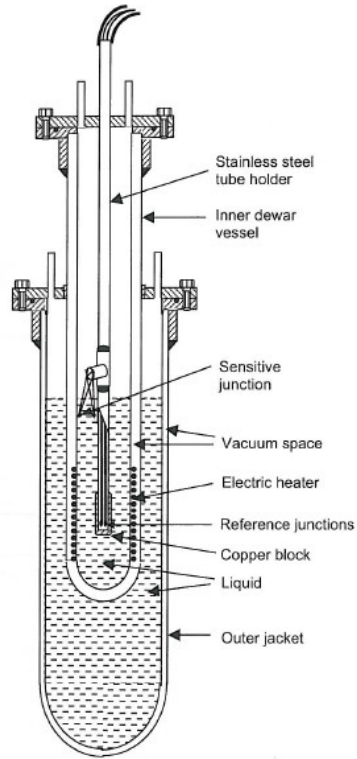
Figure 7: Experimental Rig for Cryogenic Evaporation Studies (Scurlock 2006)
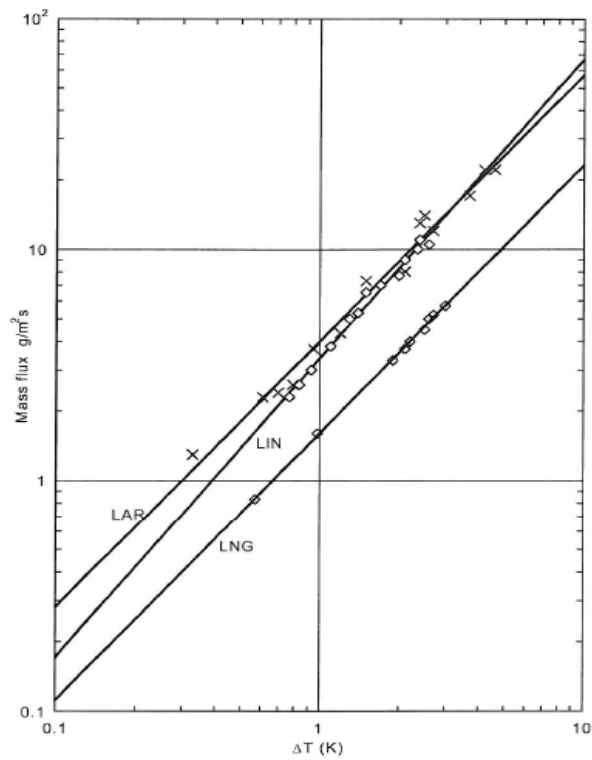
Figure 8: Results from the Cryogenic Evaporation Test, Evaporation Mass Flux versus Bulk Superheat (Scurlock 2006)

Scurlock also graphed the bulk temperature difference versus distance from the surface in Figure 9. This was produced by allowing the evaporating fluid surface to pass by a fixed microthermometer.
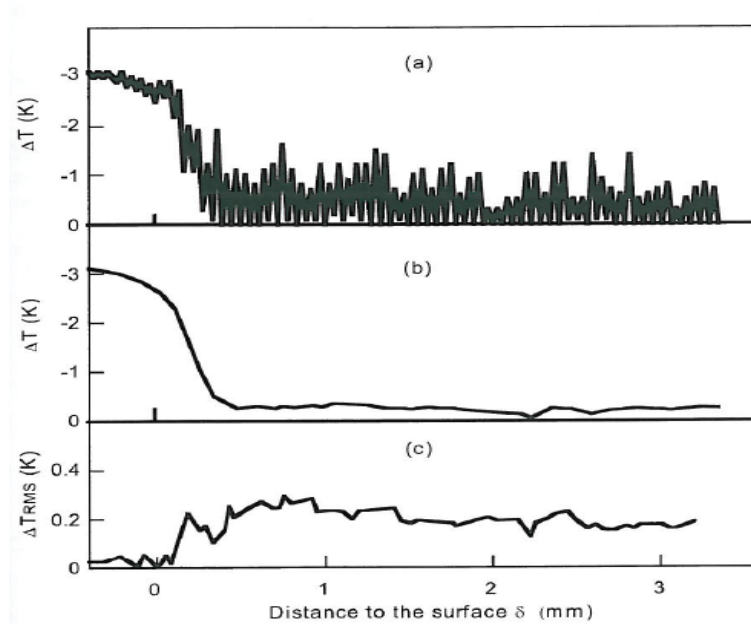
Figure 9: Bulk Superheat versus Distance to Surface, a) Local temperature variation, b) smoothed variation, c) RMS variation of fluctuations with depth (Scurlock 2006)

Using the mass flux produced by the evaporation of the cryogenic fluid and the bulk superheat versus distance from the vapor liquid interface, Scurlock came up with a number of relationships explaining the thermal impedance provided by the fluid surface. He claimed the thermal impedance created by the surface may be broken into three separate regions. Figure 10 illustrates the three regions impeding heat transfer in the surface layer of cryogenic fluids.
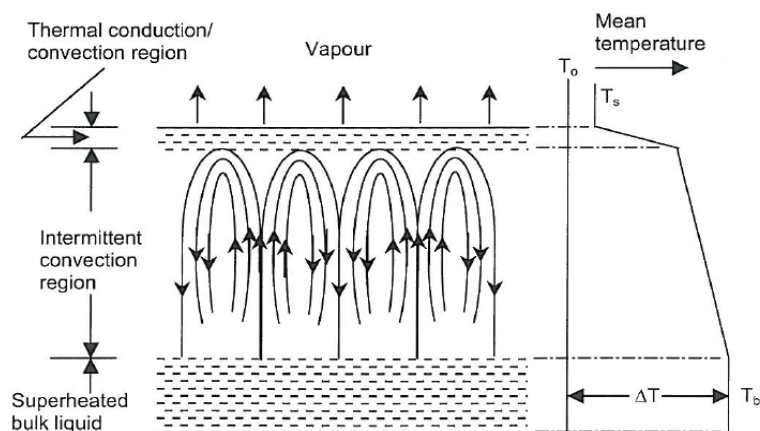
Figure 10: Heat Transfer Regions and Temperature Profile of Cryogenic Surfaces (Scurlock 2006)

Scurlock found heat transfer occurring in the top surface layer, shown as a black line below the upward pointing arrows in Figure 10, was controlled by molecular evaporation which was less than 1-2 microns thick. The mass flux and heat flux in this region are quantified in Equations (1) and (2).

$$\dot{m}_{evap}/A = 90\alpha(T_{surface} - T_{sat}) \tag{1}$$

$$W_{evap}/A = 90h_{lat}\alpha(T_{surface} - T_{sat}) \tag{2}$$

Beneath the top surface layer, Scurlock found "a thermal conduction region enhanced by some convection, about 400 microns thick, with an extraordinarily high temperature gradient" which he called "the thermal conduction / convection region" (2006). This region is illustrated as a set of dashed lines below the top surface layer in Figure 10. The heat transfer mechanism in this region is dominated by "a mixture of thermal conduction and highly damped intermittent convection" (Scurlock 2006). Equation (3) describes the heat transfer per unit area occurring in the thermal conduction / convection region.

$$W_{evap}/A = k_{eff,cond}(T_{cond} - T_{surf})/z_{cond} \tag{3}$$

Note T_{cond} stands for the temperature at the bottom of the conductive / convection region and $k_{eff,cond}$ is the effective thermal conduction coefficient for the entire region in Equation (3). Since the majority of the thermal impedance to the cryogenic fluid evaporation was found in the conductive / convection region, Scurlock published the experimental results from this region which are found in Table 2.

Table 2: Experimental Data on Effective Thermal Conductivity in Region 2 during Surface Evaporation (Scurlock 2006)

Fluid	Surface Mass Flux ($g/m^2 s$)	$T_{cond} - T_{surf}$ (K)	Temperature Gradient 10^3 K/m	$k_{eff,cond}$ (W/K)	k_{actual} (W/K)	k_{eff}/k_{actual}
LIN	13.9	3.2	7.5	370	133	2.8
LCH$_4$	3.0	2.5	5.0	305	189	1.6
LOX	9.8	2.4	6.7	305	152	2.0
LA	14.6	3.2	10.0	236	128	1.8
LNG	2.7	2.1	5.0	275	189	1.5

The lowest region in the sub-layer between the bulk cryogenic liquid in the tank and the vapor is the intermittent convection region which is illustrated as a set of swirling arrows in Figure 10. Scurlock noted that this region is shorter than the conductive / convection region and only approximately 0.2 to 5mm thick with a temperature gradient of approximately 50 K/m. Scurlock states, "The major feature is the temperature spikes which have a time constant of about 0.3 s and a mean amplitude of approximately +0.5K and -0.5K respectively within the temperature interval T_{bulk} to $T_{surface}$" (2006). These temperature fluctuations come from pockets of cryogenic fluid

that transfer heat through convection (Beduz and Scurlock 1994). Scurlock found that the heat transfer occurring in the intermittent convection region may be quantified in Equation (4).

$$W_{evap}/A = k_{eff,conv}(T_{bulk} - T_{cond})/z_{conv} \tag{4}$$

Notice that Equation (4) contains an effective thermal conductive coefficient, $k_{eff,conv}$, which incorporates the conductive and convective heat transfer occurring in the intermittent convection region. Also, z_{conv} represents the effective height of this region.

The overall thermal impedance provided by the entire surface layer (i.e. all the regions combined) is given by the temperature balance in Equation (5) and expended in Equation (6).

$$(T_{bulk} - T_{sat}) = (T_{surf} - T_{sat}) + (T_{cond} - T_{surf}) + (T_{bulk} - T_{cond}) \tag{5}$$

$$(T_{bulk} - T_{sat}) = (\dot{m}_{evap}/A)\left((1/90\alpha) + (z_{cond}/k_{eff,cond}) + (z_{conv}/k_{eff,conv})\right) \tag{6}$$

In addition to studying the evaporation heat transfer of different cryogenic fluids, Scurlock made a number of important observations about the evaporation rate occurring in cryogenic storage containers when the fluid in the container was disturbed. Scurlock agitated the contents of the tank by tapping the cryogenic tank at certain intervals. He observed that "agitation of the bulk liquid can lead to liquid motion in the surface sub-layer circumventing or bypassing the mixed conduction/convection region". In various experiments on agitated cryogenic storage containers, Scurlock noted that the evaporation rate for LIN increased by 23 fold compared to an undisturbed container. Similarly, the evaporation rate for LCH4 increased by 19 fold compared to an undisturbed container. Scurlock illustrated this increase in evaporation due to agitation of the storage container in Figure 11. The spike in boil-off rate in Figure 11 corresponds to the moment in time when the contents of the tank was disturbed.
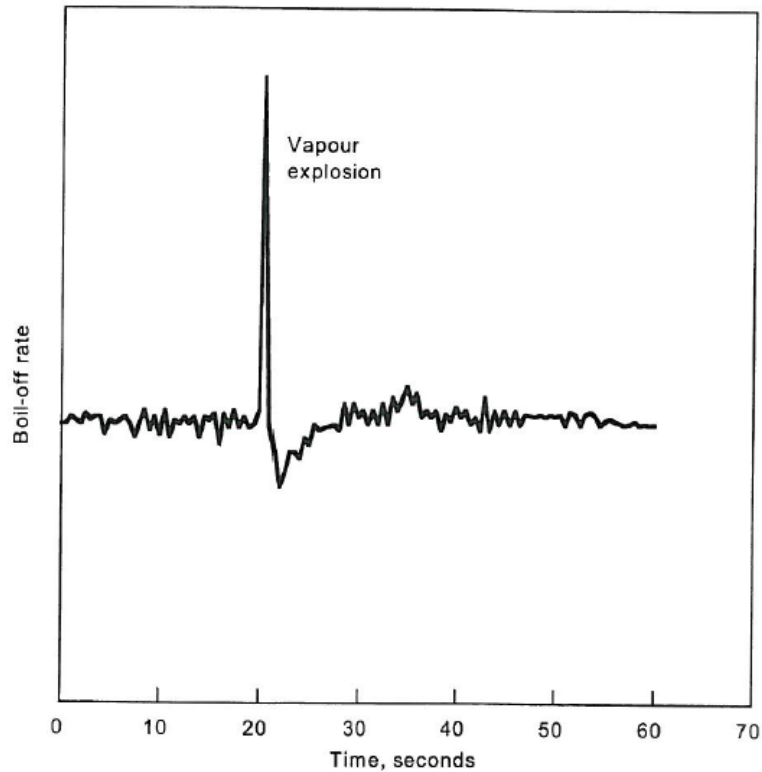
Figure 11: Increased Evaporation from Surface Agitation (Scurlock 2006)

Scurlock found during agitation experiments that the surface layer controlling the evaporation rate at the liquid surface would be repaired "in a few seconds or minutes". However, he also noted that it was possible to maintain this agitation "over a longer period of time, several seconds, or minutes, or hours in length, so as to prevent the self-repairing mechanism re-establishing the equilibrium sub-layer structure". Once the agitation abated, however, the rate of evaporation occurring inside the tank returned to the rate given by Equation (6).

Both the evaporation experiments and agitation experiments conducted by Scurlock provide insight into the heat transfer mechanism occurring at the vapor liquid interface in cryogenic containers. One of the main points in the initial report written on the topic of NG engine de-loading was that the temperature of the liquid surface layer in cryogenic tanks is at its saturation temperature which depends on the vapor pressure in the tank. An understanding of the heat transfer occurring at the vapor liquid interface is important in recognizing the relationship between the temperature of the liquid surface and the pressure in the tank. It is reasonable to assume that if the liquid surface layer was agitated in a closed cryogenic container (e.g. the LNG tank on a vessel) then the vapor pressure would change correspondingly.

The evaporation experiments conducted by Scurlock differ from the current study because the initial conditions in each study are different. In Scurlock's experiments, the bulk cryogenic liquid is assumed to be superheated because of heat leakage into the container. In order to achieve thermodynamic equilibrium, evaporation occurs at the surface layer of the cryogenic liquid to

release excess heat. In the LNG tank on KV Bergen and MF Korsfjord, the bulk LNG in the tank is sub-cooled and the vapor at the top of the tank may be superheated. These initial conditions are illustrated in Figure 12. To reach thermodynamic equilibrium, the vapor at the top of the tank will release heat to the liquid region in the form of condensation. Condensation in a closed tank will cause the vapor pressure to fall. Even though the type of latent heat exchange differs, the heat transfer fundamentals studied by Scurlock provide insight in how the surface layer controls heat transfer between the vapor and liquid in the tank.
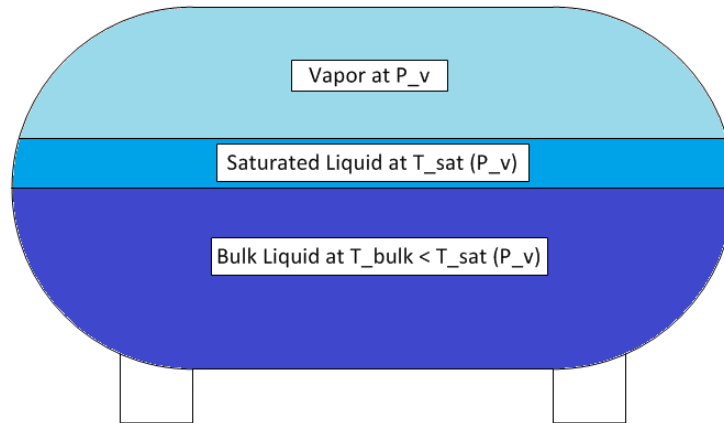
Figure 12: LNG tank conditions on vessels with NG engines

Another important point made in Scurlock's agitation experiments is that the rate of evaporation or condensation will increase when surface layer in a cryogenic tank is disturbed. This phenomenon explains the second hypothesis which assumes there is a relationship between disturbances experienced inside the LNG tank and the fall in tank pressure. The difference between these two observations, however, is that Scurlock recognized an increase in the rate of evaporation rather than an increase in the rate of condensation. Again, these differences may be attributed to different initial tank conditions.

With the relationship between the liquid vapor interface and the tank pressure established, an understanding of the time necessary to pressurize a cryogenic tank is required. The next sub-section explores the relationships governing the pressurization of cryogenic tanks.

3.2 Cryogenic Tank Pressurization

In addition to understanding how the vapor and liquid interact in a cryogenic tank, an understanding of factors affecting pressurization time is also necessary in determining the factors behind NG engine de-loading. As stated earlier, the top of the tank is pressurized (i.e. the pressure in the top of the tank increases) by vaporizing liquid at the bottom of the tank and introducing it as vaporized NG at the top of the tank. One organization which has conducted a large amount of research on the pressurization of cryogenic tanks during various operations is the National Aeronautics and Space Administration (NASA). Though related to the pressurization of

rocket fuel tanks, many of the same engineering aspects apply to the pressurization of LNG tanks on vessels using NG engines.

One particular study, produced by NASA, sought to develop an appropriate model to estimate the mass of vapor required to maintain a certain tank pressure. Roudebush (1965) endeavored to create "a simplified one-dimensional model" to simulate the pressurization of a rocket with cryogenic liquid outflow. The equations developed in this model were numerically integrated to calculate the total mass over a certain period of time required to maintain a constant tank pressure. Roudebush's results were compared to experiments conducted by the Lockheed-Georgia Company to assess the accuracy of the model. Figure 13 illustrates the model developed by Roudebush. In Figure 13, gas entering the top of the tank maintains a certain vapor pressure while liquid is leaving from the bottom of the tank.
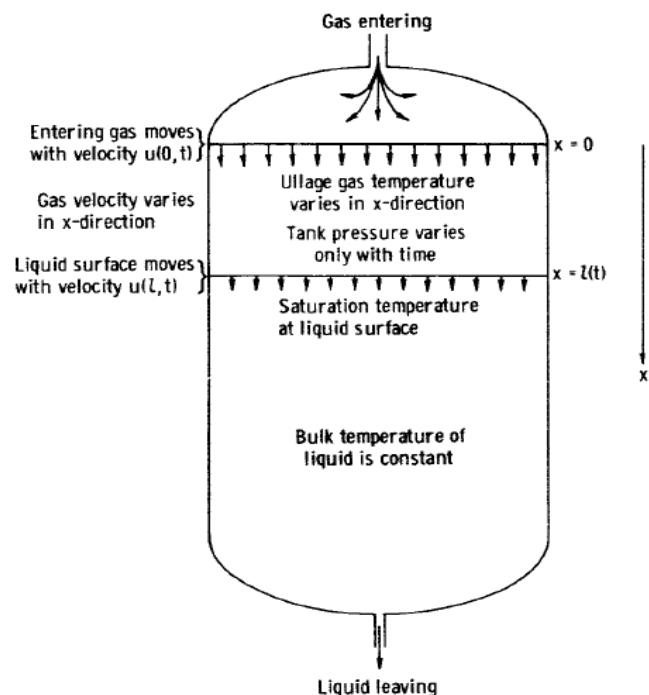
Figure 13: Cryogenic Tank Pressurization Models

Roudebush assumed the following to simplify the model:

- The vapor in the tank is able to exchange heat with the walls and liquid inside the storage vessel.
- The effect of tank sloshing is negligible.
- The mass flow rate of liquid leaving the tank is constant.
- A number of fluid properties such as: gas density, gas velocity, conductive heat transfer coefficient between the gas and wall, and gas specific heats are all assumed to be constant.

- The tank is assumed to be cylindrical.
- The speed of the vapor entering the tank does not vary radially. The vapor gas only varies in the axial tank direction.
- At a singular point in time, the tank pressure and temperature is assumed to be uniform.
- The tank wall temperature is also assumed to be uniform at a given point in time.
- Axial heat transfer is considered negligible.
- Phase change (evaporation or condensation) does not occur.
- The gas does not transfer heat to the liquid.

Using these assumptions, Roudebush developed a set of governing equations to find the mass over a certain outflow time required to maintain tank pressure. Roudebush combined the following: the First Law of Thermodynamics, the Continuity Equation, and the Equation of State for a Real Gas. The full sequence of developing these governing equations may be found in Roudebush's report. Equation (7) is developed from a combination of the First Law of Thermodynamics and the Real Gas Law. The first terms accounts for the conductive heat transfer between the tank wall and the gas in the radial direction. The second term accounts for the change in temperature from the introduction of new gas from the top of the tank. The third term accounts for the change in gas temperature due to the changing pressure in the tank over time due to the loss of liquid from the bottom of the tank. The fourth term accounts for the heat transfer to the system from internal hardware.

$$\frac{\partial T_{gas}}{\partial t} = \frac{2h_{cond}ZRT_{gas}}{r_{tank}MP_{gas}C_p}\left(T_w - T_{gas}\right) - u_{gas}\frac{\partial T_{gas}}{\partial x} + \frac{RT_{gas}Z_1\partial P_{gas}}{JMP_{gas}C_p\partial t} + \frac{RT_{gas}Zq_{hard}C_{hard}}{\pi r_{tank}^2 MP_{gas}C_p} \tag{7}$$

Similarly, Roudebush used a combination of the Continuity Equation and Real Gas Law to come up with Equation (8).

$$\frac{\partial u_{gas}}{\partial x} = \frac{Z_1}{ZT}\frac{dT_{gas}}{dt} - \frac{Z_2}{ZP_{gas}}\frac{dP_{gas}}{dt} = \frac{Z_1}{ZT_{gas}}\left(\frac{\partial T_{gas}}{\partial t} + u_{gas}\frac{\partial T_{gas}}{\partial x}\right) - \frac{Z_2}{ZP_{gas}}\frac{\partial P_{gas}}{\partial t} \tag{8}$$

To validate Equations (7) and (8), Roudebush compared a numerical analysis of the derived equations with pressurization tests conducted at the Lockheed-Georgia Company. A description of the tank used in pressurization experiments during liquid outflow is provided:

> The tank used was 27 inches in diameter and 89 inches in overall length with dished-head ends. It was constructed of 5/16-inch-thick 304 stainless steel plate. Heat leak was reduced to 40 Btu per hour per square foot by a vacuum jacket surrounding the entire tank. The inlet gas diffuser was designed to direct flow vertically downward with a flat velocity profile across the tank. The inner surface of the tank dome was insulated with a 1/2 –inch layer of cork. No slosh baffles, ribs, or other features (except for instrumentation) were present to disturb the flow. The instrumentation…provided a significant heat sink in some of the runs (Roudebush 1965).

This experiment was run several times while varying the parameters to ascertain if Equations (7) and (8) accurately described the amount of propellant required to hold the top tank pressure constant. Table 3 and Table 4 list what parameters were used for the different tank pressurization experiments.

Table 3: Experimental Values for Lockheed-Georgia Company Tank Pressurization Experiments (Roudebush 1965)

Experiment	Tank Pressure [lb/in^2]	Outflow Rate [ft^3/s]	Time of outflow [s]	Initial Ullage Depth [ft]	Heat to Internal Hardware, $q_I C$, [Btu/ft*s]
1	160	0.0669	350	0.525	0.334
2	161	0.2375	93	0.467	1.462
3	57	0.0780	284	0.483	0.296
4	58	0.2238	101	0.375	1.213
5	164	0.2340	95	0.583	0.628
6	40	0.2550	88	0.483	1.577
7	159	0.0634	355	0.658	0.293
8	159	0.2598	90	0.675	1.427
9	159	0.2365	100	0.458	0.323
10	40	0.0703	309	0.442	0.240

Table 4: Experimental Values for Lockheed-Georgia Company Tank Pressurization Experiments Continued (Roudebush 1965)

Experiment	Gas Temperature at Interface [R]	Wall Temperature at Interface [R]	Initial Inlet Gas Temperature [R]	Initial Inlet Wall Temperature [R]	Pressurizing Gas	Heat Transfer Coefficient [Btu/ (ft^2)*hr*R]
1	57	46	488	206	H_2	13.75
2	57	46	484	210	H_2	12.25
3	47	46	373	170	H_2	7.09
4	47	46	398	157	H_2	6.67
5	57	46	395	194	H_2	11.34
6	44	46	385	176	H_2	5.13
7	57-46	46	521	207	He	12.31
8	57-48	46	524	161	He	11.15
9	57-50	46	324	153	He	10.45
10	44-35	46	347	148	He	5.25

Using the initial values listed in Table 3 and Table 4, the mass required to maintain a constant tank pressure from the different experiments is given in Table 5. The deviation between the calculated results and the experimental results are given in Table 6.

Table 5: Calculated and Experimental Tank Pressurization Results (Roudebush 1965)

Experiment	Mass of Pressurant [lb]				
	Experimental	Previously Calculated	For Zero Heat Flow to Interior Hardware	From Ideal Gas Law	From Computed Heat transfer coefficient
1	3.98	3.95	3.70	3.79	4.07
2	2.72	2.60	2.36	2.55	2.90
3	1.76	1.69	1.50	1.61	1.79
4	1.24	1.27	1.05	2.54	1.43
5	3.76	3.51	3.31	3.45	3.81
6	0.83	0.93	0.69	0.91	1.06
7	8.14	7.61	7.18	7.61	7.81
8	5.59	5.57	5.03	5.57	6.17
9	9.24	8.48	8.19	8.48	9.04
10	2.70	2.56	2.25	2.56	2.76

Table 6: Deviation between Calculated and Experimental Results (Roudebush 1965)

Experiment	Experimental Mass [lb], m_e	Calculated Mass [lb], m_c	Deviation, $\frac{m_c - m_e}{m_e} * 100$
1	3.98	3.95	-0.75
2	2.72	2.60	-4.41
3	1.76	1.68	-4.54
4	1.24	1.27	2.42
5	3.76	3.51	-6.65
6	0.83	0.93	12.04
7	8.14	7.61	-6.51
8	5.59	5.57	-0.36
9	9.24	8.48	-8.23
10	2.70	2.56	-5.18

Roudebush claimed the deviations between the calculated and measured results listed in Table 6 were acceptable for use of modeling the amount of propellant required to maintain a certain pressure during liquid propellant outflow. Using some of the assumptions made by Roudebush and similar modeling techniques, a set of equations may be used to calculate the amount of time required to pressurize an LNG tank on a vessel.

The models created by Roudebush will differ from the models created in this report. The biggest difference between the two modeling goals is that Roudebush desired to maintain a constant tank pressure during liquid outflow while this study requires a model which examines a system where the tank pressure is increased from a lower value. Additionally, the goal of the NASA experiment was to find the total amount of propellant required to maintain a constant tank pressure during the pressurization process. The study conducted in this report is interested in the heat and mass required over time to increase the tank pressure. Roudebush's study is useful in that some of the

same assumptions and governing equations may be modified to derive a similar set of equations governing the pressure build up in the LNG tank. In addition to studying the factors affecting pressurization time, an understanding of the fall in tank pressure from tank sloshing is desired. The next sub-section will explore different studies conducted on the correlation between cryogenic tank sloshing and fall in tank pressure.

3.3 Cryogenic Mixing and Excitation

A number of studies relating the pressure drop in cryogenic tanks to external excitation have been performed. An experiment conducted by Ludwig, Dreyer, and Hopfinger (2013) measured "the pressure change in a partially filled liquid nitrogen tank, subjected to periodic lateral forces". In the experiment, liquid nitrogen was subjected to different sloshing conditions which were able to be externally controlled. The liquid and vapor temperature profiles were observed and recorded during all phases of the experiment. Equation (9) was developed to calculate the pressure in the cryogenic tank over time given different sloshing conditions.

$$P = P_{int}\frac{\bar{T}_v(t)}{\bar{T}_{v,int}} - \frac{R_{sl}\bar{T}_{v,int}\rho_{v,sl}}{V_v}\left[\frac{2JaS\sqrt{D_e}}{\sqrt{\pi}}\left(\sqrt{t'_{sl}} - \sqrt{\Delta t_{sl}}\right)\right] - u_e S_e t_s \tag{9}$$

Equation (9) take into account the both the thermal characteristics of the cryogenic fluid, the vapor temperature over time, geometry of the cryogenic vessel, and the character of the excitation administered.

Figure 14 provides an outline of the experimental rig used in the sloshing experiments. The rig contained one pressure sensor and 16 temperature sensors. At the beginning of the experiment, the tank was pressurized to various pressures using vaporized N2 at 294 K and added to the tank using a diffusor.
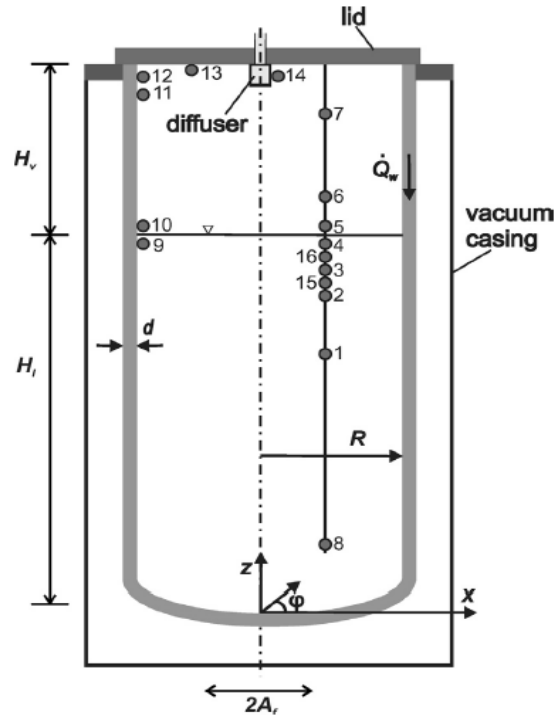
Figure 14: Experimental Rig in Excitation Experiments (Ludwig, Dreyer et al. 2013)

The experiments were conducted in four distinct phases which is illustrated in Figure 15 and described below:

1. The pressure in the cryogenic tank was increased to 300 kPa using the gas diffusor (shown as the time period $(t_{p,o}, t_{p,f})$ in Figure 15).
2. The pressure in the tank was allowed to relax and settle to about 240 kPa (shown as the time period $(t_{p,f}, t_{s,o})$ in Figure 15).
3. Once the pressure in the tank settled, sloshing commenced (shown as the time period $(t_{s,o}, t_{s,f})$ in Figure 15). This continued in the experiment until a minimum pressure was achieved.
4. After a sustained pressure was achieved, the sloshing ceased and the tank pressure was monitored while the waves formed by sloshing abated (shown as the time period $(t_{s,f}, t_{s,f+t_d})$ in Figure 15).
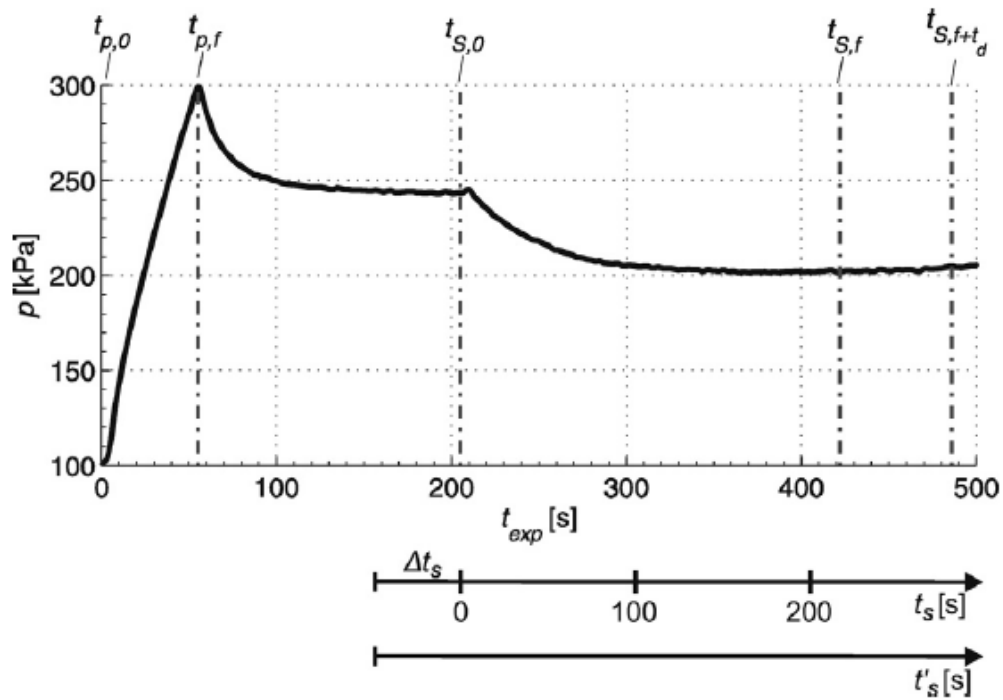
Figure 15: Recorded Pressure during Excitation Experiment (Ludwig, Dreyer et al. 2013)

During pressurization, a thermal gradient forms in the liquid and vapor layers in the tank. The development of thermal stratification during the different phases of the experiment is illustrated in Figure 16. The experiment used five different sloshing conditions including: "three stable asymmetric sloshing modes, one chaotic sloshing mode and one swirl mode" (Ludwig et al., 2013).
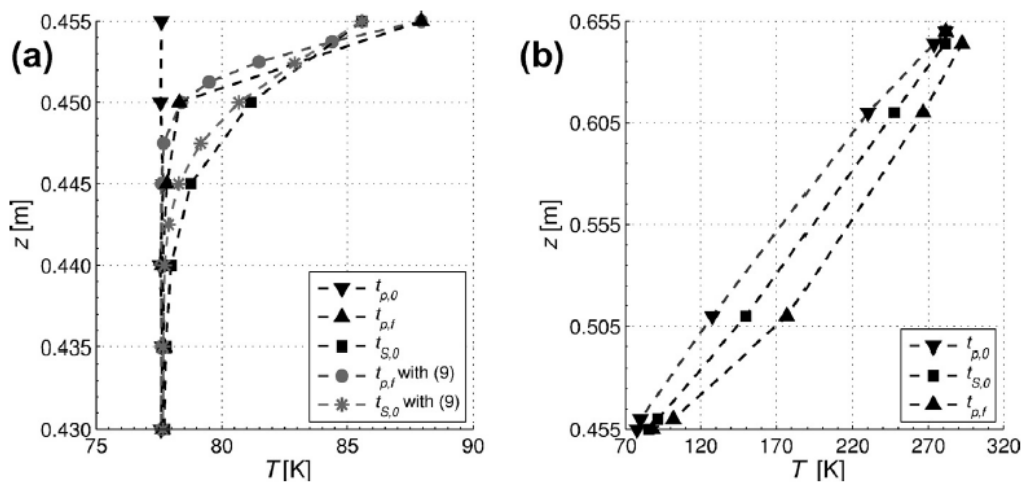
Figure 16: Thermal Gradient during Pressurization and Sloshing (Ludwig, Dreyer et al. 2013)

Ludwig et al. noted the fall in tank pressure was caused by the condensation of vapor at the liquid surface. Figure 17 shows how the calculated pressure drop estimated using Equation (9) compares with the measured pressure drop for an experiment with planar waves, E2, and chaotic waves, E4. Experimental observations show that a relatively asymptotic pressure is achieved.
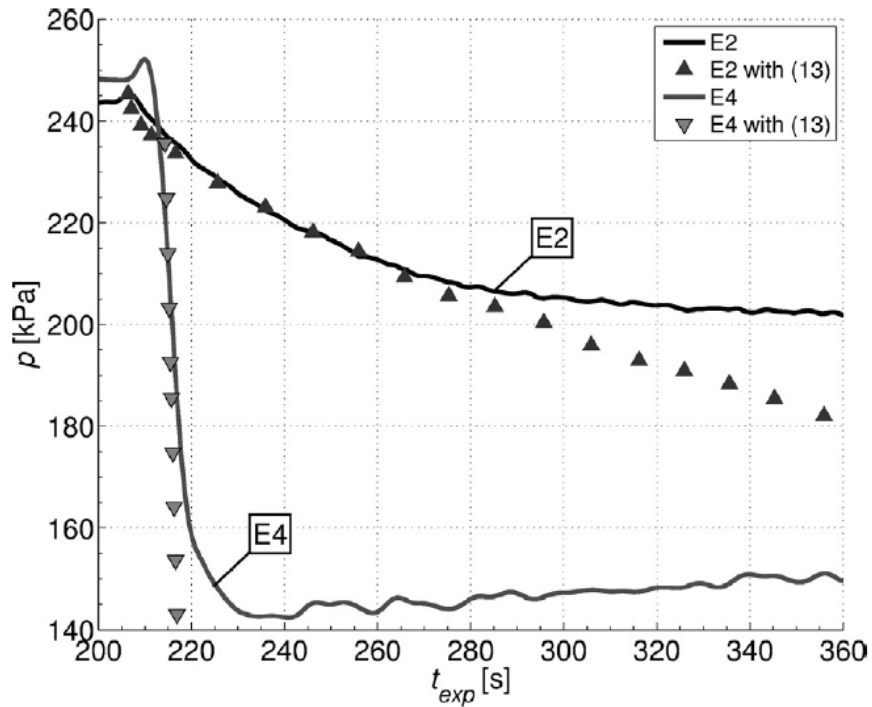
Figure 17: Calculated versus Experimental Pressure Drop in Sloshing Experiment (Ludwig, Dreyer et al. 2013)

Ludwig et al. concluded that the pressure drop the in the cryogenic tank occurs because the breaking motion of the wave disrupts the formation of the liquid boundary layer at the surface. This experiment quantifies the observations made by Scurlock who noted that the rate of evaporation increased during evaporation experiments when the cryogenic container was disturbed by tapping.

A similar set of experiments were performed by NASA to understand the effects of sloshing on tank pressure in rockets. Specifically, a sets of tests conducted by Moran, McNelis, Kudlac, Haberbusch, and Satornino (1994) studied the effects of varying "slosh frequency and amplitude, pressurant type, ramp pressure and ullage volume" on the cryogenic tank pressure. It was postulated in the study that during shuttle maneuvering sub-cooled hydrogen may be circulated "near the liquid-vapor interface resulting in increased condensation and corresponding pressure collapse". Experiments were carried out in the experimental rig shown in Figure 18.
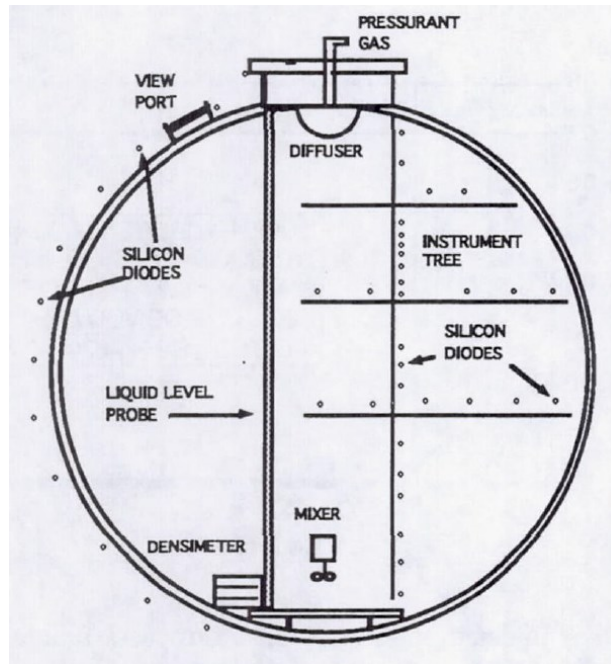
Figure 18: K-Site Test Facility Moran, McNelis et al. (1994)

These tests were performed in the following sequence:

1. The tank was filled to a certain level with liquid hydrogen and vented to 1 atm.
2. After venting, the tank was pressurized using conditioned gas.
3. After pressurization, shaking commenced using apertures capable of rocking the test rig at certain frequencies. The frequency was increased until certain wave amplitudes were met.
4. The shaking continued for two minutes at the given amplitude (set by the shaking frequency).

An example of one of the hydrogen slosh tests is provided in Figure 19.
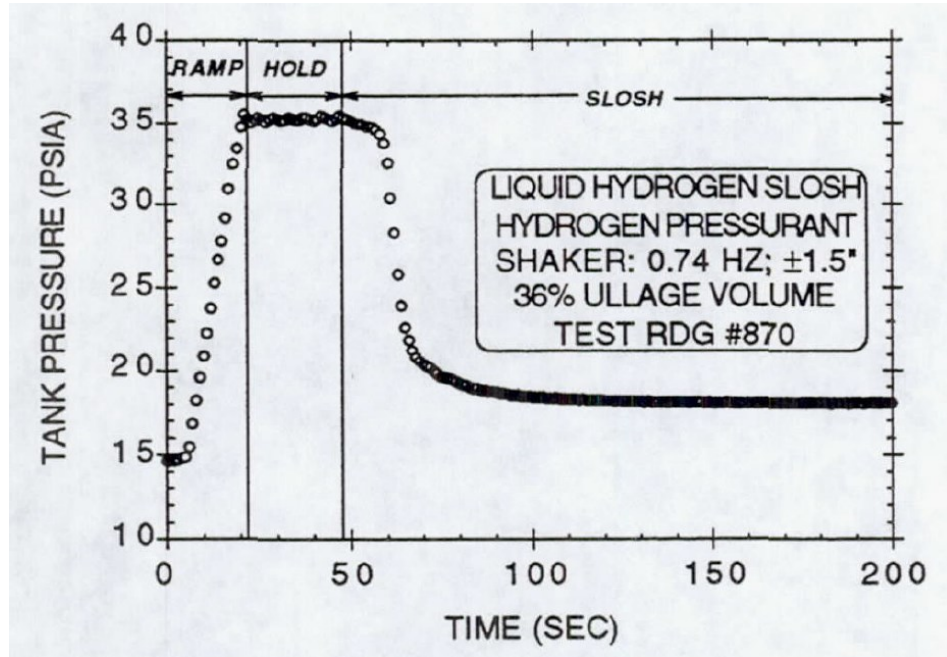
Figure 19: Tank Pressure during Liquid Hydrogen Slosh Test Moran, McNelis et al. (1994)

The amount of pressure change was measured as a percentage of the saturation pressure before the tank was pressurized. This expression, called "Percent Collapse", is given by Equation (10).

$$\%Collapse = \frac{P_{ramp} - P_{min}}{P_{ramp} - P_{int}} * 100\%$$

(10)

All recorded results from the slosh test are provided in Appendix A. The largest recorded percent collapse recorded during tests was 84 %. It was also discovered in the experiments that the fall in tank pressure was related to the amplitude of the disturbances caused inside the cryogenic tank. This was caused because sub-cooled liquid was moved to the liquid surface which increased condensation. Additionally, the experiment conducted by Moran et al. found that sloshing near the natural frequency had a much greater impact on the percentage collapse of pressure in the tank than smaller amplitude disturbances further from the natural frequency.

After performing a number of tests using vaporized hydrogen over liquid hydrogen in the cryogenic vessel, the experiment was modified to have vaporized helium over liquid hydrogen. During the experiment it was noted that the pressure in the tank increased (mainly due to hydrogen evaporation from heat leakage into the container). It was recommended in the experiment that additional research be conducted on using vapor of a different composition than the liquid during pressurization to mitigate the fall in tank pressure.

Another modification made to the test was varying the volume of the vapor region in the tank. It was found that there was a correlation between the amount of vapor in the tank and the fall in tank pressure when low amplitude waves were administered. This effective is illustrated in Figure

20. Moran et al. suggested the impact is greater in vessels with a smaller vapor region because there is less mass in the vapor region to maintain the tank pressure.
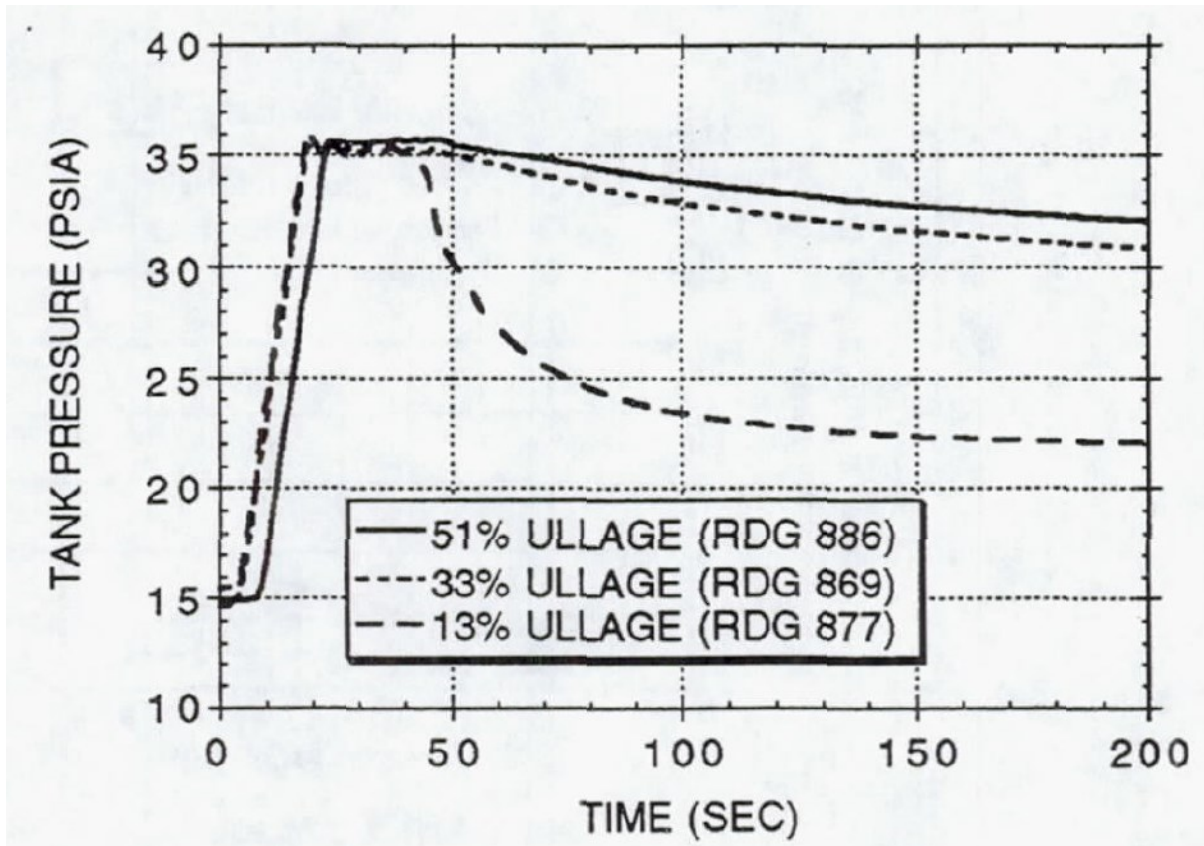
Figure 20: Vapor Volume's Impact on Sloshing Experiments Moran, McNelis et al. (1994)

In the concluding remarks of the report, Moran et al. suggested that the findings of the experiments can be "used to map the slosh stability regions for a spherical tank". These stability regions would presumably be used in future designs of rockets to prevent conditions where waves produced within the cryogenic tank would cause the tank pressure to fall below acceptable limits.

The experiments conducted by Ludwig et al. and Moran et al. are directly related to the second hypothesis which postulates that the fall in tank pressure was related to sloshing inside the LNG tank cause by either internal or external sources. It is possible the second recorded NG engine de-loading was caused by tank sloshing which was triggered by the sea state mentioned in the discussion with the Chief Engineer. Additionally, the observation that sub-cooled liquid moving to the liquid surface causes increased condensation may be relevant during the bunkering. It is possible that, after LNG is bunkered from the bottom of the tank, the liquid contents in the tank shift causing the sub-cooled LNG to travel to the surface layer. This effect causes an increased rate of condensation and a more dramatic fall in tank pressure. The fact that the fall in tank pressure is related to the percent vapor volume is also relevant. After bunkering, the vapor volume (and vapor mass) is often very small compared to the percent liquid volume. This

suggests that sloshing in the tank would have a greater impact on the top tank pressure in the LNG tank directly after bunkering since there is less vapor mass available for condensation. This theory supports the observation made in the description of the de-loading event which stated that the NG engine de-loading event occurred soon after bunkering.

The experiment conducted in this report will deviate from the experiment conducted by Ludwig et al. and Moran et al. in that it would be difficult to directly measure the sloshing experienced inside the LNG tank. However, it may be possible in future works to relate sea state to the sloshing occurring inside a LNG tank and fall in LNG tank pressure. This relationship would allow operators to determine if a certain sea state has the potential to cause the tank pressure to fall below an acceptable limit triggering NG engine de-loading. These additional experiments will be discussed in the chapter dedicated to further works.

The different studies related to the liquid vapor interface, pressurization calculations, and the relationship between the fall in tank pressure and sloshing have provided a better understanding of the condition inside the LNG tank on KV Bergen and MF Korsfjord. The sub-section on the liquid vapor interface has illustrated that the liquid surface layer is related to the top tank pressure and vice versa. A review of cryogenic tank pressurization studies has provided a set of fundamental equations and assumptions to derive a set of equations which governs the time required to pressurize the LNG tanks on MF Korsfjord and KV Bergen. Finally, the studies on sloshing in cryogenic tank have proven that there is a relationship between the disruption of the surface layer and the fall in tank pressure. The next section will discuss the measurement campaign used to test the two hypotheses behind the fall in tank pressure which caused the de-loading events.

4. Measurement Campaign

This chapter contains a description of the measurement campaign conducted onboard MF Korsfjord and KV Bergen. Included in this chapter is a description of the equipment and techniques used. Also included in this chapter is a discussion on instrumentation error and parameters which could not be measured directly. The purpose of this measurement campaign is to gain a better understanding of the interaction between the liquid heel, sub-cooled bunkered LNG, and vapor during and after the bunkering process as well as the heat and mass added by the PBU during pressurization. The information gained from this measurement campaign will be used to test the two hypotheses for the reasons behind the NG engine de-loadings.

4.1 Parameters Analyzed

In order to better understand what parameters were necessary to record during the measurement campaign, a process flow diagram was created which took into account all mass and energy entering and leaving the LNG tank on both MF Korsfjord and KV Bergen. Figure 21 illustrates the top part of the process flow diagram. Each variable necessary to perform a heat and mass balance in the Vaporizer and LNG tank were taken into consideration and matched with the installed or portable equipment which would provide this information. Alternative methods or assumptions were made for parameters which could not be measured directly.
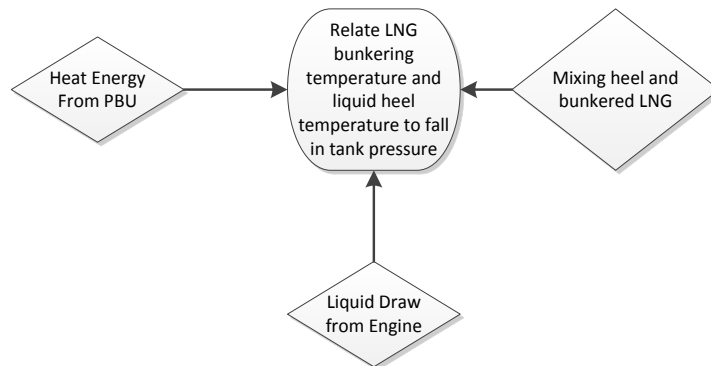
Figure 21: Top Section of the Process Flow Diagram for the Measurement Campaign

A full illustration and description of the process flow diagram used to map the measurement campaign may be found in Appendix B. Table 7 contains a list of all the parameters measured during the measurement campaign. One of the biggest challenges faced during the design of the measurement campaign was the inability to perform intrusive tests on KV Bergen or MF Korsfjord. Any equipment used could not permanently modify the LNG system. Due to this requirement, a number of indirect techniques were used to determine the changing conditions in the LNG tank during the measurement campaign.

Parameter	Symbol
Mass flow LNG to NG engines	$\dot{m}_{VAP}$
Mass flow through PBU	$\dot{m}_{PBU}$
Mass flow water / glycol flow	$\dot{m}_{GLY}$
Temperature of NG vapor exiting Evaporator to NG engines	$T_{EVAP,out}$
Temperature of LNG entering Evaporator to NG engines	$T_{EVAP,in}$
Temperature of NG vapor exiting PBU	$T_{PBU,out}$
Temperature of LNG entering PBU	$T_{PBU,in}$
Temperature of water / glycol entering Vaporizer	$T_{GLY,in}$
Temperature of water / glycol exiting Vaporizer	$T_{GLY,out}$
Temperature of Bunker LNG	T_{bunker}
Temperature of heel in tank	T_{heel}
Temperature of vapor in LNG tank	T_v
Volume heel	V_{heel}
Volume bunkered LNG	V_{bunker}
Top tank pressure	P_v
Composition of bunkered LNG	[-]

4.2 Description of Measurement Campaign

In order to better understand the changing pressure in the LNG tank during and after bunkering, a measurement campaign was designed to record different parameters in the LNG system on MF Korsfjord. Table 8 lists the portable equipment used during the measurement campaign and Table 9 lists the installed equipment used in the measurement campaign. Figure 22 illustrates the placement of the different sensors in the measurement campaign and Figure 23 shows the location of the installed measuring equipment onboard.

Table 8: Portable Equipment Used on MF Korsfjord

Parameter	Equipment
PBU Mass Flow	UF-801 P Flowmeter; SE1515 Flowmeter Probe
PBU Outlet Temperature	4 T-Type Thermocouples
Water Glycol Inlet Temperature	4 T-type Thermocouples
Water Glycol Outlet Temperature	4 T-Type Thermocouples
Water Glycol Volume Flow	UF-801 P Flowmeter; SE1515 Flowmeter Probe
Top Filling Bunkering Temperature	4 T-type Thermocouples
Instrument Cleanse Temperature	2 T-type Thermocouples

Table 9: Installed Measuring Equipment on KV Bergen and MF Korsfjord

Value Measured	Sensor Name	Equipment
Filling Gas Temperature	TE304	Pentronic PT100
Trycock Temperature	TE505	Pentronic PT100
Top Tank Gas Pressure	PI502	WIKA Pressure Indicator
LNG Tank Volume Level	LIT503	Rosemount Differential Pressure Trans.
Water Glycol Exit Temperature	TE507	Pentronic PT100
Vaporizer Gas Exit Temperature	TE509	Pentronic PT100
Vaporizer Gas Exit Pressure	PIT520	WIKA Pressure Indicator
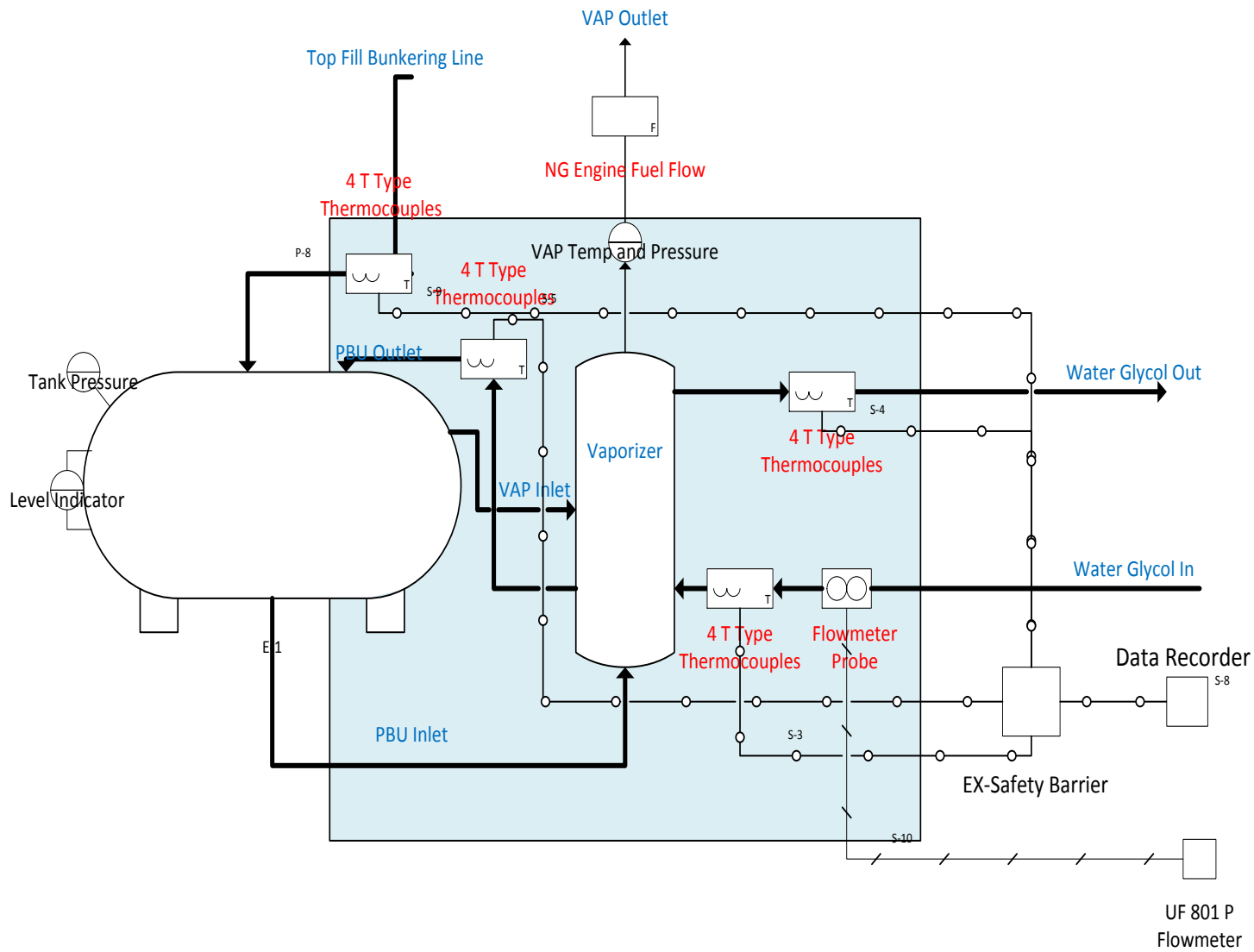
Figure 22: Portable Sensors on MF Korsfjord
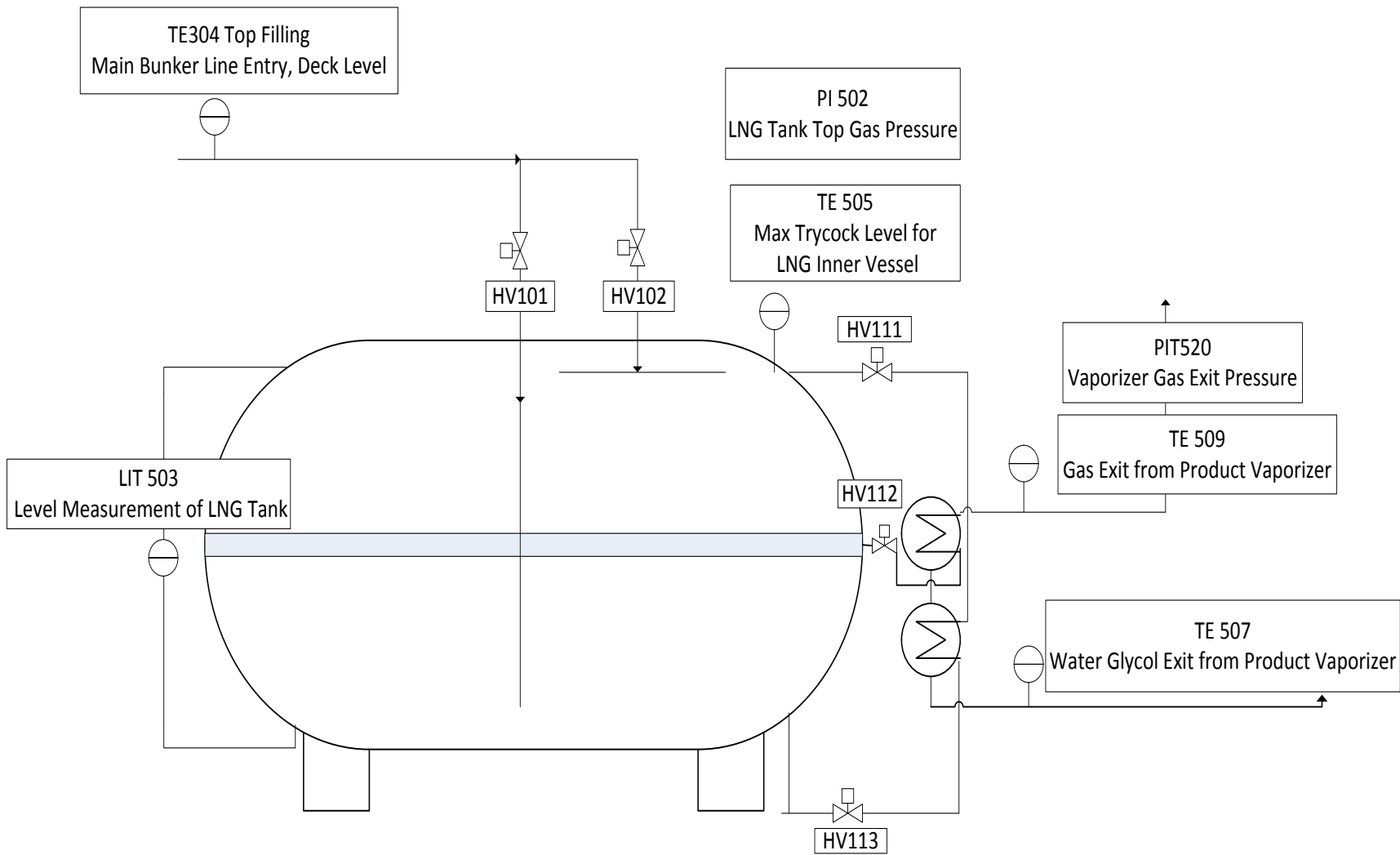
Figure 23: Installed sensors on MF Korsfjord

TE304 Top Filling
Main Bunker Line Entry, Deck Level

PI 502
LNG Tank Top Gas Pressure

TE 505
Max Trycock Level for
LNG Inner Vessel

HV101   HV102

HV111

PIT520
Vaporizer Gas Exit Pressure

TE 509
Gas Exit from Product Vaporizer

LIT 503
Level Measurement of LNG Tank

HV112

TE 507
Water Glycol Exit from Product Vaporizer

HV113

One of the biggest concerns for the measurement campaign was safety. It was stressed during the design and execution of the measurement campaign that any equipment operating inside the Cold Box on MF Korsfjord and KV Bergen were approved to be operated in Zone 1 EX areas. The Cold Box is indicated as a blue square in Figure 22. According to DNV (2014) in a regulation titled "Gas Fuelled Ship Installation", any equipment operating in the Cold Box had to be certified for temperature class, T1, and equipment group IIA since there was the possibility that natural gas could exist in the room in the event of a LNG leak. The regulation states that "tank connection spaces" including the Cold Box are considered Zone 1 hazardous areas requiring certain specifications on equipment used in these spaces. To comply with these safety standards, probes approved for Zone 1 EX areas were selected for the UF 801 P flowmeter. Additionally, an electrical explosive barrier was used with the thermocouples. These barriers altered the voltage through the thermocouple wires so that they would not act as an ignition source in the event of a LNG leak in the Cold Box. All other portable electronic equipment used in the measurement campaign was operated outside the Cold Box. Appendix C contains all HSE and risk assessment documents filled for these measurements.

As indicated in Figure 22, the following portable equipment was placed in the Cold Box. Four T-type thermocouples were placed equidistance around the PBU gas exit, water glycol inlet, and water glycol outlet piping. During a measurement performed on 18 April 2014 on MF Korsfjord, a set of four t-type thermocouples were shifted to the top filling bunkering pipe to measure the temperature of the natural gas existing in the top of the LNG tank purged from the LNG tank before bunkering. On 03 May 2014 during a measurement on KV Bergen, two additional thermocouples were placed on piping used to cleanse the installed cryogenic equipment. Table 10 provides the date and vessel where each of the measurements took place. The abbreviation for the tests will be used in later chapters when discussing the data acquired during the measurement campaign.

Table 10: Abbreviation of Measurements

Abbreviation	Date (2014)	Vessel
E1	31 March – 01 April	MF Korsfjord
E2	07 April – 08 April	MF Korsfjord
E3	18 April	MF Korsfjord
E4	03 May	KV Bergen

Appendix D contains additional information on the bunkering process and information received during measurements E1 and E2. The measurement campaign description given to Fjord 1 before the measurements is provided in Appendix E. Certain parts of the measurement campaign description were modified once a better understanding of the LNG system on MF Korsfjord was gained.

After the initial set up was complete on MF Korsfjord, the measurement campaign was carried out in the following steps. The portable equipment described above was activated before bunkering commenced. This portable equipment recorded the PBU exit temperature, water glycol inlet temperature, water glycol exit temperature, top tank temperature, and heel temperature. While bunkering, the LNG truck tank temperature, pump temperature, truck tank pressure, pump pressure, flow rate, and total mass passed was recorded from the LNG truck every minute. Unfortunately, neither Gasnor nor Skansgass could send additional information of the measuring equipment used on their trucks.

On MF Korsfjord, the LNG system remained in stand-by mode overnight while the ferry was at the pier. When the LNG system was started, the PBU exit temperature, water glycol inlet temperature, water glycol exit temperature, and water glycol flowrate were recorded using portable equipment. The flowmeter probes used in conjunction with the UF 801 P Ultrasonic Flowmeter were placed in reflex (V) configuration to measure the liquid flow in the water glycol piping. In the reflex configuration, both of the probes are placed on the same side of the piping and the ultrasonic signal is reflected from one side of the pipe downstream to the second flowmeter probe. During the pressurization period, before operating the NG engines in measurement E2, an attempt was made to measure the gas volume flow traveling through the PBU exit piping. After attempting to measure gas volume flow in the indirect configuration, the flowmeter probes were later reconfigured for direct configuration (/). In the direct configuration, one probe is placed upstream of the other probe which is placed downstream and on the other side of the pipe. An illustration on the direct and indirect configuration for the flowmeter probes may be found in Figure 24 and Figure 25.
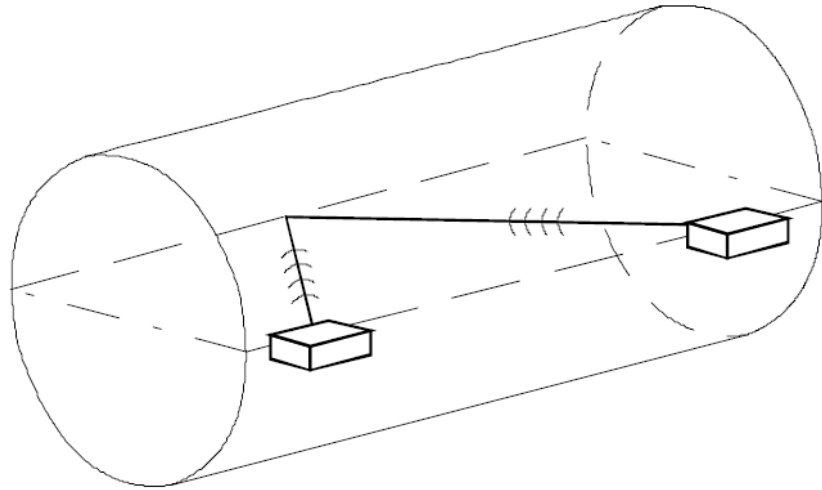
Figure 24: Indirect Flowmeter Measurement (Ultraflux 2003)
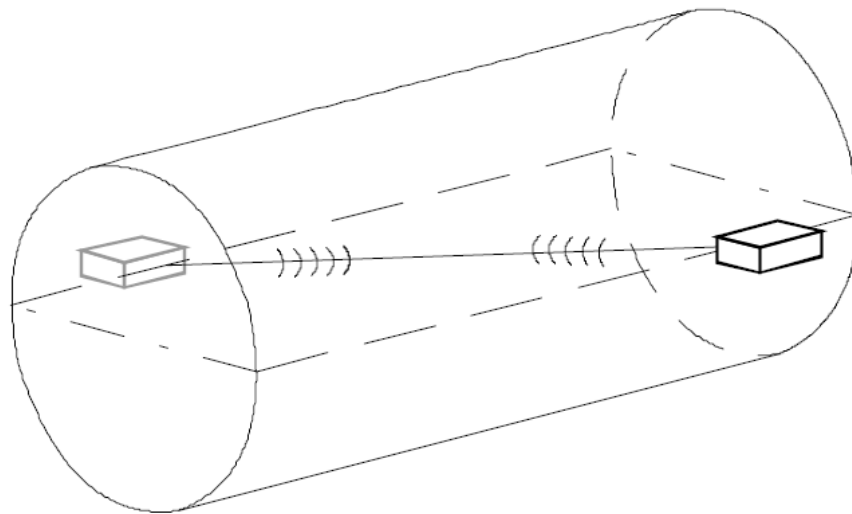
Figure 25: Direct Flowmeter Measurement (Ultraflux 2003)

According to the Ultraflux 801-P Manual, the accuracy of the UF-801-P is "often better than 1% for a wide range of flows". One of the challenges experienced while using the ultra-sonic flowmeter was that the exact state of the water glycol and natural gas was not known since intrusive tests were not allowed during the measurement campaign. Parameters used for the calibration of the measurement of the water glycol flow and NG exiting the PBU are found in Table 11.

Description	Symbol	Value	Units
Propagation Velocity Water / Glycol mixture (50% glycol, 5C)	B_{GLY}	1542	m/s
Propagation Velocity in NG exiting PBU (Methane, 15C, 1 atm)	B_{NG}	441	m/s
Outer Diameter Water / Glycol pipe	d_{GLY}	220	mm
Outer Diameter PBU exit pipe	d_{NG}	48.3	mm

T-type thermocouples were selected because it was possible to measure temperatures associated with cryogenic fluids. According to NIST (1995), the appropriate temperature range for T-type thermocouples is -200°C to 400°C making them ideal for measuring systems using LNG since temperatures do not go below -162°C. NIST also states that the error for the temperature range of 200°C to 0°C is -0.02°C to 0.04°C and for the temperature range 0°C to 400°C the error range is from -0.03°C to 0.03°C. When installing the T-type thermocouples on the different pipes in the Cold Box, aluminum tape was placed over the thermocouples and then covered with 5 cm of rubber insulation to mitigate the influence of the ambient temperature.

4.3 Installed Equipment

The instrument error from the installed equipment on the ship was also considered. CryoAB (2009) contains a list of all the installed components used on both KV Bergen and MF Korsfjord. The LNG tank systems on both vessels were designed by Cryo AB and the system drawings indicate that the same components were used in the same location in both systems. It is reasonable to assume that the errors for the installed measuring equipment on both vessels are roughly equal.

4.3.1 PT-100 Temperature Element

Installed sensors TE304, TE505, TE507, and TE509 are all PT-100 sensors produced by Pentronic. The PT-100s are considered "Resistance-Temperature Detectors" (RTD) (Pentronic 2014). According to Wheeler and Ganji (2004), RTDs are made from a "length of metal wire combined with a resistance measuring device" and unlike thermocouples are able to "measure temperatures directly, not relatively". The RTDs used on KV Bergen and MF Korsfjord are considered Class A PT-100s which suggests they have an error of +/- 1°C which is illustrated in Figure 26.
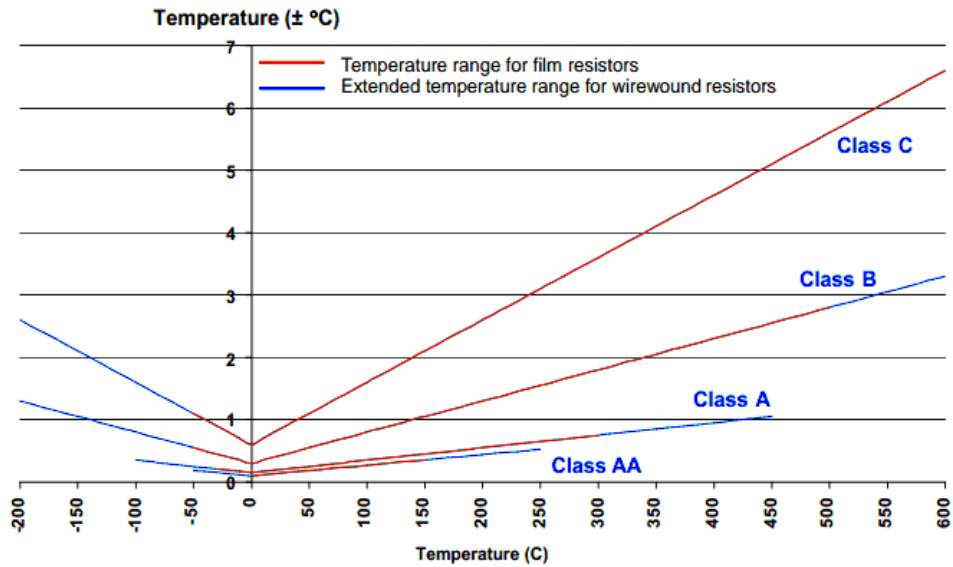
Figure 26: Tolerance Classes for PT100 Thermocouples (Pentronic 2014)

Another source of error for the PT-100s is hysteresis. According to the component manual produced by Pentronics, hysteresis is when the RTD "gives different readings depending on whether the temperature is rising or falling". Stated specifications suggest this error could be up to 0.008% of the given temperature in addition to the product tolerance given in Figure 26.

4.3.2 Differential Pressure Transmitter

The Rosemount 3051 Differential Pressure Transmitter is used to measure the pressure difference between the top and bottom of the LNG tank. This information is used to indicate the LNG level in the LNG tank on KV Bergen and MF Korsfjord. According to Rosemount (2006), the pressure transmitters on KV Bergen and MF Korsfjord (LIT503) have a total accuracy of +/- 0.15% of the actual tank pressure. The liquid level is calculated using an assumed density and the geometry of the LNG tank.

4.3.3 Pressure Indicator

Installed sensors PI 502 and PIT520, produced by WIKA, are used to measure the top tank pressure and gas vapor exit pressure from the Evaporator (EVAP) circuit in the Vaporizer. These components have an accuracy of +/- 1.0% of the actual pressure. The maximum possible amount of error for each of the portable and installed components is summarized in Table 12. Note that the maximum errors displayed in units of measurements were based on the most extreme values experienced during the measurement campaign.

Component	Max Error [%]	Max Error [Units]
Ultraflux Flowmeter (Note 1)	+/- 1.00 %	+/- 0.72 m^3/hr
T-Type Thermocouple (-200°C to 0C) (Note 2)	+/- 0.024%	+/- 0.04 °C
T-Type Thermocouple (0C to 400C) (Note 3)	+/- 0.075%	+/- 0.03 °C
PT-100s (TE304,TE505,TE507,TE509) (Note 2)	+/- 0.617%	+/- 1.00 °C
Differential Pressure (LIT503) (Note 4)	+/- 0.15 %	+/- 21.6 kPa
Pressure Indicator (PI502,PIT520) (Note 5)	+/- 1.00 %	+/- 0.05 bara

Note 1: Based on average measured water glycol flow of 72.72 m^3/hr on MF Korsfjord.
Note 2: Based on an assumed lowest LNG temperature of -162 C.
Note 3: Based on a maximum water glycol temperature of 40 C.
Note 4: Based on a maximum height of 3.6 m and density of 407 kg/m^3 in the LNG tank on MF Korsfjord.
Note 5: Based on a maximum observed tank pressure of 5 bara on MF Korsfjord.

4.4 Missing Parameters

Since it was not possible to conduct intrusive tests on KV Bergen and MF Korsfjord a few parameters could not be measured directly. Provided is a brief discussion on what parameters could not be directly measured and how appropriate assumptions were made to determine these values. Also included are comments on how future testing could directly measure these parameters.

It was not possible to measure the following parameters directly during the measurement campaign on KV Bergen and MF Korsfjord: heel composition, top tank gas composition, water glycol density, PBU mass flow rate, and LNG composition in both the PBU and EVAP. The heel, top tank gas, and LNG entering the PBU and EVAP were assumed to be the same composition as the bunkered LNG. Water glycol density was calculated using relationships produced by Conde Engineering (2011) based on the percent glycol indicated by the Chief Engineer on KV Bergen and MF Korsfjord. The PBU mass flow rate was calculated using an energy balance of the different streams exchanging heat in the Vaporizer. This calculation may be found in the Data Acquired chapter.

In future measurement it may be possible to conduct intrusive tests which allow direct measurement of the LNG and NG. Specifically, "gas chromatographic analysis" used in the sampling of LNG and NG in transfer lines between LNG tanker ships and shore facilities appears to be a promising method to acquire these missing parameters (GIIGNL 2011). The use of these intrusive techniques is discussed in greater detail in the chapter discussing future works.

Using the measurement techniques described in this chapter, four different measurement campaigns were carried out to gain a better understanding of the reasons behind the NG engine de-loading. Before these measurements were conducted, however, calculations were performed to model possible outcomes. The next chapter describes the calculations performed and discusses their results.

5. Modeling and Calculations

This chapter contains calculations performed before the measurement campaign which were used to model the changing conditions in the LNG tank before, during, and after bunkering. The three major calculations in this chapter include the mass flow rate through the PBU, the time required to pressurize the tank, and the fall in tank pressure resulting from mixing. The results from this chapter will be compared to the data acquired during the measurement campaign to assess whether the models developed in this chapter accurately reflect what is occurring in the LNG system. The models used in this chapter will also be used in the Results and Discussion chapter to determine which tank conditions will cause the NG engines to de-load.

5.1 PBU Mass Flow Rate

This sub-section describes a method to calculate the PBU mass flow rate which will be compared to measurements taken from the PBU on KV Bergen and MF Korsfjord. The mass flow rate through the PBU is required in the next sub-section to calculate the time required to pressurize the LNG tank. The purpose of the PBU in the LNG system is to restore the desired top tank pressure after a fall in tank pressure has occurred. This fall in tank pressure may come from either liquid LNG draw to the NG engines or from internal interaction from LNG mixing with vapor in the tank. The mass flow rate and pressurization time can be compared to the rate at which the top tank pressure falls in order to assess whether the pressure in the LNG tank will fall below a certain level causing a de-loading event.

The PBU is an internal loop in the LNG tank system that channels LNG from the bottom of the tank, evaporates the liquid, and injects it at the top of the tank. In the PBU, the amount of LNG which is circulated through this section is determined by the liquid height in the tank and the difference in density of the LNG. The operator is able to select an allowable pressure deviation in the tank before the PBU valve is opened allowing LNG to circulate through the unit. The mass flow rate circulated through the PBU is determined by the thermosiphon effect and is used in other process equipment, such as natural circulation reboilers. A drawing of the PBU on KV Bergen is shown in Figure 27. Note that the PBU is comprised of the lower bundle of coils in the drawing.
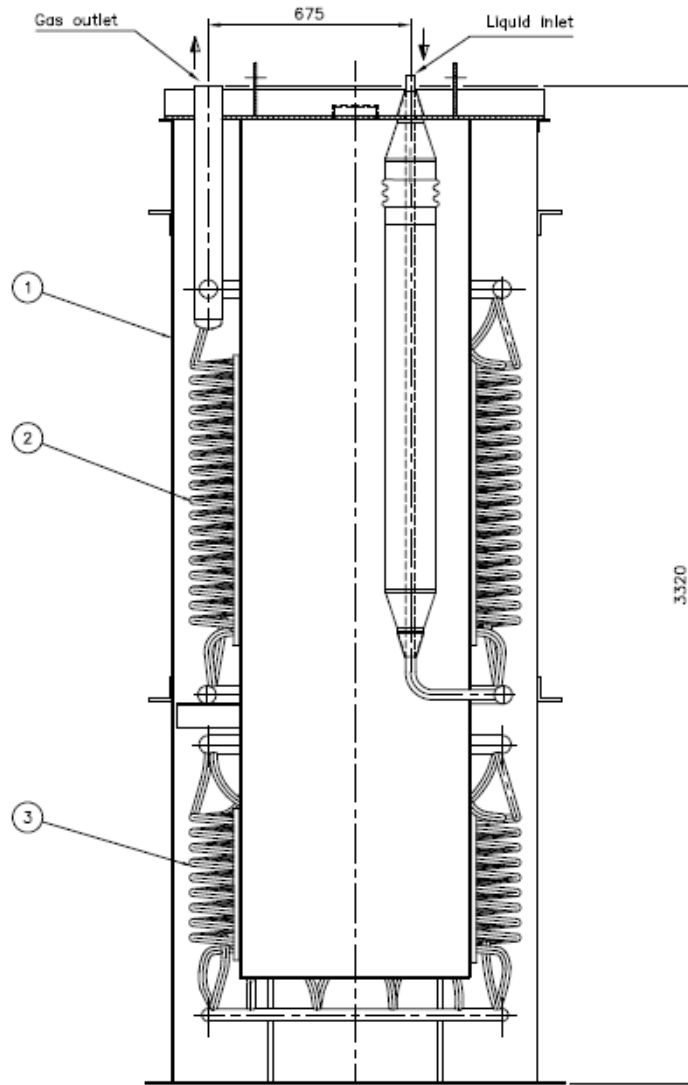
Figure 27: PBU on KV Bergen (Cryo AB 2009)

The PBU on KV Bergen and Korsfjord have several similarities between vertical thermosiphon reboilers used in distillation columns. One similarity is the driving forces used in both pieces of equipment. Serth (2007) states "the driving force for the flow is the density difference between the liquid in the feed circuit and the two-phase mixture in the boiling region and return line". In the PBU on both vessels, the density difference is caused by LNG vaporization which occurs when heat rejected from the water/glycol circuit is absorbed into the coils of the PBU. The calculation method outlined in this section was originally published by Fair (1960) and later re-published by Serth (2007) with additional information on vertical re-boiler design.

5.1.1 PBU Overall Heat Transfer Coefficient

The overall mass flow rate through the PBU is solved using a pressure balance through different sections of the tank and PBU. A generic diagram of the different points in the mass balance is shown in Figure 28.
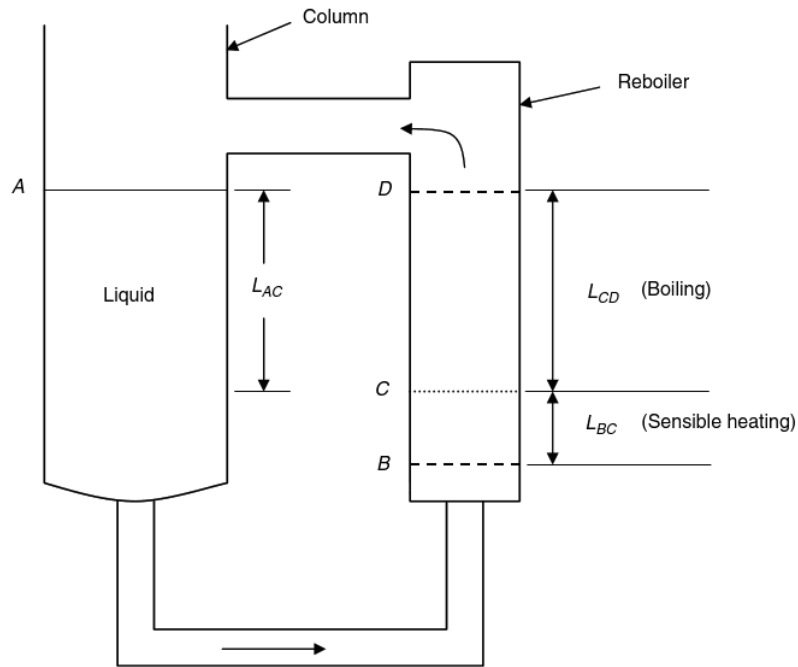
Figure 28: Pressure Balance (Serth, 2007)

The first factor which must be computed is the overall heat transfer coefficient, U, in the PBU. A number of geometric constants shown in Table 13 have been found using system drawings or assumed.

Table 13: Geometric PBU Constants

Symbol	Value (KV Bergen)	Unit	Description
N	4.5	[-]	Coil rows in PBU
n	20	[-]	Tubes in PBU
$d_{tube,i}$	0.009	[m]	PBU tubing diameter
b_{tube}	0.001	[m]	PBU tube thickness
C_{PBU}	1.22	[m]	PBU shell diameter
B_{PBU}	0.70	[m]	PBU annulus diameter
$d_{AB,i}$	0.028	[m]	Piping section AB diameter
b_{AB}	0.0015	[m]	Piping section AB thickness
z_{BD}	0.900	[m]	Vert. height section BD
$d_{DA,i}$	0.063	[m]	Piping section DA diameter
z_{tank}	4.90	[m]	Vert. height tank
L_{AB}	3.00	[m]	Piping section AB length
L_{DA}	5.00	[m]	Piping section DA length

Additionally, the composition of the LNG used for calculations in this chapter is provided in Table 14 which comes from a fueling sheet provided by Gasnor during a bunkering that occurred in October 2013 on KV Bergen.

Table 14: Bunkering Composition

Composition	Mole Fraction
Nitrogen	0.005
Methane	0.95
Ethane	0.0383
Propane	0.0055
Iso-Butane	0.0025
N-Butane	0.0007
Pentane	0.0005

Before calculating the overall heat transfer coefficient of the PBU, the Reynolds number of the water/glycol flow through the PBU must be calculated using Equations (11), (12), and (13). Notice that Equation (11) uses the average cross section between the outer and inner diameter of the PBU minus the space occupied by the tubes when calculating the Reynolds number.

$$G_{gly} = \dot{m}_{gly}/(\pi/4) * \left(d_c{}^2 - d_b{}^2\right) - n(d_{coil,avg,o}{}^2 - d_{coil,avg,i}{}^2)) \tag{11}$$

$$\dot{m}_{gly} = \dot{Q}_{gly}\rho_{gly} \tag{12}$$

$$Re_{gly} = d_e G_{gly}/\mu_{gly} = \dot{m}_{gly}/\mu_{gly}\frac{\pi}{4}d_e \tag{13}$$

The convective and conductive heat transfer occurring outside the coils of the PBU may be estimated using the relations provided by Patil, Shende et al. (1982). Equation (14) refers to laminar flow occurring inside the water / glycol stream where the Reynolds number is between 50 and 10,000. Equation (15) refers to turbulent flow occurring inside the water / glycol stream where the Reynolds number is above 10,000. Equation (15) was originally published by Kern (1950) who conducted tests on shell side film coefficients for heat exchangers used in the hydrocarbon industry. Kern (1950) claims deviations between Equation (15) and industry data may be between 0 to 20 percent.

$$\frac{h_{gly,o}d_e}{k_{gly}} = 0.6Re_{gly}^{0.5}Pr_{gly}^{0.31}; \ 50 < Re_{gly} < 10,000 \tag{14}$$

$$\frac{h_{gly,o}d_e}{k_{gly}} = 0.36Re_{gly}^{0.55}Pr_{gly}^{1/3}\left(\mu_{gly}/\mu_{gly,w}\right)^{0.14}; \ Re_{gly} > 10,000 \tag{15}$$

The fluid properties of the water glycol mixtures were calculated using mathematical models for secondary fluids published by Conde Engineering (2011). Both the mathematical models and constants used in the equations of state for the glycol mixture may be found in Appendix F.

After determining the heat transfer coefficient outside of the coils of the PBU, the heat transfer coefficient for the heat transfer occurring inside the coils were calculated. Gnielinski (1987) published a number of correlations for helically coiled tubes of circular cross sections covering laminar, transitional, and turbulent flow. These correlations were compared to other existing experimental data on helically coiled tubes. Gnielinski found that others tests studying laminar flow of water and oil "did not deviate more than +/- 15% from the values" calculated. Similarly, correlations for transitional and turbulent flow did not deviate more than +/-15% compared to existing data from experiments on the turbulent flow of air and water in helically coiled heat exchangers. Using Gnielinski's correlations, the equations for the critical Reynolds number and Nusselt number for laminar, transitional and turbulent LNG flows are provide in Equations (16), (17), (18), (19), (20), (21), and (22).

$$Re_{crit} = 2300 \left[1 + 8.6 \left(\frac{d_{tube,i}}{d_{coil,avg,i}} \right)^{0.45} \right] \tag{16}$$

When the flow inside the PBU coils is laminar, i.e., $Re_{lng} < Re_{crit}$, then Equations (17) and (18) apply.

$$Nu_{lam} = 3.65 + 0.08 \left[1 + \left(\frac{d_{tube,i}}{d_{coil,avg,i}} \right)^{0.9} \right] Re_{lng}{}^{m} Pr_{lng}{}^{1/3} \left(\frac{Pr_{lng}}{Pr_{LNG,w}} \right)^{0.14} \tag{17}$$

$$m = 0.5 + 0.2903 \left(\frac{d_{tube,i}}{d_{coil,avg,i}} \right)^{0.194} \tag{18}$$

When the flow inside the PBU coils is transitional, i.e., $Re_{crit} < Re_{lng} < 2.2 * 10^4$, then Equations (19) and (20) apply.

$$Nu_{trans} = ANu_{Lam}(Re_{lng} = Re_{crit}) + (1 - A)Nu_{turb}(Re_{lng} = 2.2 \times 10^4) \tag{19}$$

$$A = \frac{2.2 \times 10^4 - Re_{lng}}{2.2 \times 10^2 - Re_{crit}} \tag{20}$$

When the flow inside the PBU coils is turbulent, i.e., $Re_{LNG} > 2.2 * 10^4$, then Equations (21) and (22) apply.

$$Nu_{turb} = \frac{\left(\frac{f_t}{8}\right) Re_{lng} Pr_{lng}}{1 + 12.7 \sqrt{\frac{f_t}{8}} \left(Pr_{lng}^{2/3} - 1\right)} \left(\frac{Pr_{lng}}{Pr_{lng,w}}\right)^{0.14} \tag{21}$$

$$f_t = \left[\frac{0.3164}{Re_{lng}^{0.25}} + 0.03 \left(\frac{d_{tube,i}}{d_{coil,avg,i}}\right)^{0.5}\right] \left(\frac{\mu_{lng,w}}{\mu_{lng}}\right)^{0.27} \tag{22}$$

The type of flow occurring inside the coils of the PBU will depend on the LNG mass flow through the PBU. Since the LNG mass flow through the PBU is unknown, the Nusselt number for the LNG in the PBU was calculated in a MATLAB program using an initial guess for the mass flow. Within each calculation loop, the mass flow is increased until the pressure balance described in the next section is solved. The MATLAB program used to calculate the overall heat transfer coefficient, U, for the PBU is provided in Appendix G. The heat transfer coefficient for the fluid inside the coils of the PBU is given by the definition of the Nusselt number provided in Equation (23).

$$h_{lng,i} = \frac{Nu_{lng} k_{lng}}{d_{tube,i}} \tag{23}$$

Using the heat transfer coefficient inside and outside of the PBU tubing as well as the thermal conductivity of the tubing and thickness an overall heat transfer coefficient for the PBU may be calculated using Equation (24).

$$\frac{1}{U_{PBU}} = \frac{1}{h_{gly,o}} + \frac{1}{h_{lng,i}} + \frac{b_{tube}}{k_{tube}} \tag{24}$$

The pressure change within each section of the PBU is calculated and balanced with the other sections to solve for the LNG mass flow rate. Figure 28 shows the different sections of the PBU loop that are considered. This methodology is very similar to the one described by Fair (1960) and Serth (2007) in the design of vertical thermosiphons. The LNG systems drawing on KV Bergen is used to illustrate these different sections in Figure 29. Section A to B is the pressure change from the top of the liquid LNG level to the inlet of the PBU. Section B to C refers to the sensible heating zone in the PBU where the LNG is brought from its sub-cooled temperature to its saturated temperature. Section C through D refers to the section of the PBU where the LNG is vaporized.
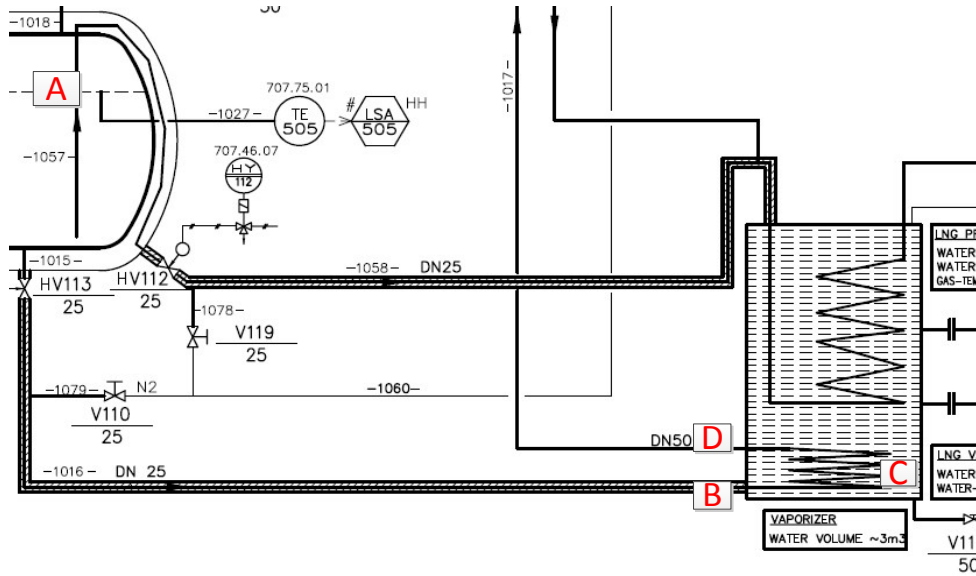
Figure 29: Pressure Balance Calculation Sections

It is assumed that the LNG is completely vaporized after traveling around one loop of the PBU circuit. This assumption is confirmed by measurements discussed in the Data Acquired chapter. Section D to A refers to the path that he NG follows after exiting the PBU to the top of the LNG in the tank. The program used to calculate this mass flow rate through the PBU is provided in Appendix H. MATLAB code provided by Brown, Lux, Muxny, Lemmon, and Wait (2011) is utilized so that MATLAB is able to call the fluid properties of the LNG mixture and water / glycol mixture at different states from NIST REFPROP. Additional MATLAB code was taken from Clamond (2008) to calculate the Colebrook friction factor for flows in pipe sections A to B and D to A.

Sub-sections 5.1.2 PBU Section A to B, 5.1.3 PBU Section B to C, 5.1.4 PBU Section C to D, 5.1.5 PBU Section D to A will examine the pressure changes in each section of the PBU. The pressure changes from each of the sections in the PBU will be balanced in sub-section 5.1.6 Pressure Balance to provide an expression which can be used to calculate the PBU mass flow rate.

5.1.2 PBU Section A to B

PBU section A to B encompasses the path from the top of the liquid level in the tank to the inlet section of the PBU. This section considers the pressure change from the static liquid height in the LNG tank and pressure losses due to fluid flow through the piping connecting point A to point B. Minor losses from valves and bends are also considered. Table 15 provides some geometric constants for section A to B.

Table 15: Geometric Constants for Piping Sections A to B

Symbol	Value (KV Bergen) [m]	Description
$d_{AB,i}$	0.028	Pipe diameter section A to B
b_{AB}	0.0015	Thickness pipe section A to B
L_{AB}	3.00	Pipe length section A to B
z_{tank}	4.90	Tank height
z_{AB}	4.00	Vert. height point A to B
e_{AB}	0.000004	Pipe roughness pipe section A to B

Note that the vertical height from point A to B includes the liquid level in the LNG tank plus the vertical height from the bottom of the tank to the inlet of the PBU. The PBU is at a lower elevation than the LNG tank bottom. The pipe roughness is based on the industry standard for DIN2391 precision steel piping which is indicated in system drawings. To estimate the fluid friction in the pipe the Reynolds number was calculated using the expression in Equation (25).

$$Re_{AB} = d_{AB,i} G_{PBU,AB} / \mu_{lng,AB} = \dot{m}_{PBU} / \mu_{lng,AB} \frac{\pi}{4} d_{AB,i} \tag{25}$$

Additionally, the LNG velocity in this section is estimated with the expression in Equation (26).

$$u_{AB} = \frac{\dot{m}_{PBU}}{\rho_{LNG,AB} \frac{\pi}{4} d_{AB,i}} \tag{26}$$

McGovern (2011) suggests using Colebrook expression for the friction factor for turbulent flow given in Equation (27) and the friction factor for laminar flow given in Equation (28).

$$\frac{1}{\sqrt{f_{AB}}} = -2 log_{10} \left(\frac{e_{AB}/D_{AB}}{3.7} + \frac{2.51}{Re_{AB}\sqrt{f_{AB}}} \right); Re_{AB} > 2300 \tag{27}$$

$$f_{AB} = 64/Re_{AB}; Re_{AB} < 2300 \tag{28}$$

A separate MATLAB program was used for Equation (27) since the solution for the fluid friction may be found using iterative methods (Clamond 2008). The total change in pressure from point A to point B is incorporated in Equations (29) which takes into account the static change in pressure from the liquid height. Equation (29) also takes into account the change in pressure due to fluid friction and minor losses from valves and bends. Instead of using the liquid height in the tank, the pressure differential from the top to the bottom of the tank may also be used since this value is measured directly from equipment installed on KV Bergen and MF Korsfjord. The total change in pressure due to minor losses is illustrated in Equation (30). Finally, the expression for a drop in pressure due to a valve or bend is given in Equation (31).

$$P_B - P_A = \rho_{lng,AB} g \Delta z_{AB} - f_{AB} \frac{L_{AB} \rho_{lng,AB} u_{AB}^2}{2 d_{AB,i}} - \Delta P_{minor,AB} \tag{29}$$

$$\Delta P_{minor,AB} = \Delta P_{valve,AB} + \Delta P_{bend,AB} \tag{30}$$

$$\Delta P_{valve/bend} = \frac{L_e}{d_e} f_{AB} \frac{u_{AB}^2}{2g} \tag{31}$$

According to LNG systems drawings, there is one globe valve (HV113) and at least one 45 degree bend and one 90 degree bend in the piping from point A to point B. Figure 30 shows the globe valve used in the LNG system on KV Bergen.

Figure 30: LNG Globe Valve KV Bergen (SPS Cryogenics)

Hardee and Sines (2012) recommend using 340, 30, and 16 for the L_e/d_e values for the globe valve, 90 degree bend, and 45 degree bend, respectively, in Equation (31). The next sub-section explores the pressure change in piping section B to C.

5.1.3 PBU Section B to C

PBU section B to C encompasses the sensible heating zone in the PBU tubing. Similar to vertical thermosiphon calculations, "boiling is assumed to begin when the liquid in the tubes become saturated; sub-cooled boiling is not considered" (Serth 2007). In section B to C, the static pressure decreases because of the change in height, while the temperature of the liquid LNG increases because of convective and conductive heat transfer occurring inside the lower part of the PBU tubing. It is assumed that the temperature at the bottom of the tank (the sub-cooled LNG introduced during bunkering) is approximately the same temperature as point B. Since the focus

of this study is on conditions after bunkering, it is assumed that the temperature of the LNG at the bottom of the tank is approximately the same temperature as the temperature in the truck during bunkering. To find the relationship between liquid temperature and pressure, "A linear relationship between the temperature and pressure is assumed [and] the saturation curve is linearized about" the sub-cooled temperature at the bottom of the tank (Serth 2007). This relationship, originally published by Serth and Fair, is provided in Equations (32) and (33) and illustrated in Figure 31.

$$\frac{T_C - T_B}{P_C - P_B} = \frac{(\Delta T / L_{BC})}{(\Delta P / L_{BC})} \tag{32}$$

The saturation curve for the LNG is linearized about the sub-cooled temperature at the bottom of the tank in Equation (33).

$$\frac{T_{sat} - T_A}{P_{sat} - P_A} = (\Delta T / \Delta P)_{sat} \tag{33}$$
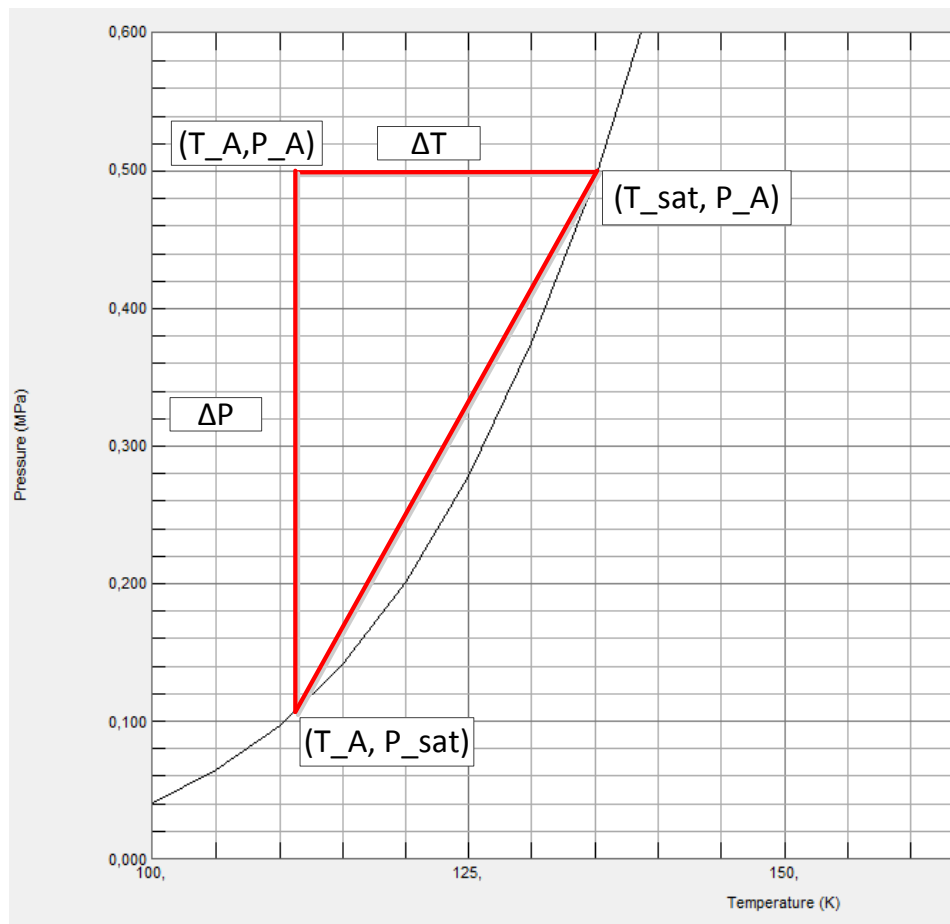
Figure 31: Linearized LNG Saturation Curve

Assuming point C is the saturation temperature and pressure, Equations (32) and (33) may be combined into Equation (34) to find the pressure at point C in the PBU (Serth 2007), (Fair 1960).

$$\frac{P_B - P_C}{P_B - P_A} = \frac{(\Delta T/\Delta P)_{sat}}{(\Delta T/\Delta P)_{sat} - \frac{(\Delta T/L_{BC})}{(\Delta P/L_{BC})}} \tag{34}$$

The temperature gradient, $\Delta T/L_{BC}$, is given by Equation (35) and the log-mean temperature difference of the streams entering and exiting the PBU are given in Equation (36). Notice that Equation (35) is given by an energy balance between the energy rejected by the water/glycol mixture and absorbed by the LNG in the PBU. This energy balance is better illustrated in Equation (37).

$$\frac{\Delta T}{L_{BC}} = \frac{n\pi d_{tube,o} U_{PBU} \Delta T_m}{\dot{m}_{PBU} Cp_{lng}} \tag{35}$$

$$\Delta T_m = \frac{\left(T_{gly,i} - T_{lng,i}\right) - \left(T_{gly,o} - T_{lng,o}\right)}{ln\left(\frac{T_{gly,i} - T_{lng,i}}{T_{gly,o} - T_{lng,o}}\right)} \tag{36}$$

$$\dot{m}_{PBU} Cp_{lng}(T_C - T_B) = n\pi d_{tube,o} U_{PBU} \Delta T_m L_{BC} \tag{37}$$

The pressure gradient, $\Delta P/L_{BC}$, is given by Equation (38). It is assumed the pressure gradient in section B to C is mainly caused by the change in static pressure over the change in vertical height in the PBU.

$$\frac{\Delta P}{L_{BC}} = \rho_{lng,B} g \tag{38}$$

Neglecting friction losses, it is possible to find the vertical length of section B to C as well as section C to D. The vertical length of section B to C may be estimated by Equation (39).

$$\frac{(P_B - P_C)}{(P_B - P_A)} \cong \frac{L_{BC}}{(z_A - z_B)} \tag{39}$$

Using the overall vertical length of the PBU, the length of section C to D may also be estimated in Equation (40).

$$L_{CD} = z_{PBU} - L_{BC} \tag{40}$$

The change in pressure due to fluid friction may be estimated using Equations (25), (26), (27), and (28), using the calculated length of section B to C. The expression for the pressure at point C is given in Equations (41) and (42).

$$P_C = P_B - Eqn(34)(P_B - P_A) - f_{BC} \frac{L_{BC} G_{BD}^2}{2\rho_{lng,B} d_{tube,i}} \tag{41}$$

$$G_{BD} = \frac{\dot{m}_{PBU}}{n\frac{\pi}{4}d_{tube,i}^{2}} \tag{42}$$

The next sub-section calculates the pressure changes in PBU section C to D.

5.1.4 PBU Section C to D

Section C to D encompasses the section within the PBU where boiling and two phase flow occurs. Point C occurs when the LNG within the PBU tubing is saturated. Section C to D includes the following factors which lead to a change in pressure: static head losses, acceleration losses, and friction losses (Fair 1960), (Serth 2007).

The first factor considered is the change in pressure due to fluid friction in section C to D. It is assumed that the LNG is completely vaporized once it leaves the tubing of the PBU, i.e. $x_{exit} = 1$. Since there is two-phase flow in section C to D, a two phase multiplier, ϕ_{LO}, must be calculated to estimate the pressure drop due to fluid friction in this section. The expression for the change in pressure due to fluid friction is provided in Equation (43) which is recommended by (Fair 1960) and (Serth 2007).

$$\Delta P_{fric,CD} \cong \frac{f_{CD}L_{CD}G_{BD}^{2}\phi_{LO}^{2}}{2d_{tube,i}\rho_{L}} \tag{43}$$

The two phase multiplier in Equation (43) may be calculated with the Lockhart Martinelli correlation for turbulent – turbulent flow in Equation (44) and (45) (Lockhart and Martinelli 1949). The flow pattern suggests that both the liquid and vapor inside the tubes of the PBU are turbulent. The turbulent – turbulent correlation is recommended by Fair (1960) since the majority of vertical thermosiphon of this design have this fluid behavior.

$$\phi_{LO}^{2} = 1 + \frac{20}{X_{tt}} + \frac{1}{X_{tt}^{2}} \tag{44}$$

$$X_{tt} = \left[\frac{1-x}{x}\right]^{0.9}\left(\rho_{lng,v}/\rho_{lng,l}\right)^{0.5}\left(\mu_{lng,l}/\mu_{lng,v}\right)^{0.1} \tag{45}$$

Fair (1960) recommends using 2/3 of the vapor quality of the flow exiting the vertical thermosiphon. Since it is assumed that the LNG is completely vaporized in the PBU a value of 2/3 is used in Equation (45).

The change in static pressure due to the change in elevation in section C to D may be calculated using Equation (46). Since there is two-phase flow in this region, an average two-phase density must be calculated for this section. The expression for the average two phase density is given by Equation (47).

$$\Delta P_{stat,CD} \cong \rho_{avg,tp} g L_{CD} \tag{46}$$

$$\rho_{avg,tp} = \varepsilon_v \rho_v + (1 - \varepsilon_v)\rho_l \tag{47}$$

Equation (47) requires the vapor void fraction, ε_v, which is described as the "fraction of the total volume that is occupied by the vapor phase" (Serth 2007). Equation (48) is the expression for the vapor void fraction. Fair (1960) recommends using 1/3 the exit vapor quality in calculations for the change in static pressure in section C to D.

$$\varepsilon_v = \frac{x}{x + SR(1 - x)(\rho_v/\rho_l)} \tag{48}$$

The Slip Ration, SR, may be calculated using the Chisholm correlations provided in Equations (49), (50), and (51) which is required in Equation (48) (Chisholm 1983).

$$SR = (\rho_l/\rho_{hom})^{0.5}; \ X_{tt} > 1 \tag{49}$$

$$SR = (\rho_l/\rho_v)^{0.5}; \ X_{tt} \leq 1 \tag{50}$$

$$\rho_{hom} = [x/\rho_v + (1 - x)/\rho_l]^{-1} \tag{51}$$

The last factor in determining the overall pressure drop in section C to D is the acceleration caused by the two-phase flow and is provided in Equation (52) (NTNU 2013).

$$\Delta P_{acc,CD} \cong \frac{G_{BD}{}^2}{\rho_l} x_{exit} \left(\frac{\rho_l}{\rho_g} - 1 \right) \tag{52}$$

Combining the change in pressure due to fluid friction, change in static pressure, and fluid acceleration gives the overall change in pressure provided in Equation (53).

$$P_D - P_C = \Delta P_{f,CD} + \Delta P_{stat,CD} + \Delta P_{acc,CD} \tag{53}$$

Note that it is assumed at point D that the LNG has been completely vaporized. The next sub-section considers the pressure change in section D to A of the PBU.

5.1.5 PBU Section D to A

The calculations in section D to A are similar to the calculations in section A to B except that now it is assumed that the vapor quality of the NG is unity. It is assumed that static pressure and fluid friction are the two forces dominating the pressure drop from point D back to point A. The overall change in pressure from point D to point A may be estimated with Equations (54), (55), and (56).

$$P_D - P_A = \rho_{lng,D} g \Delta z_{DA} - f_{DA} \frac{L_{DA}\rho_{lng,D}u_{DA}^2}{2d_{DA,i}} - \Delta P_{minor,DA} \tag{54}$$

$$\Delta P_{minor,DA} = \Delta P_{valve,DA} + \Delta P_{bend,DA} \tag{55}$$

$$\Delta P_{valve/bend} = \frac{L_e}{d_e} f_{DA} \frac{u_{DA}^2}{2g} \tag{56}$$

A similar calculation method may be used to find u_{DA} and f_{DA} as in the previous sub-sections. Additionally, system drawings indicate there is at least one globe valve, one 90 degree bend, and one 45 degree bend in the piping system from point D to point A. With relationships established for each section of the PBU, it is now possible to balance the change in pressure in each of the sections to calculate the PBU mass flow.

5.1.6 Pressure Balance

To solve for the mass flow rate through the PBU ($\dot{m}_{PBU}$) a pressure balance may be used to equate the changes in pressure within each of the sections to one another. The pressure balance is given in Equation (57).

$$(P_A - P_B) + (P_B - P_C) + (P_C - P_D) + (P_D - P_A) = 0 \tag{57}$$

Solving for $\dot{m}_{PBU}$ is an iterative process. As stated above, the MATLAB program used to perform these iterations is found in Appendix H. The next sub-section presents the calculated PBU mass flow given different initial conditions.

5.1.7 Modeling Results

To better understand how the mass flow through the PBU varies with the pressure at the top of the LNG tank on KV Bergen, the initial pressure at the LNG liquid surface and liquid height in the tank were varied while the other parameters were held constant. Table 16 indicates what parameters were held constant while the pressure at the liquid surface and liquid height were varied.

Table 16: PBU Mass Flow Variables / Constants

Parameter	Value	Units	Constant / Varied
P_A	300-500	kPa	Varied
h_A	3.92-1.96	m	Varied
T_B	113	K	Constant
T_D	294	K	Constant
P_{gly}	101.3	kPa	Constant
$T_{gly,i}$	299	K	Constant
$T_{gly,o}$	295	K	Constant
θ_{gly}	0.5	[-]	Constant

Using the MATLAB code in Appendix G and H, the pressure at point A was varied between 300 and 500 kPa and the liquid height was varied between 40 to 80 percent of its max height. The corresponding mass flow through the PBU was calculated. The results of varying the top tank pressure and liquid height are presented in Figure 32. Also, it was determined that the flow in sections AB, BC, CD, and DA were all turbulent when the top tank pressure was between 300 kPa and 500 kPa and the liquid height was between 40 to 80 percent of its max value.
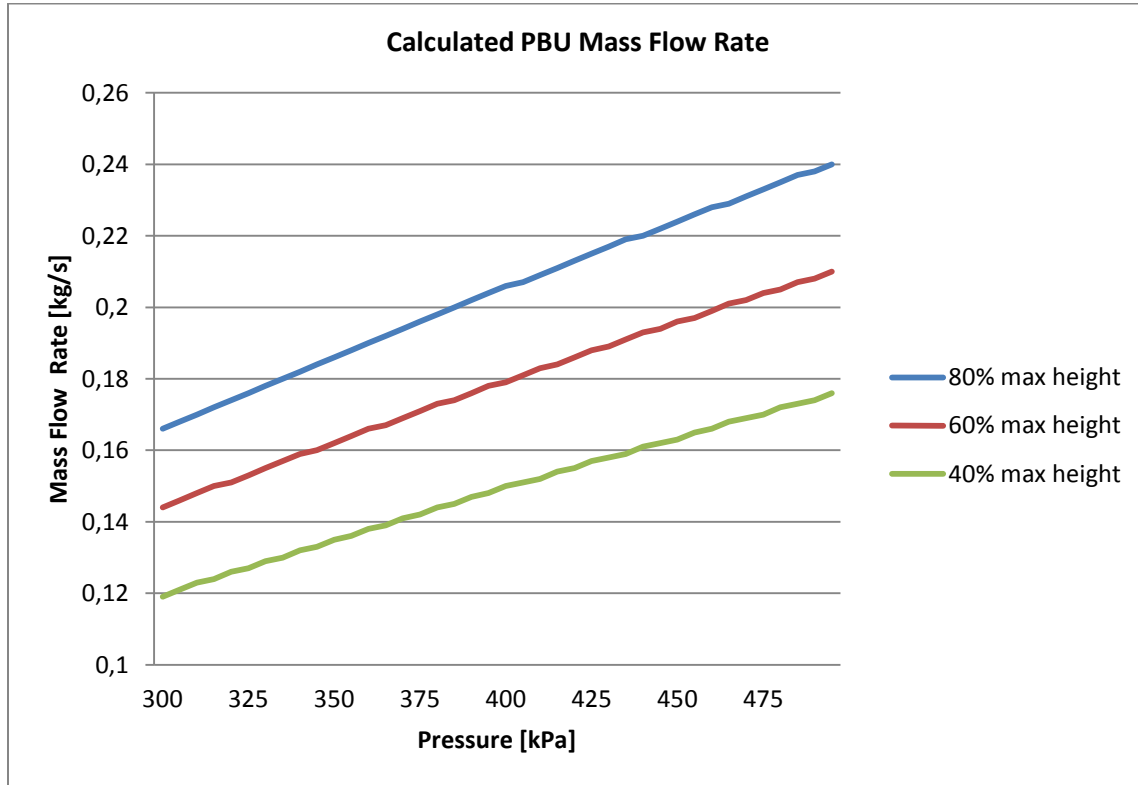
Figure 32: PBU Mass Flow versus Top Tank Pressure and Liquid Height

The relationship between tank pressure, liquid height, and PBU mass flow, shown in Figure 32, appear to be linear. A tank liquid height corresponding to 50% of the max height was selected for use in the pressurization calculations described in the next section. The linearized result of this calculation is presented in Equation (58).

$$\dot{m}_{PBU} = 0.0016 * P_v + 0.1316 \tag{58}$$

It may be assumed that the dimensions of the PBU were sized proportionally to the volume of the LNG tank on KV Bergen and MF Korsfjord since the same company designed the LNG system for both ships. This suggests that the same relationship between top tank pressure and PBU mass flow may be used for MF Korsfjord even though the PBU parameters for KV Bergen were used to calculate this relationship.

The relationship between top tank pressure, liquid height and mass flow through the PBU will be used in the next section to calculate the amount of time required to increase the top tank pressure from 400 kPa to 500 kPa. In the Data Acquired chapter, the PBU mass flow calculated in this section will be compared with the PBU mass flow rate measured indirectly during the measurement campaign.

5.2 Tank Pressurization Calculations

This section proposes an idealized methodology of calculating the time required to increase the top tank pressure from 400 kPa to 500 kPa. These results will be compared to the actual pressurization time recorded during the measurement campaign to understand how much the actual top tank pressurization differs from the idealized case. This analysis will also provide insight into how the vapor section of the LNG tank interacts with the liquid section in the LNG tank.

5.2.1 Pressure Build Up from PBU

This sub-section examines the governing equations used to create an expression for the pressurization time. A completely insulated vapor region is assumed in these calculations and will be compared with the values produced from the measurement campaign to see how much heat is exchanged between the liquid and vapor sections in the LNG tank. Figure 33 illustrates the mass and energy entering and leaving the vapor region in an uninsulated tank (e.g. what is actually occurring on KV Bergen and MF Korsfjord).
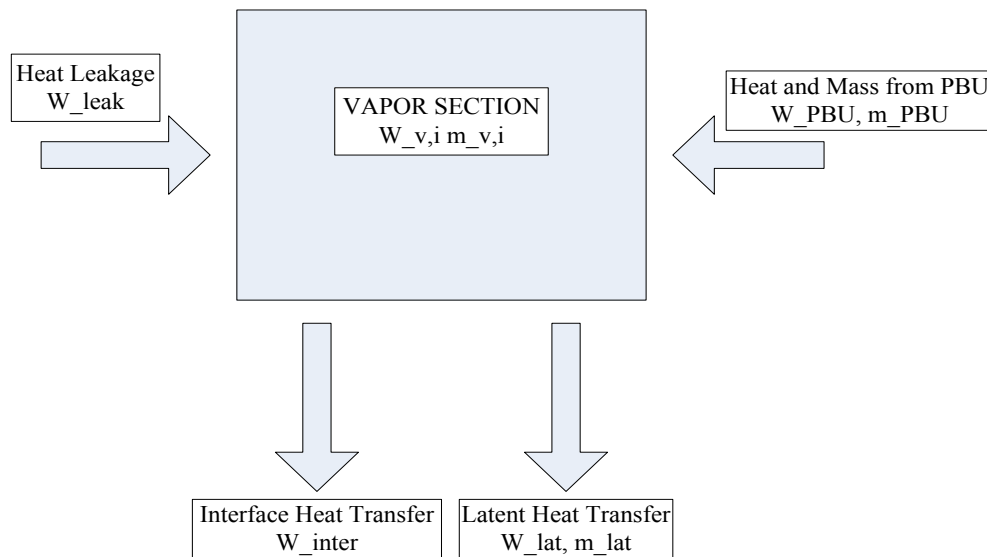
Figure 33: Heat and Mass Balance Vapor Section

Equations (59) and (60) indicate the energy and mass in the top of the tank at a particular point in time.

$$E_{v,i} - \int_0^t W_{inter}(t)\, dt - \int_0^t W_{lat}(t)\, dt + \int_0^t W_{PBU}(t)\, dt + \int_0^t W_{leak}(t)\, dt = E_v(t) \tag{59}$$

$$m_{v,i} + \int_0^t \dot{m}_{PBU}(t)\, dt - \int_0^t \dot{m}_{lat}(t)\, dt = m_v(t) \tag{60}$$

The calculations performed in this sub-section assumed that the heat leakage through the tank wall was negligible and there was no interface heat transfer or latent heat transfer (i.e. no evaporation or condensation). Only the initial energy and mass in the vapor section and the energy and mass entering the vapor from the PBU were considered in these calculations. Deviations between these idealized calculations and measured values indicate the extent of interaction between the vapor and liquid region in the LNG tank. Stated another way, the difference in the amount of time required to pressure the tank indicates the rate of condensation in the vapor section.
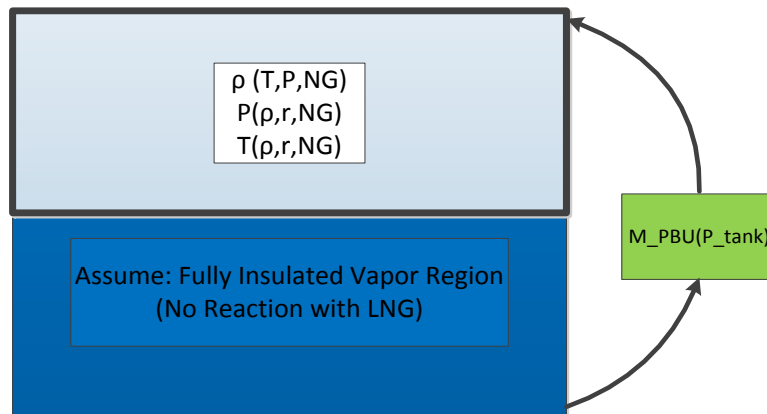
Figure 34: Top Tank Pressurization

A number of additional assumptions may be made from the main supposition that the vapor region is completely insulated. These assumptions include:

- The vapor region does not interact physically or thermodynamically with the liquid region. A control volume is placed around the vapor region.
- The pressure and temperature change inside the vapor region of the tank is isentropic.
- The vapor volume does not change during pressurization. See Section 5.2.2 Constant Volume Assumption for calculations supporting this assumption.
- Phase change (condensation /evaporation) does not occur during pressurization.
- The composition of the NG does not vary from the values listed in Table 14 since it may be assumed that the LNG through the Vaporizer is completely evaporated
- The vapor behaves ideally.

Using these assumptions, Equations (59) and (60) reduce to Equations (61) and (62).

$$E_{v,i} + \int_0^t W_{PBU}(t)\,dt = E_v(t) \tag{61}$$

$$m_{v,i} + \int_0^t \dot{m}_{PBU}(t)\,dt * t = m_v(t) \tag{62}$$

The initial conditions assumed in these calculations are provided in Table 17. Note that the vapor temperature and volume correspond to the initial conditions used in the PBU mass flow calculations from the previous subsection.

Table 17: Initial Conditions for Tank Pressurization Calculations

Variable	Value	Unit
$P_{v,i}$	400	kPa
$T_{v,i}$	294	K
$\rho_{v,i}$	2.81	kg/m^3
Δt	10	s
V_v	117	m^3

To calculate the pressurization time of the LNG tank, a simple mass balance was used along with the relationships for isentropic change of pressure and temperature in a closed container. Equation (63) illustrates the simple mass balance over time. Notice that the mass flow through the PBU at a particular point in time, $\dot{m}_{PBU}(P,t)$, varies as the pressure changes in the tank.

$$V_v \rho_{v,i} + \int_0^t \dot{m}_{PBU}(P,t)\,dt = V_v \rho_v(t) \tag{63}$$

Another relationship is required to calculate the change in temperature resulting from the increasing vapor density over time. Using the idealized assumptions stated above, the temperature change in the vapor region may be assumed to be an isentropic process of an ideal gas with constant specific heat derived from the 2nd Law of Thermodynamics (Cengel and Boles 2008). This relationship is provided in Equation (64).

$$\left(\frac{T_2}{T_1}\right)_{s=const} = \left(\frac{\rho_2}{\rho_1}\right)^{s-1} \tag{64}$$

A similar relationship is required to calculate the increasing pressure in the top of the tank as the density increases. The pressure change in the vapor region may be assumed to be an isentropic process of an ideal gas with constant specific heat derived from the 2nd Law of Thermodynamics (Cengel and Boles 2008). This relationship is provided in Equation (65).

$$\left(\frac{P_2}{P_1}\right)_{s=const} = \left(\frac{\rho_2}{\rho_1}\right)^s \tag{65}$$

Appendix I explains the iterative process used to calculate the time required to build the pressure from 400 kPa to 500 kPa. It was assumed that the ratio of specific heats was constant during each time step. The density, pressure, temperature, and ratio of specific heat were re-calculated at the end of each time step and used in the next time step. It is important to stress that the results calculated using Equations (63), (64), and (65) do not produce the actual amount of time required to increase the top tank pressure from 400 kPa to 500 kPa. Rather, the calculated top tank pressure over time will be compared with the measured top tank pressure to see how much the two values deviate. Figure 35 indicates the pressure build up in the top of the tank versus time.
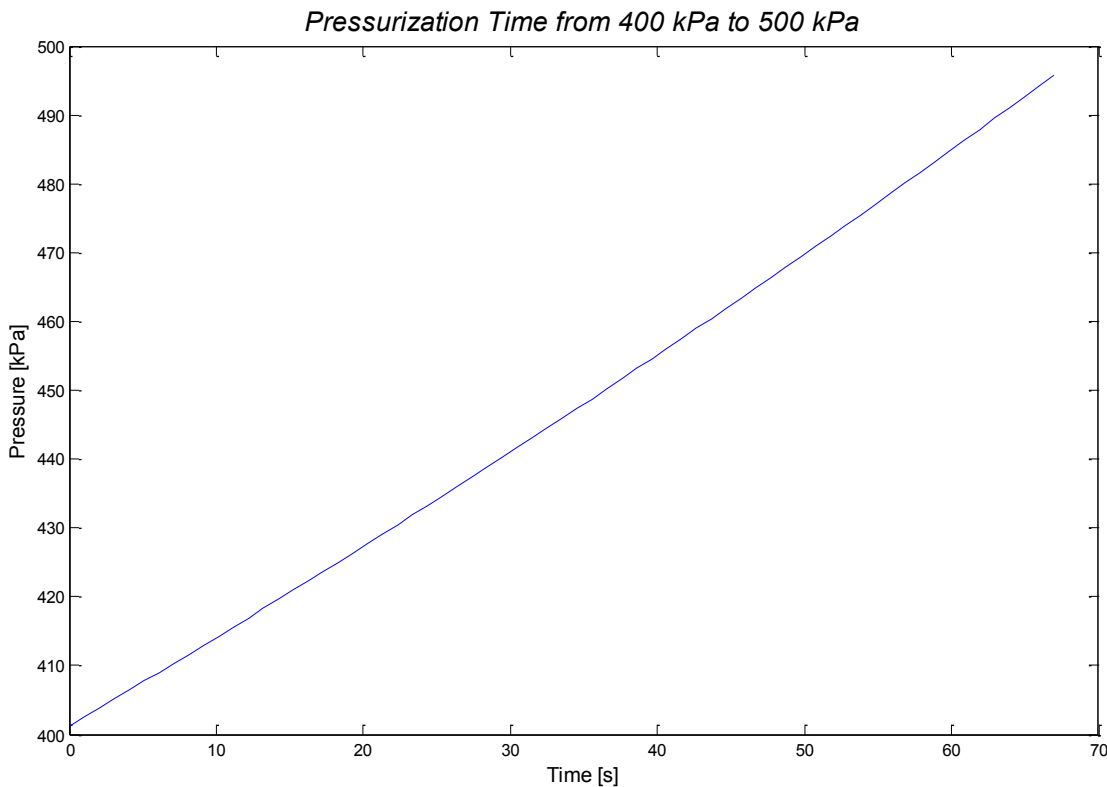
Figure 35: Top Tank Pressurization Time

The MATLAB code for the process described in this sub-section is provided in Appendix J. Using the initial conditions shown in Table 17, the change in tank pressure from 400 kPa to 500 kPa took 67 seconds. The next sub-section will validate the assumption that the change in volume due to the LNG draw from the PBU and EVAP is negligible.

5.2.2 Constant Volume Assumption
This sub-section accesses the validity of negating the liquid and vapor volume change in the pressurization calculations. The effect of the PBU and EVAP will be considered. Each of these

situations is calculated within the pressurization time, 67s, which was estimated in the previous sub-section.

The expression for the change in liquid and vapor volume is provided in Equation (66).

$$V_{heel}(t) = \left(m_{heel,i} - \int_0^t \dot{m}_{engine}\,dt - \int_0^t \dot{m}_{PBU}\,dt \right) / \rho_{heel} \tag{66}$$

Notice that the effects of condensation and evaporation were negated. Since the overall volume of the LNG tank will remain unchanged, the changing volume of the vapor in the LNG tank may be calculated using Equation (67).

$$V_v(t) = V_{tank} - V_{heel}(t) \tag{67}$$

The fuel consumption versus power produced graph for the GS 16R Mitsubishi gas engines used on KV Bergen is provided in Figure 36.
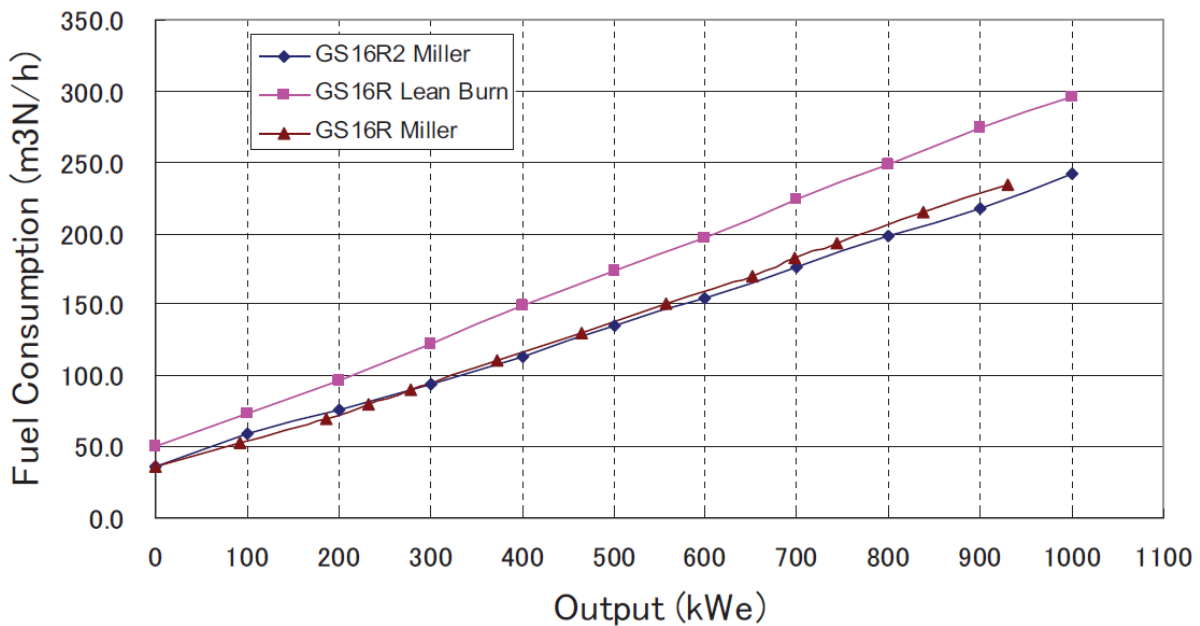
Figure 36: Fuel Consumed vs Power Output on KV Bergen

The first factor considered affecting the vapor and liquid volume in the LNG tank is the phase change in the PBU. Using the assumption that the LNG entering the PBU is completely vaporized, the total mass flow through the PBU during pressurization may be calculated by integrating the changing $\dot{m}_{PBU}$ over the pressurization time. This calculation gives the total liquid mass vaporized in the PBU while the top tank pressure is increased from 400 kPa to 500 kPa. The total mass was calculated to be 0.922 kg (0.0023 m^3 at saturated liquid conditions). This accounts for approximately 0.00002 % of the initial liquid volume in the tank assuming that the LNG tank is half full of saturated LNG of the composition listed in Table 14. These results

58

suggests volume change from the PBU would have a negligible effect on the changing liquid and vapor volume in the LNG tank and may be ignored in pressurization calculations.

The next factor affecting the liquid and vapor volume change in the LNG tank is the liquid draw from the LNG engines. The reported power produced during the de-loading event on KV Bergen will be used to estimate the fuel consumption while the top tank pressure is increasing from 400 kPa to 500 kPa. According to Espeland (2012), KV Bergen was producing 2200 kW leading up to the de-loading event. Assuming that there were three NG engines (nr_{eng}) sharing the load equally, each engine would be consuming approximately $190 Nm^3/hr$ according to Figure 36. This power production level is considered a maximum value and represents a conservative estimate for the amount of liquid vaporized in the EVAP. A simplified way of estimating the liquid draw from the NG engines during tank pressurization is to multiply the time required to pressurize the tank from 400 kPa to 500 kPa by the average fuel consumption for this engine load. This estimation is shown in Equation (68) and using the linearized fuel consumption in Figure 36. Equation (69) uses the ideal gas law to find the volume of the NG directly after it leaves the Vaporizer. Equation (70) uses the conservation of mass to find the mass of the LNG used by the NG engine before and after it is vaporized.

$$\int_0^t \dot{m}_{eng} dt / \rho_{heel} \approx t_{press} \left(W_{eng} \left(\frac{\dot{Q}_{eng,1000kW} - \dot{Q}_{eng,0kW}}{1000kW} \right) + 40 \right) nr_{eng} \approx V_{ng,1} \tag{68}$$

$$\frac{P_{ng,1} V_{ng,1}}{T_{ng,1}} = \frac{P_{ng,2} V_{ng,2}}{T_{ng,2}} \tag{69}$$

$$V_{ng,2} \rho_{ng,2} = V_{lng,3} \rho_{lng,3} \tag{70}$$

Table 18 provides the values assumed for the different states. Since the volume flow presented in Figure 36 is given in normal cubic meters it is assumed that the pressure at state 1 is 1 atm (101.3 kPa) and temperature is 0 C (273 K).

Variable	Value	Units
W_{engine}	733	kW
nr_{eng}	3	[-]
t_{press}	67	s
$\dot{Q}_{engine,1000kW}$	245	Nm^3/hr
$\dot{Q}_{engine,0kW}$	40	Nm^3/hr
$P_{ng,1}$	101.3	kPa
$P_{ng,2}$	450	kPa
$P_{ng,3}$	450	kPa
$T_{ng,1}$	273	K
$T_{ng,2}$	294	K
$\rho_{ng,2}$	3.26	kg/m^3
$\rho_{lng,3}$	407.42	kg/m^3
$V_{ng,1}$	10.6	m^3
$V_{ng,2}$	2.58	m^3
$V_{lng,3}$	0.0206	m^3
$m_{lng,3}$	8.40	kg

Using the assumptions listed in Table 18, it was found that the NG engine drew 8.40 kg of LNG (0.0206 m^3) at sub-cooled bunkering conditions during the 67 second pressurization period. This accounts for approximately 0.000176 % of the initial liquid volume in the tank assuming that the LNG tank is half full of saturated LNG of the composition listed in Table 14. The estimate performed in this sub-section suggests that the volume change caused by the PBU and EVAP may be ignored during shorter operations like the pressurization of the LNG tank.

Now that an idealized relationship for the time required to pressurize the LNG tank has been established, it is desirable to know how much the tank pressure is expected to fall. As stated in the hypothesis section, it is probable that the fall in tank pressure which caused the NG engine to de-load was related to either a change in the LNG system introduced during bunkering or disruptions of the liquid surface layer between the vapor and liquid section. This next section will create a model to calculate the maximum fall in tank pressure if the heel in the tank mixes completely with the vapor in the tank. The effects of bunkering will also be considered by creating a relationship for the fall in tank pressure given that the heel, bunkered LNG, and vapor mix together completely.

5.3 Mixing Calculations
This section uses a simple energy and mass balance to calculate tank conditions after the LNG and vapor in the tank have mixed together completely. Similar to the previous sub-section, these calculations represent an idealized situation which may deviate from what actually occurs in the

tank. The results from the calculations in this sub-section will be compared with the data from the measurement campaign to assess how much mixing actually occurs between the LNG and NG inside the tank.

5.3.1 Two Layer Mixing

This subsection considers the situation where the liquid heel mixes completely with the vapor in the tank. It is assumed in these calculations that the heel is sub-cooled below the bubble point. This situation represents the status of the LNG tank a certain amount of time after bunkering where the bunkered LNG has mixed completely with the heel in the tank. The extent that the heel is sub-cooled will be determined during the measurement campaign. To simplify calculations, complete mixing is assumed to occur independent of time. Before constructing a set of equation for the heat and mass balance in the tank, a number of assumptions must be made.

5.3.1.1 Two Layer Mixing Assumptions

This sub-section outlines the assumption used to estimate the conditions inside the LNG tank after complete mixing between the vapor and liquid in the tank has occurred. The following assumptions were made:

- Complete mixing occurs between the liquid heel and vapor.
- Mixing time is not relevant.
- The initial vapor temperature and pressure is 294 K and 500 kPa, respectively.
- The molar composition of the NG changes during the mixing process.
- The molar composition of the LNG in the tank changes very little and may be assumed constant.
- The PBU is not affecting the pressure or temperature in the LNG tank during mixing.
- The EVAP is not affecting the pressure or temperature in the LNG tank during mixing.
- There is no heat leakage into the LNG tank from the surroundings.
- The volume occupied by the liquid and vapor does not change during mixing.
- After mixing, the liquid and vapor in the tank are at the same temperature.
- The effect of static liquid and vapor pressure are negligible.

Using these assumptions, a set of governing equations may be developed in the next sub-section.

5.3.1.2 Governing Equations

Equations for the Conservation of Energy and Conservation of Mass were used to calculate the total amount of energy and mass existing in the system before and after mixing occurred.

The initial energy in the LNG tank is given by Equation (71).

$$E_{tank,i} = V_{heel,i}\rho_{heel,i}(T_{heel,i}, P_{heel,i})h_{heel,i}(T_{heel,i}, P_{heel,i}) + V_{v,i}\rho_{v,i}(T_{v,i}, P_{v,i})h_{v,i}(T_{v,i}, P_{v,i})$$ (71)

The initial mass in the LNG tank is given by Equation (72).

$$m_{tank,i} = V_{heel,i} \rho_{heel,i}(T_{heel,i}, P_{heel,i}) + V_{v,i} \rho_{v,i}(T_{v,i}, P_{v,i}) \tag{72}$$

The total tank volume is related to the liquid and vapor volume in Equation (73). Note that the volume in the LNG tank, V_{tank}, is a fixed value.

$$V_{tank,i} = V_{heel,i} + V_{v,i} \tag{73}$$

Table 19 provides the assumed initial conditions inside the LNG tank. Note that the initial liquid heel temperature is varied in these calculations. Within the MATLAB program created for these calculations, different initial heel temperatures are tested by changing the amount of sub-cooling based on a reference temperature. A reference temperature was calculated based on the bubble point temperature of the LNG composition listed in Table 14 at 500 kPa. This reference point temperature was calculated to be -137.1°C (135.9 K). The initial liquid sub-cooling is indicated based on this reference temperature.

<div align="center">

Table 19: Initial Tank Conditions 2 Layers Mixing

Variable	Value	Units
V_{tank}	234	m^3
$T_{v,i}$	294	K
$P_{v,i}$	500	kPa

</div>

After determining the initial temperature, pressure and composition of the liquid heel, the initial composition of the vapor may be determined. The composition of the vapor was calculated using Raoult's law which is provided in Equation (74) (Cengel and Boles 2008). Equation (74) recognizes the relationship between the mole fraction of a specific compound in the vapor region, $y_{mol,v}$, the mole fraction of a specific compound in the liquid region, $y_{mol,l}$, the total vapor volume, $P_{tot,v}$, and the saturation pressure of a specific compound at the interface temperature, $P_{mol,sat}(T_{inter})$. During mixing calculation, the interface temperature between the liquid and the vapor becomes the same as the temperature throughout the entire tank.

$$P_{mol,v} = y_{mol,v} P_{tot,v} = y_{mol,l} P_{mol,sat}(T_{inter}) \tag{74}$$

The initial composition of the vapor in the tank at the conditions listed in Table 19 is provided in Table 20 to illustrate that the vapor composition is different than the liquid composition in the tank. As stated in the assumptions, the initial liquid composition, $y_{mol,l}$, of the different components were assumed to the same throughout the mixing process. The vapor composition at the end of each mixing calculation was found to be different from the initial vapor composition listed in Table 20. As expected, the combined mole fractions of lighter components (e.g. N2, CH4, and C2) are higher in the vapor region than the liquid region.

Table 20: Vapor Composition at 294 K and 500 kPa

Composition	Mole Fraction
Nitrogen	0.034
Methane	0.9149
Ethane	0.0501
Propane	9.729E-4
Butane	1.762E-5
Pentane	1.917E-6

After considering the changing composition of the vapor before and after mixing, a set of relationships were developed to calculate the tank energy before and after mixing. One of the features of NIST REFPROP is the ability to calculate both liquid and vapor enthalpy, density, and pressure for mixtures. This feature was used in the calculations described in this sub-section. These calculations assumed that mixing caused the liquid and vapor layers to transfer heat and mass with one another until both layers were at the same temperature. The final temperature of the liquid and vapor in the tank was related to the vapor pressure using the ideal gas law. A new vapor pressure was calculated within each iterative loop of the MATLAB code. The MATLAB code used to calculate the final temperature and pressure during these mixing calculations is provided in Appendix K. Within the MATLAB code, a forward loop uses an initial guess for the final temperature in the tank. This temperature guess is used to calculate the enthalpy and density of the liquid and vapor in the LNG tank after mixing. If the calculated energy and mass is lower than a certain tolerance from the initial energy and mass then the final temperature guess is increased by a small amount and the total tank energy and mass is calculated again in a forward loop. This process continues until the final energy and mass in the LNG tank matches the initial energy and mass. This assumptions is reflected in Equations (75), (76), and (77) shown below.

The final energy is the LNG tank is given by Equation (75).

$$E_{tank,f} = V_{heel,f}\rho_{heel,f}(P_{v,f}, T_f)h_{heel,f}(P_{v,f}, T_f) + V_{v,f}\rho_{v,f}(P_{v,f}, T_f)h_{v,f}(P_{v,f}, T_f) \tag{75}$$

The final mass in the LNG tank is given by Equation (76).

$$m_{tank,f} = V_{heel,f}\rho_{heel,f}(P_{v,f}, T_f) + V_{v,f}\rho_{v,f}(P_{v,f}, T_f) \tag{76}$$

Similar to Equation (73), the final heel volume and vapor volume is related to the total tank volume which remains constant through the mixing calculations. This relationship is provided in Equation (77).

$$V_{tank,f} = V_{heel,f} + V_{v,f} \tag{77}$$

These mixing calculations are visually portrayed in Figure 37.
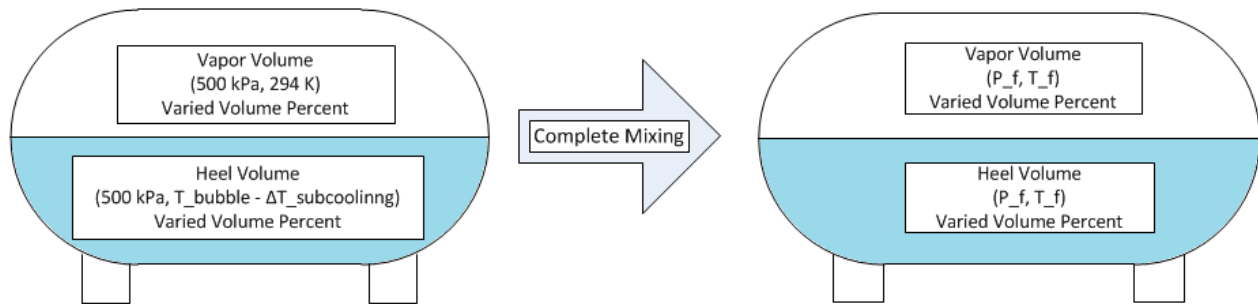
Figure 37: 2 Layers Mixing

The next sub-section provides the results of this model and discusses what may be inferred from the results.

5.3.1.3 Calculation Results

Using the governing equations provided in the previous sub-section, mixing calculations were performed over a certain span of sub-cooled temperatures relative to the liquid bubble point temperature. The results from the mixing of the liquid heel and vapor layers are showed in Figure 38 and Figure 39. The initial liquid bubble point temperature using the LNG composition in Table 14 at 500 kPa was -137.1°C (135.9 K). As mentioned in the previous sub-section, the initial energy and mass of the vapor were calculated using the initial conditions listed in Table 19 (294 K, 500 kPa). All results shown in Figure 38 and Figure 39 come from these same initial vapor conditions. The curves in Figure 38 and Figure 39 indicate a relationship between the initial liquid temperature of the heel and the calculated fall in vapor pressure and temperature.
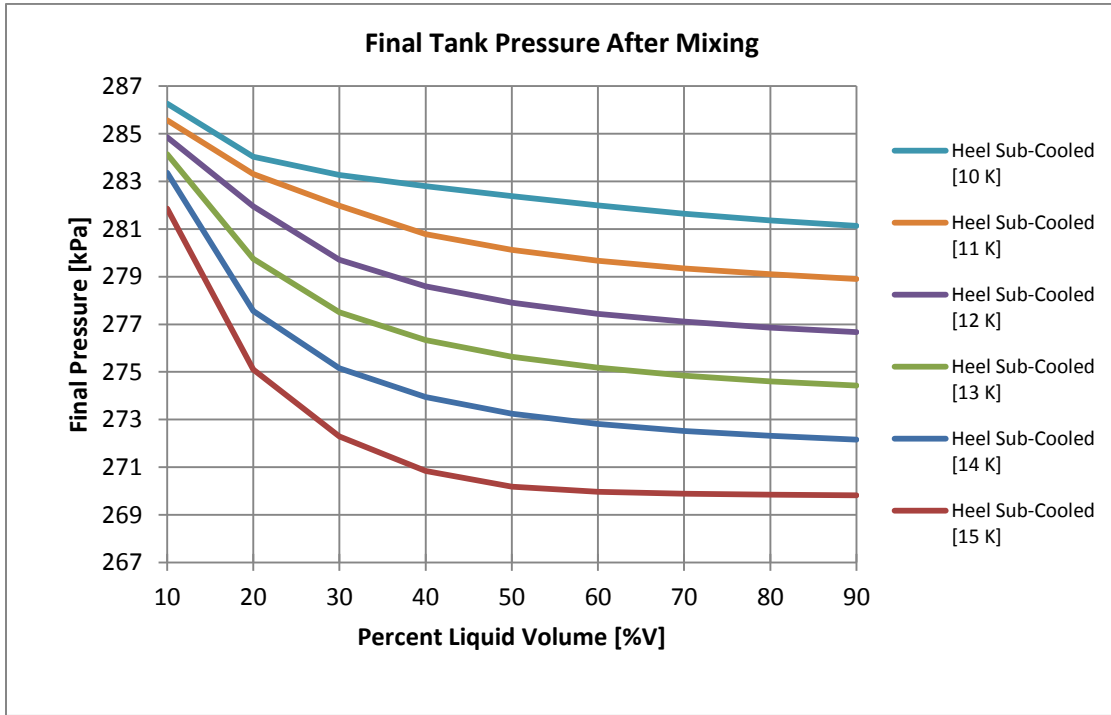
Figure 38: Final Tank Pressure Mixing Calculations
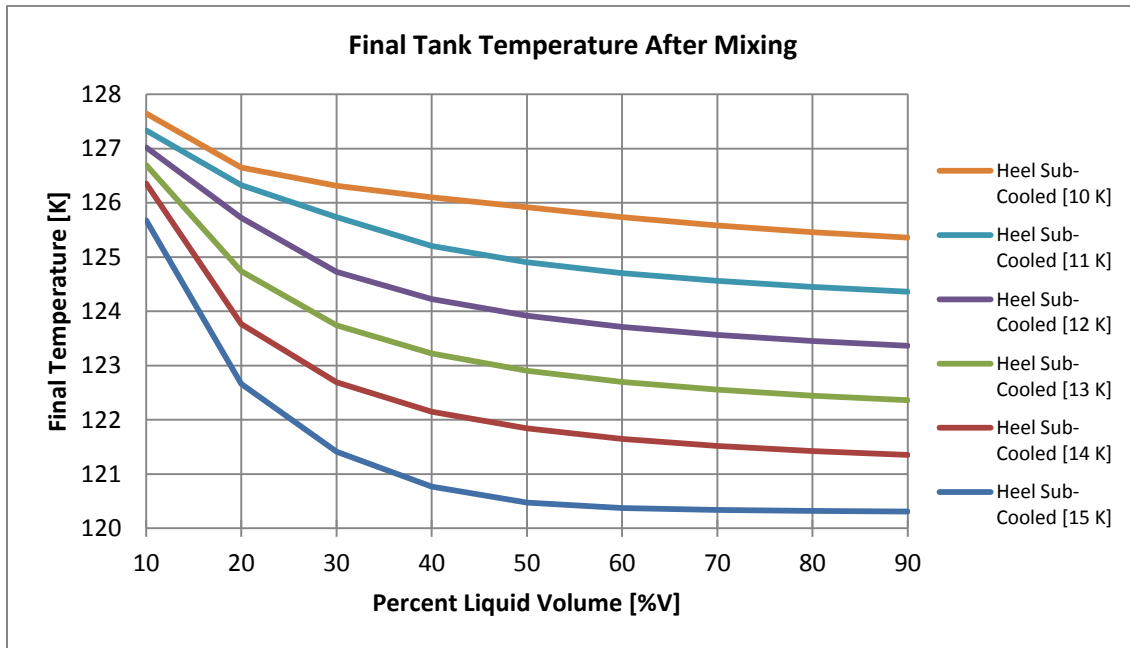
Figure 39: Final Tank Temperature Mixing Calculations

The range of initial liquid heel temperatures, between 10 and 15 K below the liquid bubble temperature, were chosen because they covered the measured heel temperature which will be discussed in the Data Acquired chapter. As shown in Figure 38, the final pressures for all the selected combinations fall below the 350 kPa de-loading pressure. These results suggest that if the contents of the LNG tank are completely mixed over a long period of time then the tank pressure criteria will be met causing a de-loading event. This suggests NG engine de-loading can results from liquid and vapor mixing in the tank. It is uncertain, however, how much of the liquid and vapor mix with one another in different situations. The extent of liquid and vapor mixing will be explored in the Results and Discussion chapter.

The results presented in this section represent the lowest possible temperature and pressure which may be achieved in an isolated LNG tank given certain initial conditions. This sub-section has developed a set of governing equations for the two layer mixing case. These equations must be modified to include the cooling influence of the bunkered LNG in order to adequately reflect the LNG tank conditions directly after bunkering. The next sub-section develops an additional set of equations which will be used in the Results and Discussion section to calculate the total possible fall in tank pressure due to complete mixing of the liquid and vapor in the LNG tank.

5.3.1.4 Three Layers Mixing

Three layers mixing calculations involve an additional dimension compared to the two layer mixing calculations. In three layers mixing calculations, the bunkered LNG, liquid heel, and NG vapor mix completely with one another. This situation represents the period directly after bunkering has occurred. It is assumed that external forces have caused the three different liquid and vapor phases in the tank to interact with one another.

Similar to the previous subsection, the equations for the Conservation of Energy and Conservation of Mass were used to calculate the total amount of energy and mass existing in the system before and after mixing occurred. The initial energy in the LNG tank is given by Equation (78). The third term in Equation (78) accounts for initial energy of the LNG delivered during bunkering.

$$E_{tank,i} = V_{heel,i}\rho_{heel,i}h_{heel,i}(T_{heel,i}, P_{heel,i}) + V_{v,i}\rho_{v,i}h_{v,i}(T_{v,i}, P_{v,i}) \\ + V_{sc,i}\rho_{sc,i}h_{sc,i}(T_{sc,i}, P_{sc,i})$$

(78)

The initial mass in the LNG tank is given by Equation (79).

$$m_{tank,i} = V_{heel,i}\rho_{heel,i} + V_{v,i}\rho_{v,i} + V_{sc,i}\rho_{sc,i}$$

(79)

The total tank volume is related to the liquid and vapor volume in Equation (80). Note that the volume in the LNG tank, V_{tank}, is a fixed value.

$$V_{tank,i} = V_{heel,i} + V_{v,i} + V_{sc,i}$$

(80)

The final energy is the LNG tank is given by Equation (81). The final liquid volume in Equation (81) combines the bunker and heel liquid volumes (e.g. $V_{l,f} = V_{heel,i} + V_{sc,i}$).

$$E_{tank,f} = V_{l,f}\rho_{l,f}(P_f,T_f)h_{l,f}(P_f,T_f) + V_{v,f}\rho_{v,f}(P_f,T_f)h_{v,f}(P_f,T_f) \tag{81}$$

The final mass in the LNG tank is given by Equation (82).

$$m_{tank,f} = V_{l,f}\rho_{l,f}(P_f,T_f) + V_{v,f}\rho_{v,f}(P_f,T_f) = m_{tank,i} \tag{82}$$

Similar to the two layer mixing calculations, the final heel volume and vapor volume is related to the total tank volume which remains constant through the mixing calculations. This relationship is provided in Equation (83).

$$V_{tank,f} = V_{l,f} + V_{v,f} \tag{83}$$

The MATLAB program created to calculate the fall in tank pressure from three layers mixing was modified from the code provided in Appendix K. This calculation methodology will be used in the Results and Discussion chapter to determine the total fall in tank pressure possible using measurements discussed in the Data Acquired chapter.

The methodology presented in this sub-section does not completely consider all the different factors leading to a de-loading event. One major relationship missing from this analysis is the connection between mixing time and extent of mixing between the liquid and vapor. Another major link missing is an understanding of what conditions (internal or external to the LNG system) will cause tank mixing to occur. These factors are necessary to determine if the PBU will be able to maintain a certain pressure in the tank while mixing of the liquid and vapor inside the tank cause the existing vapor in the tank to condensate. The Results and Discussion chapter provide a simplified calculation methodology to test whether the de-loading event will occur when the surface area between the liquid and vapor and liquid surface layer thickness are altered. The next sub-section in this chapter explores the gliding evaporating temperature in the Vaporizer which will be used to confirm some values obtained in the measurement campaign.

5.4 Gliding Evaporation Temperature in Vaporizer

This section considers the gliding evaporation temperature of LNG in the Vaporizer. Since LNG is made of a number of components with different fluid properties, the temperature over which evaporation occurs in the Vaporizer will change throughout the process. In the EVAP and PBU, it may be assumed that the composition of the LNG entering both circuits is the same composition of the NG leaving both circuits. This assumption is not valid for evaporation or condensation occurring in the LNG tank and is an important distinction to maintain while evaluating each sub-system. To better understand the gliding temperature at which evaporation occurs inside the Vaporizer circuits (EVAP and PBU) a saturation curve was produced in NIST REFPROP using the LNG composition listed in Table 14. This saturation curve is provided in Figure 40. Different

iso-bars were selected for the curve in Figure 40 to illustrate the gliding evaporating temperatures at certain pressures.
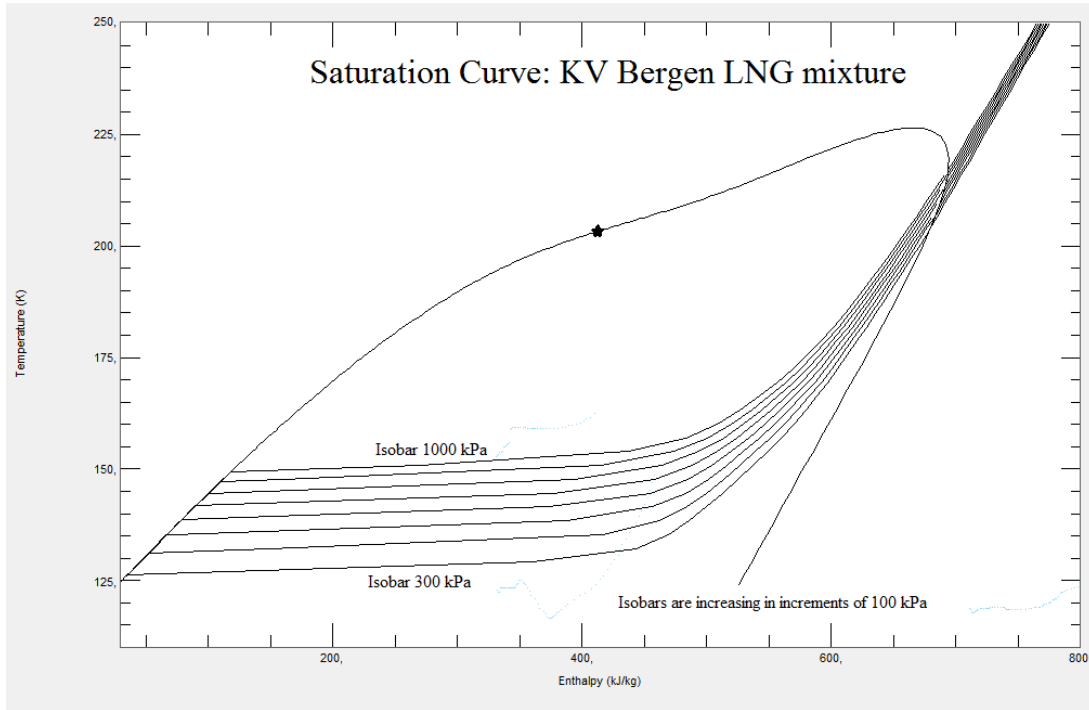
Figure 40: LNG Gliding Evaporation Temperature

The temperature difference between the bubble point and dew point is provided in Table 21 for a range of different isobars. This information provides the temperature rise required in the PBU and EVAP for the LNG to be fully vaporized.

Table 21: Bubble Point and Dew Point at certain Pressures (KV Bergen)

Isobar [kPa]	Bubble Point [K]	Dew Point [K]	Temperature Rise [ΔK]
200	119.91	199.37	79.46
250	123.32	201.77	78.45
300	126.24	203.76	77.52
350	128.82	205.46	76.64
400	131.14	206.94	75.80
450	133.25	208.26	75.01
500	135.19	209.44	74.25

The information provided in Table 21 will be compared with temperature measurements of NG leaving the PBU and EVAP in the measurement campaign to confirm the assumption that the NG is superheated in the Vaporizer. This information will also be used to confirm the assumptions used to calculate the PBU mass flow rate and tank pressurization time.

5.5 Chapter Conclusion

Calculations were performed in this chapter to gain a better understanding of how the different sub-components in the LNG system on KV Bergen and MF Korsfjord behave during normal and extreme circumstances. The first sub-section developed a set of relationships which may be used to estimate the mass flow rate from the PBU given different operating conditions in the LNG tank. This information will be compared to measured PBU mass flow rates in the Data Acquired chapter to determine whether the approach taken to calculating the PBU mass flow rate in this chapter was accurate. In the Results and Discussion chapter, the PBU mass flow rate will be compared to the rate of condensation caused by disruptions of the surface layer to determine if the tank pressure will rise or fall over time.

The second calculation performed in this section determined the amount of time required to pressurize an idealized LNG tank. This calculation will be compared to the actual time required to pressurize the tank. In the Results and Discussion chapter, the difference between the idealized pressurization calculations and the actual pressurization time will be used to determine the amount of condensation occurring when the tank is not disturbed.

The third calculation performed shows the lowest possible fall in tank pressure achievable from two layer mixing. A separate set of equations were created for a LNG tank with three layers (heel, bunkered LNG, and vapor). In the Results and Discussion chapter, this methodology will be used to determine the extent of mixing in the LNG tank based on results gathered during the measurement campaign.

The fourth calculation will be used to determine if the NG leaving the Vaporizer is above the dew point temperature and if the LNG entering the Vaporizer is below the bubble point temperature. These values will be used to confirm the measurements gathered in the Data Acquired chapter.

6. Data Acquisition

This chapter analyzes and discusses the data collected onboard MF Korsfjord and KV Bergen during the measurement campaign. The date each measurement took place is indicated using symbols (E1, E2, E3, and E4) established in Table 10. Data presented in this chapter is organized into sections by sub-components of the LNG system (e.g. LNG, EVAP, and PBU). At the end of each section, there is a discussion of the interpretation of the data collected in each section. The focus of this chapter is to provide data supporting the calculations on the PBU mass flow rate, pressurization time, and initial and final tank conditions after bunkering. In the Results and Discussion chapter, the data analyzed in this chapter will be used with calculations performed in the Modeling and Calculations chapter to determine if the PBU is able adequately maintain tank pressure while tank sloshing and mixing causes vapor condensation.

6.1 LNG Tank

The data presented and analyzed in this section will focus on conditions in the LNG tank before, during, and after bunkering. The first sub-section will focus on the temperature and composition of the heel before bunkering. The second sub-section will focus on the temperature and composition of the vapor before bunkering. The third sub-section explores the conditions of the LNG delivered to the ship's LNG tank during bunkering. The final sub-section considers the changing conditions in the tank when the heel mixes with the LNG introduced during bunkering. At the end of this section, implications of the changing conditions in the LNG tank related to NG engine de-loading are discussed.

6.1.1 Initial Heel Temperature

A number of different measurements were taken to calculate the temperature, pressure and composition of the vapor and heel in the LNG tank before bunkering. The first set of data considers the physical properties of the liquid heel before bunkering. Two separate methods were used to obtain the liquid heel temperature. The first method, which may be called the "purge method", sought to indirectly obtain the liquid heel temperature while the vapor was purged from the ship's LNG tank before bunkering. The second methods, which may be called the "instrument flush method", directly measured the LNG which was used to clean the cryogenic measuring equipment.

The "purge method" was employed during measurements E3 and E4 in an attempt to indirectly obtain the heel temperature. In preparation for this measurement, 4 K-type thermocouples were placed equidistance around the top filling bunkering piping leading to the LNG tank. The top filling bunkering pipe is labeled as item 2 in Figure 41. Before bunkering, the standard practice onboard MF Korsfjord and KV Bergen is to inert all piping which will handle LNG with NG from the top of the ship's LNG tank. This is done to remove any impurities from the piping before bunkering. A full description of the preparation undertaken before the bunkering process is provided in Appendix D.

During the purging process, it is possible that the tank pressure may be lowered to the evaporation pressure. At the evaporation pressure, the liquid surface of the LNG tank is assumed to be at its bubble point condition. If the bubble point pressure is measured during purging it may be used to find the bubble point temperature which corresponds to the top liquid layer in the ship's LNG tank. Before conducting the measurement, the amount time required to purge NG from the tank was calculated. The methodology used to estimate the maximum amount of time required to purge the tank is provided in Appendix L.

The top fill bunkering pipe temperature and tank pressure for measurement E3 is shown in Figure 42. Note 1 in Figure 42 refers to the moment when NG purging began at second 20 (i.e. HV 102 was opened). Note 2 at second 35 marks the time that the vapor temperature and pressure reached a relatively horizontal value. Presumably, this is the point during the purge where the evaporation pressure is achieved. Note 3 at second 90 denotes the time when the main value on the top fill bunkering line, HV 102, was closed. Between the period of time marked in Note 2 and 3, the average NG temperature was -44.47°C (228.53 K) and the average tank pressure was 4.719 bara. The recorded temperature rises slightly after Note 3 because the thermocouples are located upstream of HV102. When HV 102 is closed, the vapor contents of the top filling bunkering line is warmed slightly by heat leakage which accounts for the slight rise in temperature before LNG flows through the pipes and drives the recorded temperature down again. These results from this method will be evaluated at the end of this sub-section to determine if data recorded during tank purging is able to provide the heel liquid surface temperature.

The "instrument flush method" was employed during E4 to measure the liquid heel temperature directly. In preparation for the "instrument flush method", 2 K-type thermocouples were placed on the short section of exposed pipe where the tubing for the cryogenic instrument flush protrudes from the LNG tank. It was not possible to take a picture of the location and set up for the instrument flush method because it was difficult to obtain a camera that met Ex Zone 1 criteria. A diagram of the general location of the instrument flush line is shown with an arrow in Figure 43. A discussion with the Chief Engineer on KV Bergen revealed that the instrument flush was completed approximately twice a year. To flush the cryogenic instruments, valve V56 (shown in Figure 43) was opened manually within the Cold Box. During E4, the Chief Engineer held V56 open until the lowest surface temperature of the instrument flush piping was recorded. The data from the instrument flush method is presented in Figure 44. Note 1 in Figure 44 at second 89 denotes the moment V56 was opened and the instrument flush began. Note 2 at second 129 denotes the time the lowest pipe surface temperature was recorded. Note 3 at second 248 denotes the moment V56 is fully closed and the instrument flush was concluded. Before the instrument flush was conducted, V56 was opened briefly to insure that the flushing system still was operational since the last flush. This is the reason why the temperature before note 1 in Figure 44 is below ambient temperature. The entire duration of the instrument flush was 159 seconds and the lowest pipe surface temperature recorded was -148.748°C (124.252 K). The

information inferred from the data collected using the instrument flush method will be discussed at the end of this sub-section.
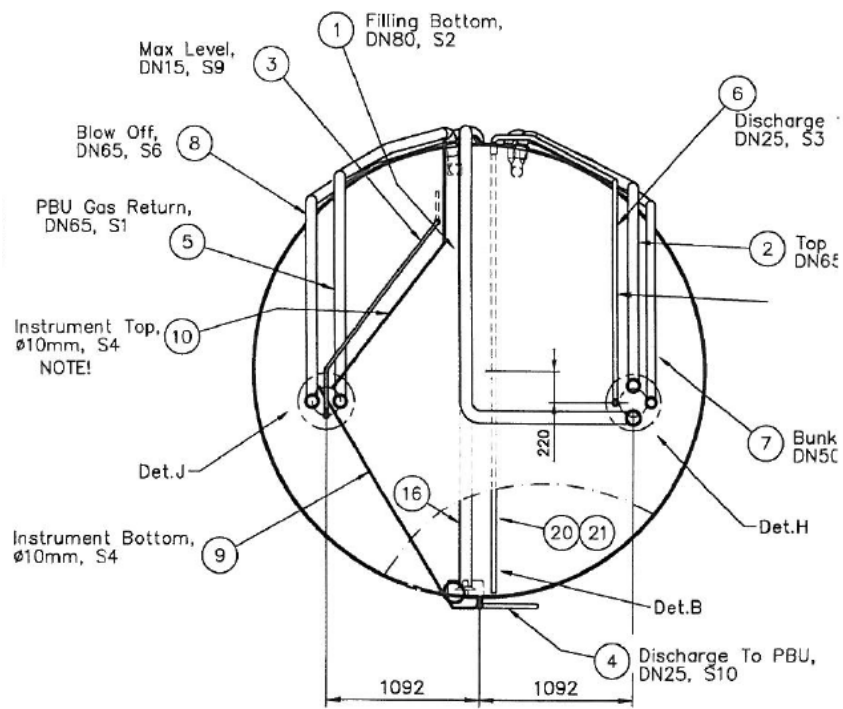
Figure 41: Head Profile Inner Tank on MF Korsfjord
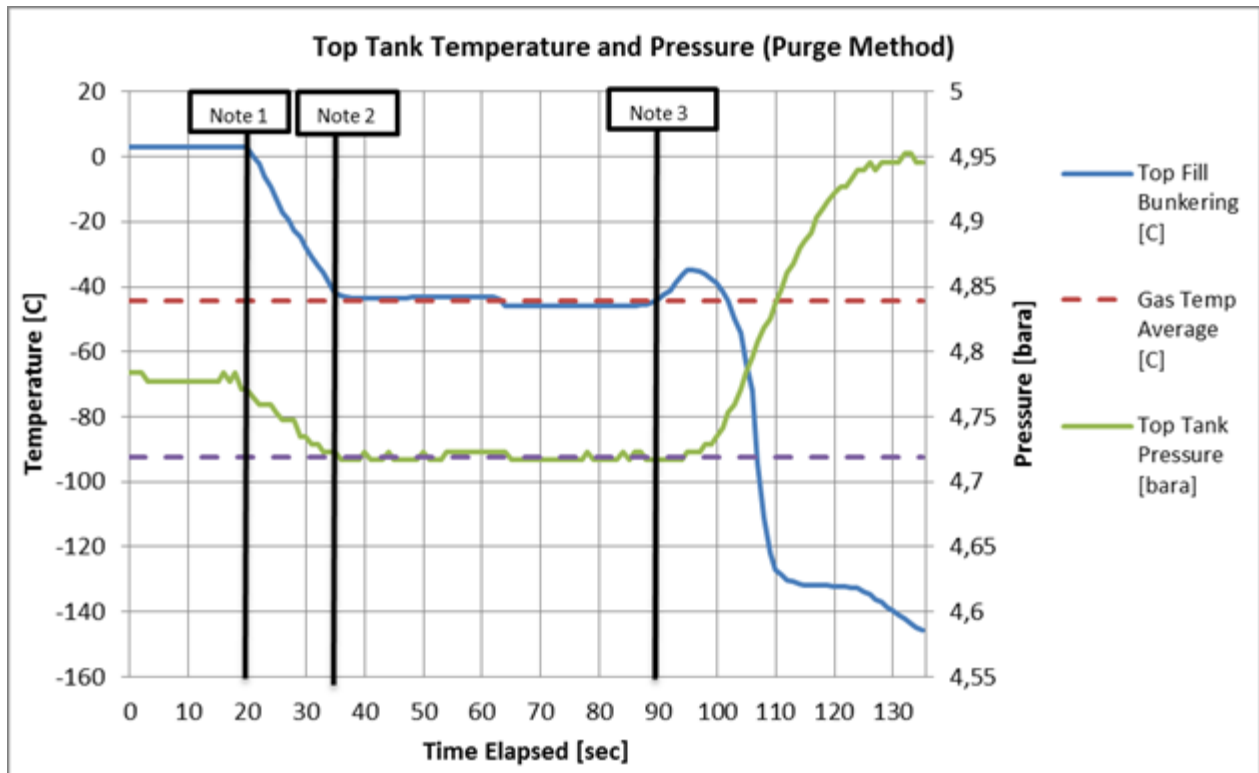
Figure 42: Top Tank NG Temperature and Pressure during E3
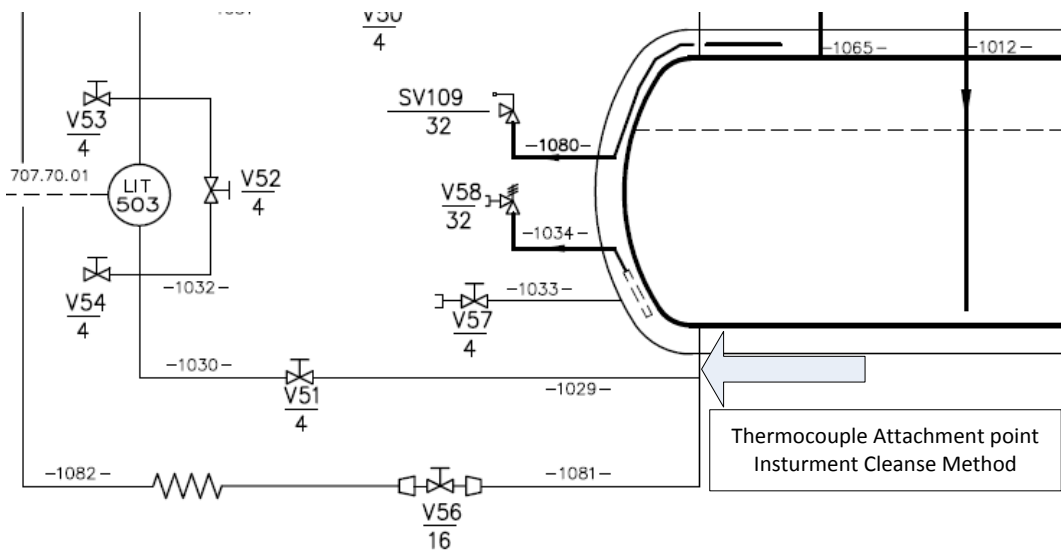
Figure 43: Thermocouple Attachment Point Instrument Cleanse Method
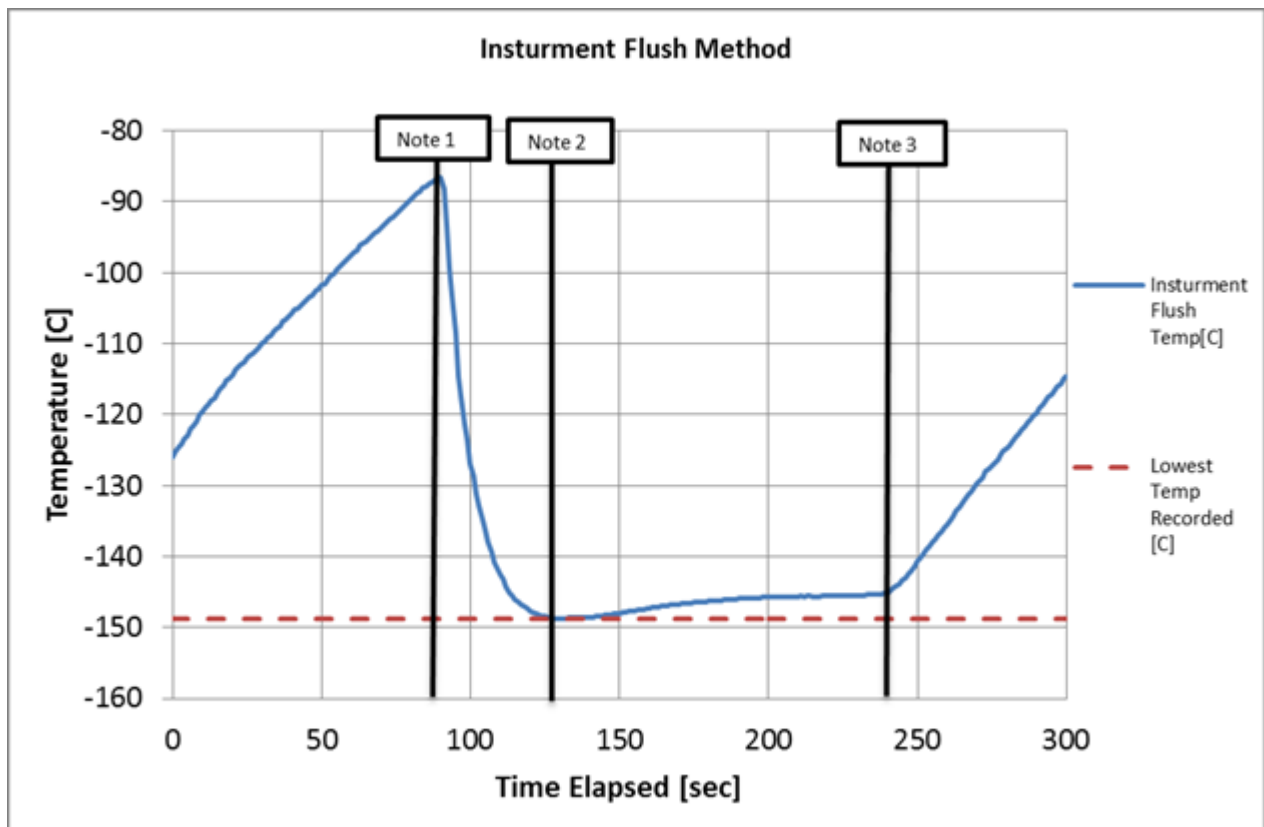
Figure 44: Instrument Flush Piping Temperature during E4

Both the purge method and the instrument flush method allow the temperature of the liquid surface layer and the bulk heel to be measured before bunkering. The purge method is best suited to provide the liquid surface temperature. Scurlock found, as noted in the Literature Review, the liquid surface layer in the tank exists at the bubble point temperature corresponding to the saturation pressure in the tank. Before purging, the pressure in the tank corresponds to the superheated temperature of the vapor pillow established from superheated NG introduced by the PBU. The vapor pressure is brought down to a saturated state during purging. As stated at the beginning of the sub-section, evaporation will commence once the bubble point pressure is reached. This suggests that the approximately constant pressure of 4.719 bara achieved at second 35 (note 2) denotes the bubble point pressure. Using the LNG composition provided in Table 14, it is possible to calculate the liquid bubble point temperature in NIST REFPROP. Calculations reveal that the liquid bubble point temperature at 4.719 bara is -138.88°C (134.12 K). This temperature may be used to approximate the liquid surface temperature in the LNG tank during E3 and is a general indication of the temperature of the liquid surface layer during operation of the LNG system.

The instrument flush method is better suited to determine the bulk heel temperature. Since the thermocouples in E4 were attached directly to the instrument flush pipes they are able to directly measure the LNG drawn from the tank. It may be assumed that the lowest temperature measured, -148.748°C (124.252 K), reveals the liquid heel temperature. One possible reason that the pipe surface temperature increases after the lowest temperature is achieved (Note 2) in Figure 44 is that the temperature recorded by the thermocouple was slightly altered by the formation of frost on the outside of the pipe during the instrument flush. It is possible that this frost acted as a thermal insulator between the thermocouple and pipe surface resulting in a higher measured temperature. Using the bubble point temperatures shown at different iso-bars in Table 21, it may also be concluded that the heel in the LNG tank exists in a sub-cooled state directly before bunkering.

Both the liquid surface temperature and the bulk heel temperature established in this sub-section will be used in the Results and Discussion chapter to illustrate the actual fall in tank pressure from mixing between the liquid heel, vapor, and bunker LNG. These temperatures will also be used to calculate what mixing conditions would cause the pressure in the LNG tank below the NG engine de-loading pressure. The next sub-section will consider data used to determine the initial vapor temperature and composition in the tank before bunkering.

6.1.2 Initial Vapor Temperature
This sub-section evaluates the data acquired to determine the top tank temperature and composition before bunkering. Two separate methods were considered when determining the initial vapor temperature before bunkering. The first method considers using the Trycock temperature to accurately determine the vapor temperature. The second method considers the temperatures recorded during the purging method described in the sub-section above.

During measurement E1, the Trycock temperature was evaluated as a means of determining the vapor temperature. In Figure 41, the Trycock piping is labeled as item 3. A picture the Trycock piping covered in frost in the Cold Box on MF Korsfjord is shown in Figure 45. The primary purpose of the Trycock temperature sensor is to signal a closing of the bunkering valve if the liquid level in the tank goes above a height corresponding to 95% of the tank liquid volume at bunkering conditions. This height is considered the "over-fill limit". The entrance to the Trycock piping is situated so that if the over-fill limit is exceeded LNG will travel down the Trycock piping causing a dramatic drop in temperature recorded by the Trycock temperature sensor. This temperature drop will trigger a closing of bunkering valves HV 101 and HV 102. When MF Korsfjord and KV Bergen are not bunkering, a vapor temperature is recorded by the Trycock temperature sensor. The Trycock temperature recorded during the full duration of E1 is provided in Figure 46. Note 1 corresponds to minute 10 when bunkering from the top of the LNG tank on MF Korsfjord began. Note 2 corresponds to minute 102 when LNG stopped flowing from the bunkering truck to the ship's LNG tank (e.g. the bunkering valves are closed). Note 3 (minute 123) corresponds to when the tank reaches a relatively constant pressure. Note 4 at minute 481 indicates when the PBU began to increase the tank pressure before the NG engines were started. Note 5 refers to the moment the NG engines were started at minute 500. Finally, Note 6 refers to a period where the tank pressure rises and falls during the operation of the vessel. The accuracy of the Trycock temperature sensor in providing the vapor temperature will be evaluated at the end of this sub-section.

The other method of determining the vapor temperature considers the temperature recorded during the purge method. Unlike the assessment of the heel temperature and composition, it is not valid to assume that the vapor composition is the same as the LNG composition listed in Table 14. It is possible, however, to estimate the composition of the vapor in the top of the tank using the same relationship from the Modeling and Calculations chapter to estimate the vapor composition before mixing. As stated previously, Raoult's Law (Equation (74)) may be used to estimate the vapor composition in a mixed component tank given that the liquid composition, tank pressure, and saturation pressure for each component is known. Assuming the pressure between Note 2 and 3 in Figure 42 provides the bubble point pressure and the liquid composition of the heel is the same as listed in Table 14, the composition of the vapor before bunkering may be calculated. The MATLAB code from Appendix K was used to calculate the vapor composition before bunkering which is provided in Table 22. This calculated vapor composition will be used later in this section to determine the extent of mixing that occurred between the heel, bunkered LNG, and vapor after bunkering.

Figure 45: Trycock piping in the Cold Box on MF Korsfjord
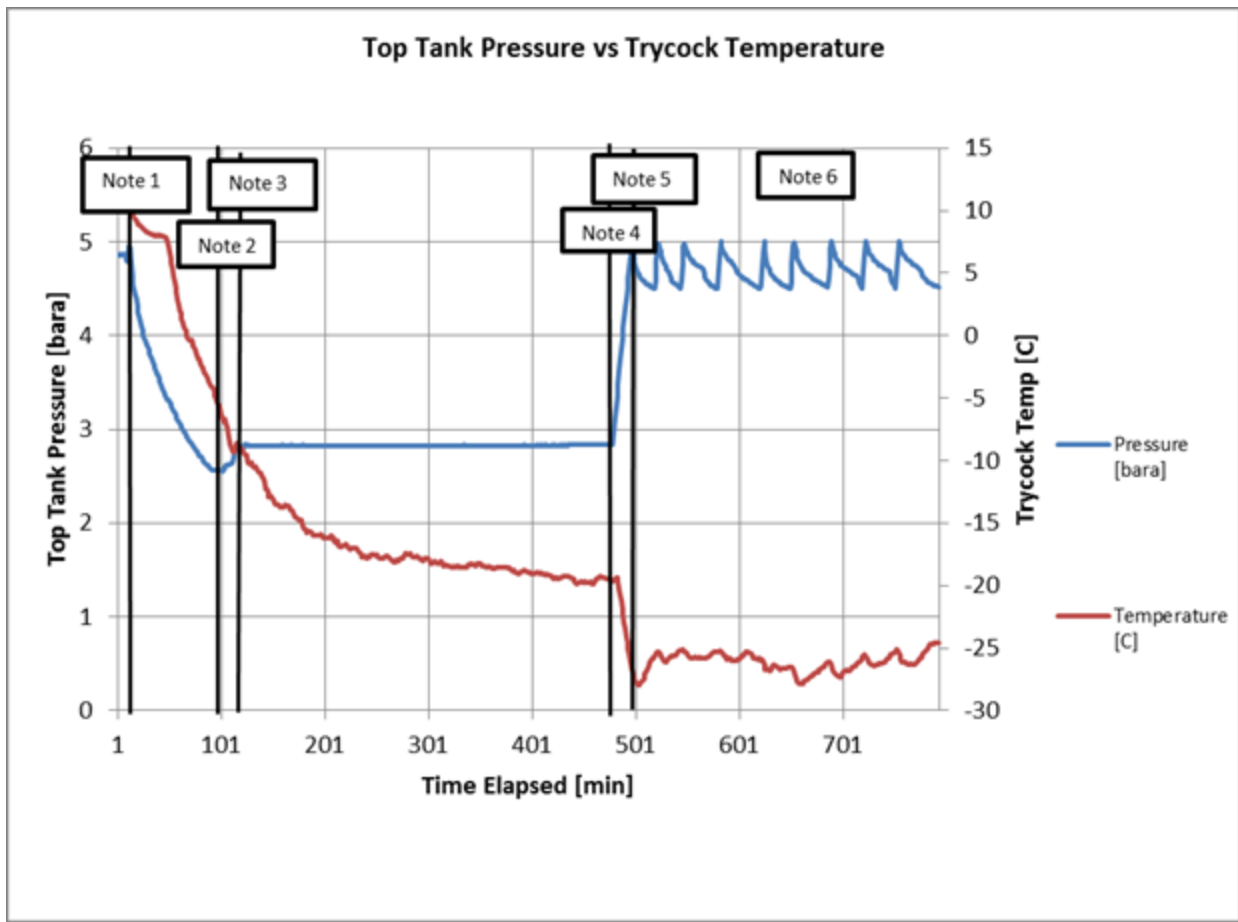
Figure 46: Tank Pressure and Trycock Temperature during E1

Composition	Mole Fraction
Nitrogen	0.0360
Methane	0.9089
Ethane	0.0541
Propane	0.0011
Butane	1.925E-5
Pentane	2.107E-6

The data presented in this sub-section suggest that the NG purging method is more accurate than the Trycock temperature in determining the vapor temperature and composition before bunkering. One of the reasons the Trycock temperature was rejected as an accurate indication of the vapor temperature is that the recorded temperature does not react to changes in pressure as indicated in Figure 46. The most noticeable deviation between the expected change in temperature and pressure is between notes 4 and 5 in Figure 46. As stated earlier, during this period the PBU injects superheated vapor to the top of the tank to build up the tank pressure. During this time span, the vapor temperature is expected to increase while the tank pressure is increasing. Instead, the Trycock temperature falls during this period of time. One explanation why the Trycock temperature does not accurately reflect the vapor temperature is that the piping from the entrance of the Trycock piping to the point where the temperature is measure is too long to accurately reflect the vapor temperature in the tank. For these reasons, the Trycock temperature is rejected as an appropriate method of determining the vapor temperature. Comparatively, the purging method has the benefit of measuring the NG temperature directly as it is being released from the top of the tank. Given these considerations the data from the purging method is selected over the data from the Trycock temperature sensor.

The data from the purging method suggests that the vapor in the top of the tank may be slightly superheated even though the vapor directly adjacent to the liquid surface layer is saturated. Using the asymptotic pressure (4.719 bara) observed in Figure 42, the corresponding bubble point temperature was calculated to be -64.21°C (208.79 K). The asymptotic temperature in Figure 42 between note 2 and 3 is -44.47°C (228.53 K) and approximately 19.7°C warmer than the calculated bubble point temperature. One possible explanation why a superheated temperature was measured in the vapor region during the purge is that there is a thermal gradient in the vapor region. It is possible that the vapor in the top of the tank is superheated while the vapor which exists directly adjacent the liquid surface layer is saturated. Since the opening to the top fill bunkering pipe exists at the top of the LNG tank it is likely that the temperature recorded during the purge method is the superheated vapor at the top of the tank instead of the saturated vapor near the liquid surface. For this reason, the superheated vapor temperature is selected to perform additional calculations.

These first two sub-sections in this chapter established the temperature and composition of the heel and vapor in the LNG tank before bunkering. The next sub-section will consider the temperature of the LNG which is loaded into the ship's LNG tank during bunkering.

6.1.3 Bunker LNG Temperature

In order to examine how the tank pressure changes as a result of bunkering, the temperature of the LNG loaded during bunkering is required. This information was obtained from two different sources: 1) temperature measurements taken from the bunkering truck and 2) temperatures recorded by the top fill bunkering pipe. The information obtained from both sources complement one another and provides a reasonable indication of the bunkering temperature.

The first source examined for the bunker LNG temperature is the bunkering truck tank temperature recorded during E2. The temperature sensor on the bunkering truck is located near the bottom of the tank close to the location of the connection point for the bunkering line. In addition to the installed temperature sensor on the truck, there is a temperature sensor at the bunkering station on MF Korsfjord and KV Bergen where the bunkering hose is connected. Figure 47 illustrates the truck tank temperature, bunkering station temperature, ship tank pressure, and the saturation temperature (bubble point) corresponding to the measured temperature. Within Figure 47, minute 0 refers to the point in time when the bunkering valve at the bunkering stationed was opened. During measurement E2, LNG was only filled from the top of the ship's tank. Note 1 in Figure 47 at minute 77 refers to a slight rise in the recorded temperature at both the truck tank sensor and the bunkering station sensor. The reason for this slight rise in recorded temperature is that the liquid content of the bunkering truck is almost empty and both sensors are recording temperature close to the liquid surface layer. As shown in Figure 16 in the Literature Review, a thermal gradient is expected at the liquid surface in a cryogenic container. The presence of this thermal gradient is captured by the slight increase in recorded bunker temperature near the end of bunkering. The average truck bunker temperature between minute 0 and minute 77 is -153.74 (119.26 K). An assessment of information collected from the bunkering truck and bunker station is provided at the end of this sub-section.

Another source which may provide the LNG temperature during bunkering is the thermocouples attached to the top fill bunkering pipe. The temperature recorded by these thermocouples was used in the previous sub-section for the tank purging measurements. Figure 48 illustrates the pipe surface temperature recorded at the top fill bunkering piping during measurement E3. Note 1 in Figure 48 (minute 2) refers to the moment that the bunkering valve is opened and LNG flows into the ship's tank. Similar to the observation made in the bunkering temperature from E2, a slight rise in bunkering temperature is indicated by note 2 in Figure 48 near the end of bunkering. The average bunker temperature between note 1 and note 2 in Figure 48 is -153.64°C (119.36 K). This average temperature has only a 0.10°C temperature difference between the average temperature recorded within the truck tank. The results from both methods are discussed at the end of the sub-section.
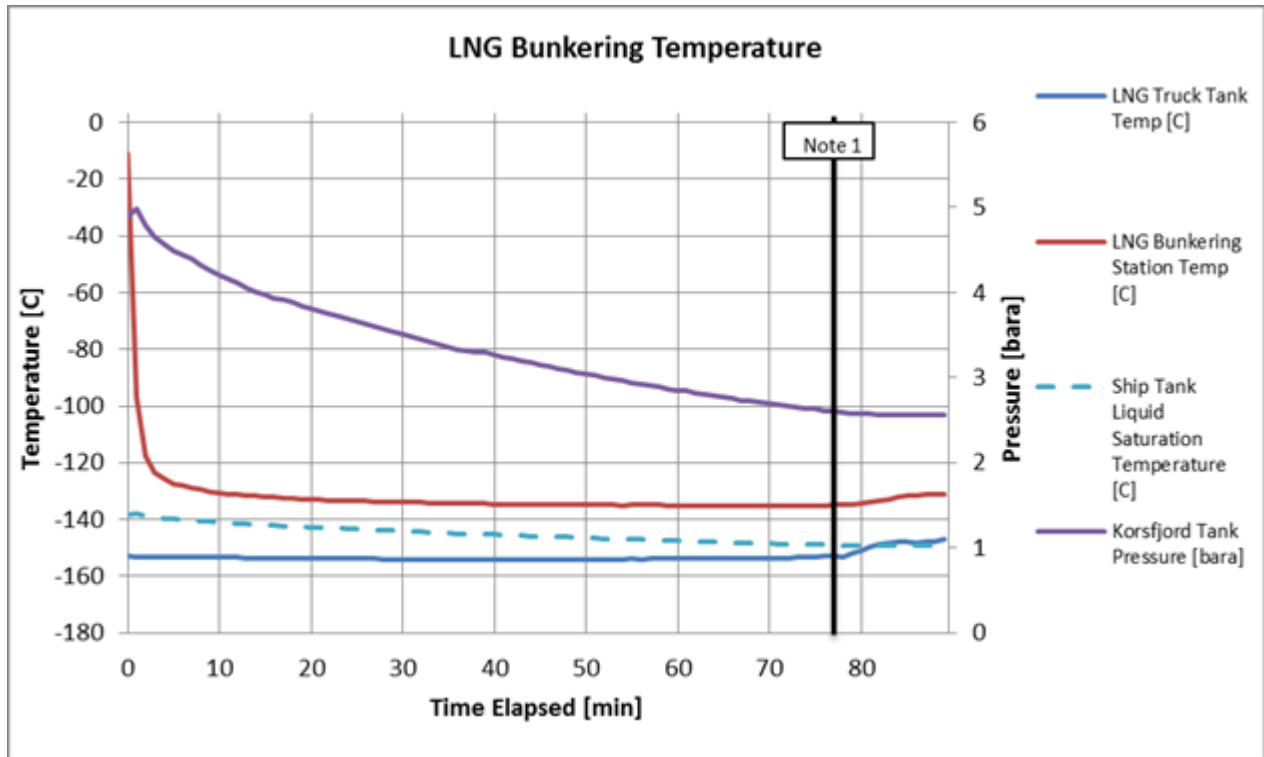
Figure 47: LNG Bunkering Temperature Recorded at LNG truck during E2
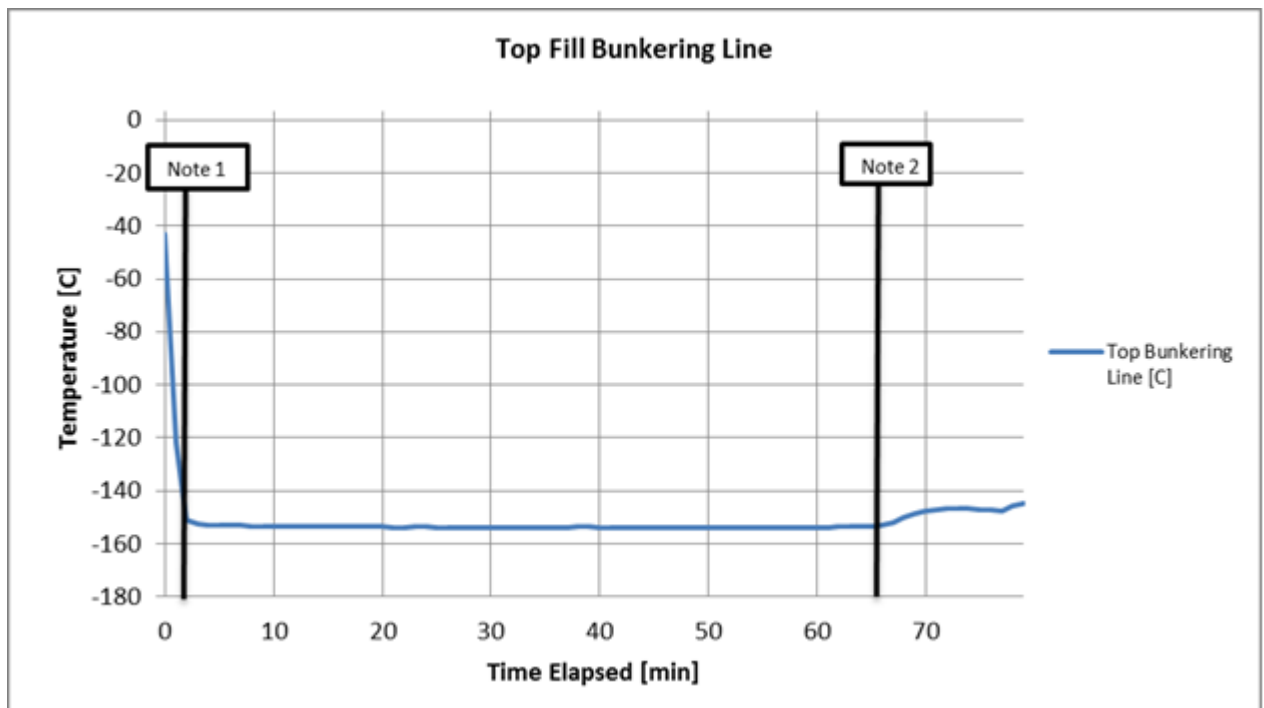
Figure 48: LNG Bunkering Temperature recorded at the top fill bunkering line during E3

Since the top fill bunkering line is closer to the ship's tank, the bunker LNG temperature recorded by the thermocouples attached to the top fill bunkering pipe is selected over the temperature in

the tank truck. One possible reason for the 0.10°C temperature increase between the truck tank temperature and the top fill bunkering pipe temperature is that the LNG is warmed slightly from fluid friction and heat leakage in the bunkering piping.

It may also be concluded that the temperature sensor located at the bunkering station on the deck on the ship, shown as the red line in Figure 47, is not a good indication of the LNG entering the tank during bunkering. One reason this sensor does not accurately reflect the bunker temperature is that it is located above the bubble point temperature which is calculated from the tank pressure. Temperatures above the bubble point suggest the LNG being sent to the tank is two phase, which is not accurate since the pressure in the ship's tank is decreasing during the bunkering process.

From the explanation in this sub-section, a temperature of -153.64°C (119.36 K) is assumed to reflect the LNG temperature introduced during bunkering. A discussion with a Gasnor representative suggested that the composition of the LNG delivered by the bunkering truck changes very little between each bunkering. This suggests that the LNG composition in Table 14 provides an appropriate approximation of the composition of the LNG delivered during bunkering.

The last three sub-sections have established the initial conditions of the heel, vapor, and bunker LNG before bunkering. The next sub-section will analyze the fall in tank pressure when the three components mix. This analysis will determine what percentage of the lowest possible tank pressure established in the Modeling and Calculations chapter actually occurs during bunkering.

6.1.4 Heel and Bunker LNG Mixing

An understanding of the interaction between the heel and bunkered LNG may be gained by observing the tank pressure during and after bunkering. The previous three sub-sections have established the properties of the heel, vapor, and bunker LNG. This sub-section will describe the reaction in the tank when the three components mix.

The interaction between the heel and liquid may be examined using the pressure recorded during and after bunkering in measurement E1. Figure 49 shows the pressure change over a smaller time period than in Figure 46. Note 1 (minute 101) in Figure 49 marks when the valve at the bunkering station closes. At this moment, LNG stops flowing from the bunkering truck to the tank. Directly after the bunkering valve is closed, the pressure in the tank ceases to fall. A slight increase in tank pressure is observed before note 1. This slight rise in tank pressure may be attributed to the warmer LNG near the liquid surface in the bunkering truck which is delivered to the ship's tank near the end of bunkering. At note 2 (minute 112) the top fill bunkering valve (HV 102) is closed. As noted earlier, HV 102 is located close to the LNG tank within the Cold Box. During the period between note 1 and note 2, any remaining liquid in the piping between the valve located at the bunker station and HV 102 is heated because of heat leakages into the uninsulated pipes. Heat leakages cause residual LNG in the bunkering lines to evaporation and expand into the LNG tank on the ship. The evaporation of the residual liquid in the bunkering piping is the reason for the

rise in tank pressure between note 1 and note 2. After HV 102 is closed (note 2), the tank pressure continues to rise until note 3. At note 3 (minute 114), the tank pressure begins to fall until note 4 (minute 121). One possible reason for the rise in tank pressure between note 2 and note 3 is that heat contained in the warmer heel is released through the liquid surface in the form of evaporation. This surface evaporation causes the tank pressure to rise. Between note 3 and 4, it is possible that the bunkered LNG, which was only loaded from the top of the tank during the bunkering, shifted places with the warmer heel at the bottom of the tank. One explanation for this liquid shift is the density difference between the bunkered LNG and the heel. The bunker LNG is denser than the heel because it is initially colder. This liquid shift may have disturbed the top liquid layer which caused the vapor and bulk liquid to exchange heat. Direct heat exchange between the vapor and liquid caused rapid condensation of the vapor in the tank. This rapid condensation may be the reason for the fall in tank pressure noticed between note 3 and note 4. At note 5 (minute 128), the tank pressure remains relatively constant at 282.84 kPa for several hours while MF Korsfjord remains at the pier until the next morning. It can be presumed at note 5 that the bunkered LNG and heel have become relatively well mixed. Using the constant pressure from note 5, a comparison may be made with the full mixing calculations performed in the Modeling and Calculations chapter.
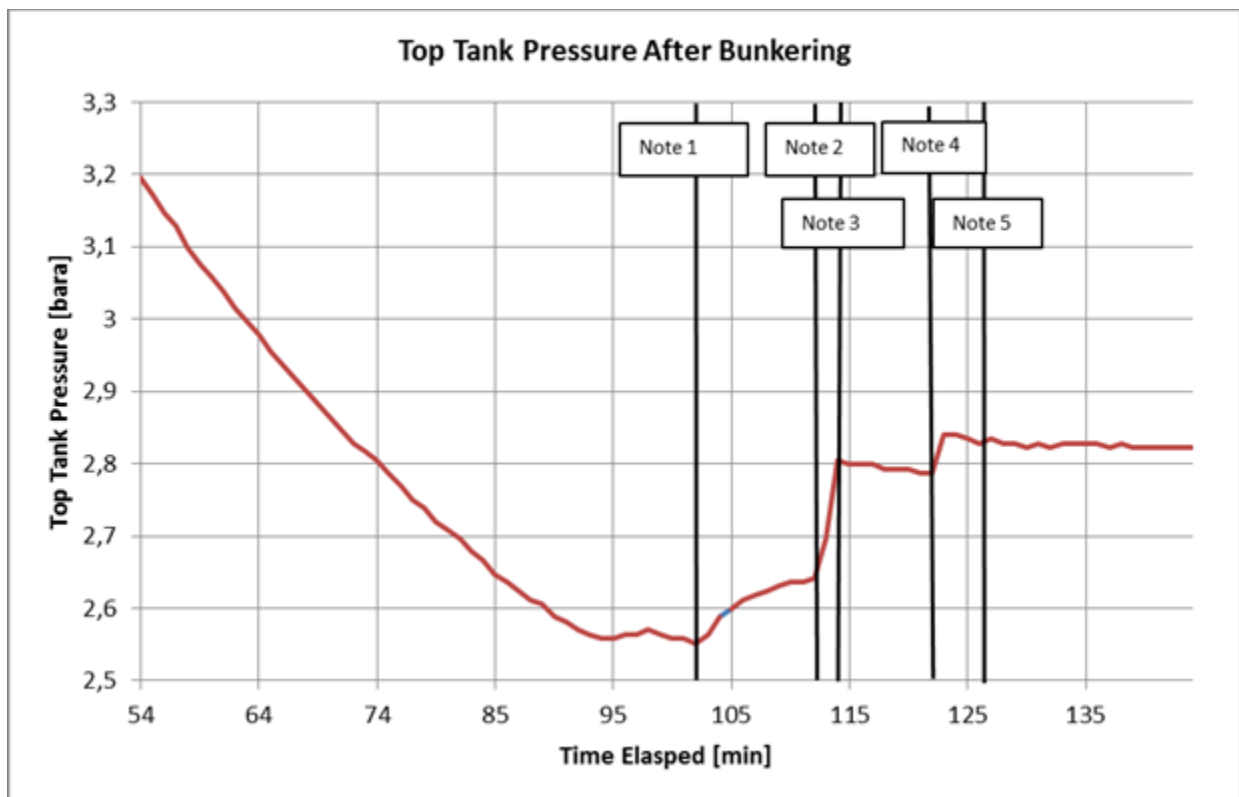
Figure 49: Post Bunkering Pressure Change

Using the process described in the Modeling and Calculations chapter for three layer mixing and the initial values found for the temperature and composition of the heel, vapor, and bunkered

LNG, the expected fall in tank pressure from full tank mixing may be calculated. Table 23 displays the values from the previous sub-sections which are used in the full mixing calculation. Even though the values used in Table 23 come from different measurements, they are assumed to be fairly indicative of conditions during a standard bunkering.

Table 23: Initial Values for Expected Fall in Tank Pressure from 3 Layers Mixing during E1

Variable	Value	Units
$V_{heel,i}$	27.16	m^3
$V_{sc,i}$	54.57	m^3
$V_{v,i}$	43.27	m^3
$T_{v,i}$	228.53	K
$T_{heel,i}$	124.25	K
$T_{sc,i}$	119.36	K
$P_{v,i}$	486.78	kPa

In order to use the MATLAB code in Appendix K to calculate the lowest tank pressure from full mixing, a weighted average for the liquid temperature was determined based on the volume of the heel and bunker LNG. This weighted liquid average was calculated to be -152.01°C (120.99 K).The lowest possible pressure from full tank mixing was found to be 264.18 kPa with a liquid and vapor temperature of -151.64°C (121.36 K). As indicated in

Figure 49, the tank pressure settle to 282.84 kPa after the heel and bunkered LNG finished mixing. This result suggests actual mixing between the heel, vapor, and bunkered LNG during bunkering causes the tank pressure to fall to 93.4 % of the lowest possible pressure. It is important to note that the weather conditions during E1 were negligible (e.g. the strongest wind guest recorded at the Værnes weather station was 7.4 m/s) and most likely did not affect the mixing inside the LNG tank between the heel, vapor, and bunkered LNG. Rather, the internal mixing of the heel, vapor, and bunkered LNG had the biggest influence on the fall in tank pressure. This observation suggests similar events, such as internal sloshing from waves striking the hull of the ship, may cause the tank pressure to fall in a similar manner. The observed fall in tank pressure from mixing during bunkering also proves that it is possible to achieve a tank pressure below 350 kPa from interaction between the bulk liquid and vapor in the tank. An estimation of the fall in tank pressure due to sloshing is provided in the Results and Discussion chapter. The next section in this chapter evaluates the data gained from measurement taken on the EVAP circuit.

6.2 Evaporator (EVAP) Measurements

This section will consider different measurements taken on the EVAP circuit during the measurement campaign. As mentioned earlier, the EVAP circuit is used to evaporate LNG from the tank before traveling to the GRU. The goal of this section is to find how much heat is

absorbed by LNG traveling through the EVAP. This information will be used in the next section to calculate the PBU mass flow rate.

In order to calculate the heat absorbed by LNG traveling through the EVAP, the temperature of the LNG entering the EVAP, NG exiting the EVAP and mass flow through the EVAP are required. The LNG temperature entering the EVAP may be estimated from the previous sub-section by using the weighted liquid temperature of the heel and bunkered LNG (e.g. -152.01°C (120.99 K)). Using installed temperature and pressure sensors in the Vaporizer, the exit conditions of the NG upon leaving the EVAP may also be determined. The EVAP exit temperature and pressure during E2 are shown in Figure 50. The reason for temperature and pressure fluctuation of NG exiting the EVAP is uncertain. These fluctuations have no correlation to the PBU valve opening or the changing power produced by the NG engines. Note that the temperatures and pressures recorded in Figure 50 are above the bubble point temperatures listed in Table 21from the Modeling and Calculations chapter. This indicates that the NG leaving the EVAP is superheated as initially assumed. The last remaining item required to calculate the heat absorbed by the EVAP is the LNG mass flow rate through the circuit.

The mass flow rate through the EVAP was calculated by using a correlation between the power produced by the NG engines and the total amount of fuel consumed by both engines. Figure 51 illustrates the powered produced by NG engine 1 (NG1) and NG engine 2 (NG2). The pattern of power usage shown in Figure 51 is repeated on MF Korsfjord since the vessel runs the same pattern as it transits from one side of the shore to the other at regular half hour intervals. Note 1 to Note 2 in Figure 51 refers to the power produced by both engines as it is leaving the pier. It is assumed that more power is required in this evolution since the vessel must overcome its inertia to reach transit speed. Note 2 to 3 refers to the period of time that MF Korsfjord is transiting between ports and note 3 to 4 is the power consumed while the vessels is alongside the pier. The exact time at which each event occurs is irrelevant since the pattern is repeated every half hour in accordance with the ferry schedule. A separate gas engine performance curve was created by collecting 100 data points recorded by the Woodward gas engine performance monitoring system. A linear curve was fit to these data points. The data points and fitted curve are presented in Figure 52. Note that the y-intersect of the curve does not start at zero which may indicate the engine losses experienced during idling. As expected, the gas engine performance curve shown in Figure 52 resembles Figure 36 since the same engines models are used on MF Korsfjord as on KV Bergen. Using the method described to determine the temperature and mass flow of the LNG entering and exiting the EVAP, the heat absorbed by LNG in the EVAP may be calculated.
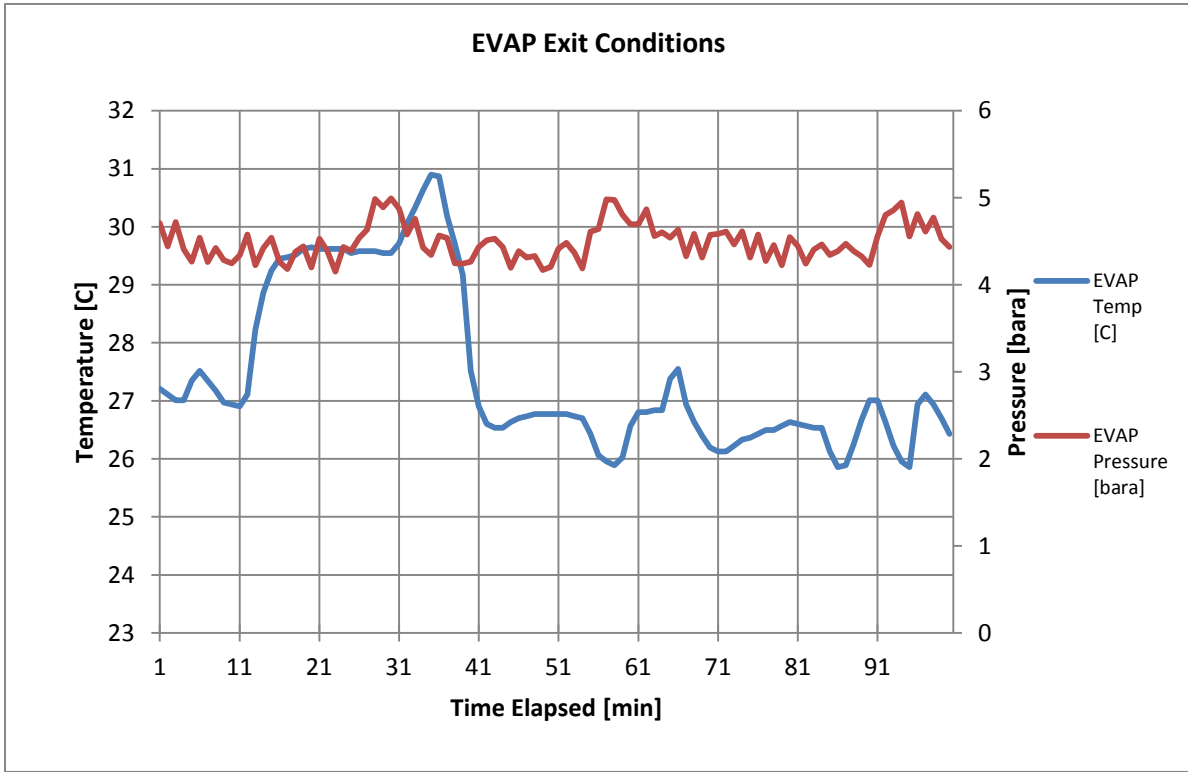
Figure 50: EVAP Exit Conditions during E2
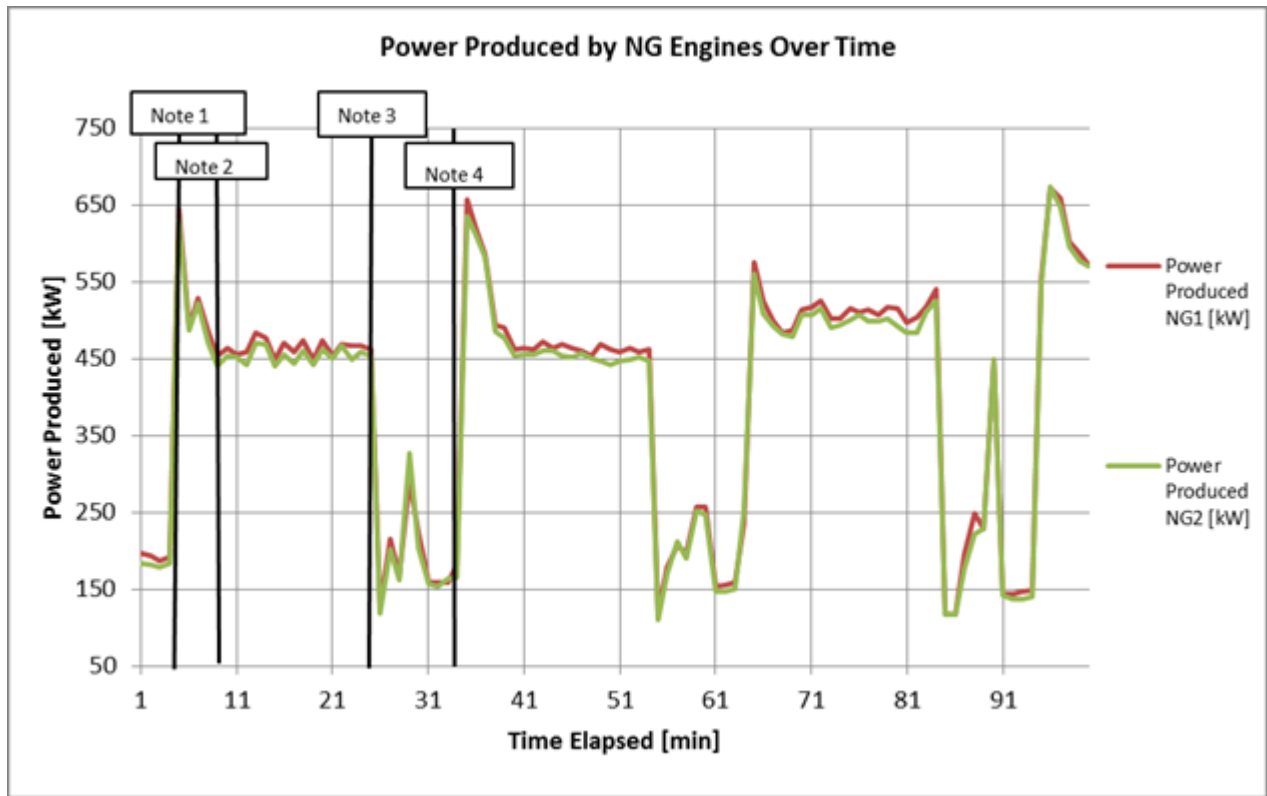
Figure 51: Powered Produced by NG1 and NG2 during E1
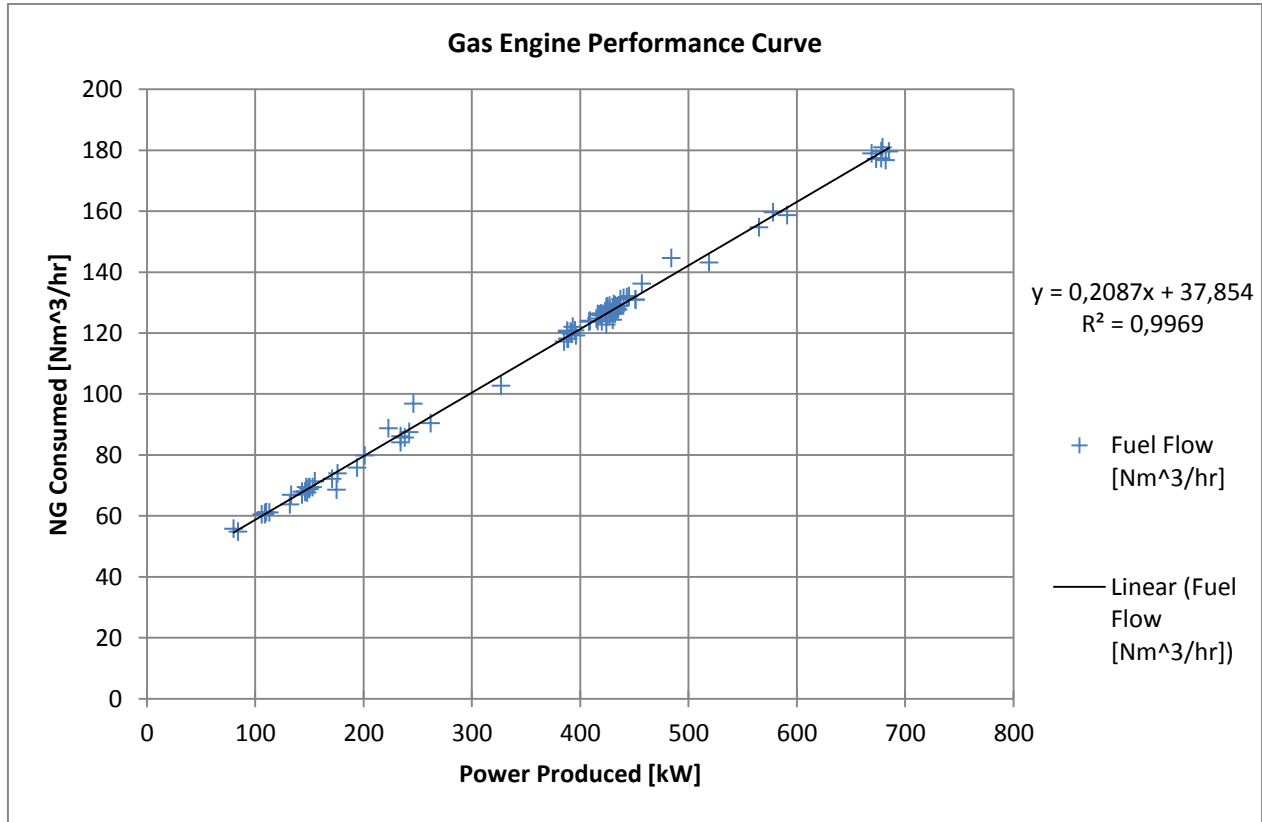
Figure 52: NG2 Engine Performance Curve

To determine the heat absorbed by the EVAP, the fluid properties from Table 24 were used.

Table 24: Fluid Properties in EVAP

Parameter	Symbol	Value	Unit
Average LNG temperature entering Vaporizer Circuit	$T_{lng,in}$	120.99	K
Average NG temperature exiting Vaporizer Circuit	$T_{ng,out}$	227.47	K
Bubble Point Temperature at 4.58 bara	$T_{sat,in}$	133.57	K
Dew Point Temperature	$T_{sat,out}$	208.46	K
LNG Pressure entering Vaporizer	$P_{lng,in}$	4.66	bara
NG Pressure exiting Vaporizer	$P_{ng,out}$	4.49	bara
Evaporating Pressure in EVAP	$P_{evap,avg}$	4.58	bara
NG density at 4,49 bara and 227 K	$\rho_{ng,out}$	4.12	kg/m^3
LNG density at 4,66 bara and 121 K	$\rho_{lng,in}$	426.72	kg/m^3
LNG density at Normal Condition (0C, 1atm)	$\rho_{lng,0C,1atm}$	0.76	kg/m^3
LNG heat capacity at 4,66 bara and 121 K	$Cp_{lng,in}$	3.38	kJ/(kg*K)
LNG heat capacity at 4,58 bara and 133.57 K	$Cp_{sat,in}$	3.51	kJ/(kg*K)
NG heat capacity at 4,58 bara and 208.46 K	$Cp_{sat,out}$	2.10	kJ/(kg*K)
NG heat capacity at 4,49 bara and 227 K	$Cp_{ng,out}$	2.10	kJ/(kg*K)
Average Latent Heat of Evaporation	h_{evap}	625.66	kJ/kg

The linearized fuel consumption versus power produced shown in Figure 52 is given in Equation (84) where the volume flow is provided in normal units (0°C, 1 atm).

$$\dot{Q}_{lng} = 0.2087W_{NG\ engine} + 37.854 \tag{84}$$

The heat absorbed by the LNG in the EVAP during the vaporization process is provided by Equations (85) and (86). In Equation (86), evaporation is assumed to occur at an average pressure of 4.58 bara. Refer to Figure 40 in the Modeling and Calculations chapter for a visualization of the gliding temperature rise of the LNG during the evaporation that occurs in the EVAP. The first term in Equation (86) refers the sensible heat of the LNG from a sub-cooled state to the bubble point temperature. The second term accounts for the latent heat of evaporation and the third term accounts for the sensible heat absorbed to bring the NG to a superheated state.

$$\dot{m}_{EVAP} = \dot{Q}_{lng,0C,1atm}\rho_{lng,0C,1atm} \tag{85}$$

$$W_{Evap} = \dot{m}_{EVAP}\left[\left(\left(Cp_{sat,in} * T_{sat,in}\right) - \left(Cp_{lng,in} * T_{lng,in}\right)\right) + h_{evap} \right. \tag{86}$$
$$\left. + \left(\left(Cp_{ng,out} * T_{ng,out}\right) - \left(Cp_{sat,out} * T_{sat,out}\right)\right)\right]$$

The heat absorbed in the EVAP over time is provided in Figure 53.
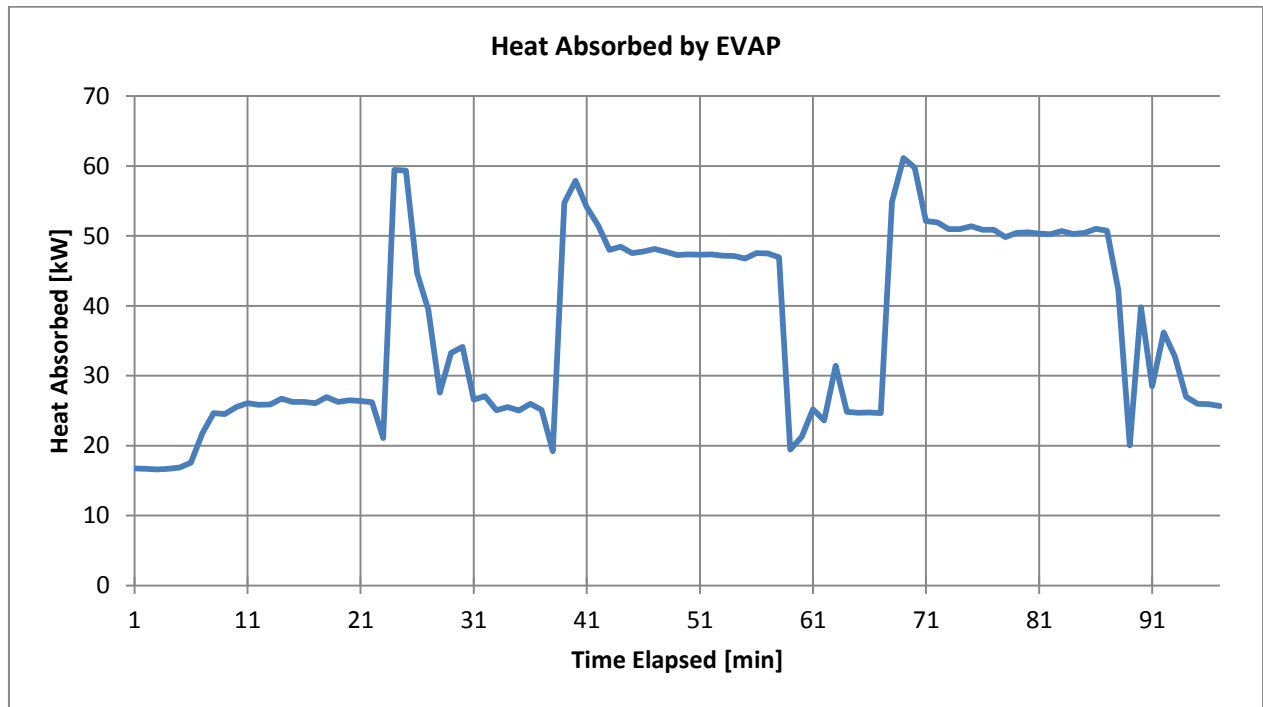
Figure 53: Heat Absorbed in the EVAP over time during E2

As expected, the curve for the heat absorbed in the EVAP in Figure 53 resembles the power produced by the NG engines over time shown in Figure 51 even though the data was taken from two separate measurements. Since the heat absorbed by the EVAP over time has been established, the heat rejected by the water glycol circulation through the Vaporizer and the heat absorbed by the PBU is required to calculate the mass flow rate circulated through the PBU.

6.3 PBU Measurements

Before calculating the heat absorbed by the PBU, the heat rejected by the water glycol entering the Vaporizer must be calculated. Once both of these values are determined, the mass flow rate circulated through the PBU may be calculated. The mass flow rate circulated through the PBU will be used in the Results and Discussion section to determine the actual pressurization time in the tank and how much vapor condensation may be tolerated before the PBU is unable to maintain the tank pressure.

In order to calculate the heat rejected by the water glycol circulated through the Vaporizer, the mass flow rate and temperature of the water glycol entering and exiting the Vaporizer is required. During measurement E2, four T-type thermocouples were each placed around the water glycol entrance and exit pipes to the Vaporizer. The average temperature recorded for each pipe may be found in Appendix M. The temperature difference between the water glycol entering and exiting the pipe is found in Figure 54. Also shown in Figure 54 is the valve opening of the PBU. As expected, there is a correlation between the spikes in water glycol temperature difference and PBU valve opening. One explanation for these spikes is that additional heat is required to vaporize the LNG in the PBU circuit in addition to the EVAP circuit. An ultrasonic flow meter was also used during measurement E2 to determine the average volume flow of the water glycol through the Vaporizer. The flow measurements recorded are found in Appendix N. Also included in Appendix N is the pump curve for the Allweiler pumps which circulate the water glycol through the Vaporizer. The recorded water glycol flow falls within the published capacity of the pumps. An average volume flow of 72.42 m^3/hr was recorded. Table 25 shows the additional fluid properties which are required to calculate the heat rejected by the water glycol in the Vaporizer. The heat rejected by the water glycol traveling through the Vaporizer may be calculated using Equation (87) and is provided in Figure 55.

$$W_{gly} = \dot{Q}_{gly,avg}\rho_{gly,avg}Cp_{gly,avg}\left(T_{gly,in} - T_{gly,out}\right) \tag{87}$$
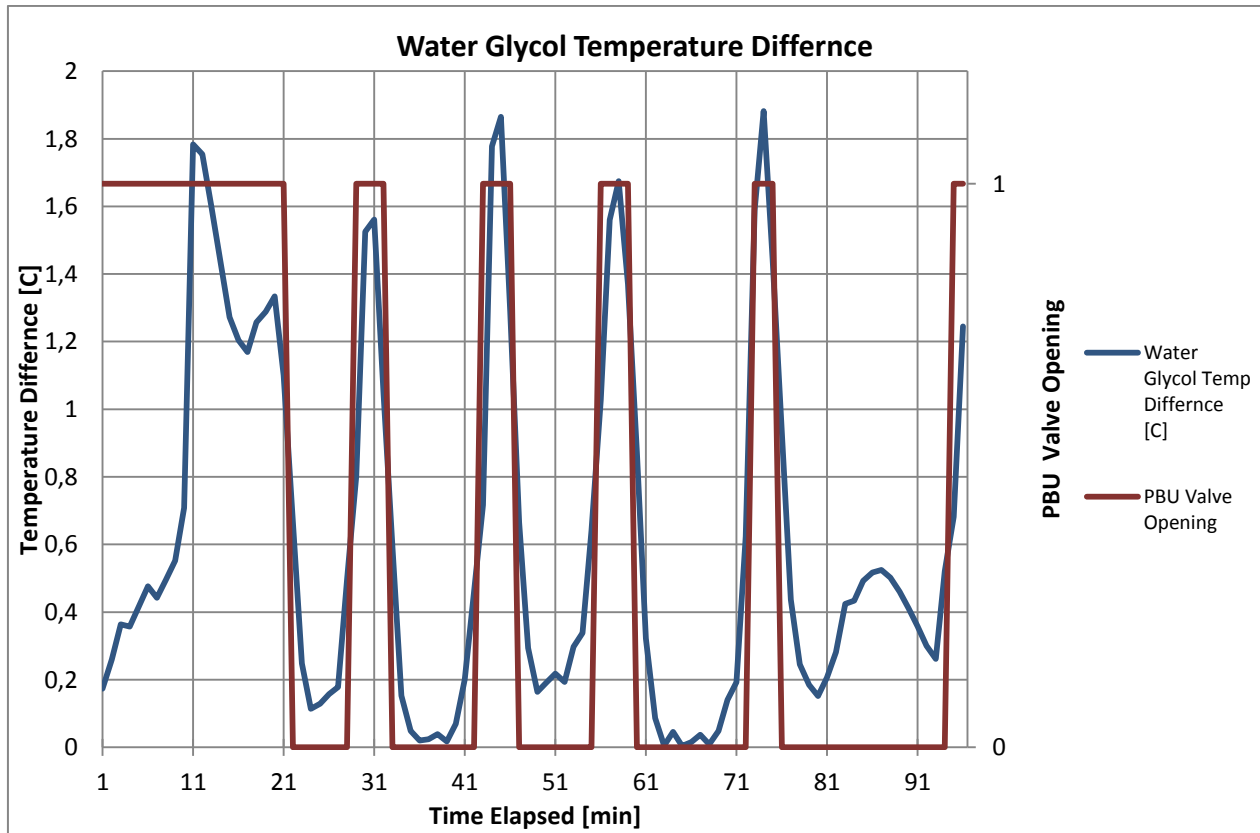
Figure 54: Water Glycol Temperature Difference during E2

Table 25: Water Glycol Fluid Properties

Variable	Symbol	Value	Unit
Average Inlet Temperature	$T_{gly,avg,in}$	33.07	C
Average Outlet Temperature	$T_{gly,avg,out}$	32.60	C
Average Heat Capacity	$Cp_{gly,avg}$	3.38	kJ/(kg*K)
Average Flow	$\dot{Q}_{gly,avg}$	72.42	m^3/hr
Average Density	$\rho_{gly,avg}$	1070	kg/m^3
Concentration	θ_{gly}	0.5	-
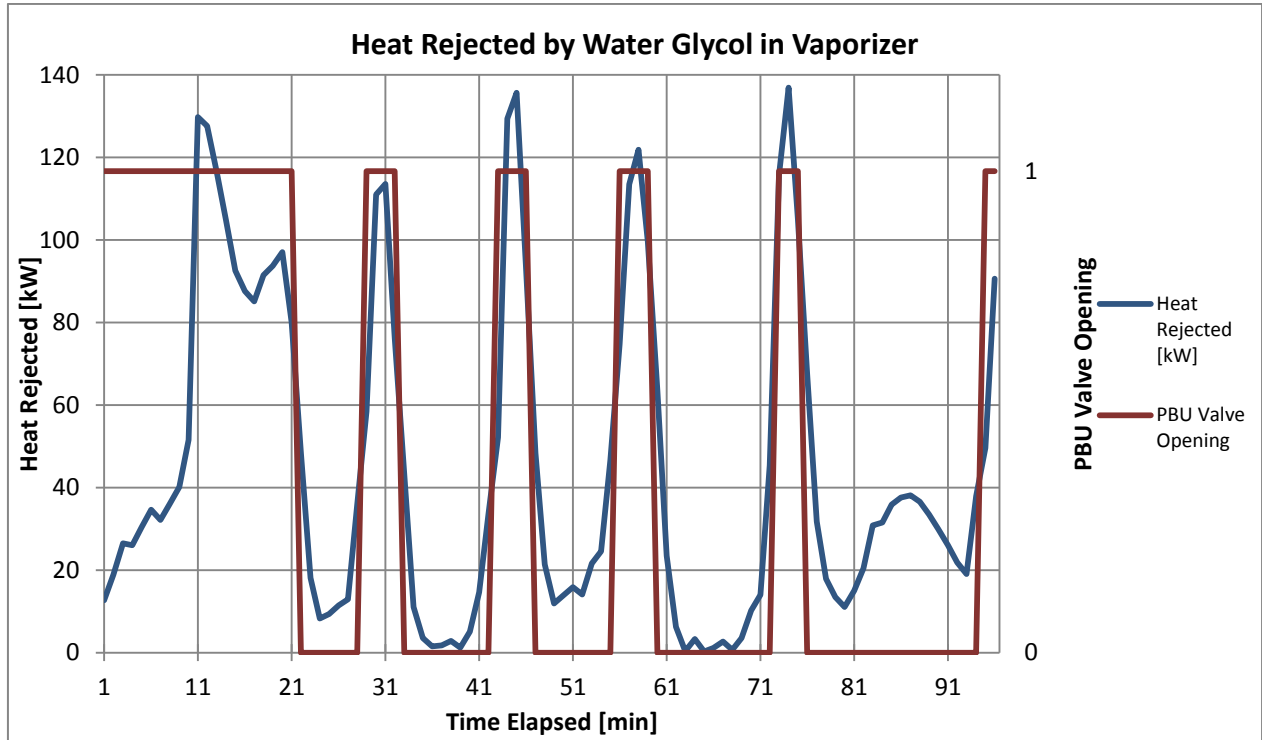
As expected, the spikes of heat rejected by the water glycol in Figure 55 correspond to the time the PBU valves are open. Using the heat rejected by the water glycol and the heat absorbed by the EVAP, the heat absorbed by the PBU may be calculated.

The heat absorbed by the PBU is calculated using a simple heat balance of the different streams entering and leaving the Vaporizer. Equation (88) was used to calculate the heat absorbed by the PBU. Terms which were not included in Equation (88) were the heat leakage from the Vaporizer to the surroundings and any frost solidification which may form on the coils of the PBU or EVAP.

$$W_{gly} = W_{PBU} + W_{EVAP} \tag{88}$$

The heat absorbed and rejected by each circuit is shown in Figure 56. The periods of time where the combined heat absorbed by the PBU and EVAP exceeds the heat rejected by the water glycol indicate the formation of frost on the coils within the Vaporizer. It may be assumed that this frost is liquefied once the PBU is closed. Using the heat absorbed by the PBU, the PBU mass flow rate may be calculated. Similar to Equation (86), the mass flow rate through the PBU may be calculated by re-arranging Equation (89) which accounts for both the sensible and latent heat absorbed by LNG circulated through the PBU.

$$W_{PBU} = \dot{m}_{PBU} \left[\left(\left(Cp_{sat,in} * T_{sat,in} \right) - \left(Cp_{lng,in} * T_{lng,in} \right) \right) + h_{evap} \right.$$
$$\left. + \left(\left(Cp_{ng,out} * T_{ng,out} \right) - \left(Cp_{sat,out} * T_{sat,out} \right) \right) \right]$$

<div align="right">(89)</div>

The LNG circulated through the PBU during E2, is presented in Figure 57 where the highest amplitude of PBU mass flow is approximately 0.30 kg/s. The average PBU mass flow rate may be calculated by dividing the total mass of LNG circulated through the PBU by the PBU valve opening time. This average was calculated to be 0.16 kg/s which will be used the Results and Discussion section to determine the relationship between the actual and idealized pressurization time.

Using the methodology discussed in the Modeling and Calculations chapter, the average PBU mass flow rate from this chapter may be compared to a PBU mass flow rate calculated at the tank conditions for the period of time shown in Figure 55. During the period of time shown in Figure 55, the tank height was 62.2% of its maximum value and the average tank pressure was 467 kPa. These values produced a calculated PBU mass flow rate of 0.20 kg/s. This calculated value is 25% more than the average measured value found in this chapter. One reason for this deviation is that some of the PBU constants (e.g. tube diameter and length) assumed in Table 13 may be incorrect. These values should be updated if more accurate PBU dimensions become available. Since the PBU mass flow rate provided in this chapter was measured directly this value is selected over the calculated PBU mass flow rate when performing additional calculations. In the next chapter, the average measured PBU mass flow rate will be compared with the rate of condensation to determine if the PBU is able to maintain tank pressure.
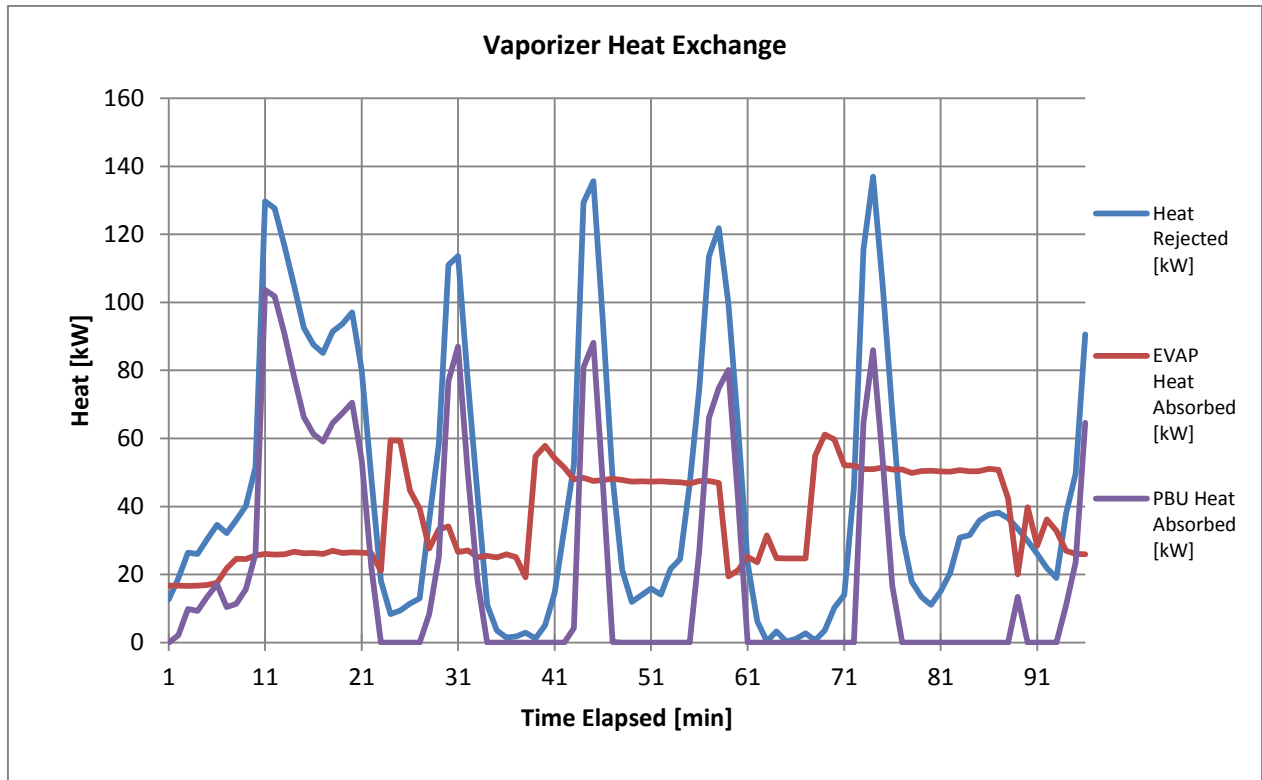
Figure 56: Heat Exchange in Vaporizer during E2
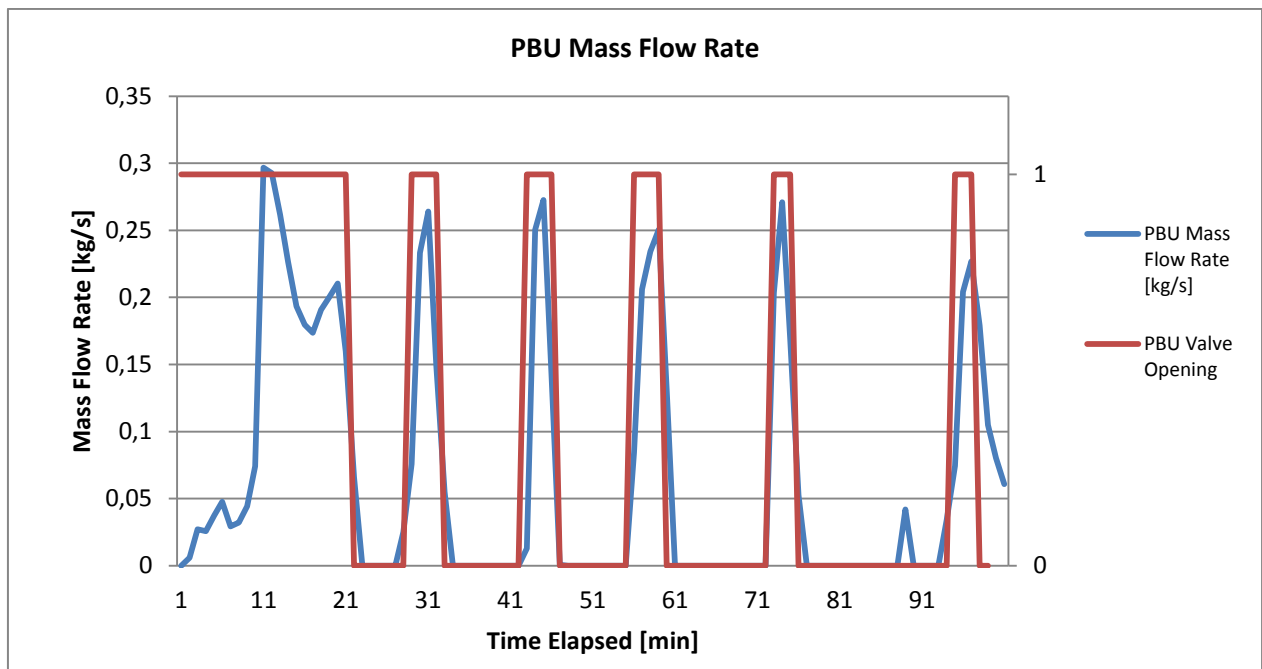
Figure 57: Calculated PBU Mass Flow during E2

6.4 Chapter Conclusion

This chapter has examined the data collected during the measurement campaign to gain a better understanding of how the different components in the LNG system behave before, during, and after bunkering. In this chapter, the initial conditions of the heel and vapor were determined. The initial fluid properties of the LNG added to the ship's tank during bunkering were also examined. Using these initial values, a study was conducted which compared the actual fall in tank pressure from mixing during bunkering to the lowest possible fall in tank pressure calculated in the Modeling and Calculations chapter. A comparison of the calculated fall in tank pressure from mixing to the actual fall in tank pressure during bunkering during E1 indicated that the tank pressure fell to 93.4% of the lowest possible mixing value. This comparison indicated that NG de-loading was possible if sustained mixing between the bulk liquid and vapor in the tank is maintained.

A separate investigation was conducted on the heat exchanged between the different streams in the Vaporizer. Using the heat rejected by the water glycol circuit and absorbed by the EVAP and the PBU, it was possible to calculate the mass flow rate circulated by the PBU. The average PBU mass flow rate calculated from the measurement campaign was 0.16 kg/s. The fall in tank pressure from mixing and PBU mass flow rate will be important in the next chapter to consider how these two factors affect the time required to pressurize the tank. A study will be conducted in the Results and Discussion chapter to determine if the PBU is able to maintain the tank pressure while the surface layer is altered causing vapor condensation.

7. Results and Discussion

The Results and Discussion chapter combines elements from the previous chapters to determine the major factors behind NG engine de-loading. To determine these factors, the idealized pressurization time from the Modeling and Calculations chapter is compared with the recorded pressurization time from the Data Acquired chapter. A comparison of the two methods indicates what rate superheated vapor produced by the PBU condenses while the vessel is undisturbed. Values from this comparison provide a base case while parameters related to the surface layer are altered to calculate the corresponding change in vapor pressure. Simulations are performed which determine how much of the liquid surface layer must be altered by sloshing to produce vapor condensation which would cause NG engine de-loading. The estimated time to NG engine de-loading is calculated based on situations where the rate of vapor condensation exceeds the mass flow rate from the PBU.

7.1 Idealized versus Actual Pressurization Time

The purpose of this section is to find the rate of condensation that occurs while the tank is undisturbed (e.g. no external forces are causing sloshing). This was done by comparing the idealized pressurization calculation with the actual amount of time required to pressurize the tank during E1 and E2. A comparison of the idealized pressurization time with the actual pressurization time in the tank suggests that vapor condensation occurs while the PBU builds the tank pressure. Only a portion of the superheated vapor supplied to the top of the tank by the PBU remains in vapor form. The mass rate of vapor retained in the vapor section, $\dot{m}_v$, may be illustrated by a simple mass balance shown in Equation (90).

$$\dot{m}_v = \dot{m}_{PBU} - \dot{m}_{cond} \tag{90}$$

A positive value for $\dot{m}_v$ suggests that the pressure in the tank will increase and a negative value suggests the tank pressure will decrease. Using the same process described in the Modeling and Calculations section for tank pressurization, the mass rate retained in the vapor section $\dot{m}_v$ may be substituted for the PBU mass flow rate $\dot{m}_{PBU}$ in Equations (63), (64), and (65). These relationships provided a way to estimate the actual amount of time required to change the tank pressure.

The time required to build the top tank pressure was calculated using the parameters shown in Table 26. An initial vapor pressure of 299.15 kPa was selected because it closely resembled the initial tank pressure in E1 and E2 before the tank pressure was increased. Using this tank pressure, an initial vapor temperature of 203.11 K was calculated based on the dew point temperature of the vapor. The dew point temperature was used because tank pressurization occurs after bunkering when the tank vapor has been cooled to saturated conditions. The initial dew point temperature was calculated in NIST REFPROP and accounts for the difference in molar fractions between the liquid and vapor sections of the tank. The liquid composition of the LNG provided in Table 14 was used in these pressurization calculations. An initial liquid temperature

of 120.99 K was selected based on the volume weighted value of the bunkered and heel temperatures discussed in the Data Acquired chapter. A PBU mass flow rate of 0.16 kg/s was also selected based on the average PBU mass flow rate measured during E2. Finally, a vapor volume of 43.27 m^3 was selected based on the average vapor volumes measured during E1 and E2 directly after bunkering.

Using different vapor condensation rates, a range of pressurization times were calculated. Figure 58 illustrates how the pressurization time changes as the rate of condensation varies. It was determined that when 66.2% of the PBU mass flow rate condensed the calculated pressurization time deviated no more than 3.6% of the actual tank pressure versus time for E1 and no more than 3.2% for E2. This suggests that approximately 0.106 kg/s of vapor condenses while the tank is un-disturbed. Using the values for an un-disturbed tank, the thickness of the liquid surface layer may be estimated.

Table 26: Pressurization Parameters

Parameter	Symbol	Value	Unit
Initial vapor pressure	$P_{v,i}$	299.15	kPa
Initial vapor temperature	$T_{v,i}$	203.11	K
Initial liquid temperature	$T_{l,i}$	120.99	K
Measured PBU mass flow	$\dot{m}_{PBU}$	0.16	kg/s
Rate of Condensation	$\dot{m}_{cond}$	Varied	Kg/s
Vapor Volume	V_v	43.27	m^3
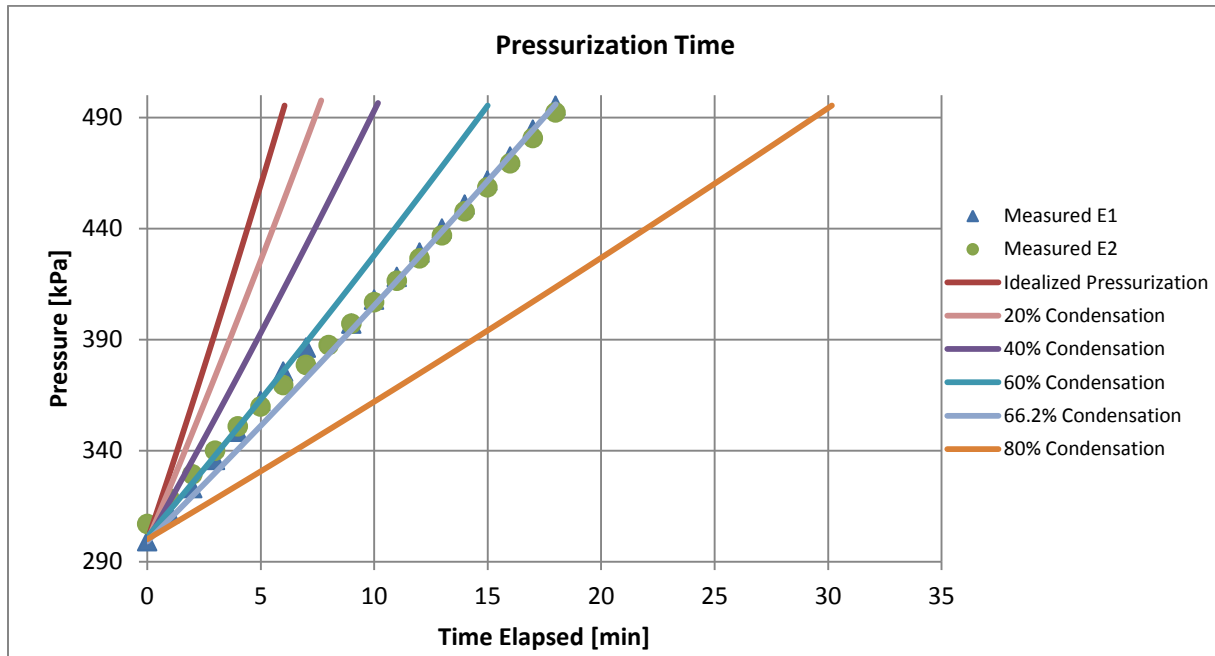
Figure 58: Pressurization Time with Vapor Condensation

The results discussed in this section suggest that condensation will occur in the tank even while the ship is alongside the pier. Using the condensation rate determined in this section, it is possible to calculate the thickness of the surface sub-layer in the next section. Once the thickness of the surface sub-layer for the undisturbed case has been calculated, the thickness of the surface sub-layer and interface surface area may be varied to illustrated how the rate of condensation changes. These modifications are representative of the conditions inside the tank while forces external to the vessel cause sloshing.

7.2 Vapor Condensation

This section determines the rate of vapor condensation and de-loading time under different tank conditions. To perform these calculations, the thickness of the surface layer of an undisturbed tank is estimated. The effects of sloshing are illustrated by diminishing the surface layer thickness while increasing the vapor liquid interface surface area to show how the rate of condensation in the tank increases. Using the vapor condensation rate calculated from these modified tank conditions, the time require to reach the NG engine de-loading pressure is calculated.

The approach used to calculate the thickness of the liquid surface layer is similar to the method used by Scurlock. As stated in the Literature Review, Scurlock determined that the majority of the thermal impedance in the surface layer existed in the "thermal conductive / convection region". Scurlock used a modified version of Fourier's law of conduction in Equation (3) to calculate the heat transfer occurring in this region. A similar approach may be used if it is assumed that the total heat transfer occurring between the top and bottom of the liquid surface occurs in a thin conductive region. A modified version of Fourier's law of conduction is provided in Equation (91). Equation (91) assumes that the conductive and convective heat transfer occurring in the liquid surface may be shown as a layer of effective conduction.

$$W_{cond,eff} = \left[\frac{k_{eff,cond} \, S\left(T_{sat}(P_{v,i}) - T_{bulk}\right)}{x_{eff,cond}} \right]$$

(91)

Additionally, it may also be assumed that the primary means of heat rejection in the vapor section to maintain the thickness of the surface sub-layer is the latent heat release through condensation. To simplify calculations, the sensible heat rejected by the superheated vapor is neglected. Equation (92) provides the heat rejected during vapor condensation to the liquid surface layer.

$$W_{cond,eff} = \dot{m}_{cond} h_{lat}$$

(92)

The effective thickness of the surface layer may be calculated by combining Equation (91) and Equation (92). Table 27 provides the values used to calculate the effective thickness of the surface layer in an undisturbed tank. A liquid surface layer thickness of 1.71 mm was calculated using the vapor condensation rate from the previous section.

Parameter	Symbol	Value	Unit
Effective Thermal Conductivity	$k_{eff,cond}$	1.73E-3	kW/(kg*K)
Flat Liquid Vapor Inferface Area	S_{flat}	44.21	m^2
Vapor Pressure	$P_{v,i}$	500	kPa
Liquid Bubble Point Temperature	$T_{sat}(P_{v,i})$	134.9	K
Bulk Liquid Temperature	T_{bulk}	120.99	K
Rate of Condensation	$\dot{m}_{cond}$	0.16	kg/s
Latent Heat of Condensation	h_{lat}	579	kJ/kg
Effective Surface Layer Thickness	$x_{eff,cond}$	1.71	mm

Using the undisturbed surface layer thickness and vapor liquid interface area as a base case, the two values may be varied to illustrate how the rate of condensation in the tank changes. As shown in Equation (91), when the thickness of the effective surface layer decreases the rate of heat transferred through the effective conduction region increases. This causes the rate of condensation to increase. The sloshing experiments conducted by Ludwig et al. shows that the liquid surface layer erodes when sloshing begins. This effect is illustrated in Figure 16 by the change in temperature versus height when sloshing begins. Similarly, when the liquid vapor interface area is increased the rate of condensation also increases. Figure 59 shows how the rate of condensation changes given different values for the liquid surface thickness and the surface area of the liquid vapor interface. Equation (93) indicates what percentage of the surface layer thickness remains during sloshing. Additionally, the vapor liquid interface area was multiplied by difference factors above unity to illustrate the increased surface area from sloshing. These factors are indicated by the symbol, S, shown in the legend in Figure 59.

$$b_\% = \left(\frac{x_{eff,cond} - x_{destroyed}}{x_{eff,cond}} \right) * 100\%$$

(93)

When the rate of vapor condensation exceeds the mass flow rate from the PBU the tank pressure will begin to fall. This is illustrated in Figure 59 by the dotted line labeled "de-loading threshold". When a level of condensation exceeding this line is maintained for a long period of time then NG engine de-loading will occur.

An additional calculation is performed to estimate the time until NG engine de-loading occurs given a certain rate of sustained condensation. The conservation of mass and the ideal gas law may be used iteratively to calculate the fall in pressure over time. Mass in the vapor section at a given point in time may be calculated using Equation (94). The density at a given point in time is provided by Equation (95). Finally, the ideal gas law may be used to calculate the tank pressure over time. This expression is provided in Equation (96). Equations (94), (95), (96) assume that the vapor volume remains constant during sustained vapor condensation.

$$m_v(t) = m_{v,i}(T_{v,i}, P_{v,i}) + \int_0^t \dot{m}_{PBU}(t)\, dt - \int_0^t \dot{m}_{cond}(t)\, dt \tag{94}$$

$$\rho_v(t) = m_v(t)/V_v \tag{95}$$

$$P_v(t) = \frac{\rho_v(t) * R * T_v}{M_v(t)} \tag{96}$$

Similar to the mixing calculations performed in the Modeling and Calculation chapter, the composition of the vapor was calculated within each iterative step using Raoult's law. The liquid composition in the tank was assumed to be constant. Table 28 provides the constants used to calculate the time until de-loading occurs. The vapor temperature was set to a constant value equal to the temperature of the vapor pillow measured in the Data Acquired chapter. In reality, the vapor temperature is expected to fall while the surface layer is disturbed. The average vapor volume and PBU mass flow rate, originally found in Table 26, were also used to calculate de-loading time. Figure 60 provides the falling pressure versus time for different surface layer thicknesses and vapor liquid interface surface areas.

Table 28: De-loading Time Parameters

| Parameter	Symbol	Value	Unit
Initial Tank Pressure	$P_{v,i}$	500	kPa
De-loading Pressure	$P_{v,f}$	350	kPa
Vapor Temperature	T_v	228	K
Vapor Volume	V_v	43.27	m^3
PBU mass flow	$\dot{m}_{PBU}$	0.16	kg/s
Rate of Condensation	$\dot{m}_{cond}$	varied	kg/s
Effective Surface Layer Thickness	$x_{eff,cond}$	varied	Mm
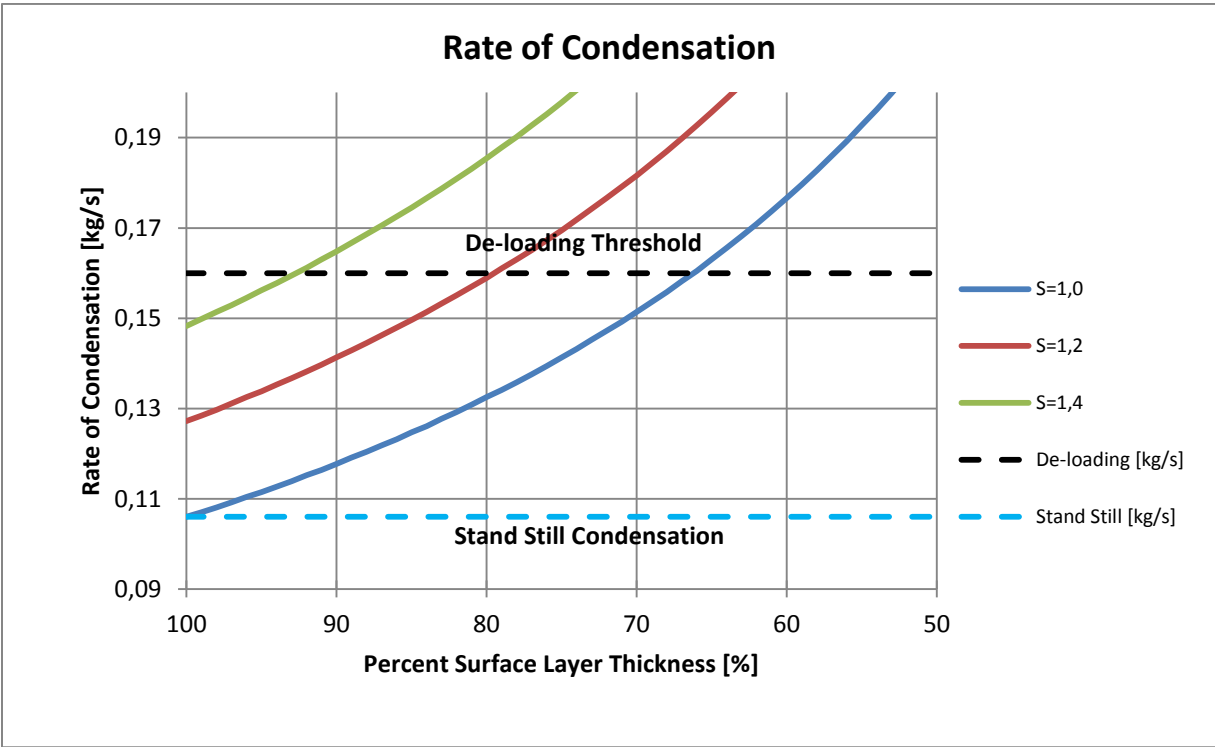
Figure 59: Rate of Vapor Condensation
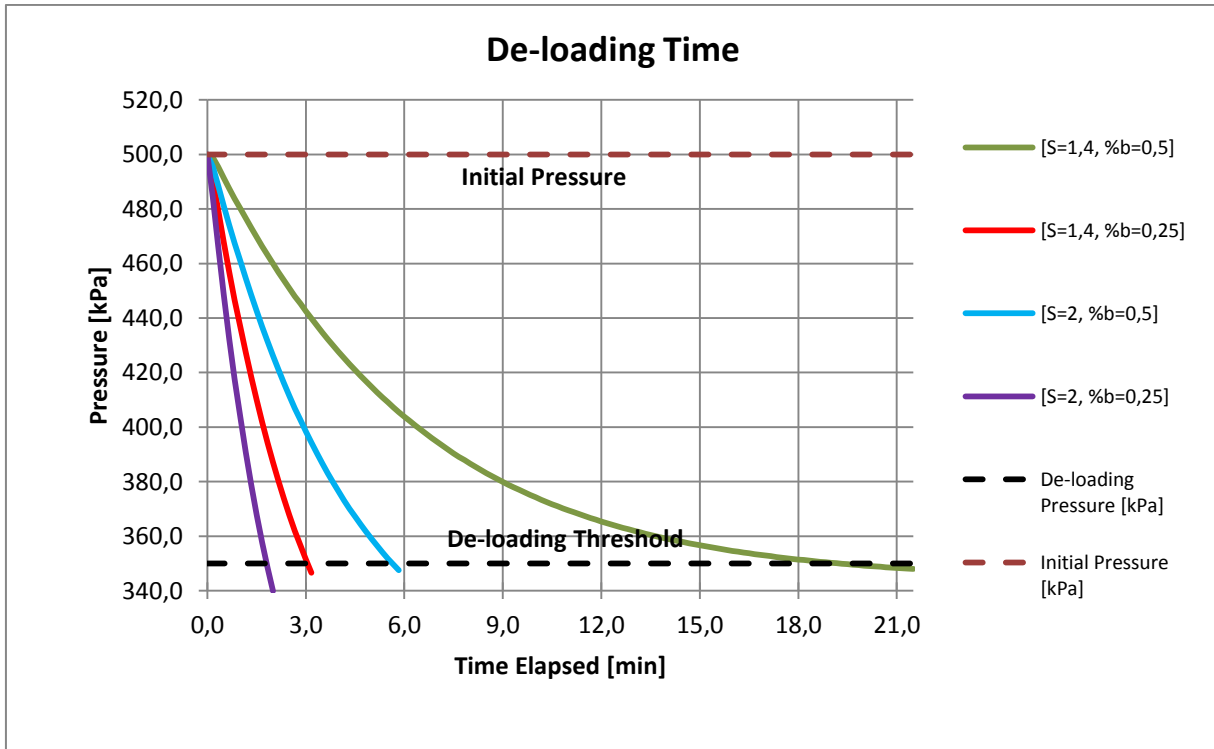
Figure 60: De-loading Time

This section illustarted de-loading conditions will occur when the liquid surafce layer and vapor liquid interface area are modified. Different vapor condensation rates have been calculated by varying these two paramteres. The different condensation rates were used to calculate the time to NG engine de-loading. The next section will discuss how the results from the first two sections fit into the larger study of NG engine de-loading on LNG fueled vessels and provide possible explinations for the two de-loading events on KV Bergen.

7.3 Discussion

This section uses the information from the previous sections to provide a general description of why NG engine de-loading occurs, how this information may be related to the two NG engine de-loading descriptions, and what additional topic should be studied. As illustrated in the chapter outlining the Thesis Objectives, the goal of this thesis was to determine if there was a relationship between NG engine de-loading on MF Korsfjord and KV Bergen and external conditions which cause sloshing inside the tank. The Literature Review examined previous studies which indicated a relationship between the liquid surface layer in the tank and the vapor pressure. Experiments by Ludwig et al. and Morgan et al. illustrated that tank sloshing caused by cryogenic tank rocking led to a drop in pressure. The calculations performed in the Modeling and Calculations section estimated the capacity of the LNG system on MF Korsfjord and KV Bergen to build up the tank pressure over time and proved NG engine de-loading was possible if the entire contents of the tank mixed. Conditions inside the different components of the LNG system were examined in the Data Acquisition chapter and provided realistic values that were used in this chapter. The first two sections of this chapter illustrated the connection between the changing condition of the liquid surface layer and fall in tank pressure. This process has shown that NG engine de-loading is possible when the liquid surface layer in the LNG tank is altered in a certain way.

The small temperature difference between the heel temperature and bunkering temperature examined in the Data Acquired chapter indicate that the conditions for NG engine de-loading are possible well after bunkering has occurred. One of the biggest impacts, however, that bunkering has on NG engine de-loading is that it decreases the vapor mass available for vapor condensation if the rate of vapor condensation exceeds the PBU mass flow rate. A smaller vapor mass after bunkering suggests NG engine de-loading will occur sooner compared to a relatively empty tank with more vapor mass. This point was illustrated in the Literature Review by the experiments conducted by Moran et al. where it was shown that the tank pressure fell sooner from sloshing when the tank was fuller.

An examination of the systems drawings on KV Bergen and MF Korsfjord indicate the presence of installed structures inside the LNG tanks to reduce the effects of sloshing. These structures are called "swash bulkheads" and are designed to inhibit the effects of sloshing in LNG tanks. Figure 61 illustrates the types of swash bulkheads that are used on KV Bergen. Since the analysis in this report supports the claim that NG engine de-loading was attributed to tank sloshing it is likely that the swash bulkheads currently installed on KV Bergen are ineffective in preventing the amount of sloshing which would lead to NG engine de-loading.

Surprisingly, these swash bulkheads are not required according to Det Norske Veritas' (DNV) standards for the design of the LNG tanks on KV Bergen and MF Korsfjord. Guidance regarding slosh analysis is provided in the DNV classification note titled "Strength Analysis of Independent Type C Tanks". According to the document, the tanks on KV Bergen and MF Korsfjord are categorized as type C independent tanks. The section of the analysis dedicated to sloshing loads indicate that when the length of the tank meets the criteria ($L_{tank} \leq 0.16 L_{ship}$), then the "tank may be designed without internal swash bulkheads" and "sloshing evaluation is not required" (DNV 2013). LNG tanks on both KV Bergen and MF Korsfjord fall below the length requiring swash bulkheads and sloshing evaluations. This suggests that if swashing bulkheads were not installed, as indicated in DNV's standard, then the effects of vapor condensation from sloshing would be even more severe. In light of the documented de-loading cases and the analysis conducted in this study, a further investigation should be conducted into the design of the swash bulkheads in tanks on LNG fueled vessels. DNV should also consider updating their classification note to include an analysis of how sloshing will affect LNG system pressure.
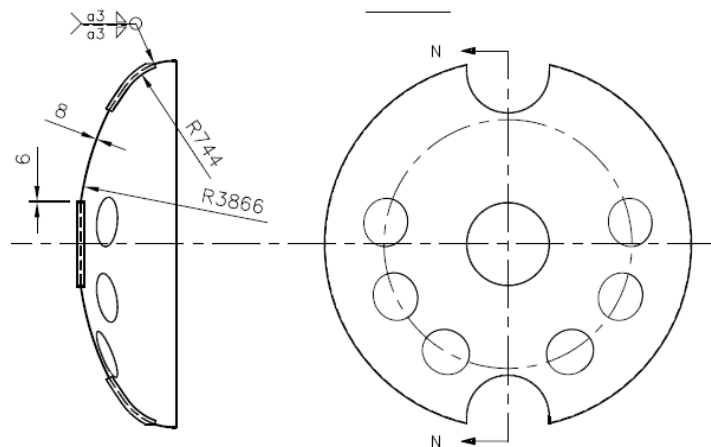
Figure 61: Swash Bulkhead on KV Bergen

The finding of this report supports the hypothesis that the second NG engine de-loading event occurred because of sloshing caused by rough weather even though swash bulkheads were present. It is reasonable to conclude that sloshing from sea and wind loads cause sustained vapor condensation which was greater than the PBU mass flow rate. Since the rate of condensation was greater than the mass flow rate from the PBU the LNG tank pressure fell until the de-loading threshold was exceeded. It is difficult to calculate the liquid wave characteristics inside the tank during this de-loading event because the time to NG engine de-loading was omitted from the description provided by the Chief Engineer. The first de-loading event, on the other hand, occurred for different reasons since it was reported that the weather was relatively calm.

One possible explanation for the first de-loading event is operator error. A discussion with the Chief Engineer indicated that when KV Bergen is inport for a long period of time the manual

valve on the hot side of the heat exchanger for the LNG Evaporator is closed partially to reduce the load on the ship's boiler system while the LNG system is not being used. The heat exchanger for the LNG evaporator provides heat for the water glycol circuit which is pumped through the Vaporizer. A full description and line drawing of the different elements which provide heat to the heat exchanger for the LNG evaporator is provided in Appendix O. The heat exchanger being discussed is circled in red in Figure 81 in Appendix O. The Chief Engineer noted that on a few occasions the valve on the hot side of the heat exchanger for the LNG Evaporator has not been opened completely before the vessel gets underway. This suggests that a reduced amount of water glycol flowed through the heat exchanger for the LNG Evaporator which results in less heat being transferred to the water glycol circuit on the cold side. A reduced amount of heat available in the water glycol circuit for the Vaporizer suggests there was a reduced amount of heat for the PBU circuit. It is possible the tank pressure fell during the first de-loading because the PBU was only able to supply a portion of its full vapor mass flow capacity. During this event, the condensation from a relatively undisturbed tank may have been greater than the reduced mass flow rate provided by the PBU.

In order to better understand what conditions cause NG engine de-loading, a separate study should be conducted which relate external forces acting on the vessel to the changing liquid surface layer in the LNG tank. This studied may be carried out in two parts. The first part should be conducted in a controlled experimental environment where external forces which act on the LNG tank may be monitored and adjusted. This study should establish a correlation which relates external forces on the tank to falling tank pressure inside the tank. The second part of the study should perform an additional set of measurements on MF Korsfjord and KV Bergen during rough weather conditions. This study would provide a relationship between measured weather conditions and observed fall in tank pressure. The next chapter will discuss recommendations for additional studies which may provide a better understanding of the external conditions which cause NG engine de-loading and some abatement measures which should be considered in future system designs.

7.4 Chapter Conclusion

The Results and Discussion chapter provide one possible explanation for the underlying cause of NG engine de-loading due to falling LNG system pressure. Analysis from this chapter supports the claim that NG engine de-loading will occur when disruptions of the surface layer cause sustained vapor condensation. The thickness of the surface layer and the liquid vapor interface area were varied to illustrate how the rate of vapor condensation changes compared to the rate of condensation in an undisturbed tank. When the rate of vapor condensation exceeded the PBU mass flow rate it was determined that the LNG tank pressure would begin to fall. Different de-loading times were estimated for different scenarios where the surface layer was altered.

Two explanations were offered for the de-loading events reported on KV Bergen. One possible reason for the second de-loading event is that tank sloshing from bad weather caused the vapor in the tank to condense at a rate greater than vapor was provided by the PBU despite the presence of

swashing bulkheads. The first de-loading event may have been caused by reduced capacity of the PBU brought about from a misalignment of the water glycol circuit. In the next chapter, topics for further understanding of NG engine de-loading are proposed.

8. Recommendations for Further Work

This section describes different subjects which may be researched further to provide a better understanding of NG engine de-loading caused by falling tank pressure. One area which requires additional insight is the relationship between external forces acting on tank and sloshing and mixing that occurs inside the tank. Insight may be gained by building and performing tests in an experimental rig where external conditions are controlled and internal response measured. Another avenue where insight may be gained is by conducting an additional measurement campaign which focuses on the falling tank pressure on KV Bergen and MF Korsfjord in rough weather. Also addressed are different abatement technologies which may be tested to prevent a fall in tank pressure during poor weather conditions.

8.1 Experimental Rig

One possible way to establish the relationship between forces acting externally on the tank and the subsequent mixing and sloshing inside the tank is by building an experimental rig. This methodology has an advantage over field measurements in that different variables may be controlled and conditions inside the tank may be measured directly from installed sensors. One of the difficulties encountered during the measurement campaign was controlling or verifying some of the variables measured during the tests. One crucial item which was not possible to control or verify was the character of the disturbances in the LNG tank (e.g. the amplitude of the slosh wave, liquid vapor interface surface area, and the thickness of the surface layer during sloshing). Moran et al. and Ludwig et al. both used an experimental rig which made it possible to control the disturbances inside the cryogenic tank. They did this by using electric motors attached to rocker arms. These rocker arms could produce waves inside the LNG tank at a desired amplitudes and speeds. A similar rig should be produced which can model the LNG system on KV Bergen and MF Korsfjord. This rocker arm should be able to simulate the same responses of a ship in different sea states and at different speeds. For example, the rocker arm system should be able to simulate the pitch, roll, yawl, and heave of a ship in different sea conditions while performing different maneuvers. A separate study should be conducted in how to accurately simulate the pitch, roll, yawl, and heave of the ship's LNG tank in an experimental rig.

In addition to the rocker arm system, this experimental rig should have installed sensor which allow the changing conditions in the LNG tank to be measured directly. The proposed experimental rig should have a model sized PBU circuit and LNG outlet connected to a service tank to model the LNG being drawn by the gas engines. A sketch of the proposed experimental rig is shown in Figure 62.
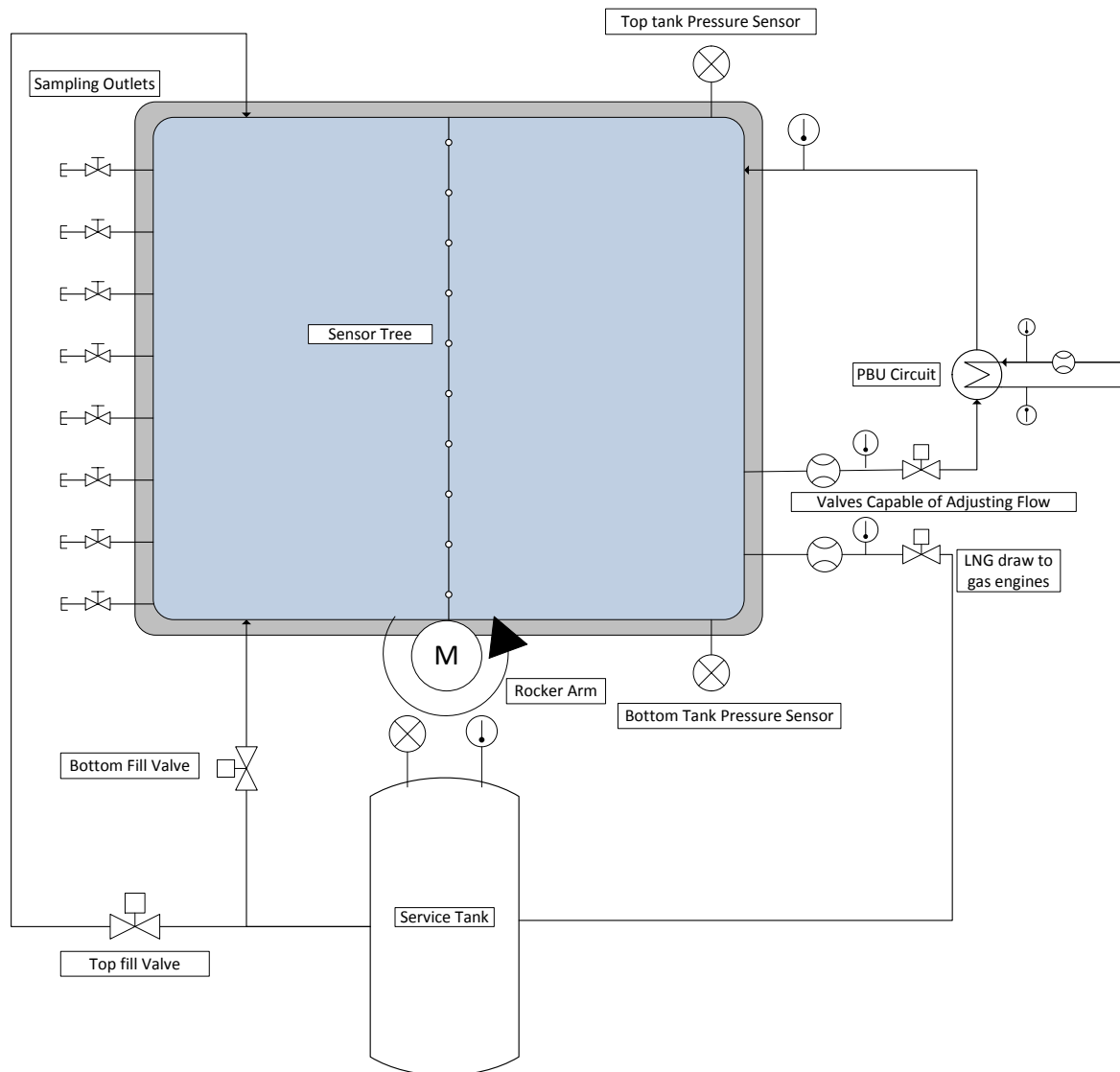
Figure 62: Proposed Experimental Rig

In the proposed design, the experimental rig would contain more sensors than are available on MF Korsfjord and KV Bergen. A sensor tree should be placed vertically in the experimental with temperature sensors at certain intervals to see the development of thermal gradients during the simulated bunkering process and tank pressurization process. There would be a pressure sensor at the top and bottom of the tank to calculate the liquid layer in the tank. Additionally, a control valve should be able to regulate the LNG flow vaporized by the PBU. The ability to regulate PBU flow would allow additional tests which measure the required mass flow rate necessary to maintain tank pressure given certain conditions. Thermocouples would be placed on the entrance and exit of the PBU circuit to be able to calculate the exact amount of heat which is absorbed during the vaporization process as well as a flowmeter at the inlet of the PBU circuit. Spaced at certain intervals vertically along the tank would be tubes which allow the sampling of the

105

contents of the LNG tank at different intervals. This would make it possible to measure the composition of the NG and LNG at different layers inside the tank. The composition of the liquid and vapor may be used to verify the temperature readings provided by the thermocouples Attached to the main LNG tank would be a service tank filled with LNG capable of being cooled and warmed to a desired temperature. Flow from this service tank could simulate the top and bottom bunkering which occurs on KV Bergen and MF Korsfjord.

Though not currently in service, the commissioning of an experimental rig which allows certain parameters to be controlled or measured directly would provide additional insight into the problem of NG engine de-loading from a fall in tank pressure. The next section discusses modifications which may be made to the measurement campaign on KV Bergen and MF Korsfjord which would draw the relationship between external tank conditions and fall in tank pressure.

8.2 Additional Data Points

In addition to building an experimental rig where certain parameters in the measurement campaign may be controlled, additional data points from the field should be taken during extreme weather conditions. The measurements performed in the report focus on conditions where the contents of the vessel are undisturbed. NG engine de-loading occurs, however, during extreme weather conditions when external forces cause internal sloshing and mixing inside the LNG tank.

Unlike the experimental rig described in the previous section, it would be difficult to control some of the variables in a measurement campaign during poor weather. A number of additional tools would be required in addition to the measuring equipment listed in the Measurement Campaign chapter. Specifically, the dynamic motion of the LNG would need to be measured to estimate the sloshing occurring inside the tank. It may be possible to monitor and record the multi-directional motion of the LNG tank using an accelerometer. This device would record how the position of the LNG tank changes in reference to an inertial frame. Using the position of the tank over time, the corresponding changing tank conditions may be calculated and equated to the fall in tank pressure.

One possible outcome of these measurements would be a general relationship between recorded weather conditions and estimated fall in tank pressure. This would provide the operators on KV Bergen and MF Korsfjord a general indication of expected fall in tank pressure given certain weather conditions. Estimated fall in tank pressure could then be used as a decisional tool to determine whether weather conditions may lead to NG engine de-loading which may lead to an unsafe situation.

The first two sections in this chapter have considered additional tests which will provide insight in the relationship between external forces acting on the LNG system and fall in tank pressure. The next section considers different possible abatement methods which may be used to prevent the fall in tank pressure.

8.3 Abatement methods

Besides developing a better understanding of the relationship between external tank disturbances and internal sloshing and mixing, addition research should be conducted on various abatement measures which may be used to prevent falling tank pressure. As indicated in the Results and Discussion chapter, both KV Bergen and MF Korsfjord have swash bulkheads installed in the LNG tanks. This study has shown that these swash bulkheads are ineffective in preventing the amount of sloshing leading to NG engine de-loading. Additional studies should be conducted which draw the connection between the sloshing characteristics and fall in tank pressure. The goal of this research should be to determine the best possible way to implement sloshing barriers to preserve the liquid surface layer. Different abatement methods may be researched which prevent the full or partial destruction of the thickness of the liquid surface layer and keep the interface surface area as low as possible. These types of LNG system changes may be categorized as alternations to the LNG tank.

Another way to mitigate the impact of falling tank pressure is by modifying the connection between the LNG tank and the GRU. In the GS16 Mitsubishi generator set description, a footnote mentioned it was possible to increase the pressure of the NG using a gas compressor before entering the GRU. This mitigation technique has a number of drawbacks, however. One drawback is that it would increase the complexity of the LNG system and introduce another potential failure point in the design. Another drawback is that it would add additional weight and space on LNG fueled vessels.

A third mitigation tactic is to prevent the condensation of the vapor in the LNG tank. One possible mitigation technique was offered by Moran et al. in the sloshing experiments described in the Literature Review chapter. Moran et al. found vapor condensation was considerably reduced when an inert gas was used to pressurize the tank instead of vaporizing the liquid in the tank to build up the tank pressure. This technique offers a number of challenges if introduced in the LNG system on KV Bergen and MF Korsfjord. Specifically, the inert vapor must come from a separate source than the LNG tank. Similar to the addition of the gas compressor, components used to store and produce inert vapor would make the LNG system more complex and require additional space onboard the vessel. This mitigation technique would also introduce impurities into the LNG tank which may affect the performance of the NG engine. These different concerns would need to be addressed if this mitigation technique was utilized.

8.4 Chapter Conclusion

This chapter has considered subjects which may be studied further to gain a better understanding of the relationship between external forces acting on the tank and fall in tank pressure. Also discussed in this chapter are different abatement techniques which should be researched to prevent tank pressure from falling below the NG engine pressure threshold. An outline of an experimental rig which may be constructed to perform additional tests is discussed. Also provided is a description of a measurement campaign during extreme weather conditions on MF Korsfjord and KV Bergen. Abatement technologies may focus on preserving the liquid surface

layer, building the NG pressure before the GRU, and using vapor which is less likely to condense.

9. Conclusion

This chapter summarizes the finding of this report and explains how it has led to a better understanding of NG engine de-loading due to falling tank pressure. Additionally, this chapter indicates where the information presented in this study fits into the larger body of knowledge regarding falling pressure in cryogenic tanks from sloshing or mixing.

The analysis conducted in this report has developed a series of models and measured values which indicate how the LNG systems on KV Bergen and MF Korsfjord should behave during normal operation. One model predicts the PBU mass flow rate given different liquid heights and vapor pressures in the LNG tank. The values predicted in the PBU mass flow rate model were compared to measurements taken on KV Bergen and MF Korsfjord. Both the model and the measured PBU mass flow rate measurements established the maximum capacity of the PBU to build up the tank pressure over time.

Another model created was an idealized method to calculate the time required to pressurize the tank. This method was compared with measurements taken during the measurement campaign to see how the two pressures deviated over time. Using this comparison, it was possible to argue that a portion of the PBU mass flow rate condenses in an undisturbed tank. Using the rate of condensation, it was possible to calculate the thickness of the surface layer when the tank was not disturbed.

The third model calculated the lowest possible fall in tank pressure possible when the liquid contents of the tank mixed completely with the vapor contents. These calculations indicated that it is possible to go below the pressure threshold which causes NG engine de-loading. The time over which the fall in pressure took place was not addressed in the liquid and vapor mixing model. Rather, the fall in tank pressure over time was addressed in the Results and Discussion section where it was illustrated that a fall in tank pressure occurred when the rate of vapor condensation exceeded the PBU mass flow rate. A range of condensation rates were calculated given that the thickness of the surface layer and area of the liquid and vapor interface were altered. Using these different condensation rates, it was possible to estimate the amount of time over which the tank pressure fell until it crossed the NG engine de-loading pressure threshold.

The reasons for the two documented de-loading situations were also addressed in the Results and Discussion chapter. It was concluded that the second de-loading event occurred because external forces initiated tank sloshing and mixing which caused the vapor in the tank to condense over a sustained period of time. The rate of condensation during this de-loading event was greater than the mass flow rate from the PBU. It was postulated that the first de-loading event was caused by operator error. Specifically, a reduced amount of heat delivered to the Vaporizer from system misalignment led the PBU to produce a lower mass flow rate than designed.

Additional experiments were proposed for further insight into the problem of NG engine de-loading. The largest existing gap in knowledge includes the relationship between external forces

acting on the LNG tank and the response of the contents inside the tank. An experimental rig was proposed which would allow certain variables to be controlled and monitored. Also proposed were additional tests which may be performed on KV Bergen and MF Korsfjord under extreme weather conditions which may lead to NG engine de-loading. Recommendations for different abatement technologies which would inhibit the conditions leading to NG engine de-loading were also discussed.

The research conducted in this report complements the larger field of cryogenic tank sloshing and mixing by drawing on the established knowledge of the characteristics of the liquid surface layer in cryogenic tanks and how altering this surface layer may lead to a fall in tank pressure. Using empirical data on heat transfer occurring in the surface layer collected by Scurlock, it was possible to estimate the thickness of the surface layer in the LNG tank on KV Bergen and MF Korsfjord. This work extends the observations made by Scurlock who notice a significant increase in the rate of phase change occurring inside the LNG tank when the tank was tapped at certain intervals. Furthermore, this study acknowledges the relationship between tank sloshing and fall in tank pressure established by Ludwig et al. and Moran et al. and provides an industry example of how these phenomena could disrupt the normal operation of LNG fueled vessels.

Solidifying the relationship between external tank disturbances and the fall in tank pressure is a necessary first step in improving the reliability of LNG fueled vessels. Continued research in the subject of NG engine de-loading should be made because improved reliability will reduce the requirement for expensive backup systems like the diesel generator installed on KV Bergen and MF Korsfjord. This would reduce the cost and maintenance associated on LNG fueled vessels and would accelerate the shift towards LNG as a source of maritime fuel

10. References

Ameln, C. (2014, 04 April 2014). [NTNU Project with MF Korsfjord].

Ammouri, Fouad, & Macron, Jonathan. (2011). Estimation of the quantity of product within cryogenic storage vessels. *Chemical Engineering Research and Design, 89*(10), 2003-2011. doi: http://dx.doi.org/10.1016/j.cherd.2011.01.018

Baek, S., Nam, H., Yeo, M., & Kim, K. (2012). *Development of a Zonal Model to Analyze a Thermal Storage Tank with an Electric Heater* Paper presented at the International Building Performance Simulation Association www.ibpsa.org/proceedings/asim2012/0090.pdf

Beduz, C., & Scurlock, R. G. (1994). Evaporation Mechanisms and Instabilities in Cryogenic Liquids. In P. Kittel (Ed.), *Advances in Cryogenic Engineering* (Vol. 39, pp. 1749-1757): Springer US.

Brown, P., Lux, J., Muzny, C., Lemmon, E. , & Wait, K. . (2011). refpropm.m: NIST REFPROP Retrieved from http://www.boulder.nist.gov/div838/theory/refprop/Frequently_asked_questions.htm

Burel, Fabio, Taccani, Rodolfo, & Zuliani, Nicola. (2013). Improving sustainability of maritime transport through utilization of Liquefied Natural Gas (LNG) for propulsion. *Energy, 57*(0), 412-420. doi: http://dx.doi.org/10.1016/j.energy.2013.05.002

BurnsEngineering. (2011). Error Sources that Effect Platinum Resistance Thermometer Accuracy.   Retrieved January 28, 2014, from www.burnsengineering.com/BEnews/

Cengel, Y. , & Boles, M. . (2008). *Thermodynamics : An Engineering Approach*. New York: McGraw-Hill.

Chisholm, D. (1967). *A Theoretical Basis for the Lockhart-Martinelli Correlation for Two-phase Flow*: National Engineering Laboratory.

Chisholm, D. (1983). Gas-liquid flow in pipeline systems. In N. P. Cheremisinoff & R. Gupta (Eds.), *Handbook of Fluids in Motion* Boston Butterworth.

Clamond, D. (2008). colebrook.m: Clamond, D. Retrieved from http://www.mathworks.com/matlabcentral/fileexchange/21990-colebrook-m/content/colebrook.m

Conde Engineering. (2011) Thermophysical Properties of Brines Zurich, Switzerland: Conde Engineering.

Corpening, J. . (2010). Analytic Modeling of Pressurization and Cryogenic Propellant Conditions for Liquid Rocket Based Vehicle Design In T. B. Engineering (Ed.). Huntsville, Alabama: Teledyne Brown Engineering/NASA.

CryoAB. (2009). Manual for Mykelbust vert, Yard building No. 48, 49, 52. In L. Engineering (Ed.).

CryoAB. (2009). Supply Vessel Kystvakt Component Manual. In CryoAB (Ed.), *Project Kystvakten*. Gothenborg, Sweden.

DNV. (2014). Gas Fuelled Ship Installations *Ships / High Speed. Light Craft and Naval Surface Craft* (Vol. Part 6 Chapter 13). Norway Det Norske Veritas AS.

DNV (2013). Strength Analysis of Independent Type C Tanks. 31.13. D. N. V. (DNV). Norway, Det Norske Veritas (DNV)**:** 26.

Drube, T., Haukoos, B. , Thompson, P., & Williams, G. . (2012). An Initial Qualitative Discussion on Safety Considerations for LNG Use in Transportation In N. P. Council (Ed.), *NPC Future Transportation Fuels Study: Advancing Technology for America's Transportation Future* National Petroleum Council.

Espeland, J. . (2012). 005-12-0074 - Black Out *Helse, Miljø, Sikkerhet & Kvalitetssikring* (pp. 2). Bergen, Norway Norge Kystvakten.

Espeland, J. . (2012). 005-12-0074 - Black Out *Helse, Miljø, Sikkerhet & Kvalitetssikring* (pp. 2). Bergen, Norway Norge Kystvakten.

Espeland, J. (2013, 24 October 2013). [KV Bergen Visit].

Espeland, J. (2014). [Master's Project].

Fair, J. (1960). What You Need to Design Thermosiphon Reboilers *Petroleum Refiner 39*(2), 105-123.

GIIGNL. (2011). *LNG Custody Transfer Handbook* (3rd ed. Vol. 3.01). Paris, France International Group of Liquid Natural Gas Importers.

Gnielinski, V. . (1987). Critical Reynold's Number of Helically Coiled Tubes Heat Exchanger Design Handbook (2nd Ed.) Hemisphere Publishing Corporation

Hands, B.A. (1986). *Cryogenic engineering*: Academic Press.

Hardee, R., & Sines, J. . (2012). *Piping Systems Fundamentals: The Complete Guide to Gaining a Clear Picture of Your Piping System* (2nd edition ed.). Lacey, Washington ESI Press.

Ho, Son H., & Rahman, Muhammad M. (2012). Forced convective mixing in a zero boil-off cryogenic storage tank. *International Journal of Hydrogen Energy, 37*(13), 10196-10209. doi: http://dx.doi.org/10.1016/j.ijhydene.2012.03.108

Holler, G., Fuchs, A., & Brasseur, G. (2008, 12-15 May 2008). *Fill level measurement in a closed vessel by monitoring pressure variations due to thermodynamic equilibrium perturbation.* Paper presented at the Instrumentation and Measurement Technology Conference Proceedings, 2008. IMTC 2008. IEEE.

Kern, D. . (1950). *Process Heat Transfer*. New York: McGraw-Hill.

Kew, P. A., & Reay, D. A. (2006). *Heat pipes: theory, design and applications*. Oxford [Eng.]: Butterworth-Heinemann.

Lee, Jisung, Kim, Youngkwon, & Jeong, Sangkwon. (2010). Transient thermodynamic behavior of cryogenic mixed fluid thermosiphon and its cool-down time estimation. *Cryogenics, 50*(5), 352-358. doi: http://dx.doi.org/10.1016/j.cryogenics.2010.02.001

Lockhart, R. W., & Martinelli, R. C. (1949). Proposed correlation of data for isothermal two-phase, two-component flow in pipes. *Chem. Eng. Prog, 45*(1), 39-48. doi: citeulike-article-id:12672573

Lowell, D. , Lutsey, N., & Wang, H. . (2013). Assessment of the Fuel Cycle Impact of Liquefied Natural Gas as Used in International Shipping International Council on Clean Transportation

Ludwig, C., Dreyer, M. E., & Hopfinger, E. J. (2013). Pressure variations in a cryogenic liquid storage tank subjected to periodic excitations. *International Journal of Heat and Mass Transfer, 66*(0), 223-234. doi: http://dx.doi.org/10.1016/j.ijheatmasstransfer.2013.06.072

Mandell, D. , & Roudebush, W. . (1965). Parametric Investigation of Liquid Hydrogen Tank Pressurization During Outflow *NASA Technical Note* (pp. 28). Cleveand, Ohio: Lewis Research Center

Martin, T. A., beekman, D. H., & Dillard, J. E. (1992). The design and testing of a cryogenic mixer pump. *Cryogenics, 32*(2), 243-250. doi: http://dx.doi.org/10.1016/0011-2275(92)90274-E

McGovern, J. (2011). Technical Note: Friction Diagram for Pipe Flow Dublin, Ireland: Dublin Institute of Technology.

Mitsubishi. (2014). GS16R-PTK Gen Set Rating In G. R.-P. G. S. Rating (Ed.), (pp. Generator Specifications): Mitsubishi Heavy Industries, LTD.

Moran, M. , McNelis, N., Kudlac, M. , Haberbusch, M. , & Satornino, G. . (1994). *Experimental Results of Hydrogen Slosh in a 62 Cubic Foot (1750 Liter) Tank* Paper presented at the 30th Joint Propulsion Conference Indianapolis, Indiana.

NIST. (1995). Tables of Thermoelectric Voltages and Coefficients In T. T (Ed.). USA: National Institute of Science and Technology.

NTNU. (2013). *Kompendium i TEP-07 Industriell Varmeteknikk* Trondheim, Norway Norwegian University of Science and Technology

Nurge, M. A., Youngquist, R., & Walters, D. (2003). Capacitance based mass metering for cryogenic fluids. *Cryogenics, 43*(9), 501-506.

PalmerWahl. (2007). The Evolution of Thermal Imaging Cameras.

Patil, R., Shende, B. , & Ghosh, P. (1982). Designing a Helical-Coil Heat Exchanger *Chemical Engineering*

Pentronic. (2014). Resistance Thermometer Theory. *Temperature Sensors* Retrieved 27 January, 2014, from http://www.pentronic.se/home/temperature-sensors/theory-of-sensors/pt100-sensors.aspx

Rosemount. (2006). Rosemount 3051 Pressure Transmitter In R. Inc. (Ed.). Chanhassen,MN.

Roudebush, W. . (1965). An Analysis of the Probelm of Tank Pressurization During Outflow *NASA Technical Note* (pp. 25). Cleveland, Ohio: Lewis Research Center.

Sarma, N. V. L. S., Reddy, P. J., & Murti, P. S. (1973). A Computer Design Method for Vertical Thermosyphon Reboilers. *Industrial & Engineering Chemistry Process Design and Development, 12*(3), 278-290. doi: 10.1021/i260047a012

Scurlock, R. G. (1988). Cryogenics at the university of southampton: a review. *Cryogenics, 28*(7), 439-466. doi: http://dx.doi.org/10.1016/0011-2275(88)90112-9

Scurlock, R.G. (2006). *Low-Loss Storage and Handling of Cryogenic Liquids: The Application of Cryogenic Fluid Dynamics*: Kryos Publications.

Seo, Mansu, & Jeong, Sangkwon. (2010). Analysis of self-pressurization phenomenon of cryogenic fluid storage tank with thermal diffusion model. *Cryogenics, 50*(9), 549-555. doi: http://dx.doi.org/10.1016/j.cryogenics.2010.02.021

Serth, R. W. (2007). *Process heat transfer: principles and applications*. Amsterdam: Elsevier Academic Press.

Siemens. (2013). SITRANS F: Ultrasonic Flowmeters FUP1010 IP67 Portable. Nurnberg, Germany.

Ultraflux. (2003). Ultrasonic Transit Time Flowmeter Didactic Handbook (A ed.). Cedex, France Ultraflux.

Ultraflux. (2010). UF 801-P/ UF 801-PB: New Gneration Ultrasonic Portable Flowmeters Poissy Cedex, France

Wheeler, Anthony J., & Ganji, Ahmad R. (2004). *Introduction to engineering experimentation*. Upper Saddle River, N.J.: Pearson/Prentice Hall.

Younger, A. (2004). *Natural Gas Processing Principles and Technology*. Calgary, Alberta: University of Calgary.

11. List of Appendices

Appendix A: Results of Sloshing Tests Conducted by Moran et al. (1994)

Appendix B: Measurement Campaign Process Diagram

Appendix C: HSE Documentation

Appendix D: Description of the bunkering process

Appendix E: Description of Measurement Campaign for Fjord 1

Appendix F: Water Glycol Fluid Properties

Appendix G: MATLAB program for the Overall Heat Transfer Coefficient, U, of the PBU

Appendix H: MATLAB program calculating the mass flow through the PBU

Appendix I: Iterative Vapor Pressurization

Appendix J: MATLAB program idealized tank pressurization

Appendix K: MATLAB code for mixing calculation

Appendix L: Required Purge Time

Appendix M: Water Glycol Temperature Measurements from E2

Appendix N: Water Glycol Volume Flow Measurements / Allweiler Pump Curve

Appendix O: Description of the Water Glycol System

Appendix A: Results of Sloshing Tests Conducted by Moran et al. (1994)

Freq & Ampl (Hz; +/- in)	Pressurant Type	Ullage Volume (%total)	Initial Pressure (psia)	Ramp Pressure (psia)	Ramp Time (s)	Ramp Pressurant Added (lbm)	Hold Time (s)	Total Pressurant Added (lbm)	Pressurant Temperature (°R)	Min Pressure During Sloshing (psia)	Pressure Collapse (%)	Max dP/dt During Sloshing (psi/s)	Test Rdg#
0.95; 0.5	He	17	14.1	20.6	5	0.099	1	0.110	233	n/a	n/a	0.07	187
0.95; 0.5	He	31	14.1	19.8	40	0.137	0	0.137	171	n/a	n/a	0.03	197
0.95; 0.5	He	51	-	19.9	-	-	10	-	172	n/a	n/a	0.03	200
0.95; 0.5	He	33	-	34.7	-	-	-	-	170	n/a	n/a	0.03	160
0.95; 0.5	H_2	17	14.5	20.1	3	0.057	15	0.075	222	18.4	30	-0.07	302
0.95; 0.5	H_2	28	14.0	19.8	6	0.115	18	0.153	221	18.1	29	-0.08	261
0.95; 0.5	H_2	49	14.7	20.7	8	0.236	4	0.264	212	18.9	30	-0.19	370
0.95; 0.5	H_2	13	14.6	36.1	13	0.314	14	0.382	81	22.1	65	-1.11	877
0.95; 0.5	H_2	17	14.2	35.0	14	0.273	36	0.353	193	26.7	40	-0.25	235
0.95; 0.5	H_2	31	14.4	34.7	17	0.369	16	0.452	234	28.6	30	-0.27	246
0.95; 0.5	H_2	33	15.4	35.4	13	0.625	28	0.816	71	29.5	29	-0.11	869
0.95; 0.5	H_2	49	14.2	34.7	23	0.587	13	0.685	249	28.6	30	-0.29	242
0.95; 0.5	H_2	51	14.9	35.7	14	0.920	16	1.052	76	31.2	21	-0.08	886
0.74; 1.5	He	17	14.2	19.5	4	0.075	1	0.083	238	n/a	n/a	0.11	190
0.74; 1.5	H_2	17	14.1	20.2	3	0.068	11	0.100	169	16.1	67	-0.26	303
0.74; 1.5	H_2	28	14.1	19.9	5	0.106	11	0.134	199	15.9	69	-0.39	260
0.74; 1.5	H_2	54	14.0	19.8	8	0.169	11	0.208	200	16.1	64	-0.11	263
0.74; 1.5	H_2	13	15.3	35.8	12	0.301	13	0.366	72	18.9	80	-1.04	892
0.74; 1.5	H_2	15	14.6	35.7	14	0.342	17	0.417	76	18.1	83	-1.57	878
0.74; 1.5	H_2	19	14.2	34.9	14	0.260	24	0.326	224	19.8	73	-1.06	236
0.74; 1.5	H_2	31	15.1	35.7	38	0.535	13	0.641	78	18.2	83	-2.49	893
0.74; 1.5	H_2	36	14.6	35.5	14	0.634	27	0.813	74	18.0	84	-2.55	870
0.74; 1.5	H_2	49	14.5	34.7	20	0.495	16	0.598	263	21.0	68	-0.52	243
0.74; 1.5	H_2	51	14.8	35.4	14	0.818	14	0.973	83	19.4	77	-0.48	895
0.74; 1.5	H_2	54	14.7	35.7	15	0.781	19	0.899	111	19.4	78	-0.34	887

Appendix B: Measurement Campaign Process Diagram

Before conducting the measurement campaign, the governing equations in the Vaporizer and LNG tank were considered and a full process diagram was created to determine what sources would provide the parameters required. Figure 63 shows the overall heat and mass balance from the LNG tank and Vaporizer which would be used to relate the bunkering process with the response in the LNG system on KV Bergen and MF Korsfjord.
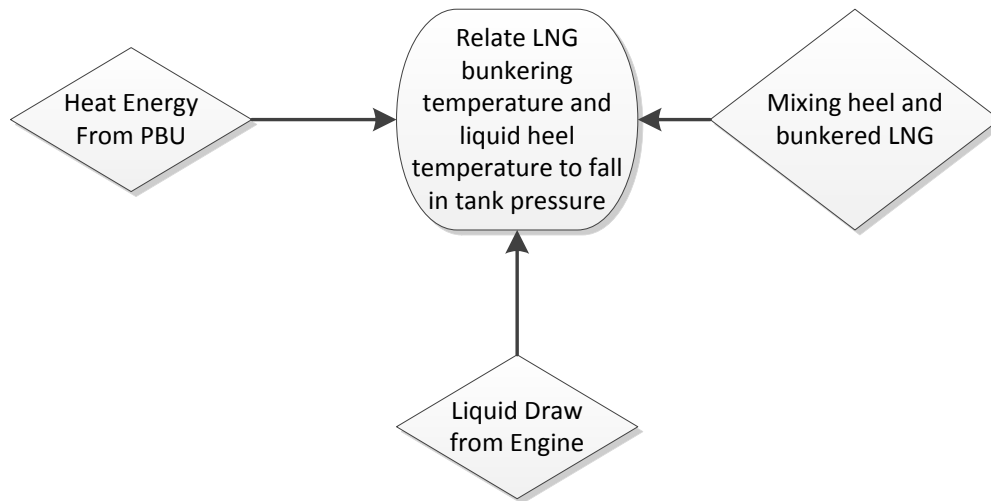
Figure 63: Overall Heat and Mass Balances Used to Organize Measurement Campaign

Figure 64 indicated the parameters required to calculate the liquid draw from the LNG tank by the NG engines.
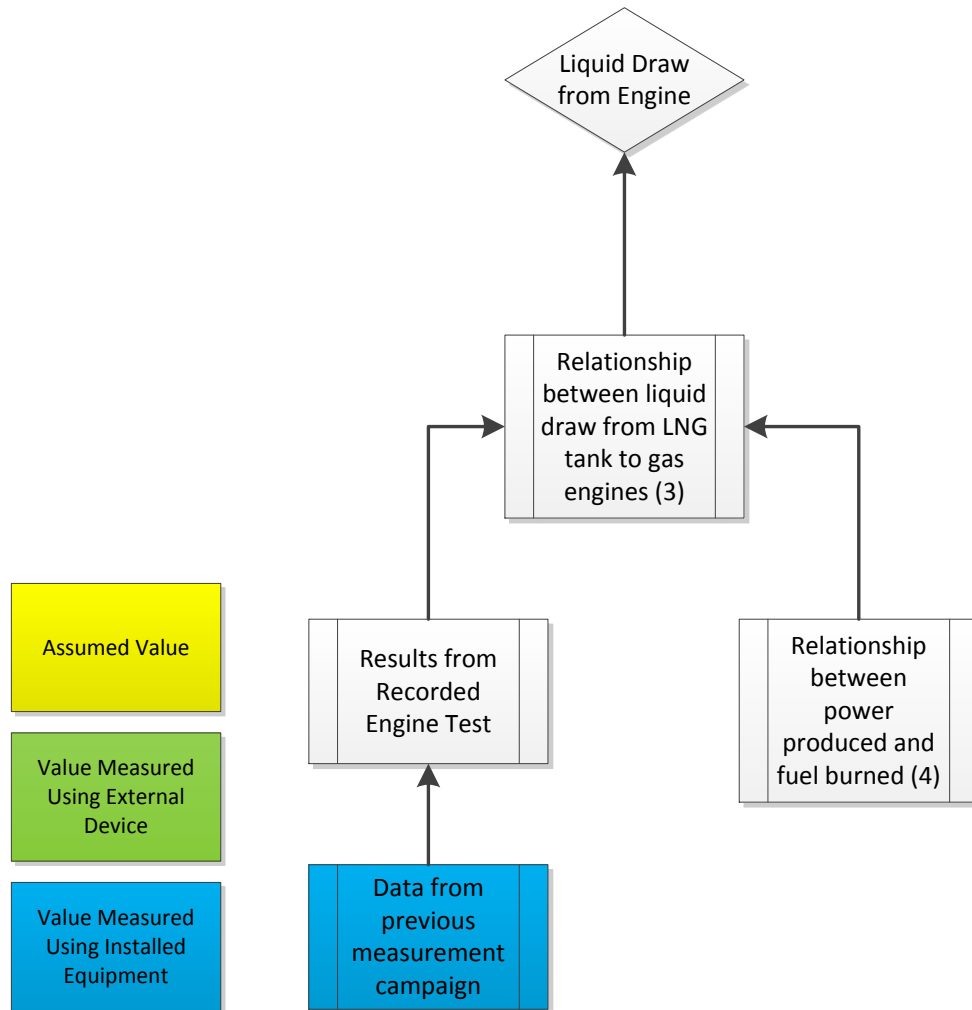
Figure 64: Process Flow to Measure LNG draw from NG Engines

Figure 65 indicates the parameters necessary to calculate the heat rejected from the water glycol traveling through the Vaporizer to the PBU circuit.
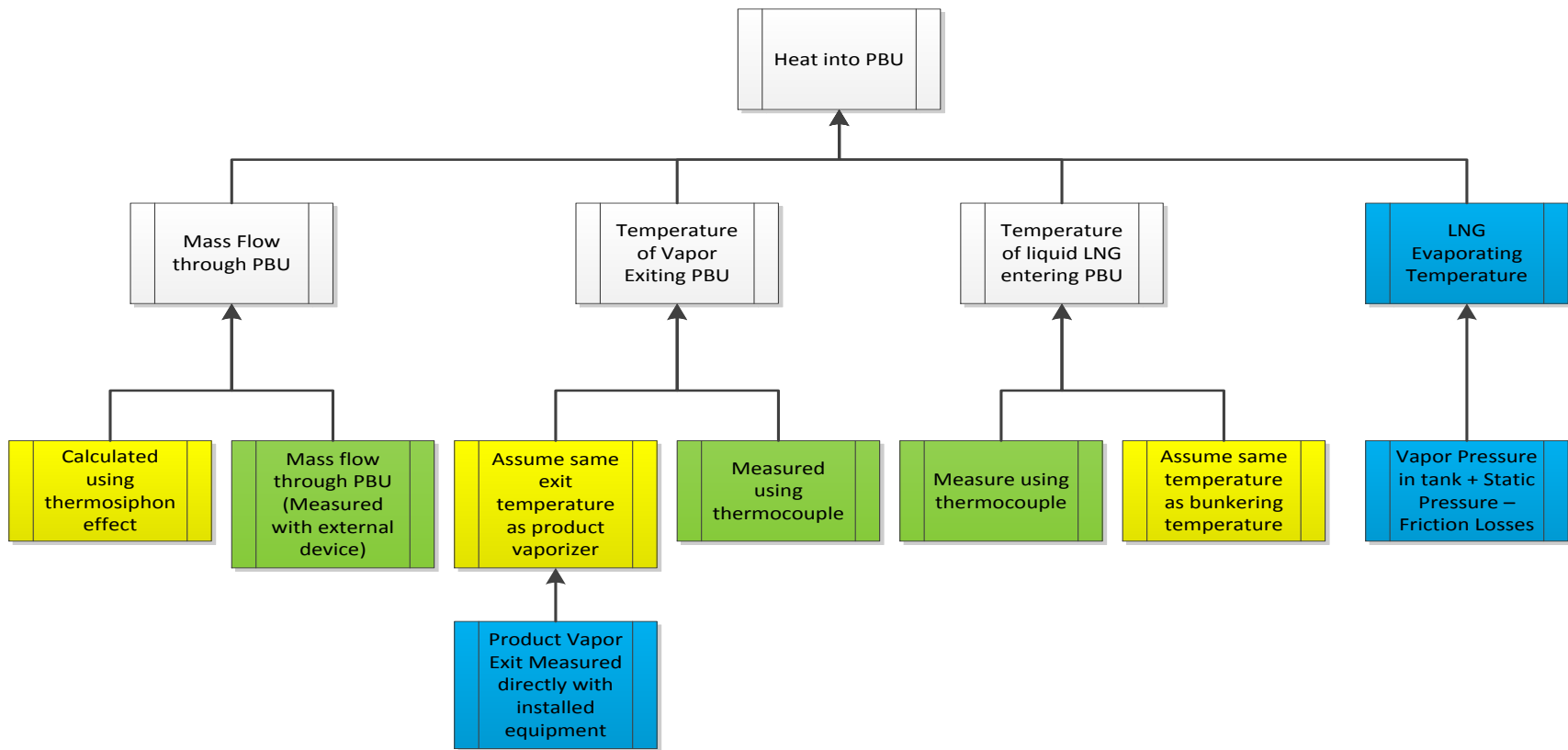
Figure 65: Process Diagram Heat Rejected to PBU Circuit

120

Figure 66 indicates the parameters required to calculate the heat rejected by the water glycol circuit traveling through the Vaporizer.
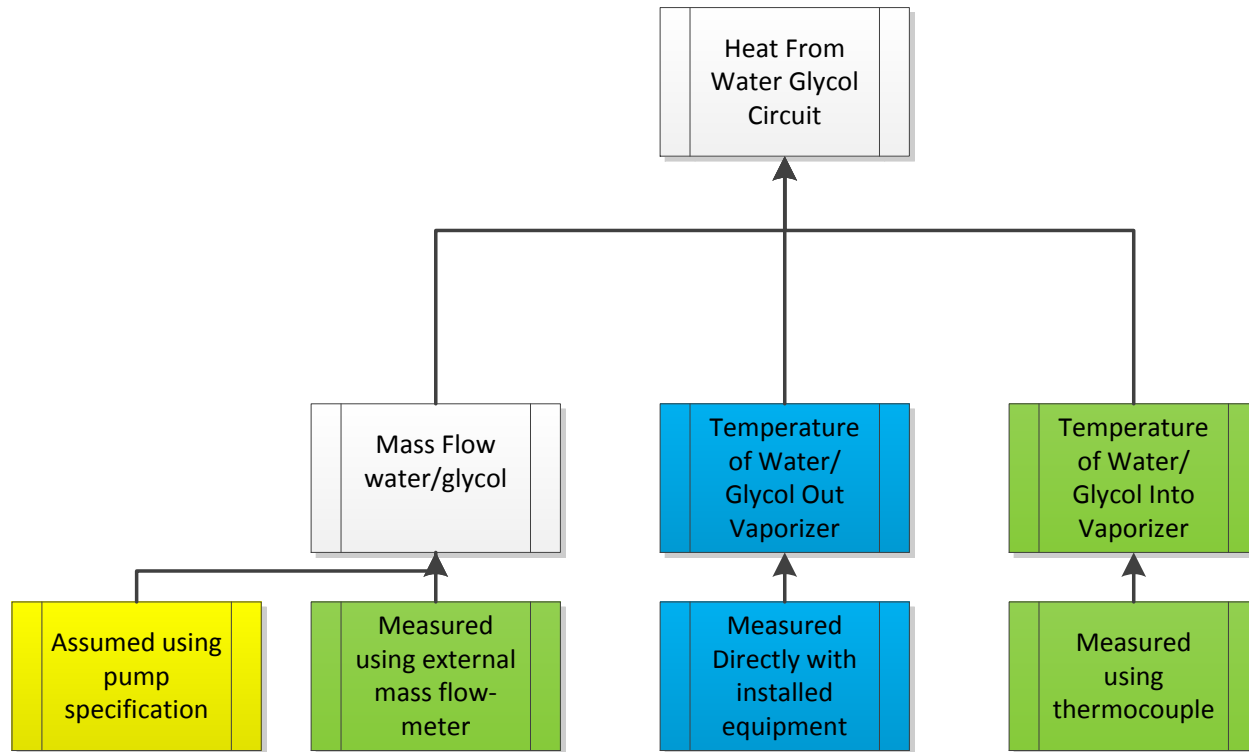
Figure 66: Process Diagram Heat Entering Vaporizer from Water Glycol Circuit

Figure 67 illustrates the parameters required to calculate the heat absorbed by the LNG which is vaporized in the Vaporizer on its way to the NG engines.
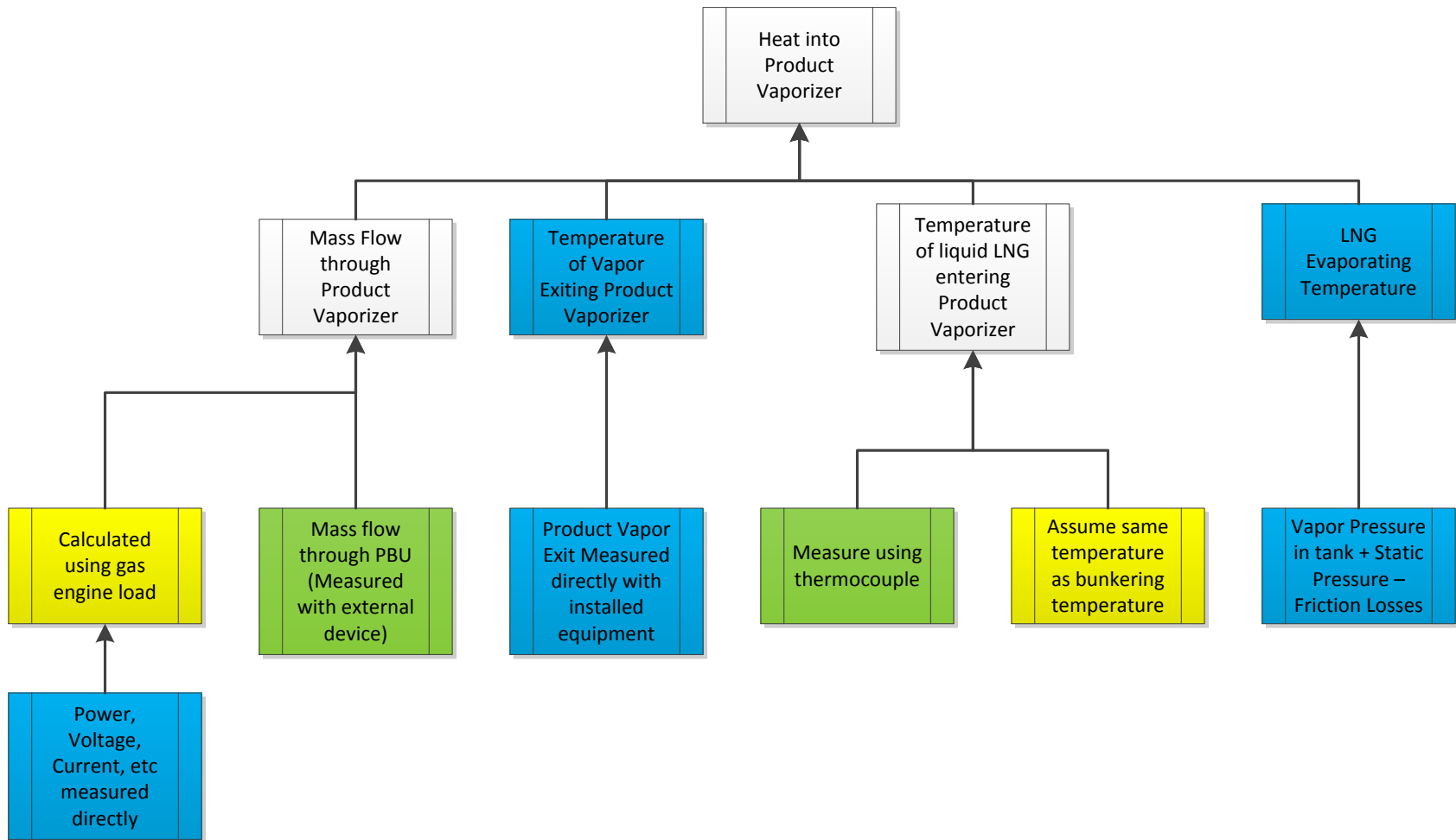
Figure 67: Heat Rejected Into Product Vaporizer Circuit

Figure 68 indicates the parameters required to find the mass in the LNG tank over given amount of time. The process diagram in Figure 68 considers the heel in the tank before bunkering, LNG added during bunkering, and LNG drawn by the NG engines.
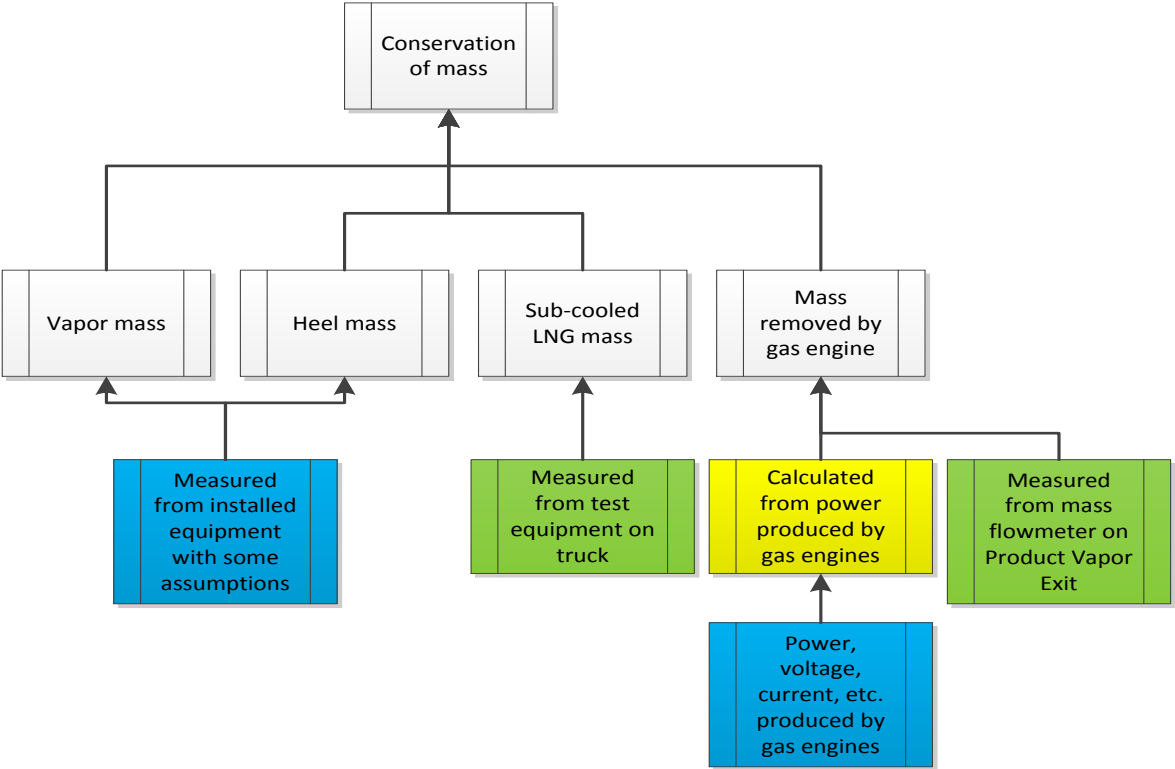
Figure 69 illustrates the parameters required to calculate the thermal energy in the LNG tank after the mixing of heel and bunkered LNG occurs.
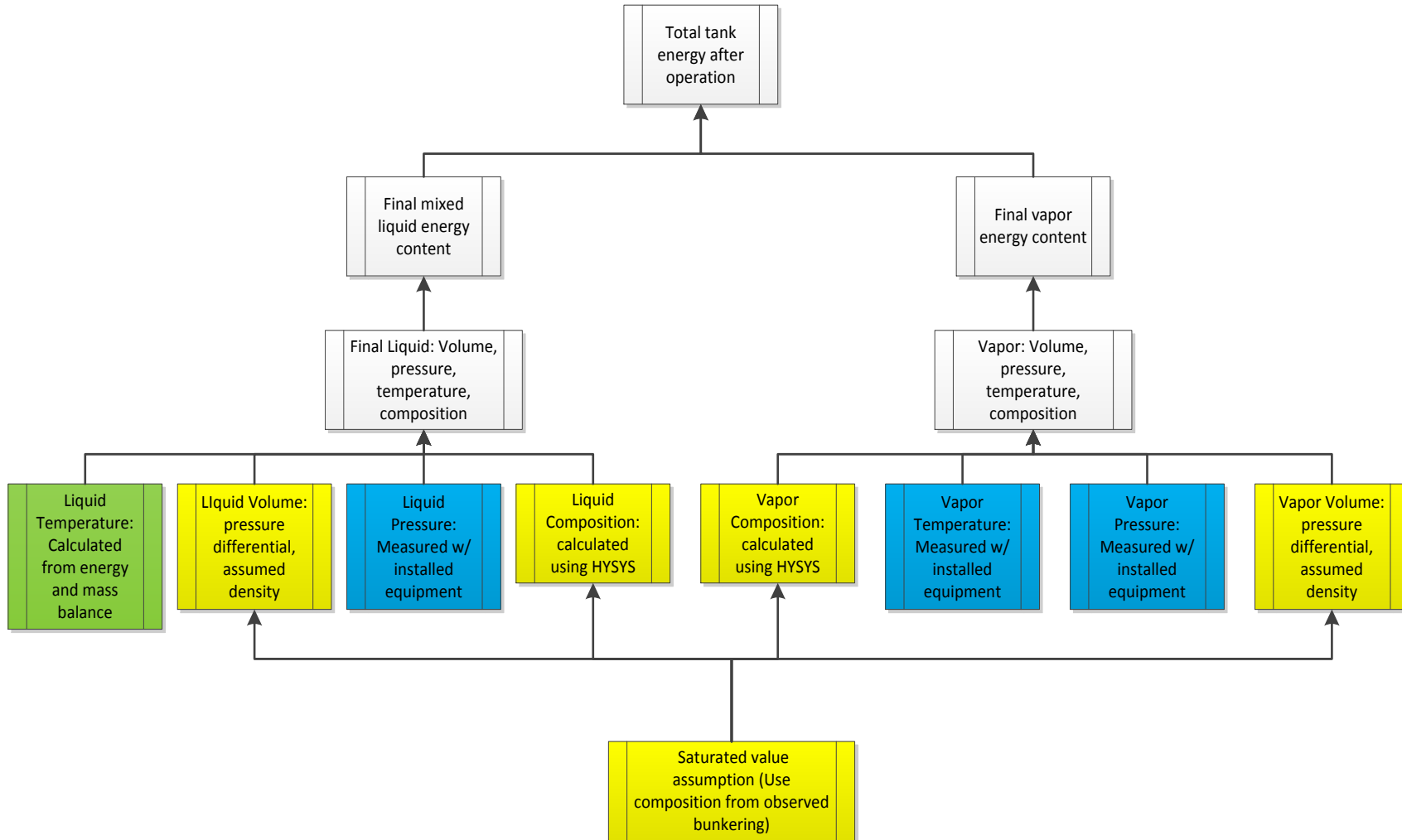
Figure 69: Process Diagram Energy in System After Mixing

Figure 70 indicates the thermal energy in the LNG tank before bunkering.
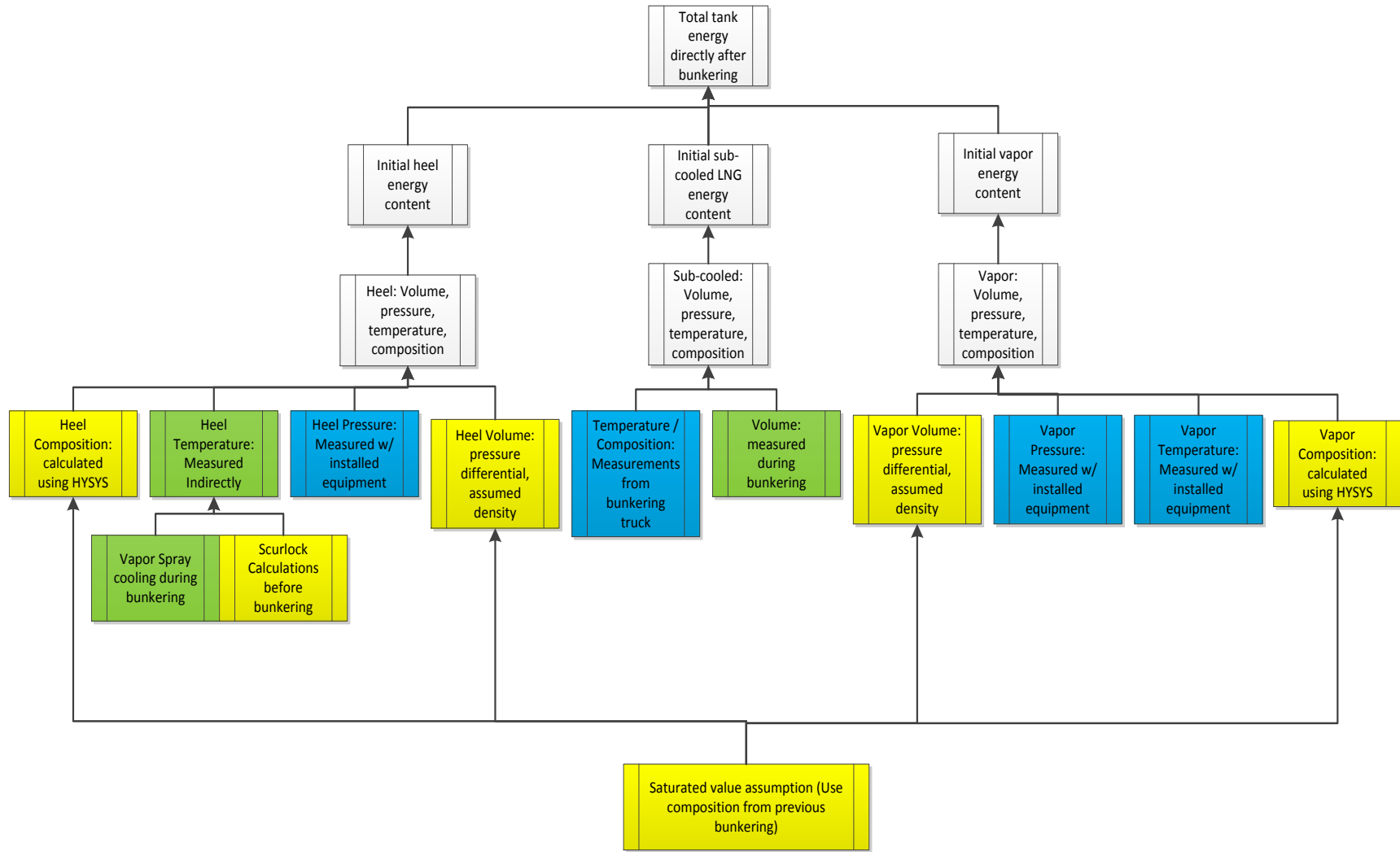
Figure 70: Process Diagram Energy in System Before Mixing

Appendix C: HSE Documentation

FIELD CARD - FOR LEADERS

Name: Joseph DiRenzo   Tel.   90 14 00 47   Insurance company: Tricare International

Home address in Norway: _____Skansegata 2a, Trondheim 7044_____

Communication equipment: _____N/A_____
What kind of equipment will you bring? What frequencies will you use, if applicable?

Next of kin (name, residence and tel.):
Joseph DiRenzoIII and Karen DiRenzo, Suffolk VA (USA), 23435 Home phone (757) 538 2907

FIELDWORK DETAILS*
Fieldwork name/type, contents/activities:

Conducting meaurements of an LNG system on MF Korsfjord and KV Bergen

Fieldwork area/workplace: __Flakk Ferry Terminal / Port of Bergen_____
It is especially important to describe this carefully if the fieldwork area/workplace is difficult to access.

Number of participants (incl. leader): __1_____

Duration From: ___31March2014_____ To: ___30April2014_____

When will participants have time off during their fieldwork? _____N/A_____

Itinerary: _____N/A_____
If applicable, please include flight numbers, flight times and scheduled stopovers/destinations.

Lodging/housing: _____N/A_____
Name, address, phone numbers for hotels/motels, etc. Please fill in if you are using a tent or caravan.

Means of transportation: Trondheim Regional Bus / Regional Flight to Bergen (only one time) _
Please fill in registration number if you are using your own car or a state-owned vehicle.

Safety equipment: face shield used while monitoring bunkering, gloves, all equipment used in Cold Box during monitoring is EX safe

CONTACT PERSONS*
Contact person at your faculty/department: Petter Nekså   Tel. 92606519

Other contact person: Dag Stinersen   Tel. 90503459
* Fill in if you are conducting fieldwork that does not involve any particular risks. (For more information: Fieldwork- for leaders). In the event that your fieldwork is more involved or complicated, you must write a travel plan.

I confirm that I have read NTNU's guidelines on Fieldwork – for leaders.

I confirm that I will comply with the security procedures applicable to the fieldwork, and that I will act in a way to ensure the safety of myself and others.

City/date: __Trondheim 04APR14___   Signature:
Field cards are stored at your faculty/institute during the fieldwork.

NTNU	Safe Job Analysis (SJA) - general	prepared by	Number	Date	
◻ HMS		HSE section	HMSRV2606	29 March 2011	
		Approved by	Page	Replaces	
		Rector	1 of 2		

SJA title: Measurements on KV Bergen and MF Korsfjord fuel tank system

Date:	Location: **KV Bergen and MF Korsfjord**
- Tick for completed checklist: **X**	

Participants:		
Joseph DiRenzo		
Responsible for SJA:	Petter Nekså	

Work description: (What and how?)
Perform non-intrusive measurements of mass flow and temperature with own equipment, as well as recording from onboard instrumentation onboard the ships, as well as onboard the bunkering truck

Risks associated with the work:
See risk assessment documentation

Protection/safety measures: (action plan – see the next page)
Described in measurement campaign documents
Use of protective equipment
Being informed about safety procedures and escape routes

Conclusion/comment:
The work involves risks, but all necessary precautions should have been done

Recommendation/ approval:	Date/Signature:	Recommendation/ approval:	Date/Signature:
Responsible for SJA:	2014-04-04	Responsible for area:	
Responsible for implementation:	2014-04-04	Other (position):	

NTNU	Hazardous activity identification process	Prepared by	Number	Date	
		HSE section	HMSRV-26/01	09.01.2013	
		Approved by	Page	Replaces	
HSE		The Rector	1 out of 1	01.12.2006	

Unit: **Date:**   2014-04-04

Participants in the identification process (including their function):   Joseph DiRenzo, MSc student (JDR)

     Petter Nekså, Prof. and Supervisor NTNU (PN)

Short description of the main activity/main process:

Perform non-intrusive measurements on KV Bergen and MF Korsfjord related to the LNG fuel tank system

Activity/process	Responsible person	Existing documentation	Existing safety measures	Laws, regulations etc.	Comment
Travel to the ship	JDR	NA	Safety belt when available	NA	Use common transport practices
Preparation for measurements	JDR and PN	Measurement plan	Following all procedures specified by the ship owners	Rules for classification of ships/high speed, light craft and naval surface craft Part 6 Chp 13, DnV rule of January 2014 for Gas fuelled ship installations	Ship owners are controlling the measurements
Performing measurements	JDR	As above	As above	As above	
Logging measurements from the ship and trucks logging system	JDR	As above	As above	As above	
Precense in machinery room, within and outside ex zone	JDR	With permission from ship captain and chief engineer	As above	As above	
Recording measurments from the bunkring LNG truck	JDR	With permission from truck driver	As above	As above	

NTNU		Risk assessment		Prepared by HSE section	Number HMSRV2603E	Date 04.02.2011	
				Approved by The Rector	Page 1 out of 3	Replaces 01.12.2006	
HSE/KS							

Unit: **Date:**
Line manager:
Participants in the risk assessment (including their function):

Activity from the identification process form	Potential undesirable incident/strain	Likelihood: Likelihood (1-5)	Consequence: Human (A-E)	Environment (A-E)	Economy/material (A-E)	Risk value	Comments/status Suggested measures
Travel to the ship	Traffic accident	1	E			E1	Use safety precautions, e.g. safety belt….
Preparation for measurements	Falling when installing measurement equipment	2	B			B2	Approach the job in a systematic way and avoid installations in bad weather
Performing measurements	N Gas leak	1	C	C	B	C1 C1 B1	Evacuate the space and follow instructions by the chief engineer
Logging measurements from the ship and trucks logging system	N Gas leak	1	C	C	B	C1 C1 B1	Evacuate the space and follow instructions by the chief engineer
Presence in machinery room, within and outside ex zone	N gas leak and potentially fire	1	C	C	B	C1 C1 B1	Using ex proof equipment where required. Evacuate as above
Recording measurments from the bunkring LNG truck	N gas or LNG spill if a hose rupture	1	C	C	B	C1 C1 B1	Use of gloves and face mask and machine boots Evacuate as above

Likelihood, e.g.:	Consequence, e.g.:	Risk value (each one to be estimated separately):
1. Minimal	A. Safe	Human = Likelihood x Human Consequence
2. Low	B. Relatively safe	Environmental = Likelihood x Environmental consequence

129

Appendix D: Description of the bunkering process

Below is a description of the bunkering process on MF Korsfjord and KV Bergen. This description is based on the bunkering process observed onboard MF Korsfjord on 01 April 2014 and 07 April 2014. Figure 71 provides the process flow diagram of the bunkering process from the LNG truck's tank to the ship's tank.
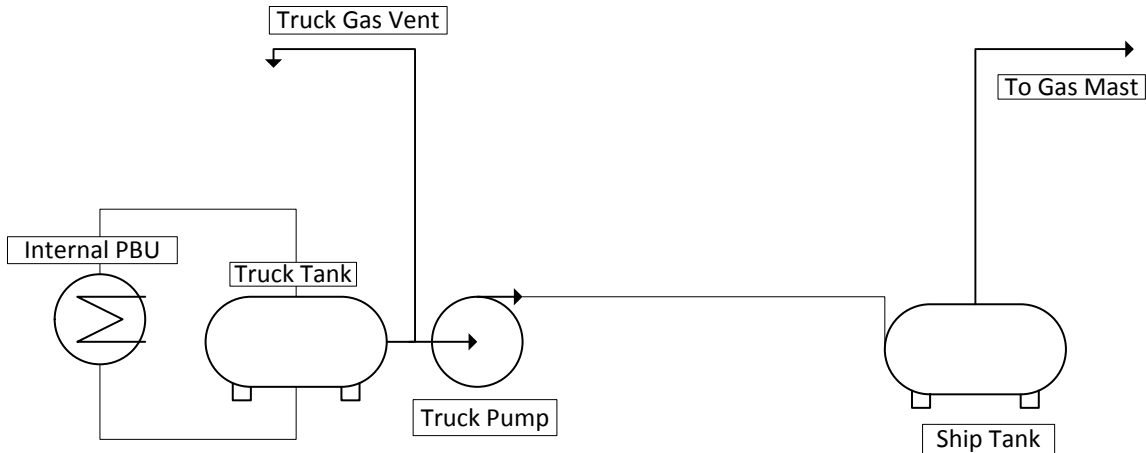
Figure 71: Process Flow Diagram Bunkering Process

According to the Manual for Natural Gas Propulsion System produced by Cryo AB (2009), the following steps are taken in the bunkering process:

1. The vessel receiving LNG is placed in "Normal Standby (NSD) – gas system shut down". This means that the LNG system on the ship is secured including the gas engines and PBU.

2. The bunkering line is connected between bunkering truck and ship. Note that MF Korsfjord employs a fixed shore connection where both the ship and bunkering truck connect. The shore connection is shown in Figure 72. The bunkering station located on MF Korsfjord is shown in Figure 73.

Figure 72: Shore Connection for MF Korsfjord

Figure 73: MF Korsfjord Bunkering Station

3. The bunkering line is inerted with nitrogen from bottles stored on the ship. This nitrogen used for inerting is vented through the gas mast located on the truck. This process takes approximately 5 minutes. The line used for bunkering is shown in Figure 74.

Figure 74: Bunkering Line on MF Korsfjord

4. During this process, the tank pressure in the bunkering truck is increased using an internal PBU.

5. After inerting the bunkering line with nitrogen, gas is purged from the top of the LNG tank on the ship to the gas vent on the bunkering truck. The NG purging from the tank on the ship occurs for approximately 4 minutes.

6. After the line is inerted and the top of the ship's LNG tank is purged, cold tank bunkering commences. LNG is only bunkering from the top of the tank on MF Korsfjord. This method of bunkering causes the top tank pressure in the ship's tank to decrease during bunkering. On KV Bergen, the bunkering system uses an automatic top tank pressure set point. Bunkering initially starts from the top of the tank. When the top tank pressure falls below a predetermined set point then bunkering occurs from the bottom of the tank. This causes the ship's tank pressure to increase. Bunkering from the bottom of the tank continues until an upper top tank pressure limit is reached. The automatic bunkering system then switching back to bunkering from the top of the tank.

7. Once bunkering has concluded, liquid line stripping occurs in which residual liquid inside the bunkering line evaporates and is pushed to the ship's tank.

8. After liquid line stripping is finished, the bunkering valves closest to the LNG tank are shut and any gas that is trapped within the bunkering line is released from the ship's gas mast for approximately 2 minutes. The gas mast on MF Korsfjord is shown in Figure 75.

Figure 75: Gas Mast on MF Korsfjord

9. After releasing the trapped gas from the bunkering line, the bunkering line is inerted and purged using nitrogen. The nitrogen and any remaining trapped gas are released from the ship's gas mast. This is done for approximately 3 minutes.

10. After the line has been inerted, the bunkering hose is disconnected and the bunkering process is secured.

It is also interesting to consider the conditions inside the LNG truck during bunkering. Figure 76 shows the LNG truck tank temperature, tank pressure, pump temperature, and pressure after the LNG pump measured during the bunkering on MF Korsfjord on 07 April 2014.
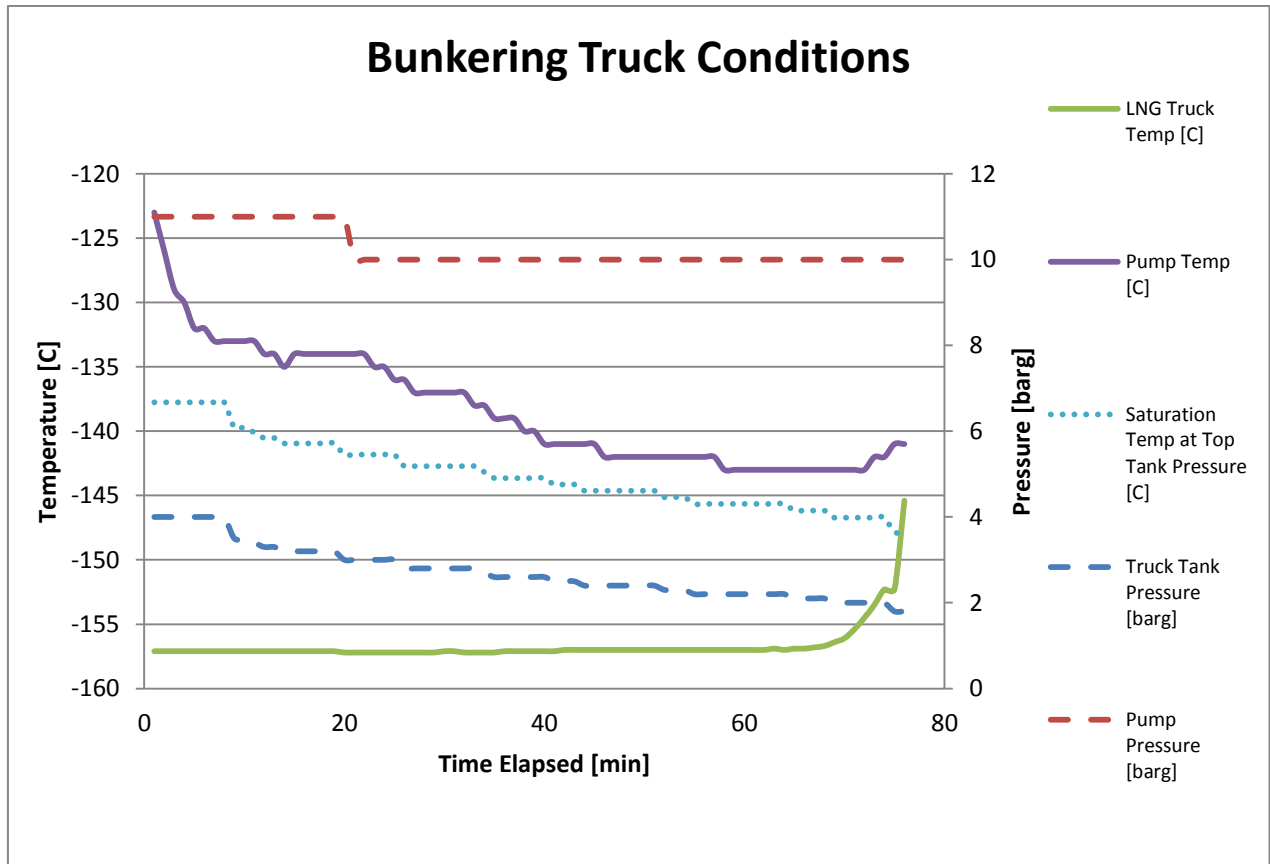
Figure 76: LNG Truck Conditions during Bunkering (Measured 07 April 2014)

Before bunkering begins, the displacement pump used to transfer liquid from the LNG truck to the LNG tank onboard the ship is cooled to a certain temperature before bunkering commences. This is done to avoid evaporation when the content of the LNG truck contacts the pump. As mentioned in the description of the bunkering process, the LNG truck tank is brought to a certain pressure before bunkering begins. As shown in Figure 76, the tank pressure inside the LNG truck decreases as LNG is pumped from the truck to the ship. Also note that the LNG truck temperature increases rapidly near the end of the bunkering process. One possible explanation for this increase in LNG tank temperature is that the sensor inside the LNG tank on the bunkering truck measures the LNG close to the liquid surface layer. Studies indicated in the Literature Review indicate the liquid temperature at the liquid surface is warmer than the liquid near the bottom of the tank. Notice also that the LNG temperature inside the truck tank is sub-cooled below the saturation temperature (bubble point) corresponding to the top tank pressure.

Appendix E: Description of Measurement Campaign for Fjord 1

Purpose:

The purpose of this measurement campaign is to gain a better understanding of the interaction between the liquid heel and sub-cooled bunkered Liquefied Natural Gas (LNG) during and after the bunkering process. Currently, there exists little knowledge about the interactions between these two liquid layers inside an LNG tank. The intended outcome of this project is to gain better insight into the physical interactions between liquid heel and sub-cooled LNG as well as make recommendations to ensure these interactions do not lead to the de-loading of the Natural Gas (NG) engines. At the end of the measurement campaign, a report will be produced with the findings of the project. A copy of this report will be supplied to Fjord 1 to be shared with vessel operators. It is requested that permission be granted by Fjord 1 to conduct this measurement campaign on one of their LNG ferries.

Equipment:

The following equipment will be required for the measurement campaign.

- UF 801-P Ultraflux Portable Flowmeter
- SE 1596-A Flowmeter Probe
- SITRANS FUP1010 Portable Flowmeter
- SITRANS Flowmeter Probe (1011HP-T1 recommended)
- (24) thermocouples and a lab recorder
- Video Recorder (if unable to record plant status using the control panel)
- Stop watch
- Tape measure

Timeline

Table 29 shows the approximate breakdown of time it would take to set up the measurement campaign and portions of the campaign that would require crew involvement.

Event	Approximate Time Required	Crew Involvement
Instrumentation Mounting	<u>2.5 hours</u> (before bunkering)	Requires (1) crew member to gain access to the Cold Box
Initial Conditions Before Bunkering	<u>30 minutes</u> (requires using the PBU before bunkering)	Requires Chief Engineer to activate the PBU to gain initial condition in the LNG tank
Bunkering	No extra time required	Requires (1) member of the crew to record truck variables during bunkering
In Operation	No extra time required	No crew involvement
Dismounting	<u>1 hour</u> (after LNG plant shutdown)	Requires (1) crew member to gain access to the Cold Box

In order to ensure that the data has reasonable reliability, it is preferable that this measurement campaign be <u>performed during (5) different bunkering evolutions</u>. If assistance from the crew is possible during LNG bunkering recording then no additional external personnel will be required.

Configuration of the Measurement Campaign:

Figure 77 shows how the measuring equipment will be set up inside and outside the Cold Box.
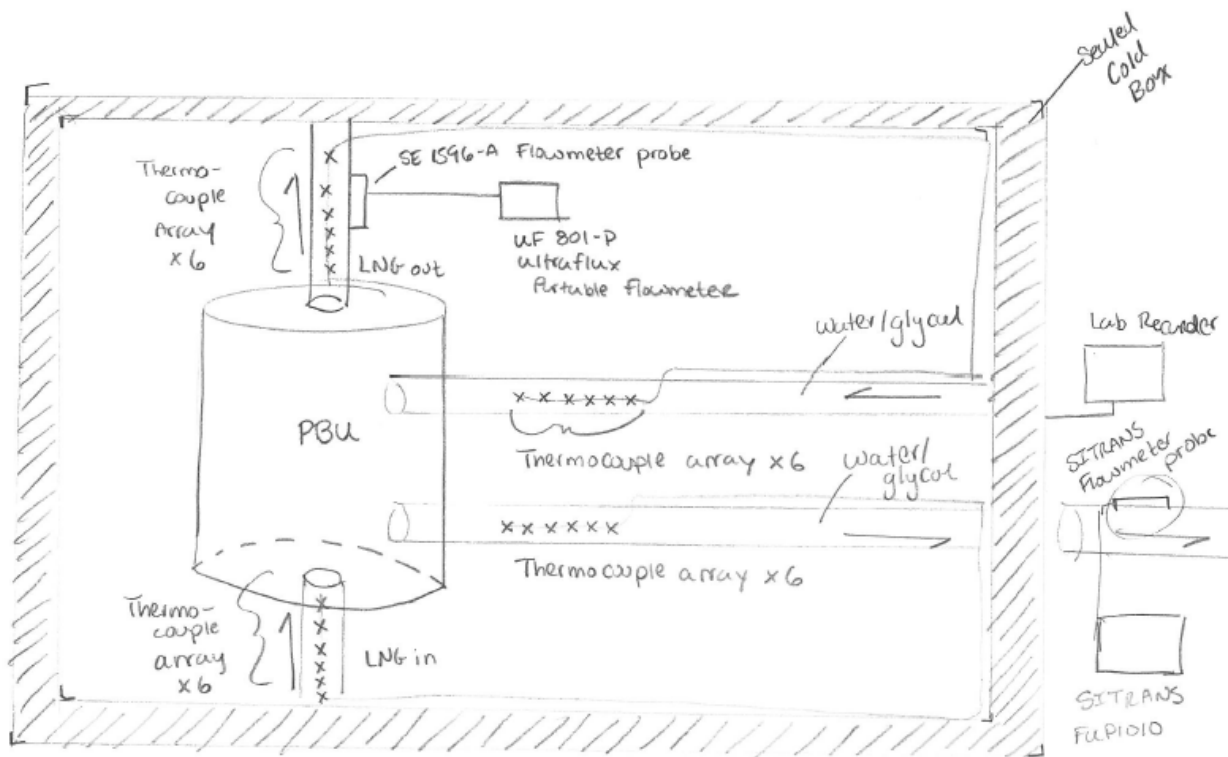
Figure 77: Measuring Equipment Set Up

This configuration makes it possible to measure the following parameters: water/ glycol inlet and outlet temperature to the PBU, LNG inlet and outlet temperature to the PBU, water/glycol volume flow through the PBU, and LNG volume flow through the PBU. In this set up, the SE 1596-A Flowmeter Probe will be connected to the UF 801-P Ultraflux Portable Flowmeter. The SE 1596-A Flowmeter Probe is able to magnetically clamp onto a 20 cm horizontal or vertical surface on the NG outlet pipe from the PBU. According to the Ultraflux UF801-P User's Manual both the UF 801-P Ultraflux Portable Flowmeter and SE 1596-A Flowmeter Probe complies with ATEX Directive 94 /4/CE and Directive 99/92/CE, meaning that they are appropriate for use within the Cold Box.

Four sets of (6) thermocouples will be attached to the outer surfaces of the water/glycol inlet and outlet pipes to the PBU and LNG inlet and outlet pipes to the PBU. The wires from the thermocouples will be led through the hatch of the Cold Box and connected to a lab recorder. Since the lab recorder will not be within the Cold Box the ATEX requirement is not applicable. Since the wires of the thermocouples are small (<1mm) the Cold Box may be resealed after all the measuring equipment has been set up in the Cold Box.

Outside of the Cold Box, the SITRANS Flowmeter and probe will be attached to water/glycol pipe entering the Cold Box. Similar to the UF 801-P Ultraflux Portable Flowmeter, the probe on

137

the SINTRANS flowmeter is able to be magnetically clamped onto the metal surface of the water/glycol pipe before it enters the Cold Box.

Sequence of Events:

1. Initial Set-Up:
   a. *Status of the LNG plant*: Gas Engines not operating
   b. *Time Required*: Approximately 3 hours (2.5 hours for set up; 0.5 hours to obtain initial conditions)
   c. *Process*:
      i. Gain access to the Cold Box on MF Tresfjord. This step requires (1) member of the crew to gain access to the Cold Box.
      ii. Attach the SE 1596-A Flowmeter Probe to a horizontal or vertical surface of the NG gas return line on the PBU circuit.
      iii. Attach (6) thermocouples to the LNG inlet pipe to the PBU and attach (6) thermocouples to the NG outlet pipe from the PBU.
      iv. Attach (6) thermocouples to the water/glycol inlet pipe to the PBU.
      v. Attach (6) thermocouples to the water/glycol outlet pipe to the PBU.
      vi. Connect all (24) thermocouples to the lab recorder and confirm they are zeroed out and the lab recorder is recording properly.
      vii. Seal access to the Cold Box on MF Tresfjord. This step requires (1) member of the crew to seal the Cold Box.
      viii. Attach the SITRANS Flowmeter Probe to the inlet water / glycol pipe (i.e. water / glycol entering the PBU). Both the SITRANS probe and flowmeter will be in the engine room and outside the Cold Box.
      ix. Operate the PBU circuit for 5 minutes or until max operating tank pressure is achieved. Ensure the NG piping to the gas engines is not receiving any NG. This step requires Chief Engineer to activate equipment / machinery to run the PBU circuit.
   d. *Purpose*: This stage of the measurement campaign serves two purposes. The first purpose is to mount the equipment that will be used to measure the plant during and after bunkering. The second purpose is to obtain the liquid heel temperature in the tank (i.e. the temperature of the LNG existing in the tank before bunkering). Depending on the pressure in the LNG tank, the PBU will increase the pressure in the tank rapidly since there is no liquid draw from the NG gas engines. It is preferred that the pressure in the LNG tank be kept as low as possible the previous time the system is operated (i.e. the day before the measurement campaign).
   e. *Other Considerations*:
      i. *Ex safe equipment*: According to the Ultraflux UF801-P User's Manual both the UF 801-P Ultraflux Portable Flowmeter and SE 1596-A

Flowmeter Probe complies with ATEX Directive 94 /4/CE and Directive 99/92/CE.

ii. *Thermocouple*s: The wires from the (24) thermocouples will be led from the pipes to the entrance of the Cold Box. Since the thermocouple wires are small (<1mm) they should not affect the seal provided by the Cold Box hatch.

2. Bunkering:
   a. *Status of the LNG plant*: In operation
   b. *Process*: This step requires (1) member of the crew to assist in recording the conditions at the LNG truck.
      i. Before bunkering note the following:
         1. Top tank temperature
         2. Top tank pressure
         3. Liquid Height / Liquid Volume
         4. Assumed LNG Density (**Note: input determined by the plant operator)
         5. Approximate time since LNG plant was last operated
      ii. After the bunkering connection has been established and the bunkering line inerted, the crew member recording will note the LNG temperature exiting the bunkering truck, pressure, and flowrate. These three measurements will be taken every minute until bunkering is complete.
      iii. I will be in the engine room recording the following information every minute:
         1. Top Tank Pressure
         2. Top Tank Temperature
         3. Liquid height / Liquid Volume
         4. Assumed LNG Density (If value has changed)
      iv. I will also note when bunkering has commenced. During bunkering, I will note if the LNG is being filled from the top of the tank or the bottom of the tank and when any switching occurs between top and bottom filling.
      v. *Post bunkering*:
         1. After bunkering the LNG remaining in the pipes will be "blown down" into the tank and the pipes inerted with N2. I will record how long the "blow down" occurs as well as the top tank pressure and temperature before and after the "blow down".
         2. I will also note if the PBU is used to increase the top tank pressure after bunkering. If so, I wil note the initial top tank pressure and temperature, PBU operating duration, percent open of the PBU valve, and final tank pressure and temperature.
   c. *Purpose*: The purpose of this section of the measurement campaign is to record how much sub-cooled LNG is bunkered and approximately where it is placed

within the LNG tank. Having a clear idea of where the different liquid layers exists and at what amount will be important in estimating how the plant will react once operations begin.

   d.   *Other Considerations*:
        i.   *Plant Recording*: Before conducting the measurement campaign, it should be established whether the vessel is capable of electronically recording the output from the different sensors on the control panel over a period of time. If this is not possible the next best solution is to have video recorder recording the control panel during the bunkering process to ensure that the plant status is recorded correctly over time.

3.   Post Bunkering Operation:
   a.   *Status of the LNG plant*: In operation
   b.   *Process*: While the ferry is operating, I will note the following from the control panel:
        i.   Top Tank Pressure
        ii.   Top Tank Temperature
        iii. Liquid height / Liquid Volume
        iv.   Assumed LNG Density (If value has changed)
        v.   Power produced by gas engines
        vi.   Voltage and current produced by gas engines
        vii. Percent open PBU versus time
        viii. Ship movement information
              1.   Average Speed
              2.   Distance traveled
              3.   Direction traveled
              4.   Sea state (wind, wind direction, wave height, etc.)
   c.   *Purpose*: The purpose of this portion of the measurement campaign is to record the changing conditions inside the LNG tank while the system is operating. Note that external factors like the weather and sea state are also taken into considerations.
   d.   *Other Considerations*:
        i.   *Recovering measuring equipment*: At the end of each measurement day, the flowmeter and probe will be collected from the Cold Box once the LNG plan is secured. If the measurement campaign will be conducted on the same ferry the next day then the thermocouples and lab recorder will remain attached to the pipes in the Cold Box. This will reduce the set up time the next by approximately 1 hour.

Benefits from the Measurement Campaign: This measurement campaign was initially conceived after receiving reports from other LNG vessels that the NG engines de-loaded after bunkering due to low pressure in the LNG tank. The results of the report may be shared with the

operators on Fjord 1 ferries to understand the physical interactions inside the LNG tank while the plant is operating. This information may be taken into consideration when mixing old and new LNG to avoid situations where the contents of the LNG tank react undesirably.

Appendix F: Water Glycol Fluid Properties

The mathematical models and constants used to calculate the fluid properties of the glycol mixture were taken from mathematical models developed by Conde Engineering (2011). The model used to calculate the density, thermal conductivity, and specific thermal capacity are given in Equation (97).

$$P_x = A_1 + A_2\theta + A_3\frac{273.15}{T_{GLY}} + A_4\theta\frac{273.15}{T_{GLY}} + A_5\left(\frac{273.15}{T_{GLY}}\right)^2 \tag{97}$$

The model used to calculate the dynamic viscosity and Prandtl number are given in Equation (98).

$$\ln(P_x) = A_1 + A_2\theta + A_3\frac{273.15}{T_{GLY}} + A_4\theta\frac{273.15}{T_{GLY}} + A_5\left(\frac{273.15}{T_{GLY}}\right)^2 \tag{98}$$

Table 30 provides the constants used in these models to calculate the different fluid parameters.

Table 30: Ethylene Glycol Parameters

Parameter Order	ρ_{GLY}	Cp_{GLY}	k_{GLY}	μ_{GLY}	Pr_{GLY}
1	658.49825	5.36449	0.83818	-4.63024	3.96951
2	-54.81501	0.78863	-1.37620	-2.14817	0.70076
3	664.71643	-2.59001	-0.07629	-12.70106	-12.98045
4	232.72605	-2.73187	1.07720	5.40536	2.64789
5	-332.61661	1.43759	-0.20174	10.98990	11.58900

The temperature values entered into Equations (97) and (98) are provided in Kelvin. These equations were programmed into MATLAB and used while calculating the mass flow through the PBU. The water / glycol temperature used to calculate the PBU mass flow was an average of the inlet and outlet temperatures according to values listed on system drawings.

Appendix G: MATLAB program for the Overall Heat Transfer Coefficient, U, of the PBU

```matlab
%Overall Heat Transfer coefficient of PBU
%LNG values based on October 2013 bunkering


function[U_PBU]=UPBU(m_PBU,P_A,T_A)
N=4.5; %Number of coil rows in PBU
n=20; %Number of tubes
d_tube_i=0.0090; %inner diameter of tube [m]
t_tube=0.001; %tube thickness [m]
d_tube_o=d_tube_i+2*t_tube; %outer diameter of tube [m]
p_tube=1.5*d_tube_o; %coil pitch [m]
C_PBU=1.220; %Diameter of PBU [m]
B_PBU=0.7000; %Diameter of Annulus [m]
r_coil=(B_PBU+(.5*(C_PBU-B_PBU)))/2;
%Mole fraction of LNG
Nitrogen=0.005;
Methane=0.95;
Ethane=0.0383;
Propane=0.0055;
Nbutane=0.0007;
Pentane=0.0005;


%Dummy Variables - Measured Values at a specific point in time
T_GLY_in=299; %[K] water / glycol temp in (drawing 3530-707-002D)
T_GLY_out=295; %[K] water / glycol temp out (drawing 3530-707-002D)
T_GLY_m=(T_GLY_in+T_GLY_out)/2; %temperature in K
T_GLY_w=T_A; %assumed pipe wall temp [K]
CNT_GLY=0.5; %Concentration of Ethelyene Glycol to Water
Q_GLY=60; %Volume flow of water / glycol [m^3/hr]



%Defining the LNG properties
%Pr_LNG is unitless (Prandtl number)
Pr_LNG=refpropm('^','T',T_A,'P',P_A,'nitrogen','methane','ethane','propane','butane','pentane',[Nitrogen Methane Ethane Propane Nbutane Pentane]);
%V_LNG is given in Pa*s (dynamic viscosity)
V_LNG=refpropm('V','T',T_A,'P',P_A,'nitrogen','methane','ethane','propane','butane','pentane',[Nitrogen Methane Ethane Propane Nbutane Pentane]);
%L_LNG is given in W/(m*K) (thermal conductivity)
L_LNG=refpropm('V','T',T_A,'P',P_A,'nitrogen','methane','ethane','propane','butane','pentane',[Nitrogen Methane Ethane Propane Nbutane Pentane]);

%Defining the water/glycol mixture properties
%The EOS must be programmed into MATLAB directly because REFPROP cannot
%process water/ glycol mixtures; Information from M.Conde Engineering (2011)
%Parameters for density [kg/m^3]
A_1_D=658.49825;
A_2_D=-54.81501;
A_3_D=664.71643;
A_4_D=232.72605;
A_5_D=-322.61661;
%Parameters for heat capacity [kJ/kg K]
%A_1_Cp=5.36449;
%A_2_Cp=0.78863;
```

```matlab
%A_3_Cp=-2.59001;
%A_4_Cp=-2.73187;
%A_5_Cp=1.43759;
%Parameters for thermal conductivity [W/m K]
A_1_L=0.83818;
A_2_L=-1.37620;
A_3_L=-0.07629;
A_4_L=1.07720;
A_5_L=-0.20174;
%Parameters for dynamic viscocity [Pa s]
A_1_V=-4.63024;
A_2_V=-2.14817;
A_3_V=-12.70106;
A_4_V=5.40536;
A_5_V=10.98990;
%Parameters for Prandtl number [-]
A_1_Pr=3.96951;
A_2_Pr=0.70076;
A_3_Pr=-12.98045;
A_4_Pr=2.64789;
A_5_Pr=11.58900;
%Equation for density of Ethelyene Glycol mixture [kg/m^3]
D_GLY=A_1_D+(A_2_D*CNT_GLY)+(A_3_D*(273.15/T_GLY_m))+(A_4_D*CNT_GLY*(273.15/T_
GLY_m))+(A_5_D*((273.15/T_GLY_m).^2));
%Equation for thermal conductivity of Ethelyene Glycol mixture [W/m K]
L_GLY=A_1_L+(A_2_L*CNT_GLY)+(A_3_L*(273.15/T_GLY_m))+(A_4_L*CNT_GLY*(273.15/T_
GLY_m))+(A_5_L*((273.15/T_GLY_m).^2));
%Equation for dynamic viscosity of Ethelyene Glycol mixture [Pa s]
V_GLY=exp(A_1_V+(A_2_V*CNT_GLY)+(A_3_V*(273.15/T_GLY_m))+(A_4_V*CNT_GLY*(273.1
5/T_GLY_m))+(A_5_V*((273.15/T_GLY_m).^2)));
%Equation for prandtl number of Ethelyene Glycol mixture [-]
Pr_GLY=exp(A_1_Pr+(A_2_Pr*CNT_GLY)+(A_3_Pr*(273.15/T_GLY_m))+(A_4_Pr*CNT_GLY*(
273.15/T_GLY_m))+(A_5_Pr*((273.15/T_GLY_m).^2)));


%Sequence of equations needed to calculate U_PBU
%Calculating additional PBU geometry
%Calculation methodology based on Patil, Shende, and Ghosh (1982)
l=N*sqrt(((2*pi*r_coil).^2)+(p_tube.^2)); %Length of one of the coils [m]
L=n*l; %Overall length of piping [m]
V_c=(pi/4)*(d_tube_o.^2)*L; %Volume of piping occupied by coil [m^3]
V_a=(pi/4)*((C_PBU.^2)-(B_PBU.^2))*p_tube*N; %Volume between PBU shell and
Annulus [m^3]
V_f=V_a-V_c; %Space available for glycol flow [m^3]
D_e=(4*V_f)/(pi*d_tube_o*L); %Equivalent diameter of tube [m]


%Heat transfer occuring outside the PBU, [ho]
M_GLY=(Q_GLY/3600)*D_GLY; %Mass flowrate of water / glycol [kg/s]
D_H1=(2*r_coil)-(d_tube_o); %inside diameter of helix [m]
D_H2=(2*r_coil)+(d_tube_o); %outside diameter of helix [m]
G_GLY=M_GLY/((pi/4)*((((C_PBU.^2)-(B_PBU.^2))-(n*((D_H2.^2)-(D_H1.^2))))));
%mass velocity [kg/m^2*s]
Re_GLY=(G_GLY*D_e)/V_GLY; %Reynolds number for water/glycol flow [-]


%Laminar / turbulent flow determines outter heat transfer coefficient
[W/(m^2*K)]
if Re_GLY < 10000;
```

```matlab
    h_o=(1/D_e)*(0.6*(Re_GLY.^0.5)*(Pr_GLY.^0.31)*L_GLY);
else

V_GLY_w=exp(A_1_V+(A_2_V*CNT_GLY)+(A_3_V*(273.15/T_GLY_w))+(A_4_V*CNT_GLY*(273
.15/T_GLY_w))+(A_5_V*((273.15/T_GLY_w).^2)));

h_o=(1/D_e)*0.36*(Re_GLY.^0.55)*(Pr_GLY.^(1/3))*((V_GLY/V_GLY_w).^0.14)*L_GLY;
end


%Determining the inner heat transfer coefficient
%First we must assume a Reynold's number for the inside flow
%Coorelations based on Gnielinski (1987) [-]
Re_LNG=(m_PBU/((pi/4)*d_tube_i*n))*(1/V_LNG);
Re_crit=2300*(1+8.6*((d_tube_i/(2*r_coil)).^0.45));

%Calculating Nu for LNG [-]
m_LNG=0.5+0.2903*((d_tube_i/(2*r_coil)).^0.194);
f_BD=(0.3164/(Re_LNG.^0.25))+(0.03*((d_tube_i/(2*r_coil)).^0.5));
A_LNG=(22000-Re_LNG)/(22000-Re_crit);
if Re_LNG < Re_crit

Nu_LNG=3.65+(0.08*(1+0.8*((d_tube_i/(2*r_coil)).^0.9)*(Re_LNG.^m_LNG)*(Pr_LNG^
(1/3))));
elseif Re_LNG > 22000
    Nu_LNG=((f_BD/8)*Re_LNG*Pr_LNG)/(1+(12.7*sqrt(f_BD/8)*((Pr_LNG.^(2/3))-
1)));
else

Nu_LNG=(A_LNG*(3.65+(0.08*(1+0.8*((d_tube_i/(2*r_coil)).^0.9)*(Re_crit.^m_LNG)
*(Pr_LNG^(1/3))))))+((1-
A_LNG)*((((1/8)*22000*Pr_LNG)/(1+(12.7*sqrt(f_BD/8)*((Pr_LNG.^(2/3))-1))))));
end


%Calculating inner heat transfer coefficient h_i
h_ic=(Nu_LNG*L_LNG)/d_tube_i; %[W/(m^2*K)]
h_io=h_ic*((2*r_coil)/d_tube_i);
%Calculating the Overall Heat Transfer Coefficient for PBU
L_steel=16; %Thermal conductivity stainless steel (W/(m*K))

U_PBU=1/((1/h_io)+(1/h_o)+(t_tube/L_steel)); % Units give in[W/(m^2*K)]

end
```

Appendix H: MATLAB program calculating the mass flow through the PBU

```matlab
clear all
clc
%Geometrical Constants of PBU Unit
N=4.5; %Number of coil rows in PBU
n=20; %Number of tubes
d_tube_i=0.0090; %inner diameter of tube [m]
t_tube=0.001; %tube thickness [m]
d_tube_o=d_tube_i+2*t_tube; %outer diameter of tube [m]
p_tube=1.5*d_tube_o; %coil pitch [m]
C_PBU=1.220; %Diameter of PBU [m]
B_PBU=0.7000; %Diameter of Annulus [m]
r_coil=(C_PBU+B_PBU)/4;
%Mole fraction of LNG
Nitrogen=0.005;
Methane=0.95;
Ethane=0.0383;
Propane=0.0055;
Isobutane=0.0025;
Nbutane=0.0007;
Pentane=0.0005;
%Geometric Constants of additional piping
d_inner_AB=0.028; % [m] diameter of pipe AB (drawing 3530-707-002D)
t_AB=0.0015; % [m] thickness of pipe AB (drawing 3530-707-002D)
tank_B=1.55; % [m] vert height from tank bottom to B (drawing B600083751-1)
h_BD=0.900; % [m] vert hieght from B to D (drawing B600083494-0)
d_inner_DA=0.063; % [m] diameter of pipe DA (drawing 3530-707-002D)
t_DA=0.002; % [m] thickness of pipe DA (drawing 3530-707-002D)
d_tank=4.900; % [m] tank diameter (drawing B600083618-03)
e_AB=0.000004; % [m] surface roughness pipe AB (precision steel DIN2391
standard)
e_DA=0.000004; % [m] surface roughness pipe DA (precision steel DIN2391
standard)
L_AB=3;% [m] length of pipe from A to B
L_DA=5;% [m] length of pipe from D to A

%Dummy Variables - Measured Values at a specific point in time
P_A=300; % Pressure at A [kPa]
T_A= 113; %Liquid Temperature at A [K]
h_LNG=d_tank*0.9; %tank liquid height [m] Corresponds to half full
P_GLY=101.3; %presure in [kPa]
T_GLY_in=299; %[K] water / glycol temp in (drawing 3530-707-002D)
T_GLY_out=295; %[K] water / glycol temp out (drawing 3530-707-002D)
T_LNG_out=294; % [K] LNG temp out of PBU (estimation; assumed 1 K temp
approach)
T_GLY_m=(T_GLY_in+T_GLY_out)/2; %temperature in K
T_GLY_w=T_A; %assumed pipe wall temp [K]
CNT_GLY=0.5; %Concentration of Ethelyene Glycol to Water
Q_GLY=60; %Volume flow of water / glycol [m^3/hr]

%Forward loop to calculate mass flow
e_tol=1;
P_surface=510;
m_PBU=0.1;
```

```matlab
X=[];
dP_loop=5;
while P_A<500

while (abs(P_A - P_surface) > e_tol)
    m_PBU=m_PBU+.001;

    if m_PBU > 10;
        disp('circulation rate too high');
        break
    end

%D_LNG is given in kg/m^3 (density)
D_LNG_A=refpropm('D','T',T_A,'P',P_A,'nitrogen','methane','ethane','propane','butane','pentane',[Nitrogen Methane Ethane Propane Nbutane Pentane]);
dP_tank=(h_LNG+tank_B)*D_LNG_A*9.8*0.001; %Pressure difference [kPa]


%Defining the LNG properties at A
%H_LNG is given in J/kg (ethalpy)
H_LNG_A=refpropm('H','T',T_A,'P',P_A,'nitrogen','methane','ethane','propane','butane','pentane',[Nitrogen Methane Ethane Propane Nbutane Pentane]);
%Pr_LNG is unitless (Prandtl number)
Pr_LNG_A=refpropm('^','T',T_A,'P',P_A,'nitrogen','methane','ethane','propane','butane','pentane',[Nitrogen Methane Ethane Propane Nbutane Pentane]);
%V_LNG is given in Pa*s (dynamic viscosity)
V_LNG_A=refpropm('V','T',T_A,'P',P_A,'nitrogen','methane','ethane','propane','butane','pentane',[Nitrogen Methane Ethane Propane Nbutane Pentane]);
%L_LNG is given in W/(m*K) (thermal conductivity)
L_LNG_A=refpropm('V','T',T_A,'P',P_A,'nitrogen','methane','ethane','propane','butane','pentane',[Nitrogen Methane Ethane Propane Nbutane Pentane]);


%Pressure at point B
%Accout for static pressure and pressure losses due to friction

%Guess Reynold's number from A to B [-]
Re_AB=(m_PBU/((pi/4)*(d_inner_AB)))/V_LNG_A;
%Guess circulation speed of LNG [m/s]
V_AB=m_PBU/(D_LNG_A*((pi/4)*(d_inner_AB.^2)));

%Calculating friction factor in the pipe [-]
%The turbulent friction factor uses the Colebrook white
%disp(Re_AB);
if Re_AB>2300
    f_d_AB=colebrook(Re_AB,(e_AB/d_inner_AB));
else
    f_d_AB=64/Re_AB;
end


%term for the pressure drop from A to B because of pipe roughness [kPa]
dP_AB_sr=(f_d_AB*L_AB*D_LNG_A*(V_AB.^2)*(1/(2*d_inner_AB))/1000; %this term
accounts for surface roughness
%this term accounts for minor losses from valves and bends
%there is one globe valve (HV113) and at least one 45 deg bend and one 90
%deg bend in the design
```

```
dP_AB_globe=340*f_d_AB*(V_AB.^2)*(1/(2*d_inner_AB))/1000; %pressure loss from
globe valve
dP_AB_45=16*f_d_AB*(V_AB.^2)*(1/(2*d_inner_AB))/1000; %pressure loss from 45
deg bend
dP_AB_90=30*f_d_AB*(V_AB.^2)*(1/(2*d_inner_AB))/1000; %pressure loss from 90
deg bend

%Calculating the pressure at point B
P_B=P_A-dP_AB_sr-dP_AB_globe-dP_AB_45-dP_AB_90+dP_tank; %Pressure at point B
[kPa]
%disp(P_B);
%Calculations from point B to point C
%Sensible Heating Zone - Assume only liquid
P_sat_1=refpropm('P','T',T_A,'Q',0,'nitrogen','methane','ethane','propane','bu
tane','pentane',[Nitrogen Methane Ethane Propane Nbutane Pentane]);
P_sat_2=refpropm('P','T',(T_A+10),'Q',0,'nitrogen','methane','ethane','propane
','butane','pentane',[Nitrogen Methane Ethane Propane Nbutane Pentane]);
dT_dP_sat=(10)/(P_sat_2-P_sat_1); %[K/kPa] saturation curve linearized about A
% density at [kg/m^3]
D_LNG_B=refpropm('D','T',T_A,'P',P_B,'nitrogen','methane','ethane','propane','
butane','pentane',[Nitrogen Methane Ethane Propane Nbutane Pentane]);
dP_L_BC=(D_LNG_B*9.81)/1000; % [kPa/m] pressure gradient zone B to C
dT_m=((T_GLY_in-T_LNG_out)-(T_GLY_out-T_A))/(log((T_GLY_in-
T_LNG_out)/(T_GLY_out-T_A))); %[K] Log-mean temp difference PBU
Cp_LNG_B=refpropm('C','T',T_A,'P',P_B,'nitrogen','methane','ethane','propane',
'butane','pentane',[Nitrogen Methane Ethane Propane Nbutane Pentane]);
U=UPBU(m_PBU,P_A,T_A); %[W/(m^2*K)] ftn calling overall heat transfer
coefficient
dT_L_BC=(pi*d_tube_i*n*U*dT_m)/(m_PBU*Cp_LNG_B); % [K/m] temperature gradient
zone B to C
P_BC_BA=(dT_dP_sat)/(dT_dP_sat+(dT_L_BC/dP_L_BC)); %Pressure change B minus C
over presure change B minus A [-]
L_BC=(h_BD)*P_BC_BA; %Length of Sensible Heating Zone (B to C) [m]
V_BD=m_PBU/(D_LNG_B*(n*(pi/4)*(d_tube_i.^2))); %LNG velocity through PBU [m/s]
%Turbulent Friction from B to C
%Dynamic Viscocity at B [Pa*s]
V_LNG_B=refpropm('V','T',T_A,'P',P_B,'nitrogen','methane','ethane','propane','
butane','pentane',[Nitrogen Methane Ethane Propane Nbutane Pentane]);
Re_BD=m_PBU/((pi/4)*d_tube_i*V_LNG_B);
Re_crit=2300*(1+8.6*((d_tube_i/(2*r_coil)).^0.45));
%disp(Re_BD);
if Re_BD < Re_crit
    dP_BC_sr=0;
else
    f_BD=colebrook(Re_BD,(e_AB/d_tube_i));
    dP_BC_sr=(f_BD*L_BC*D_LNG_B*(V_BD.^2)*(1/(2*d_tube_i))/1000; %Pressure
drop in Zone B to C b/c of friction [kPa]
end
%Calculating the pressure at point C [kPa]
P_C=P_B-(P_BC_BA*(P_B-P_A))-dP_BC_sr;%[kPa]
%disp(P_C);
%Temperature at point C [K]
T_C=refpropm('T','P',P_C,'Q',0,'nitrogen','methane','ethane','propane','butane
','pentane',[Nitrogen Methane Ethane Propane Nbutane Pentane]);

%Calculation from point C to point D
L_CD=h_BD-L_BC; %Length of Vaporization zone from C to D
```

```matlab
%Assuming exit fractional vaporization
x_e=1; %Assumed vapor quality at exit
x_f=(x_e)/3; %assumed vapor quality for friction pressure drop calcs

%This section accounts for friction loss in section C to D
%Dyanmic Viscoity of liquid at C [Pa*s]
V_LNG_C_l=refpropm('V','P',P_C,'Q',0,'nitrogen','methane','ethane','propane','
butane','pentane',[Nitrogen Methane Ethane Propane Nbutane Pentane]);
%Dynamic Viscoity of vapor at C [Pa*s]
V_LNG_C_v=refpropm('V','P',P_C,'Q',1,'nitrogen','methane','ethane','propane','
butane','pentane',[Nitrogen Methane Ethane Propane Nbutane Pentane]);
%Density of liquid at C [kg/m^3]
D_LNG_C_l=refpropm('D','P',P_C,'Q',0,'nitrogen','methane','ethane','propane','
butane','pentane',[Nitrogen Methane Ethane Propane Nbutane Pentane]);
%Density of vapor at C [kg/m^3]
D_LNG_C_v=refpropm('D','P',P_C,'Q',1,'nitrogen','methane','ethane','propane','
butane','pentane',[Nitrogen Methane Ethane Propane Nbutane Pentane]);
%Lockhart-Martinelli parameter [-]
%Assume liquid and vapor are turbulent
X_tt_1=(((1-
x_f)/x_f).^0.9)*((D_LNG_C_v/D_LNG_C_l).^0.5)*((V_LNG_C_l/V_LNG_C_v).^0.1);
%Homogenous two phase density [kg/m^3]
rho_tp_homo=1/((x_f/D_LNG_C_v)+((1-x_f)/D_LNG_C_l));
%First calculate the slip ration (SR) using the Chislom Correlation
if X_tt_1>1
    SR=(D_LNG_C_l/rho_tp_homo).^0.5;
else
    SR=(D_LNG_C_l/D_LNG_C_v).^0.25;
end
%Void Fraction [-]
e_vo=x_f/(x_f+(SR*(1-x_f)*(D_LNG_C_l/D_LNG_C_v)));
%Average two phase density [kg/m^3]
rho_tp_avg=(e_vo*D_LNG_C_v)+((1-e_vo)*D_LNG_C_l);

%Average Two-phase multiplier sqrted [-]
x_avg=(x_e*2)/3;
Y_tp=((D_LNG_C_l/D_LNG_C_v).^0.5)*((V_LNG_C_v/V_LNG_C_l).^(.25/2));
Phi_sqrd_avg=((Y_tp.^2)*(x_avg.^3))+((1+2*x_avg*((Y_tp.^2)-1))*(1-
x_avg).^(1/3));

%Exit Two-phase multiplier sqrted [-]
Phi_sqrd_exit=((Y_tp.^2)*(x_e.^3))+((1+2*x_e*((Y_tp.^2)-1))*(1-x_e).^(1/3));

%Exit Void Fraction []
X_tt_exit=(((1-
x_e)/x_e).^0.9)*((D_LNG_C_v/D_LNG_C_l).^0.5)*((V_LNG_C_l/V_LNG_C_v).^0.1);
if X_tt_exit>1
    SR_exit=(D_LNG_C_l/rho_tp_homo).^0.5;
else
    SR_exit=(D_LNG_C_l/D_LNG_C_v).^0.25;
end
%Exit Void Fraction [-]
e_vo_ext=x_e/(x_e+(SR_exit*(1-x_e)*(D_LNG_C_l/D_LNG_C_v)));

%Acceleration Pressure drop C to D [kPa]
```

```
dP_CD_acc=((((m_PBU/(n*(pi/4)*d_tube_i.^2))).^2)/D_LNG_C_l)*x_e*((D_LNG_C_l/D_
LNG_C_v)-1)/1000;
%Calculating liquid friction pressure drop from C to D [kPa]
dP_CD_l=(f_BD*L_CD*D_LNG_C_l*(V_BD.^2)*(1/(2*d_tube_i))/1000);
%Calculating the two-phase friction pressure drop from C to D [kPa]
dP_CD_f=Phi_sqrd_avg*dP_CD_l;
%Calculating static two-phase pressure drop from C to D [kPa]
dP_CD_s=(9.81*rho_tp_avg*L_CD)/1000;

%Pressure at point D [kPa]
P_D=P_C-dP_CD_acc-dP_CD_f-dP_CD_s;
%disp(P_D);


%Pressure drop from point D to point A
%Assume that the LNG is fully vaporized x_DA=1
%Density of liquid at D [kg/m^3]
D_LNG_D=refpropm('D','P',P_D,'Q',1,'nitrogen','methane','ethane','propane','bu
tane','pentane',[Nitrogen Methane Ethane Propane Nbutane Pentane]);
%Dynamic Viscoity of vapor at D [Pa*s]
V_LNG_D=refpropm('V','P',P_D,'Q',1,'nitrogen','methane','ethane','propane','bu
tane','pentane',[Nitrogen Methane Ethane Propane Nbutane Pentane]);
%Guess circulation speed of LNG in D to A [m/s]
V_DA=m_PBU/(D_LNG_D*((pi/4)*(d_inner_DA.^2)));
%Guess Reynold's number from D to A [-]
Re_DA=(m_PBU/((pi/4)*(d_inner_DA)))/V_LNG_D;
%Calculating friction factor in the pipe [-]
%The turbulent friction factor uses the Colebrook white
if Re_DA>2300
    f_d_DA=colebrook(Re_DA,(e_DA/d_inner_DA));
else
    f_d_DA=64/Re_DA;
end
%term for the pressure drop from D to A because of pipe roughness [kPa]
dP_DA_sr=(f_d_DA*L_DA*D_LNG_D*(V_DA.^2)*(1/(2*d_inner_DA))/1000); %this term
accounts for surface roughness
%this term accounts for minor losses from valves and bends
%there is one globe valve (HV113) and at least one 45 deg bend and one 90
%deg bend in the design
dP_DA_globe=340*f_d_DA*(V_DA.^2)*(1/(2*d_inner_DA))/1000; %pressure loss from
globe valve
dP_DA_45=16*f_d_DA*(V_DA.^2)*(1/(2*d_inner_DA))/1000; %pressure loss from 45
deg bend
dP_DA_90=30*f_d_DA*(V_DA.^2)*(1/(2*d_inner_DA))/1000; %pressure loss from 90
deg bend

%Calculating the pressure at the liquid surface
P_surface=P_D-dP_DA_sr-dP_DA_globe-dP_DA_45-dP_DA_90; %Pressure at surface
[kPa]
%disp(P_surface);
end


X=[X;P_A m_PBU]; %Stores P_A and m_PBU
P_A=P_A+dP_loop; %Resets P_A
m_PBU=0; %Resets m_PBU
```

```
end

figure(1);
plot(X(:,1),X(:,2))
xlabel('Top Tank Pressure [kPa]','FontSize',12)
ylabel('Mass Flowrate [kg/s]','FontSize',12)
title('\itMass Flowrate through PBU versus Top Tank Pressure','FontSize',16)
```

Appendix I: Iterative Vapor Pressurization

In order to calculate the pressurization of the top of the LNG tank in MATLAB it was necessary to modify Equations (63), (64), and (65) so they could be iterated. Equations (99), (100), and (101) represent an iterative form of Equations (63), (64), and (65).

$$\rho_v^t + \dot{m}_{PBU}(P_v^t)^t \Delta t / V_v = \rho_v^{t+\Delta t} \tag{99}$$

$$T_v^{t+\Delta t} = T_v^t \left(\frac{\rho_v^{t+\Delta t}}{\rho_v^t} \right)^{s-1} \tag{100}$$

$$P_v^{t+\Delta t} = P_v^t \left(\frac{\rho_v^{t+\Delta t}}{\rho_v^t} \right)^{s} \tag{101}$$

The initial conditions used in these iterations are provided in Table 17. A 10 sec time step was selected for these calculations.

Appendix J: MATLAB program idealized tank pressurization

```matlab
clear all
clc
%Mole fraction of LNG
Nitrogen=0.005;
Methane=0.95;
Ethane=0.0383;
Propane=0.0055;
Isobutane=0.0025;
Nbutane=0.0007;
Pentane=0.0005;

%Constants
V=117; %[m^3] Vapor Volume based on measured

%Initial Top Tank Conditions
P_initial=400; %[kPa]
T_initial=294; %[K]
D_initial_liquid=refpropm('D','P',P_initial,'Q',0,'nitrogen','methane','ethane','propane','butane','pentane',[Nitrogen Methane Ethane Propane Nbutane Pentane]);
D_initial=refpropm('D','T',T_initial,'P',P_initial,'nitrogen','methane','ethane','propane','butane','pentane',[Nitrogen Methane Ethane Propane Nbutane Pentane]);
M_initial=refpropm('M','T',T_initial,'P',P_initial,'nitrogen','methane','ethane','propane' ,'butane','pentane',[Nitrogen Methane Ethane Propane Nbutane Pentane]);
%Initial Variables
P=P_initial;
T=T_initial;
D=D_initial;
t=0;

%Forward Loop
%Conservation of mass
dt=1; %[s] step size

X=[];

while P<495
    if t>100000
        disp('too much time')
        break
    end
K=refpropm('K','T',T,'P',P,'nitrogen','methane','ethane','propane','butane','pentane',[Nitrogen Methane Ethane Propane Nbutane Pentane]);
m_PBU=(0.0016*P)+0.1316;
D_f=((m_PBU*dt)/V)+D; %density after step
P_f=P*((D_f/D).^K); %Pressure after step
T_f=T*((D_f/D).^(K-1)); %Temperature after step
X=[X;P_f T_f D_f]; %Stores P,T and D
ZZ=m_PBU; %Records the PBU within each timestep
D=D_f; %Resets D
P=P_f; %Resets P
```

```matlab
    T=T_f; % Resets T

end


steps=length(X(:,1));
t=steps*dt;
time=linspace(0,t,steps);
% Calculating the Percent Volume Change from the PBU
PBUmass=sum(ZZ)*dt; %Total LNG Vaporized in pressurization
PBUvolume=PBUmass/D_initial_liquid; %Total LNG Volume Vaporized
InitialLiquidMass=D_initial_liquid*V; %Total initial LNG in tank
PercentTankMass=PBUmass/InitialLiquidMass; %Percent LNG mass vaporized
PercentTankVolume=PBUvolume/V; %Percent LNG volume vaporized

% Calculating the Percent Volume Change from the NG Engines


disp([num2str(t) 's Pressurization Time'])
disp([num2str(PBUmass) 'kg Liquid Mass Vaporized'])
disp([num2str(PBUvolume) 'm^3 LNG Volume Vaporized'])
disp([num2str(PercentTankMass) '% LNG Vaporized to Total Liquid Mass'])
disp([num2str(PercentTankVolume) '% Percent Liquid Volume Change'])


figure(1);
plot(time,X(:,1))
xlabel('Time [s]','FontSize',12)
ylabel('Pressure [kPa]','FontSize',12)
title('\itPressurization Time from 400 kPa to 500 kPa','FontSize',16)
figure(2);
plot(time,X(:,2))
xlabel('Time [s]','FontSize',12)
ylabel('Vapor Density [kg/m^3]','FontSize',12)
title('\itVapor Density Change During Pressurization','FontSize',16)
figure(3);
plot(time,X(:,3))
xlabel('Time [s]','FontSize',12)
ylabel('Ration of Specific Heats (Cp/Cv)','FontSize',12)
title('\itRation of Specific Heats During Pressurization','FontSize',16)
```

Appendix K: MATLAB code for mixing calculation

```matlab
clear all
clc
%Initial LNG mole fractions
Nitrogen_LNGi=0.005;
Methane_LNGi=0.950;
Ethane_LNGi=0.0383;
Propane_LNGi=0.0055;
Nbutane_LNGi=0.0007;
Pentane_LNGi=0.0005;

%Initial Vapor Parameters [kPa]
P_vi=500; % [kPa] initial tank pressure
T_vi=228; % [K] initial vapor temperature

%Initial Heel Parameters [K]
T_offset=11; %[K] Offset between the saturated temperature and heel
temperature
T_LNGi=(-
T_offset)+refpropm('T','P',P_vi,'Q',0,'nitrogen','methane','ethane','propane',
'butane','pentane',[Nitrogen_LNGi Methane_LNGi Ethane_LNGi Propane_LNGi
Nbutane_LNGi Pentane_LNGi]);

%Initial NG mole fractions (Raoult's Law)
%Mole Fraction (N2)
if T_vi>126.19
    T_N2i=126.19;
else
    T_N2i=T_vi;
end
P_satN2i=refpropm('P','T',T_N2i,'Q',1,'nitrogen');
Nitrogen_NGi=(Nitrogen_LNGi*P_satN2i)/P_vi;
%Mol Fraction (C2)
P_satC2i=refpropm('P','T',T_vi,'Q',1,'ethane');
Ethane_NGi=(Ethane_LNGi*P_satC2i)/P_vi;
%Mol Fraction (C3)
P_satC3i=refpropm('P','T',T_vi,'Q',1,'propane');
Propane_NGi=(Propane_LNGi*P_satC3i)/P_vi;
%Mol Fraction (C4)
P_satC4i=refpropm('P','T',T_vi,'Q',1,'butane');
Nbutane_NGi=(Nbutane_LNGi*P_satC4i)/P_vi;
%Mol Fraction (C5)
P_satC5i=refpropm('P','T',T_vi,'Q',1,'pentane');
Pentane_NGi=(Pentane_LNGi*P_satC5i)/P_vi;
%Mol Fraction (C1)
Methane_NGi=1-(Nitrogen_NGi+Ethane_NGi+Propane_NGi+Nbutane_NGi+Pentane_NGi);




%Initial Ethalpy [kJ/kg] and Density [kg/m^3] (LNG)
h_LNGi=(1/1000)*refpropm('H','T',T_LNGi,'P',P_vi,'nitrogen','methane','ethane'
,'propane','butane','pentane',[Nitrogen_LNGi Methane_LNGi Ethane_LNGi
Propane_LNGi Nbutane_LNGi Pentane_LNGi]);
```

```matlab
d_LNGi=refpropm('D','T',T_LNGi,'P',P_vi,'nitrogen','methane','ethane','propane
','butane','pentane',[Nitrogen_LNGi Methane_LNGi Ethane_LNGi Propane_LNGi
Nbutane_LNGi Pentane_LNGi]);
%Initial Ethalpy [kJ/kg] and Density [kg/m^3] (NG)
h_NGi=(1/1000)*refpropm('H','T',T_vi,'P',P_vi,'nitrogen','methane','ethane','p
ropane','butane','pentane',[Nitrogen_NGi Methane_NGi Ethane_NGi Propane_NGi
Nbutane_NGi Pentane_NGi]);
d_NGi=refpropm('D','T',T_vi,'P',P_vi,'nitrogen','methane','ethane','propane','
butane','pentane',[Nitrogen_NGi Methane_NGi Ethane_NGi Propane_NGi Nbutane_NGi
Pentane_NGi]);
%Total Volume
V_tot=234;
Perc_liq=0.1;
V_NGi=V_tot*(1-Perc_liq);
V_LNGi=V_tot*(Perc_liq);

%Initial Energy and Mass (LNG)
E_LNGi=h_LNGi*d_LNGi*V_LNGi;
m_LNGi=d_LNGi*V_LNGi;

%Initial Energy and Mass (NG)
E_NGi=h_NGi*d_NGi*V_NGi;
m_NGi=d_NGi*V_NGi;

%Total Tank Energy and Mass (LNG+NG)
E_tot_given=E_LNGi+E_NGi
m_tot_given=m_LNGi+m_NGi;

%Total initial moles [NG]
%Average Molar Mass NGi [kg/mol]
M_NGi=(1/1000)*refpropm('M','T',T_vi,'P',P_vi,'nitrogen','methane','ethane','p
ropane','butane','pentane',[Nitrogen_NGi Methane_NGi Ethane_NGi Propane_NGi
Nbutane_NGi Pentane_NGi]);
%Total moles in NGi (kmol)
n_NGi=(m_NGi/M_NGi)*(1/1000);

%Total initial moles [LNG]
%Average Molar Mass NGi [kg/mol]
M_LNGi=(1/1000)*refpropm('M','T',T_LNGi,'P',P_vi,'nitrogen','methane','ethane'
,'propane','butane','pentane',[Nitrogen_LNGi Methane_LNGi Ethane_LNGi
Propane_LNGi Nbutane_LNGi Pentane_LNGi]);
%Total moles in NGi (kmol)
n_LNGi=(m_LNGi/M_LNGi)*(1/1000);

%Conditions after mixing
%P_sat is varied until E_initial = E_final
%Use the Loop below to alter the Saturation Pressure
%P_vf= 200; %initial pressure for iteration
e_tol_energy=500; %Allowable difference in energy initial and energy final
E_tot_calc=0; %to initialize energy


%Initialization
n_NGf=0; %Initializes the Composition Loop
Nitrogen_NGf=0;
```

```matlab
Methane_NGf=0;
Ethane_NGf=0;
Propane_NGf=0;
Nbutane_NGf=0;
Pentane_NGf=0;
Nitrogen_LNGf=0;
Methane_LNGf=0;
Ethane_LNGf=0;
Propane_LNGf=0;
Nbutane_LNGf=0;
Pentane_LNGf=0;
%Final Liquid and Vapor Temperature (Guess)
T_vf=126.3251;

while (abs(E_tot_given - E_tot_calc) > e_tol_energy)
T_vf=T_vf+0.0001;

P_vf=(T_vf*n_NGi*8.314462175)/V_NGi;

    if P_vf < 180;
        disp('Did not converge');
        break
    end


%Vapor Mole Composition
%Nitrogen
if T_vf>126.19
    T_N2f=126.19;
else
    T_N2f=T_vf;
end
P_satN2f=refpropm('P','T',T_N2f,'Q',1,'nitrogen');
Nitrogen_NGf=(Nitrogen_LNGi*P_satN2f)/P_vf;
%Ethane
if T_vf > 90.37
    T_C2f=T_vf;
else
    T_C2f=90.368;
end
P_satC2f_NG=refpropm('P','T',T_C2f,'Q',1,'ethane');
Ethane_NGf=(Ethane_LNGi*P_satC2f_NG)/P_vf;
%Propane
P_satC3f_NG=refpropm('P','T',T_vf,'Q',1,'propane');
Propane_NGf=(Propane_LNGi*P_satC3f_NG)/P_vf;
%Nbutane
if T_vf < 134.90
    T_C4f=134.90;
else
    T_C4f=T_vf;
end
P_satC4f_NG=refpropm('P','T',T_C4f,'Q',1,'butane');
Nbutane_NGf=(Nbutane_LNGi*P_satC4f_NG)/P_vf;
%Pethane
if T_vf < 143.47
    T_C5=143.47;
```

```matlab
else
    T_C5=T_vf;
end
P_satC5f_NG=refpropm('P','T',T_C5,'Q',1,'pentane');
Pentane_NGf=(Pentane_LNGi*P_satC5f_NG)/P_vf;
%Methane
Methane_NGf=1-(Nitrogen_NGf+Ethane_NGf+Propane_NGf+Nbutane_NGf+Pentane_NGf);

%Liquid Mole Composition
delta_Nitrogen=(Nitrogen_NGi-Nitrogen_NGf)*n_NGi; %Total moles ethane changed
in vapor
Nitrogen_LNGf=((Nitrogen_LNGi*n_LNGi)+delta_Nitrogen)/n_LNGi;
delta_Ethane=(Ethane_NGi-Ethane_NGf)*n_NGi; %Total moles ethane changed in
vapor
Ethane_LNGf=((Ethane_LNGi*n_LNGi)+delta_Ethane)/n_LNGi;
delta_Propane=(Propane_NGi-Propane_NGf)*n_NGi; %Total moles ethane changed in
vapor
Propane_LNGf=((Propane_LNGi*n_LNGi)+delta_Propane)/n_LNGi;
delta_Nbutane=(Nbutane_NGi-Nbutane_NGf)*n_NGi; %Total moles ethane changed in
vapor
Nbutane_LNGf=((Nbutane_LNGi*n_LNGi)+delta_Nbutane)/n_LNGi;
delta_Pentane=(Pentane_NGi-Pentane_NGf)*n_NGi; %Total moles ethane changed in
vapor
Pentane_LNGf=((Pentane_LNGi*n_LNGi)+delta_Pentane)/n_LNGi;
delta_Methane=(Methane_NGi-Methane_NGf)*n_NGi; %Total moles ethane changed in
vapor
Methane_LNGf=((Methane_LNGi*n_LNGi)+delta_Methane)/n_LNGi;

%NGf Physical Properties
d_NGf=refpropm('D','T',T_vf,'P',P_vf,'nitrogen','methane','ethane','propane','
butane','pentane',[Nitrogen_NGf Methane_NGf Ethane_NGf Propane_NGf Nbutane_NGf
Pentane_NGf]);
m_NGf=d_NGf*V_NGi;
M_NGf=(1/1000)*refpropm('M','T',T_vf,'P',P_vf,'nitrogen','methane','ethane','p
ropane','butane','pentane',[Nitrogen_NGf Methane_NGf Ethane_NGf Propane_NGf
Nbutane_NGf Pentane_NGf]);
n_NGf=(m_NGf/M_NGf)*(1/1000); %Calculates a new total vapor moles
Z_vf=refpropm('Z','T',T_vf,'P',P_vf,'nitrogen','methane','ethane','propane','b
utane','pentane',[Nitrogen_NGf Methane_NGf Ethane_NGf Propane_NGf Nbutane_NGf
Pentane_NGf]);
T_vf=(P_vf*V_NGi)/(Z_vf*n_NGf*8.314462175); %Calculates a new vapor
temperature


%Final Ethalpy [kJ/kg] and Density [kg/m^3] (LNG)
h_LNGf=(1/1000)*refpropm('H','T',T_vf,'P',P_vf,'nitrogen','methane','ethane','
propane','butane','pentane',[Nitrogen_LNGf Methane_LNGf Ethane_LNGf
Propane_LNGf Nbutane_LNGf Pentane_LNGf]);
d_LNGf=refpropm('D','T',T_vf,'P',P_vf,'nitrogen','methane','ethane','propane',
'butane','pentane',[Nitrogen_LNGf Methane_LNGf Ethane_LNGf Propane_LNGf
Nbutane_LNGf Pentane_LNGf]);
%Final Ethalpy [kJ/kg] and Density [kg/m^3] (NG)
h_NGf=(1/1000)*refpropm('H','T',T_vf,'P',P_vf,'nitrogen','methane','ethane','p
ropane','butane','pentane',[Nitrogen_NGf Methane_NGf Ethane_NGf Propane_NGf
Nbutane_NGf Pentane_NGf]);
```

```matlab
d_NGf=refpropm('D','T',T_vf,'P',P_vf,'nitrogen','methane','ethane','propane','butane','pentane',[Nitrogen_NGf Methane_NGf Ethane_NGf Propane_NGf Nbutane_NGf Pentane_NGf]);


%Final Volume (LNG)
V_LNGf=(m_tot_given-(V_tot*d_NGf))/(d_LNGf-d_NGf);
V_NGf=V_tot-V_LNGf;




%Final Energy and Mass (LNG)
E_LNGf=h_LNGf*d_LNGf*V_LNGf;
m_LNGf=d_LNGf*V_LNGf;

%Final Energy and Mass (NG)
E_NGf=h_NGf*d_NGf*V_NGf;
m_NGf=d_NGf*V_NGf;

%Total final moles [NG]
%Average Molar Mass NGf [kg/mol]
%M_NGf=(1/1000)*refpropm('M','T',T_vi,'P',P_vi,'nitrogen','methane','ethane','propane','butane','pentane',[Nitrogen_NGf Methane_NGf Ethane_NGf Propane_NGf Nbutane_NGf Pentane_NGf]);
%Total moles in NGi (kmol)
%n_NGf=(m_NGf/M_NGf)*(1/1000);

%Total Tank Energy and Mass (LNG+NG)
E_tot_calc=E_LNGf+E_NGf
m_tot_calc=m_LNGf+m_NGf;

end

disp([num2str(P_vf) ' Final Tank Pressure [kPa]'])
disp([num2str(T_vf) ' Final Tank Temperature [K]'])

%Display the initial LNG and NG composition
disp([num2str( Nitrogen_LNGi) ' LNG Mol Frac N2'])
disp([num2str( Methane_LNGi) ' LNG Mol Frac C1'])
disp([num2str( Ethane_LNGi) ' LNG Mol Frac C2'])
disp([num2str( Propane_LNGi) ' LNG Mol Frac C3'])
disp([num2str( Nbutane_LNGi) ' LNG Mol Frac C4'])
disp([num2str( Pentane_LNGi) ' LNG Mol Frac C5'])


disp([num2str( Nitrogen_NGi) ' NG Mol Frac N2'])
disp([num2str( Methane_NGi) ' NG Mol Frac C1'])
disp([num2str( Ethane_NGi) ' NG Mol Frac C2'])
disp([num2str( Propane_NGi) ' NG Mol Frac C3'])
disp([num2str( Nbutane_NGi) ' NG Mol Frac C4'])
disp([num2str( Pentane_NGi) ' NG Mol Frac C5'])


%Display the final LNG and NG composition

disp([num2str( Nitrogen_NGf) ' Final NG Mol Frac N2'])
disp([num2str( Methane_NGf) ' Final NG Mol Frac C1'])
```

```matlab
disp([num2str( Ethane_NGf) ' Final NG Mol Frac C2'])
disp([num2str( Propane_NGf) ' Final NG Mol Frac C3'])
disp([num2str( Nbutane_NGf) ' Final NG Mol Frac C4'])
disp([num2str( Pentane_NGf) ' Final NG Mol Frac C5'])
```

Appendix L: Required Purge Time

In the measurement campaign, the asymptotic tank pressure achieved during top tank purging was used as a way to calculate the liquid bubble point temperature of the heel. This temperature was indicative of the liquid surface temperature. An estimate was performed to determine the amount of time the tank should be purged in order to achieve saturated conditions.

Bernoulli's Law was used to estimate the time required to purge the tank before liquid evaporation began. A simplified version of Bernoulli's equation is provided in Equation (102). State 1 refers to the conditions inside the LNG tank and state 2 refers to the conditions outside the LNG tank.

$$0.5\rho_1 u_1{}^2 + \rho_1 g z_1 + P_1 = 0.5\rho_2 u_2{}^2 + \rho_2 g z_2 + P_2 \tag{102}$$

It may be assumed that the difference in vertical height between the first and second state is negligible. The density of the natural gas may also be assumed to be constant and the initial velocity of the NG in the tank is zero. Additionally, it may be assumed that the final pressure at state two is atmospheric conditions (1.013 bara). Equation (102) is reduced to Equation (103).

$$P_1 = 0.5\rho_{NG} u_2{}^2 + P_2 \tag{103}$$

Equation (103) may be rearranged to Equation (104) which provides the final velocity from the LNG tank.

$$u_2 = \sqrt{\frac{P_1 - P_2}{0.5\rho_{NG}}} \tag{104}$$

When multiplied by the diameter of the top tank filling line from which the tank is purged, the NG volume from the LNG tank may be calculated.

$$Q_2 = \frac{\pi}{4} d_{NG}{}^2 \sqrt{\frac{P_1 - P_2}{0.5\rho_{NG}}} \tag{105}$$

Finally, multiplying the volume flow from the tank by the total vapor volume in the tank indicates a conservative amount of time required to empty the initial contents of the tank during purging.

$$t_{purge} = V_{NG} \frac{\pi}{4} d_{NG}{}^2 \sqrt{\frac{P_1 - P_2}{0.5\rho_{NG}}} \tag{106}$$

The parameters used to estimate the purging time for MF Korsfjord is listed in Table 31 as well as the estimated purging time.

Table 31: Purging Time Parameters for E3

Parameter	Symbol	Experiment E3	Units
Initial Tank Pressure	P_1	477.13	kPa
Atmospheric Pressure	P_2	101.13	kPa
NG Density	ρ_{NG}	4.36	kg/m^3
Top Fill Pipe Diameter	d_{NG}	0.100	M
Vapor Volume	V_{NG}	97.84	m^3
Purge Time	t_{purge}	319	s

Appendix M: Water Glycol Temperature Measurements from E2

Figure 78 shows the recorded temperatures from the K-type thermocouples attached to the surface of the water glycol piping as well as the installed PT-100. The fact that the temperatures measured by the thermocouples move in the same direction over time suggest that this temperature is more accurate than the installed temperature sensors on MF Korsfjord.
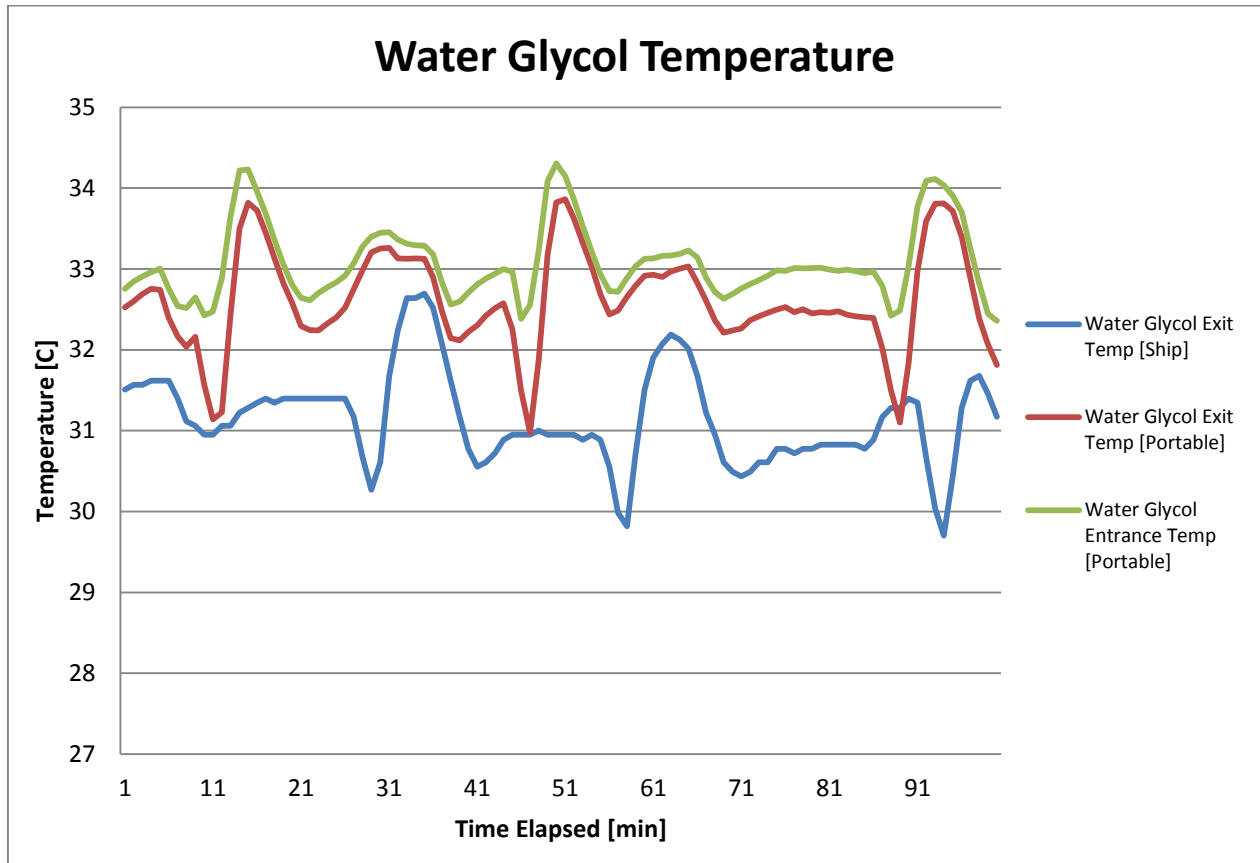

Figure 78: Water Glycol Temperature Measurements during E2

Appendix N: Water Glycol Volume Flow Measurements / Allweiler Pump Curve

Figure 79 shows a volume flow measurement collected during E2 over approximately a 60 minute period using the Ultraflux UF801 Flowmeter on MF Korsfjord. Figure 80 shows the corresponding pump characteristic curves on MF Korsfjord and KV Bergen which indicates the measured volume flow is within the published capacity of the installed pump.
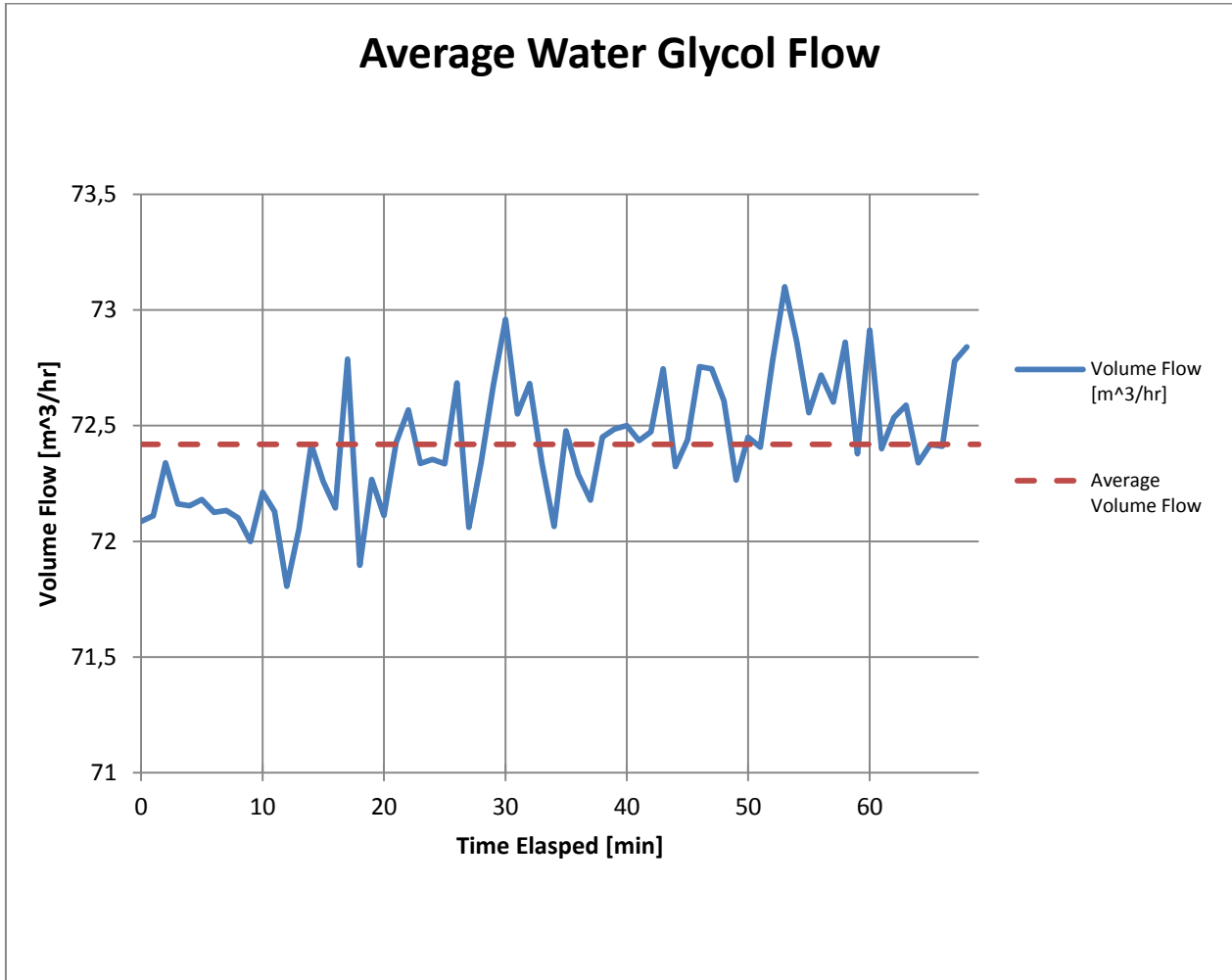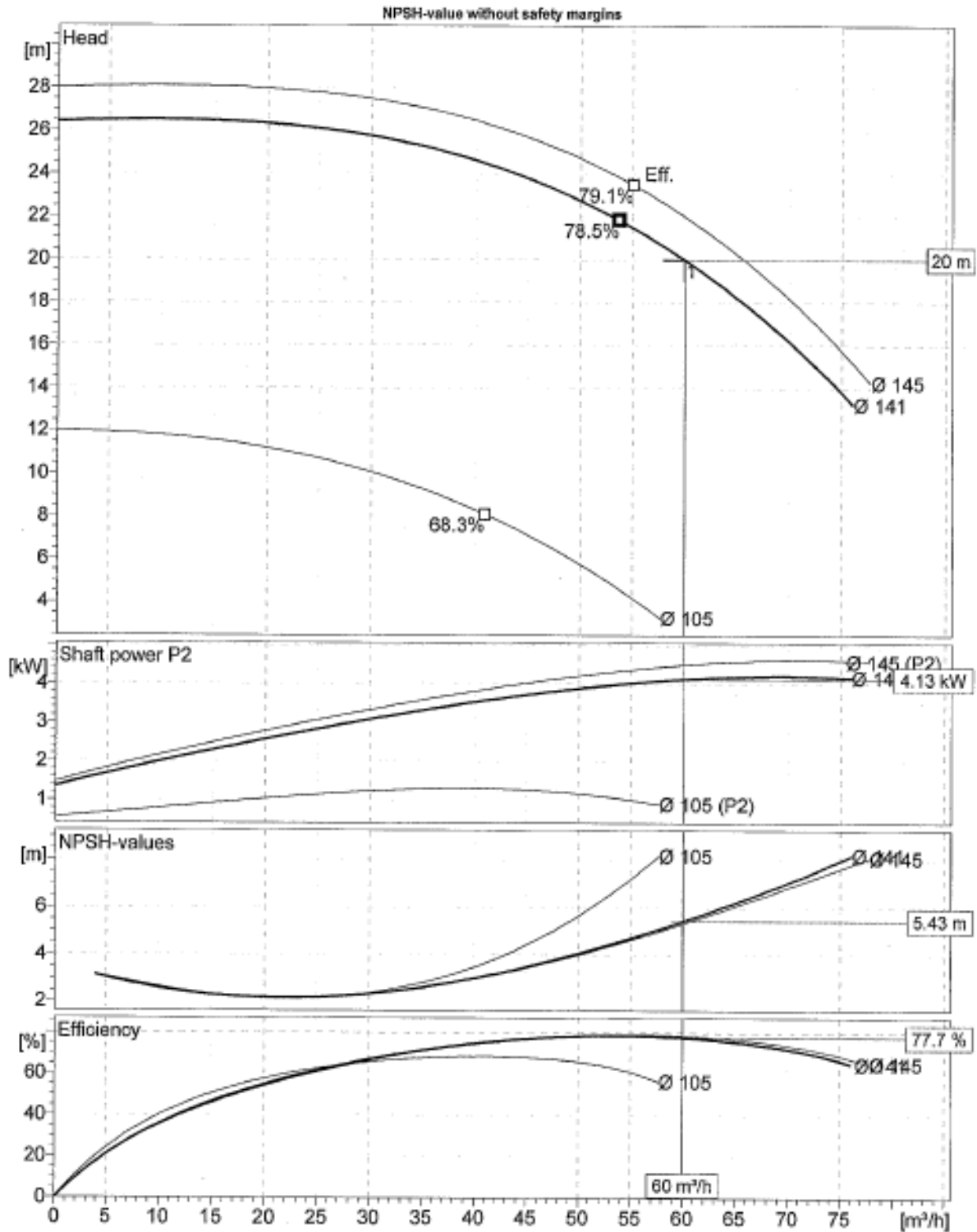

Figure 79: Water Glycol Volume Flow during E2

Figure 80: Allweiler Pump Performance Curves

Appendix O: Description of the Water Glycol System

The following is a brief description of the different components that make up the water glycol heat transfer system on MF Korsfjord. Figure 81 provides an overview of the different components that make up the heat transfer system on MF Korsfjord.
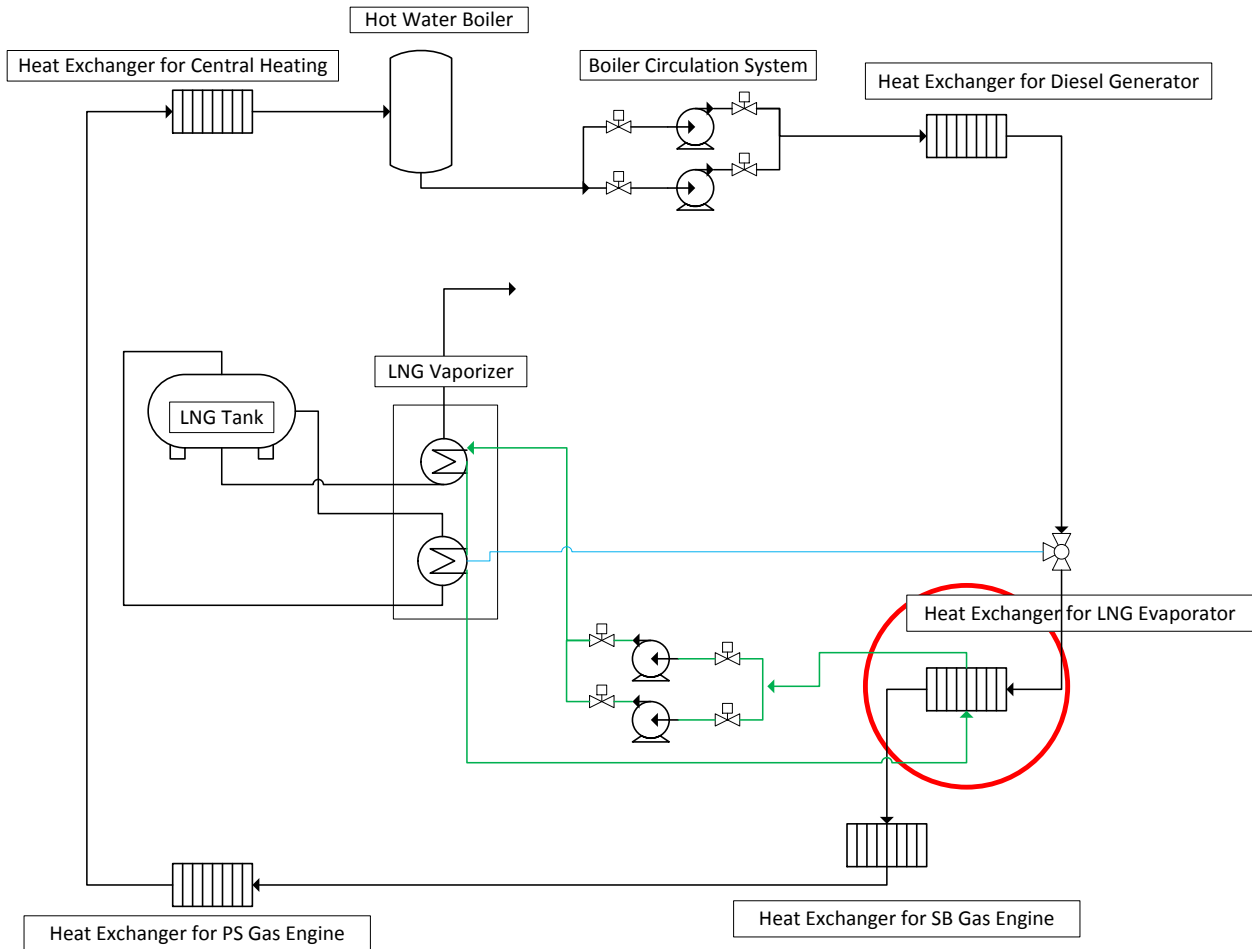

Figure 81: Water Glycol Heat Exchanger System

The following components reject heat to the Heat Exchanger System on MF Korsfjord: the Hot Water Boiler System, Diesel Generator, Port Side Gas Engine, and Starboard Side Gas Engine. According to the Chief Engineer on MF Korsfjord, the water glycol temperature exiting the LNG Vaporizer is controlled by an Amot thermo-mechanical valve made of copper which regulates the heat transferred from the main heat exchanger network to the water glycol network connected to the LNG Vaporizer. This valve is indicated by a blue line in Figure 81. A picture of the Amot thermo-mechanical vale is shown in Figure 82. The Amot valve ensures that the exit temperature of the water glycol exiting the LNG Vaporizer is roughly 32C. This is done so that complete freeze out does not occur inside the water glycol circuit running through the LNG Vaporizer. The

Heat Exchanger for the LNG Evaporator connected to the water glycol network is shown in Figure 83.

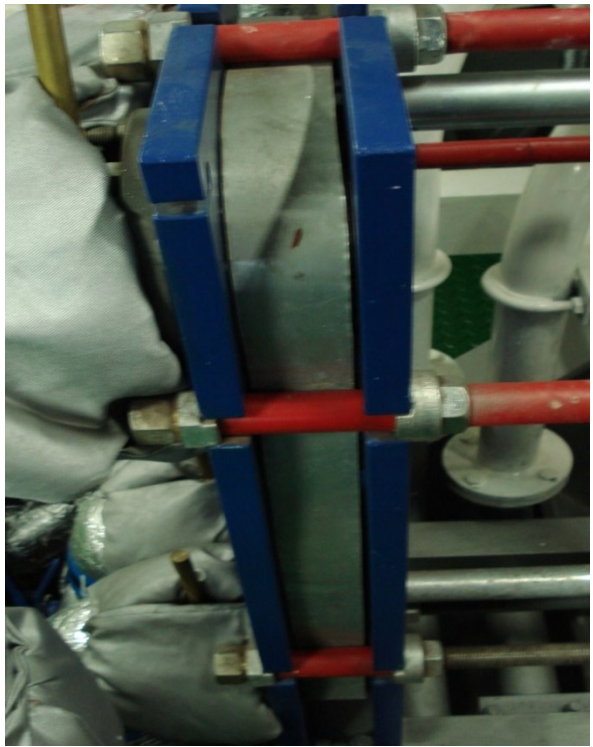Figure 82: Amot Thermo-Mechanical Valve

Figure 83: LNG Evaporator Circuit Heat Exchanger

Since heat supplied to the water glycol flow within the LNG Vaporizer circuit comes from multiple sources (including the ship's boiler which is able to store hot water while the ship is not operating along-side the pier), the NG gas engines are not required to be in operation while using the PBU circuit. This is the reason why it is possible to build up the top tank pressure the day after bunkering before the NG engines are started.